UNIVERSAL
LIBRARY

OU_156606

UNIVERSAL
LIBRARY

OSMANIA UNIVERSITY LIBRARY

Call No. 546.4 K63R Accession No. 47538

Author KLEBER, Eugene V.

Title Rare earth research. 1961

This book should be returned on or before the date last marked below

RARE EARTH RESEARCH

Edited by

EUGENE V. KLEBER

Based on

A Seminar at Lake Arrowhead, California
October, 1960

Sponsored by

The University of California
The United States Air Force,
Office of Scientific Research
The United States Navy,
Office of Naval Research
Nuclear Corporation of America,
Research Chemicals Division

THE MACMILLAN COMPANY, NEW YORK, 1961

© The Macmillan Company 1961

All rights reserved—no part of this book may be reproduced in any form without permission in writing from the publisher, except by a reviewer who wishes to quote brief passages in connection with a review written for inclusion in a magazine or newspaper.

First Printing

Library of Congress catalog card number: 61-13307

The Macmillan Company, New York
Brett-Macmillan Ltd., Galt, Ontario

Printed in the United States of America

PREFACE

The Arrowhead Research Conference was conceived with two principal aims in mind. First, we wanted to bring together many of the individuals and institutions engaged in research on that novel assortment of elements in Group III of the periodic table—the rare earths. Second, we wished to discuss current research rather than summarize previous work. With these aims in mind, we issued invitations to many speakers active in the field. The response was extremely favorable.

In accordance with the above aims, we wished to avoid the all-too-typical technical meeting where papers are read verbatim. Copies of all the papers were distributed to the attendees prior to the seminar. The sessions themselves consisted of discussion of the papers and the supplementary data presented.

It may be noted from the table of contents that some subjects dear to the hearts of rare earth researchers have not been covered. These omissions were deliberate. We felt that this symposium should be devoted to areas which are relatively new and in the forefront of today's activities rather than to those already well documented. Thus, much of the fine work on the chemistry of separation of the rare earths and on the problems and techniques of analytical chemistry is not mentioned. Conversely, the recent availability in modest quantities of purified earth metals permitted discussion of the properties of these metals and their compounds—a fact which illustrates that practical considerations played an important role in the selection of topics. There were also a substantial number of comments on the magnetic and electrical properties of the rare earths.

We were fortunate in having a large number of speakers with dissenting viewpoints on the significance and meaning of the data presented. The attendees represented many scientific fields: Government laboratories where sponsored work is being conducted; Government laboratories which monitor much of our sponsored research and development, universities representing the physical and chemical research areas, industrial research organizations, and industries which either supply raw materials or have direct uses for them.

There were five half-day sessions, during which the topics listed in the table of contents were covered. Each session was presided over by two co-chairmen, who stimulated and guided discussion. In addition to

his scheduled paper, each speaker presented supplemental and experimental data.

We gratefully acknowledge the assistance of the following chairmen:

Dr. Charles Coryell	Dr. J. Nachman
Dr. Elliot S. Pierce	Comdr. C. G. Sporer
Dr. Alton F. Armington	Dr. Alan Portis
Dr. LeRoy Eyring	Lt. S. Worcester
Dr. Don M. Yost	Dr. A. R. Bobrowsky

The culmination of a seminar is formal publication of the proceedings, for it provides the means of reaching the widest possible audience. Each author revised his paper to include comments made and experimental data discussed at the conference. Their willingness in this endeavor testifies to the success of the conference. Several of the supplementary presentations from the floor were so thorough that we have included them in this book.

We are grateful to Harry Tallman, of the University of California, and Lillian Neal for providing a smooth-running conference. Mr. Tallman helped organize the sessions and house the attendees, and Mrs. Neal assisted in accumulating the manuscripts and proofreading this book.

EUGENE V. KLEBER

Coordinator

TABLE OF CONTENTS

Preface *by Eugene V. Kleber* iii

PART ONE: SOLUTION CHEMISTRY

Some Aspects of the Stabilities of Amine Polycarboxylic Acid Chelates of the Tri-positive Rare Earth Metal Ions *by Therald Moeller, Larry C. Thompson, and Ricardo Ferrús* 3
Formation Constants and Magnetic Behavior of Some Rare Earth Chelates *by Ingmar Grenthe and W. Conrad Fernelius* 12
Some Observations Regarding Rare Earth Glycolates *by J. E. Powell and J. L. Farrell* 26
The Use of Zinc and Hydrogen Ions in the Development Columns in the Separation of Cerium-Group Rare Earths by Ion-Exchange Elution *by Jack E. Powell* 31
Liquid-Liquid Extraction of Trivalent Rare Earths Using Acidic Phosphonates As Extractants *by D. F. Peppard and G. W. Mason* 37
Some Electrochemical Differences of the Lanthanons As Related to Their Separability at Amalgam Cathodes *by E. I. Onstott*..... 51
Tetravalent Neodymium and Dysprosium *by L. B. Asprey* 58

PART TWO: OXIDE SYSTEMS AND THEIR PROPERTIES

Thermal and Electronic Properties of Rare Earth Oxides *by Edgar F. Westrum, Jr.* 69
Structure and Magnetic Properties of Perovskites *by Aaron Wold* 81
Phase-Equilibria Research in Systems Involving the Rare Earth Oxides *by Robert S. Roth* 88
The Influence of Temperature on the Cerium Oxide System CeO_2-Ce_2O_3 *by Georg Brauer and Karl Gingerich* 96
The Stoichiometry and Resistivity of PrO_x *by A. F. Clifford and Paul A. Faeth* 105
Oxygen Positions in Rare Earth Iron Garnets and Their Implications *by Ernst R. Czerlinsky and Ferdinand Euler* 113
High-Temperature Oxidation of Rare Earth Metals *by Karl S. Vorres and LeRoy Eyring* 119

PART THREE: STRUCTURE OF METALS, ALLOYS, AND INTERMETALLICS

Comparative Chemistry of the Lanthanide and Actinide Elements *by B. B. Cunningham* 127

Cell Dimensions and Magnetical Susceptibilities of the MX Compounds of Rare Earths with P, As, Sb, Bi, S, Se, Te *by A. Iandelli* 135
Magnetic and Electrical Properties of Rare Earth Metal Single Crystals *by Sam Legvold* 142
Magnetic Structure Properties of Rare Earth Metals *by W. C. Koehler, E. O. Wollan, M. K. Wilkinson, and J. W. Cable* 149
Electrical and Magnetic Properties of the Rare Earth Metals and Their Alloys and Compounds *by K. A. Gschneidner, Jr., and B. T. Matthias* 158
Saturation Magnetization, Interatomic Interactions and Remanence of Some Rare Earth Metals and Compounds *by Warren E. Henry* 165
Paramagnetism of Polycrystalline Rare Earth Metals *by Sigurds Arajs and R. V. Colvin* 178

PART FOUR: PHYSICAL PROPERTIES OF METALS, ALLOYS, AND INTERMETALLICS

Studies of Intermetallic Compounds Between the Lanthanide Metals and Iron, Cobalt, Nickel and Manganese *by W. E. Wallace and L. V. Cherry* 211
Observations on Some Gadolinium-Selenium Compounds *by R. C. Vickery and H. M. Muir* 223
Rare Earth Intermetallic Compounds with Elements of Groups V and VI *by J. F. Miller and R. C. Himes* 232
High-Temperature Semiconductors for Thermoelectric Conversion *by S. W. Kurnick, M. Cutler, R. L. Fitzpatrick, and J. F. Leavy* 241
Theory of the Electron-Transport Properties of the 4f-Electrons in Rare Earth Compounds *by R. R. Heikes* 247
Samarium Sulfides for Semiconductor Application *by M. D. Houston* 255

PART FIVE: MECHANICAL AND METALLURGICAL PROPERTIES OF METALS, ALLOYS, AND INTERMETALLICS

Scandium—Its Preparation and Properties *by A. H. Daane* 261
Mechanical Properties of Rare Earth Metals *by B. Love and C. Kirkpatrick* 269
Effects of Alloying Additions of Sc, Y, Rare Earths, Th, and Pu on the γ-α Transformation of Cerium *by K. A. Gschneidner, Jr., R. O. Elliott, and R. R. McDonald* 278
Rare Earth Metals in Metallurgy, Ceramics, and Cermets *by E. S. Funston and J. A. McGurty* 288
Rare Earth Borides and Nitrides *by Harry A. Eick* 297
A Structural Survey of the Heavy Rare Earth Silicides *by Charles E. Lundin* 306

PART ONE

Solution Chemistry

SOME ASPECTS OF THE STABILITIES OF AMINE POLYCARBOXYLIC ACID CHELATES OF THE TRI-POSITIVE RARE EARTH METAL IONS

THERALD MOELLER, LARRY C. THOMPSON, AND RICARDO FERRUS

Noyes Chemical Laboratory, University of Illinois, Urbana, Illinois

The numerical data summarized in Table I indicate that the rare earth metals are readily oxidized to tri-positive ions that differ significantly from each other only in the number of electrons in the $4f$ arrangement and in crystal radius. These ions should provide, therefore, a particularly interesting series in which to evaluate the effects of progressive changes in electronic arrangement and size upon complex-ion formation.

TABLE I: NUMERICAL DATA FOR RARE EARTH METALS AND TRI-POSITIVE CATIONS

Symbol	Atomic Number Z	Electronic Configuration		Ionization Energy ev/g atom	Standard Oxidation Potential v	Electro-negativity	Crystal Radius of Ln^{3+} A
		Ln	Ln^{3+}				
La	57	$4f^0 5d^1 6s^2$	$4f^0$	5.61	+2.52	1.1	1.04
Ce	58	$4f^2 \quad 6s^2$	$4f^1$	(6.91)	2.48	1.1	1.02
Pr	59	$4f^3 \quad 6s^2$	$4f^2$	(5.76)	2.47	1.1	1.00
Nd	60	$4f^4 \quad 6s^2$	$4f^3$	(6.31)	2.44	1.2	0.99
Pm	61	$4f^5 \quad 6s^2$	$4f^4$	...	(2.42)	(1.2)	(0.98)
Sm	62	$4f^6 \quad 6s^2$	$4f^5$	5.6	2.41	1.2	0.97
Eu	63	$4f^7 \quad 6s^2$	$4f^6$	5.67	2.41	1.1	0.96
Gd	64	$4f^7 5d^1 6s^2$	$4f^7$	6.16	2.40	1.2	0.94
Tb	65	$4f^9 \quad 6s^2$	$4f^8$	(6.74)	2.39	1.2	0.92
Dy	66	$4f^{10} \quad 6s^2$	$4f^9$	(6.82)	2.35	1.2	0.91
Ho	67	$4f^{11} \quad 6s^2$	$4f^{10}$	...	2.32	1.2	0.89
Er	68	$4f^{12} \quad 6s^2$	$4f^{11}$	...	2.30	1.2	0.87
Tm	69	$4f^{13} \quad 6s^2$	$4f^{12}$	...	2.28	1.2	0.86
Yb	70	$4f^{14} \quad 6s^2$	$4f^{13}$	6.2	2.27	1.1	0.85
Lu	71	$4f^{14} 5d^1 6s^2$	$4f^{14}$	5.0	2.25	1.2	0.84
Y	89	$4d^1 5s^2$	...	6.6	2.37	1.3	0.88

The comparative weakness of the cations as acids in the Lewis sense, as evidenced by their ease of formation, their comparatively large size (e.g., radii of Al^{3+}, Fe^{3+}, and Cr^{3+} are 0.57, 0.67, and 0.65 A, respectively), and a variety of experimental approaches (1), suggest, however, that the formation of complex species is much less characteristic

of them than it is of *d*-type transition-metal cations. Indeed, only ligands with strongly chelating properties yield complex ions of significant stabilities. Particularly important and extensively studied among these are the amine polycarboxylic acids.

The absence of extensive covalent bonding in such complexes is dictated both by the electronic configurations of the cations and by their large size. Shielding of the 4*f* electrons is sufficient to render them sterically unavailable for extensive bond formation and thereby distinguish them from the *d* electrons of the regular transition-metal ions. Participation of available 5*d* orbitals in bond formation is a possibility, but against this must be cited a wealth of evidence that most binary and ternary rare earth metal compounds have ionic properties. Furthermore, such absorption-spectra and magnetic-susceptibility data as have been published for rare earth metal complexes (2–7) indicate only perturbations of an environmental type, and show none of the profound changes that might be expected if the responsible electrons were involved in bonding. It has been quite generally concluded, therefore, that the ligands are held by electrostatic or ionic interaction.

If this type of bonding is significant, then, in terms of an extension of the Born relationship

$$\Delta E = \frac{e^2}{2r}\left(1 - \frac{1}{D}\right) \tag{1}$$

where ΔE is the energy change on solvation (complexation) of a gaseous ion of charge e and radius r in a medium of dielectric constant D, a generalized increase in the stabilities of such chelates, with decreasing crystal radii and stabilities of the yttrium complexes comparable with those of the analogous dysprosium and holmium species, may be expected. It is important, therefore, to examine and interpret existing stability data in terms of this expectation.

STABILITIES OF AMINE POLYCARBOXYLIC ACID CHELATES

The stability of a 1:1 chelate formed by reaction of an aquated rare earth metal ion (Ln^{3+}) with an amine polycarboxylate anion (Y^{n-}), according to the equation

$$Ln^{3+} + Y^{n-} \rightleftharpoons LnY^{3-n}$$

is given by the magnitude of the thermodynamic formation constant

$$K'_{\underset{LnY}{Ln}} = a_{LnY^{3-n}}/(a_{Ln^{3+}})\,(a_{Y^{n-}}) \tag{2}$$

In practice, values for concentration formation constants ($K_{\underset{LnY}{Ln}}$) have been reported, using determinations made at constant ionic strength. These

also measure stabilities, but are not of course subject to exact thermodynamic interpretation.

A number of such values, expressed in logarithmic form, are summarized in Table II. Comparisons among various chelating agents for indi-

TABLE II: FORMATION CONSTANTS OF AMINE POLYCARBOXYLIC ACID CHELATES AT μ-0.1*

	$\log K_{\frac{Ln}{LnY}}$							
Cation	IMDA (8) 25°C	NTA (9) 20°C	HEDTA (10, 22) 25°C	EDTA (11,12) 20°C	DCTA (12) 20°C	Chel-ME (13) 20°C	Chel-DE (13) 20°C	DTPA (8, 14) 25°C
La^{3+}	5.90	10.47	13.46	15.50	16.26	15.92	15.87	19.48
Ce^{3+}	...	10.70	14.11	15.98	16.76	16.76	16.09	20.5
Pr^{3+}	6.87	10.88	14.61	16.40	17.31	17.24	16.20	21.07
Nd^{3+}	6.94	11.06	14.86	16.61	17.68	17.44	16.62	21.60
Pm^{3+}	...	...	...	...	...	...	...	...
Sm^{3+}	7.10	11.33	15.28	17.14	18.38	17.88	17.28	22.34
Eu^{3+}	7.26	...	15.35	17.35	18.62	18.04	17.80	22.39
Gd^{3+}	7.02	11.43	15.22	17.37	18.77	17.84	17.53	22.46
Tb^{3+}	7.20	...	15.32	17.93	19.50	17.94	17.83	22.71
Dy^{3+}	7.32	11.62	15.30	18.30	19.69	17.92	17.87	22.82
Ho^{3+}	...	...	15.32	...	...	17.80	17.93	22.78
Er^{3+}	7.40	...	15.42	18.85	20.68	17.81	18.03	22.74
Tm^{3+}	7.50	...	15.59	19.32	20.96	17.64	17.99	22.72
Yb^{3+}	7.73	12.08	15.88	19.51	21.12	17.69	18.25	22.62
Lu^{3+}	...	...	15.88	19.83	21.51	17.55	18.51	22.44
Y^{3+}	7.11	11.55	14.65	18.09	19.15	17.42	17.19	22.05

*See notation at end of literature citations for explanation of abbreviations.

vidual cations reflect the effects upon stability of such properties of the ligand as structure, steric limitations, basicity, and number of possible rings. Of greater interest, however, are comparisons among the various rare earth metal ions and yttrium for a given chelating agent. Certain of these are presented somewhat more strikingly in Fig. 1.

In all instances, a generally regular increase in stability with increasing atomic number (or decreasing crystal radius) from La^{3+} through Eu^{3+} and a discontinuity at Gd^{3+} [the gadolinium break (9)] are noted. For the ions beyond Gd^{3+}, however, two distinct behaviors are apparent: (1) a "normal" further increase in stability with decreasing radius, with the yttrium chelate falling in the general region predicted by the size of the yttrium ion (e.g., for NTA, EDTA, and DCTA), and (2) an essential constancy or occasional maximum or minimum in stability, with the yttrium chelate falling in the cerium-earth region (e.g., for IMDA, HEDTA, Chel-ME, Chel-DE, and DTPA). Three distinct, but probably very closely related, problems are thus apparent, namely, the nature of the gadolinium

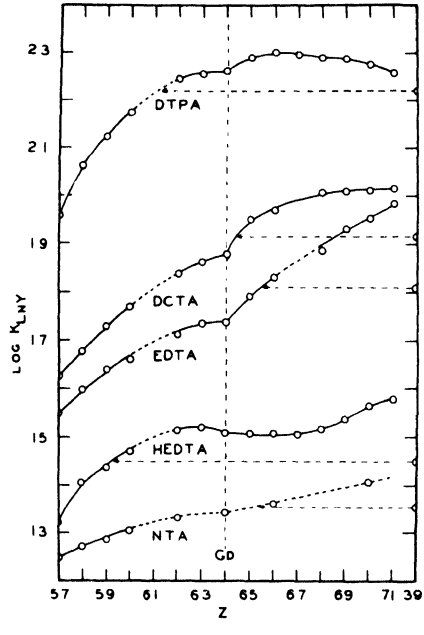


Fig. 1. Formation constants for rare earth chelates.

break, the variation of log $K_{\underset{LnY}{Ln}}$ with atomic number or crystal radius, and the position of yttrium.

INTERPRETATION OF OBSERVED VARIATIONS IN STABILITY

ELECTROSTATIC INTERPRETATION

If the bonding in these chelates is purely electrostatic, stability should be determined only by the radius of the cation present, and in terms of Eq. (1), log $K_{\underset{LnY}{Ln}}$ should then be expected to vary linearly with Z^2/r or more generally with $1/r$. Such linearity characterizes the La^{3+}-Eu^{3+} region for all the ligands under discussion, but approximations to continuing linearity for the heavier ions are noted only with EDTA, DCTA, and NTA. Indeed, any plot of this type differs only insignificantly in general appearance from the corresponding log $K_{\underset{LnY}{Ln}}$ *vs.* Z plot (Fig. 1).

It is apparent that, although the electrostatic bond picture is not unreasonable for the cerium earths, other factors must be involved in the yttrium-earth region. It can be argued that the gadolinium break is related to the discontinuity in crystal radius at gadolinium (Table I). How-

ever, this discontinuity is too minor to account for the substantial changes in formation constants at this point. It is perhaps significant to point out that this entire approach is predicated upon the assumption that trends in crystal radii are maintained in the radii of solvated and co-ordinated species. Although there is evidence for the lanthanide contraction in EDTA (15), HEDTA (7), and DCTA (7) chelates, it is probable that a smoothing out of size occurs and that differences in radii are correspondingly less pronounced than in binary ionic compounds. No explanation for the position of yttrium is apparent.

STERIC INTERPRETATIONS

It was suggested in the pioneer work on the stabilities of EDTA chelates (11) that, because of the bulkiness of the carboxyl groups, a critical point in crystal radius might be reached beyond which only three of the four carboxyl groups could fit about the central metal ion. The gadolinium break was thus associated with a change from sexidentate to quinquedentate behavior on the part of the ligand. A similar explanation can be offered for DCTA, but it cannot be applied to NTA since the three carboxyl groups can fit nicely about any cation in this series. (9)

A convincing argument for change in the polydentate character of EDTA has been offered by Betts and Dahlinger. (16) Using as normalizing values ΔH° for the formation of La(EDTA)$^-$ as measured calorimetrically and ΔF° for the formation of Nd(EDTA)$^-$ as obtained from the data of Wheelwright, Spedding, and Schwarzenbach (11), they obtained the ΔH°, ΔF°, and ΔS° values for formation of the chelates summarized in Table III from measured equilibrium constants for exchange reactions of the type

$$Ln(\text{EDTA})^- + L\acute{n}^{3+} \rightleftharpoons L\acute{n}(\text{EDTA})^- + Ln^{3+}$$

Although values for ΔF° and ΔS° are large, those for ΔH° are small and beyond europium of the wrong sign to promote complex-ion formation. The major contribution to stability is the entropy change. Of more interest, however, is the partial molal entropy of the chelate, $\bar{S}^\circ_{LnY^-}$. Although this could not be obtained directly, it could be approximated in terms of $\Delta S^\circ + \bar{S}^\circ_{Ln^{3+}}$, where $\bar{S}^\circ_{Ln^{3+}}$ can be calculated by two methods. (17, 18) Table III indicates constancy of $\bar{S}^\circ_{LnY^-}$, irrespective of method of calculation, in the La–Gd region and in the Tb–Lu region, with a difference between the two of *ca.* 6–10 e.u. Constancy within each region was interpreted as indicating constancy of structure in that region, and the difference between the two regions was then ascribed to alteration in the polydentate character of EDTA. Entropy data were correlated quite well with a change from quinquedentate to quadridentate character through opening of an *Ln–N* bond, choice of quadridentate behavior being dictated

TABLE III: THERMODYNAMIC FUNCTIONS FOR EDTA CHELATES ACCORDING TO BETTS AND DAHLINGER (16)

Cation	ΔF° kcal/mole	ΔH° kcal/mole	ΔS° e.u.	$\Delta S^\circ + \bar{S}^\circ_{Ln^{3+}}$, e.u.	
				Reference 17	Reference 18
La^{3+}	−20.72	−0.80*	66.8	32.1	27.6
Ce^{3+}	−21.07	−0.47	69.1	32.8	27.8
Pr^{3+}	−21.49	−0.80	69.4	31.9	26.4
Nd^{3+}	−21.89*	−0.80	70.7	32.2	26.2
Pm^{3+}	...	...	...	...	...
Sm^{3+}	−22.54	−0.80	72.9	32.6	25.8
Eu^{3+}	−22.72	−0.16	75.7	34.6	27.3
Gd^{3+}	−22.94	+0.43	78.4	36.6	28.9
Tb^{3+}	−23.62	+1.50	84.3	41.6	33.4
Dy^{3+}	−24.25	+1.50	86.3	42.7	34.0
Ho^{3+}	−24.61	+1.25	86.7	42.2	32.9
Er^{3+}	−25.06	+1.50	89.1	43.8	33.9
Tm^{3+}	−25.44	+1.58	90.6	44.5	34.1
Yb^{3+}	−25.91	+1.32	91.3	44.5	33.6
Lu^{3+}	−26.11	+0.64	89.7	42.2	30.9
$La^{3+} - Gd^{3+}$				33.3 ± 1.4	27.1 ± 0.9
$Tb^{3+} - Lu^{3+}$				43.1 ± 1.1	33.3 ± 0.7

* Normalizing values.

by the apparent presence of an uncomplexed carboxyl group in acids of the type H[*Ln*(EDTA)]. (19)

It must be emphasized that all of the ΔH° values employed are relative to the value for $La(EDTA)^-$. Calorimetric ΔH° values determined by Staveley (20) for a number of rare earth-EDTA chelates are some 2–3 kcal larger than the values obtained by Betts and Dahlinger. However, the trends are the same, and evaluations of $\Delta S^\circ + \bar{S}^\circ_{Ln^{3+}}$ from Staveley's data give the same two regions of constancy. (14)

However, the data summarized in Table IV indicate that in this form the thermodynamic approach provides no comparable explanation for trends in stability in either the DTPA (14, 21) or HEDTA (22) system. On the other hand, it must be emphasized that the 95 per cent confidence limits associated with evaluation of ΔH° and ΔS° from formation-constant data by the methods used are substantial, and that small differences which might be significant are thus blanketed out. Exact thermodynamic interpretations that can reflect steric effects must thus await more accurate evaluation of enthalpy changes.

LIGAND-FIELD INTERPRETATIONS

Staveley and Randall (23) have suggested that, since models reveal no likelihood of an abrupt change in polydentate character with the EDTA

TABLE IV: THERMODYNAMIC FUNCTIONS FOR FORMATION OF DTPA AND HEDTA CHELATES

Cation	DTPA (14)					HEDTA (22)		
	ΔF° kcal/mole	ΔH° kcal/mole	ΔS° e.u.	$\Delta S^\circ + \bar{S}^\circ_{Ln^{3+}}$, e.u. Ref. 17	Ref. 18	ΔH° kcal/mole	ΔS° e.u.	$\Delta S^\circ + \bar{S}^\circ_{Ln^{3+}}$ (17) e.u.
La^{3+}	−26.57	−5.7	70.0	35.3	30.8	−2.20	54.2	20
Ce^{3+}	...	...	...	...	...	−3.06	54.4	19
Pr^{3+}	−28.74	−7.1	72.0	34.5	29.0	−4.45	52.4	15
Nd^{3+}	−29.47	−5.8	79.4	40.9	34.9	−4.25	53.8	15
Pm^{3+}	...	...	...	...	...	...	...	...
Sm^{3+}	−30.48	−8.2	74.7	34.4	27.6	−4.65	54.4	15
Eu^{3+}	−30.55	−8.1	75.3	34.2	26.9	−4.81	53.8	14
Gd^{3+}	−30.65	−7.5	77.6	35.8	28.1	−4.66	54.1	12
Tb^{3+}	−30.99	−7.7	78.1	35.4	27.2	−3.39	58.8	16
Dy^{3+}	−31.14	−8.0	77.6	34.0	25.3	−2.12	63.4	19
Ho^{3+}	−31.08	−7.6	78.7	34.2	24.9	−1.14	66.3	21
Er^{3+}	−31.02	−7.3	79.6	34.3	24.4	−0.32	69.4	25
Tm^{3+}	−31.00	−5.5	85.5	39.4	29.0	+0.92	74.5	29
Yb^{3+}	−30.87	−5.5	85.1	38.3	27.4	+0.36	72.6	27
Lu^{3+}	−30.61	−4.6	87.2	40.7	28.4	+0.22	73.4	26
Y^{3+}	−30.08	−5.2	83.4	36.2	30.3	−0.29	66.1	19
Uncertainty	±(0.09–0.12)	±(1.3–2.3)	±(4.4–7.7)			±(0.3–0.6)	±(1.0–1.8)	±2

chelates, the trend in formation constants may be due to varying degrees of stabilization arising from interaction of 4*f* orbitals with the ligand field. As possible evidence, they cite the small changes in magnetic susceptibility of the neodymium ion noted upon co-ordination with EDTA (6). No ligand-field splitting can be expected for the gadolinium ion, but elsewhere it should be of the order of 100 cm^{-1}. Furthermore, they ascribe the observed reduction in stability on going from the yttrium chelate (no *f* orbitals) to the holmium chelate, where size is nearly identical but ΔH° differs by *ca.* 1 kcal, to ligand-field stabilization of the latter by *ca.* 1 kcal.

Acceptance or rejection of this argument must await the appearance of exact magnetic-susceptibility data, since, qualitatively, such data as have appeared (7) suggest little or no involvement of 4*f* electrons upon complex-ion formation. Detailed interpretation of absorption spectra should also be useful. That ligand fields are of importance has been questioned by Rossotti (24), who points out that both the yttrium- and gadolinium-EDTA chelates, where ligand-field stabilization is impossible, should have similar formation constants if this factor is determining. It is also reasonable to conclude that behaviors of the second broad class (above) would be difficult to reconcile on this basis alone.

Interaction of the ligand with 4*f* electrons should be at a maximum with strongly π-bonding ligands. It is reasonable that more light will be shed upon variations in stability as a result of magnetic and formation-constant studies on complexes formed by tailored ligands of this type (25).

CONCLUSION

It is apparent that complete solution of the problem outlined must await the acquisition of a sufficient body of accurate physical data to permit meaningful theoretical interpretation. The fallacy of extrapolating information for the lighter earths to yttrium and the heavier earths is obvious. Differences in behavior mentioned above confirm the often overlooked conclusions that can be drawn from much of the early and classic work on separations as to the really significant differences existent between the first and second halves of the series. In a way, it is unfortunate that the EDTA chelates were investigated first, for the regularities in their behavior suggested much too convincingly that all other chelates should behave similarly.

REFERENCES

1. T. Moeller and H. E. Kremers, *Chem. Revs.*, 37, 97 (1945).
2. T. Moeller and J. C. Brantley, *J. Am. Chem. Soc.*, 72, 5447 (1950).
3. T. Moeller and W. F. Ulrich, *J. Inorg. Nucl. Chem.*, 2, 164 (1956).

4. L. Holleck and D. Eckhardt, *Z. Naturforsch.*, 8a, 660 (1953); 9a, 347 (1954); 9b, 274 (1954).
5. R. C. Vickery, *J. Mol. Spectroscopy*, 2, 308 (1958).
6. L. Holleck and O. Liebold, *Naturwissenschaften*, 44, 582 (1957).
7. T. Moeller and E. P. Horwitz, *J. Inorg. Nucl. Chem.*, 12, 49 (1959).
8. R. Harder and S. Chaberek, *ibid.*, 11, 197 (1959).
9. G. Schwarzenbach and R. Gut, *Helv. Chim. Acta*, 39, 1589 (1956).
10. F. H. Spedding, J. E. Powell, and E. J. Wheelwright, *J. Am. Chem. Soc.*, 78, 34 (1956).
11. E. J. Wheelwright, F. H. Spedding, and G. Schwarzenbach, *ibid.*, 75, 4196 (1953).
12. G. Schwarzenbach, R. Gut, and G. Anderegg, *Helv. Chim. Acta*, 37, 937 (1954).
13. M. A. Hiller. Doctoral dissertation, Iowa State University (1959).
14. L. C. Thompson. Doctoral dissertation, University of Illinois (1960).
15. F. A. J. Moss. Doctoral dissertation, University of Illinois (1952).
16. R. H. Betts and O. F. Dahlinger, *Can. J. Chem.*, 37, 91 (1959).
17. R. E. Powell and W. M. Latimer, *J. Chem. Phys.*, 19, 1139 (1951).
18. K. J. Laidler, *Can. J. Chem.*, 34, 1107 (1956).
19. T. Moeller, F. A. J. Moss, and R. H. Marshall, *J. Am. Chem. Soc.*, 77, 3182 (1955).
20. L. A. K. Staveley. Private communication (1959).
21. T. Moeller and L. C. Thompson. Forthcoming publication.
22. T. Moeller and R. Ferrus. Forthcoming publication.
23. L. A. K. Staveley and T. Randall, *Discussions Faraday Soc.*, 26, 157 (1958).
24. F. J. C. Rossotti, *ibid.*, 26, 190 (1958).
25. W. C. Fernelius. Private communication (1959).

Abbreviations

IMDA—imidodiacetic acid
NTA—nitrilotriacetic acid
HEDTA—*N*-hydroxyethylethylenediaminetriacetic acid
EDTA—ethylenediaminetetraacetic acid
DCTA—1,2-diaminocyclohexanetetraacetic acid
Chel-ME—bis(2-aminoethyl) ether-*N*,*N*,*N*′,*N*′-tetraacetic acid
Chel-DE—ethyleneglycol-bis(2-aminoethyl) ether-*N*, *N*, *N*′, *N*′-tetraacetic acid
DTPA—diethylenetriaminepentaacetic acid

FORMATION CONSTANTS AND MAGNETIC BEHAVIOR OF SOME RARE EARTH CHELATES

INGMAR GRENTHE AND W. CONRAD FERNELIUS

Department of Chemistry, Lund University, Lund, Sweden; and Koppers Company, Inc., Pittsburgh, Pennsylvania

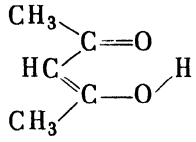
A complete investigation of the co-ordination behavior of the rare earth ions would yield much basic information which, in turn, would contribute a great deal to the understanding of this interesting group of elements. Moreover, such information would have many significant applications. For example, it is conceivable that still simpler and more economical methods for the separation of the individual rare earths in a state of high purity might result.

Among the methods for investigating the co-ordination behavior of various metal ions, the determination of formation constants and observations of magnetic behavior have proved to be particularly valuable. Both methods of attack have been used in the studies described here. There are several questions which might be answered by an investigation of the co-ordination behavior of the rare earths. Some of these are (1) what, if any, is the variation of maximum co-ordination number across the rare earth series; (2) can oxidation states other than 3+be stabilized by suitable ligands; and (3) are the 4*f* orbitals ever involved in the bonding of rare earth ions to ligands? A possible alternate way to put the last question might be; is there something analogous to π-bonding among the rare earth ions which would render complexes of some of the rare earths with favorable ligands particularly stable? Unfortunately, only a start has been made in finding answers to these questions.

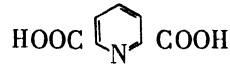
FORMATION CONSTANTS OF RARE EARTH ACETYLACETONATES AND DIPICOLINATES*

Most of the work on formation constants of complexes of the rare earths has been with ligands containing carboxyl groups as co-ordinating centers; e.g., acetic acid, glycolic acid, oxalic acid, and various aminopolyacids. In studying other types of ligands, acetylacetone (I) and dipicolinic acid (II)

*This work was supported by the Office of Naval Research through contract No. Nonr 65624 with Pennsylvania State University. Further details of the work are being published in the *Journal of the American Chemical Society*.



I



II

were chosen because both had been used previously for similar studies. (1, 2, 3) Furthermore, acetylacetone is interesting because it is not of the carboxylic acid type, and dipicolinic acid (1) because of the planar arrangement of the carboxyl groups, and (2) because of the presence of a doubly bonded (heterocyclic) nitrogen. Both of the ligands have the advantage over the aminopolyacids of possessing lower multiplicity, so that there is less likelihood of co-ordination sites not being attached to the central ion. Both ligands possess π-bonding possibilities.

EXPERIMENTAL

The measurements for the acetylacetone systems were obtained by the familiar potentiometric *p*H-titration method. Experimentally, values for the *p*H of cells of the following type were measured, using a Beckman model-G *p*H-meter

Calomel electrode	C_M m*M* rare earth 9.65 m*M* acetylacetone 3.40 m*M* perchloric acid v ml sodium hydroxide $\mu = 0.1$ *M*	Glass electrode

The general procedure in the titration was as follows: 100 ml of a solution with a metal-ion concentration, C_M, of about 2 m*M*, an acetylacetone concentration of 0.65 m*M*; a perchloric acid concentration of 3.40 m*M*, and sodium perchlorate in an amount sufficient to give an ionic strength of 0.1, was titrated with a standard sodium hydroxide solution. The *p*H of the solution was read after each addition of base. All titrations were repeated at least twice and the agreement between the *p*H-readings of the different titrations were usually within 0.02 *p*H-units. The solutions were stirred continuously by bubbling nitrogen through them. The temperature was kept constant at $30.0^\circ \pm 0.1^\circ$C.

In the study of the dipicolinate systems the *p*H-method could not be used because of the low basicity of the dipicolinate ion (dipic) and because of its very high affinity for the metal ions studied. The experimental method used is based on the competition between Cu(II) and another metal ion for the ligand. Using the known constants for the copper system, it is possible to calculate the unknown constants. [Leden (5)]

Experimentally, the emf of cells of the following type was measured:

	C_{M_I} m*M* Cu^{II}		
	$C_{M_{II}}$ m*M* rare earth	10 m*M* $HClO_4$	
Cu-Hg	C_L m*M* ligand	490 m*M* $NaClO_4$	Au
	C_H m*M* $HClO_4$	Quinhydrone	
	μ = 0.5 M		

The main measurements were carried out as titrations in the following way: A solution *S*, of known C_{M_I}, $C_{M_{II}}$, $C_H \approx 1$ m*M*, and with $C_L = 0$, was prepared in the amalgam half-cell. To this solution successive amounts of the titrant *T* were added. The titrant had the composition

$$\left\{\begin{matrix} C_L \text{ m}M \text{ } Na_2 \text{ dipic} \\ \mu = 0.5 \text{ } M \end{matrix}\right\}.$$

The titrations were made at different C_{M_I} and $C_{M_{II}}$ to show that no polynuclear species formed. A ligand titration showed that no acid complexes were formed at the pH-region where the titrations were made.

No complications arose from hydrolysis of the central ion. It is easily seen from the magnitude of the formation constants and the pH of the solutions that the hydrolysis is completely negligible for both the systems investigated. The values of the formation constants found for the two ligands are assembled in Tables I and II. They were computed by means of simultaneous equations, as described by Block and McIntyre. (6)

TABLE I: LOG K_n VALUES FOR THE REACTION OF TERVALENT RARE EARTH IONS WITH ACETYLACETONE (pK = 8.88 ± 0.02) AT $T = 30^\circ$C AND IONIC STRENGTH μ = 0.1 *M* AND 0 *M*

Metal Ion	μ = 0.1 *M*			μ = 0.0 *M*		
	log K_1	log K_2	log K_3	log K_1	log K_2	log K_3
La^{3+}	4.96 ± 0.03	3.45 ± 0.05	2.5 ± 0.1	5.1	3.8	3.0
Ce^{3+}	5.09 ± 0.04	3.3 ± 0.1	2.9 ± 0.1	5.3	4.0	
Pr^{3+}	5.27 ± 0.03	3.93 ± 0.05	3.2 ± 0.05	5.4	4.1	3.0
Nd^{3+}	5.30 ± 0.04	4.10 ± 0.03	3.20 ± 0.05	5.6	4.3	3.2
Sm^{3+}	5.59 ± 0.02	4.46 ± 0.01	2.90 ± 0.01	5.9	4.5	3.2
Eu^{3+}	5.87 ± 0.03	4.48 ± 0.03	3.29 ± 0.02	6.0	4.5	3.5
Gd^{3+}	5.90 ± 0.03	4.48 ± 0.05	3.41 ± 0.01			
Tb^{3+}	6.02 ± 0.01	4.61 ± 0.04	3.41 ± 0.01			
Dy^{3+}	6.03 ± 0.01	4.67 ± 0.02	3.34 ± 0.04			
Ho^{3+}	6.05 ± 0.01	4.68 ± 0.01	3.40 ± 0.10			
Er^{3+}	5.99 ± 0.01	4.68 ± 0.03	3.38 ± 0.01			
Tm^{3+}	6.09 ± 0.01	4.76 ± 0.02	3.48 ± 0.02			
Yb^{3+}	6.18 ± 0.01	4.86 ± 0.02	3.60 ± 0.02			
Lu^{3+}	6.23 ± 0.04	4.77 ± 0.07	3.63 ± 0.07			
Y^{3+}	5.87 ± 0.02	4.98 ± 0.06	3.25 ± 0.02			

TABLE II: LOG K_n VALUES (AND LOG β_3) FOR THE REACTION OF TERVALENT RARE EARTH IONS WITH THE DIPICOLINATE ION AT $T = 30\,^{\circ}C$ AND IONIC STRENGTH $\mu = 0.5\ M$

Metal Ion	log K_1	log K_2	log K_3	log β_3
Cu^{2+}	9.14 ± 0.01	7.37 ± 0.02		
La^{3+}	7.98 ± 0.01	5.81 ± 0.04	4.27 ± 0.02	18.06
Ce^{3+}	8.34 ± 0.02	6.08 ± 0.03	4.38 ± 0.02	18.80
Pr^{3+}	8.63 ± 0.02	6.47 ± 0.01	4.48 ± 0.02	19.94
Nd^{3+}	8.78 ± 0.02	6.72 ± 0.02	5.06 ± 0.03	20.56
Sm^{3+}	8.86 ± 0.03	7.02 ± 0.01	5.35 ± 0.01	21.23
Eu^{3+}	8.84 ± 0.01	7.14 ± 0.02	5.51 ± 0.02	21.49
Gd^{3+}	8.74 ± 0.01	7.32 ± 0.03	5.77 ± 0.03	21.83
Tb^{3+}	8.68 ± 0.03	7.43 ± 0.04	5.92 ± 0.03	22.03
Dy^{3+}	8.69 ± 0.02	7.49 ± 0.02	5.95 ± 0.01	22.13
Ho^{3+}	8.72 ± 0.02	7.51 ± 0.01	5.85 ± 0.01	22.08
Er^{3+}	8.77 ± 0.01	7.62 ± 0.04	5.74 ± 0.01	22.13
Tm^{3+}	8.83 ± 0.03	7.71 ± 0.02	5.50 ± 0.02	22.04
Yb^{3+}	8.85 ± 0.04	7.76 ± 0.03	5.12 ± 0.01	21.73
Lu^{3+}	9.03 ± 0.06	7.77 ± 0.06	4.68 ± 0.02	21.48
Y^{3+}	8.46 ± 0.01	7.27 ± 0.02	5.61 ± 0.02	21.34

DISCUSSION

The tervalent rare earth ions, all having the same configuration $5s^2 5p^6$ of the outer electron shells, form a unique series for a study of the influence of the size of the central ion on the properties of the co-ordination compounds. If the metal-ligand bond is considered to be purely electrostatic in nature, the strength of the bond should increase linearly with increasing ionic potential Z^2/r, where Z is the charge and r is the radius of the ion. A measure of this bond strength is ΔH for the reaction:

$$\mathrm{Me} + \mathrm{A} \rightleftharpoons \mathrm{Me\ A} \qquad (1)$$

Because of the experimental difficulties in the determination of ΔH, ΔF for the same reaction is often used as an alternative. $\Delta F = -RT \ln K$, where K is the equilibrium constant for the reaction. (1) This is a reasonable approximation if the entropy change of reaction (1) is small, or if it is constant through the entire rare earth series.

In Fig. 1, the logarithms for the first formation constants, log K_1, between the rare earths and acetylacetone have been plotted as a function of the ionic potential. Instead of the expected linearly increasing course, a curve is obtained where only the first part, lanthanum to europium, increases linearly, while the second part, gadolinium to lutetium, is nearly constant. The difference in log K_1 between consecutive elements in the first part is about 0.15, and the total variation from Tb to Lu is only 0.2. There is evidently a sharp decrease in stability for the

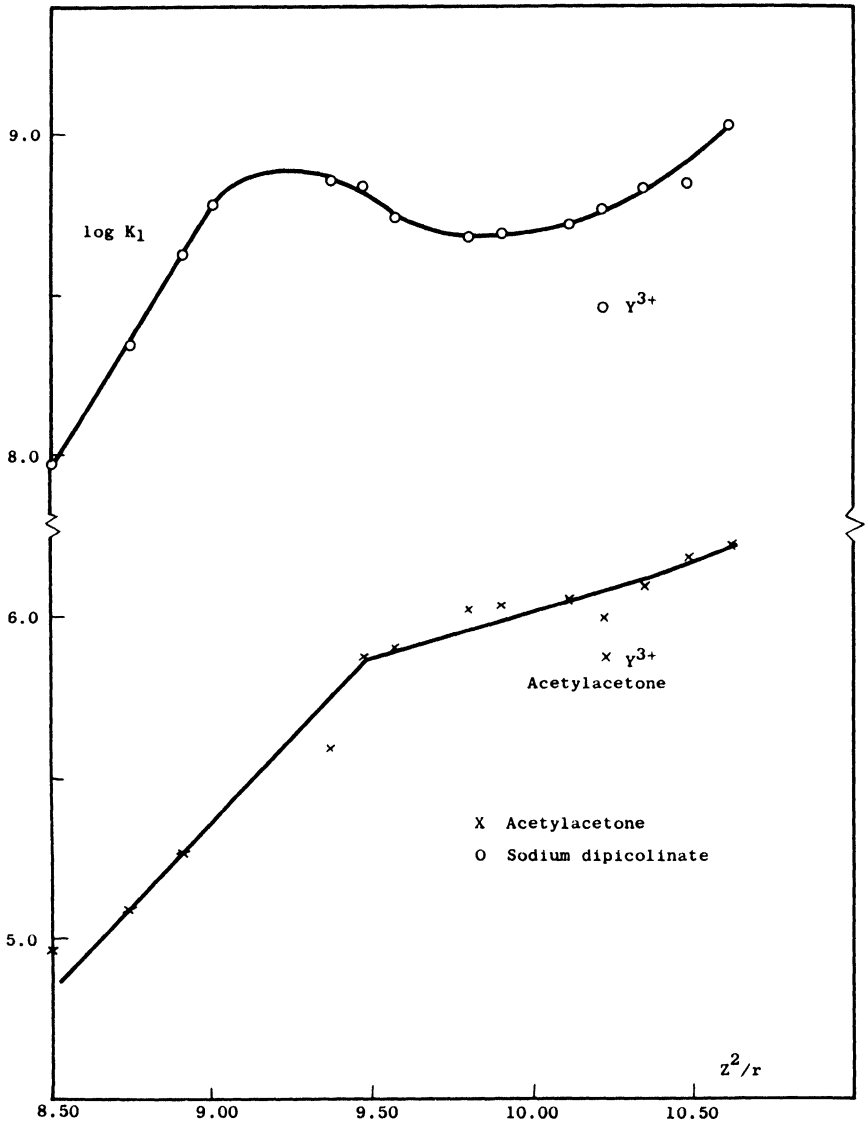


Fig. 1. Log K_1 as a function of ionic potential, Z^2/r, for various rare earth complexes.

Gd–Lu group as compared with the La–Eu group—a behavior which cannot be explained by the electrostatic bond theory.

For the dipicolinate complexes, the logarithm of the first constant, log K_1, shows the same deviations from the expected increase in stability with increasing atomic number. The logarithm of the second con-

stant increases through the entire series, though the mean differences in log K_2 between consecutive elements are smaller for the elements after gadolinium. The logarithm of the third constant increases to terbium, is constant for terbium and dysprosium, and then decreases. The total effect of this behavior is a maximum for the total complexity in the same region, as is seen from the log β_3 values in the last column of Table II.

This departure from linearity is not peculiar for the acetylacetonates and dipicolinates; on the contrary, it seems to be common for most of the rare earth complexes. Complexes of different substituted ethylenediamine acetic acids have been thoroughly investigated. (7–12) Log K *vs.* ionic-potential data for these compounds obtained from the literature have been plotted in Fig. 2 and 3. From the figures, it can be seen that all the ligands investigated, except ethylenediamine tetraacetic acid (EDTA) and cyclohexanediaminetetraacetic acid (DCTA), show deviation from the expected linear relation. In all cases the first part, La–Eu, shows a fairly good linearity. Because of the many possible co-ordination sites in these types of ligands, there is a possibility of a change in the number of points of attachment before and after gadolinium. This will result in a change both in ΔH and ΔS, and the approximation $\Delta H \approx \Delta F$ is thus no longer valid. That such a configuration change really can occur has been shown by infrared studies of Moeller *et al.* (13) and by the thermodynamic work by Betts and Dahlinger. (14) In both cases complexes with EDTA were studied, and the exceptional stability of the later rare earths was found to be due to an entropy contribution to ΔF. Formation constants are also available for the rare earth acetates, glycolates, and oxalates. A steric effect for the addition of the first ligand is very improbable both for these ligands and for acetylacetone, the entropy contribution is expected to be constant, and ΔF should thus be a good approximation of the relative bond strength.

Sonesson's data (15) for acetates and glycolates are reproduced in Fig. 3. Crouthamel and Martin (16) found log K_1 for Ce, Nd, and Yb to be 6.52, 7.21 and 7.30; that is, Yb is much less stable than expected.

The inadequacy of the electrostatic description is also seen if we look at the position of yttrium in the above diagrams. Yttrium with an ionic radius between Ho and Er should have a formation constant between log K_1 for these two ions. However, it is seen from the figures that yttrium actually falls in the Nd–Sm–Eu region for complexes of acetylacetone, bis(2-aminoethyl)ether tetraacetic acid, ethyleneglycolbis-(aminoethylether)tetraacetic acid, *N*-hydroxyethylethylenediamine triacetic acid, and cylohexanediamine tetraacetic acid.

The decrease in log K_3 for the dipicolinates probably arises because the progressively smaller radii of the rare earths impose increasing steric hindrance by the interaction between the ions and the ligands. This ef-

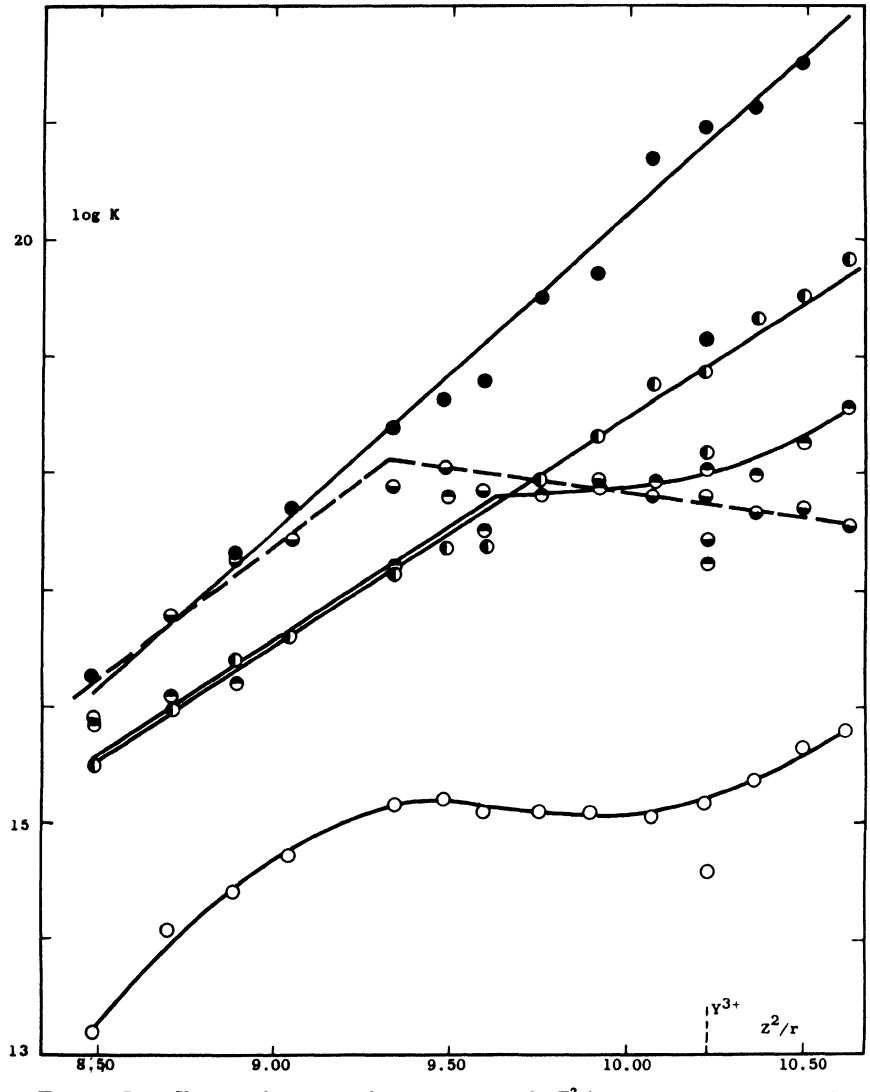


Fig. 2. Log K_1 as a function of ionic potential, Z^2/r, for various rare earth complexes: ○, *N*-hydroxyethylethylenediaminetetraacetic acid; ◓, ethyleneglycolbis (aminoethylether) tetraacetic acid; ◒, bis (2-aminoethyl) ether tetraacetic acid; ◐, EDTA; ●, DCTA.

fect should be most pronounced on the addition of the third ligand, because of the presence of two bulky groups. Steric effects have been noted before. (11, 17) As has been pointed out by Betts and Dahlinger (14) a steric effect probably causes a change in the number of co-or-

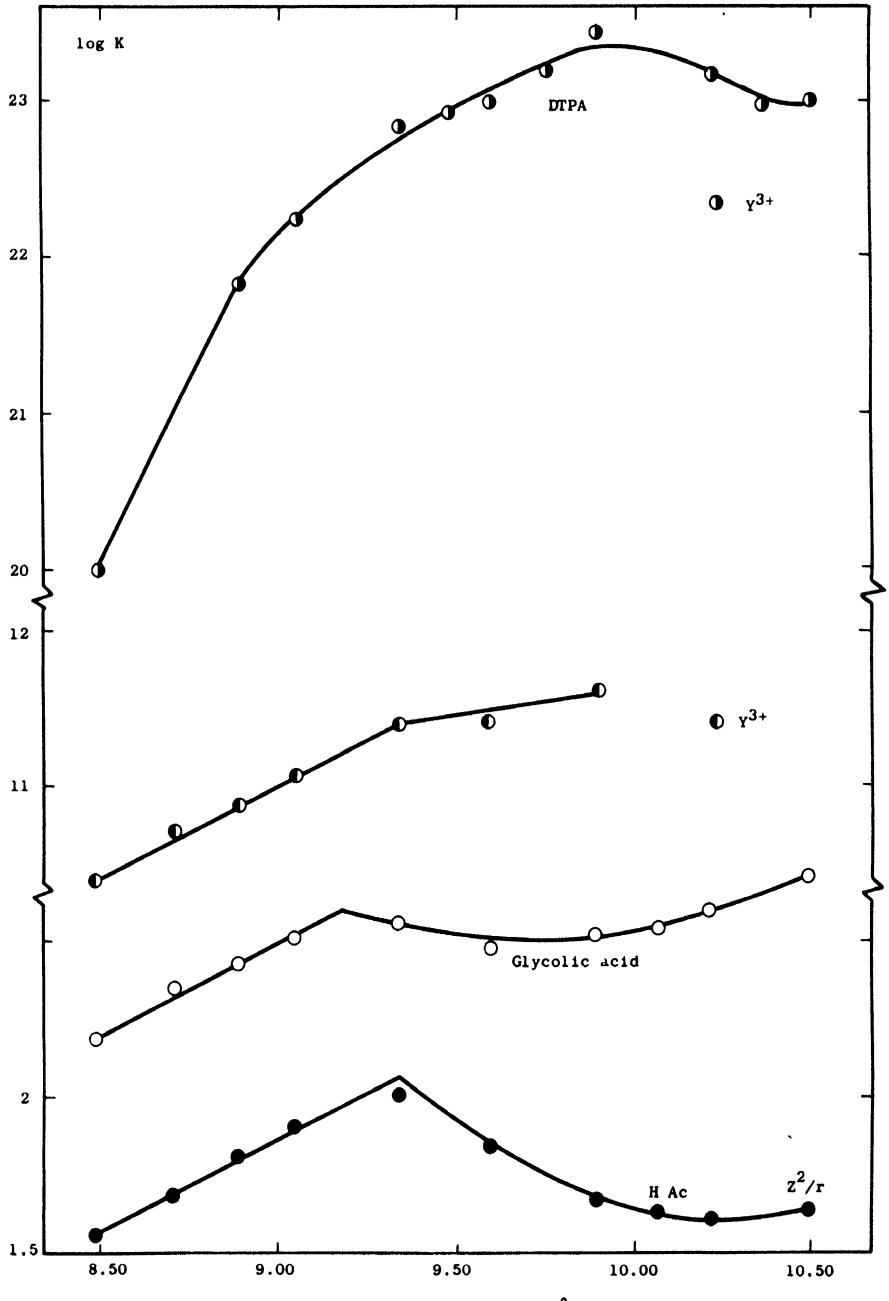


Fig. 3. Log K_1 as a function of ionic potential, Z^2/r, for rare earth complexes: ●, acetic acid; ○, glycolic acid; ◐, nitrilotriacetic acid; ◑, diethylenetriaminepentaccetic acid.

dinated carboxyl groups in the EDTA complexes of the rare earths—one carboxyl group less is coordinated after gadolinium.

If the irregularities in log K_1 were caused by a steric factor, this would be present and even more pronounced on the addition of the second ligand, thus causing variations in log K_2 similar to, but stronger than, the variations in log K_1. As is seen from Table II, this is not the case —a confirmation of views given above. The presence of several possible co-ordinating sites on a ligand leads to the question of what groups actually are involved in the chelation. Most authors are of the opinion that the amine nitrogen in the amino polyacids is involved, thus giving a maximum co-ordination number of 8 for the nitrilotriacetate complexes investigated by Anderegg. (17) For the ions of the very strong electropositive rare earth elements, it is expected that the relative affinities of ligand atoms should be in the order $F > O > N$. (18) Furthermore, the rare earths form very weak complexes with amines, even with such a strong complexing agent as triaminotriethylamine. In the light of these facts, it is perhaps more reasonable to assume that the co-ordination only occurs through the carboxyl groups. This is very likely also the case for the pyridine nitrogen. The maximum co-ordination number for all the rare earths is thus 6 in both the systems investigated here. Anderegg found in his work on the dipicolinate complexes of other metal ions (3) that only two ligands were attached to the central atom. Because at least a few of the metal ions are expected to give octahedral complexes, this shows that the pyridine nitrogen is involved here. Another interesting fact about the dipicolinate complexes is that the difference between the two consecutive constants log K_1-log K_2 is very near to that between log K_2-log K_3, indicating an unusually high affinity for the attachment of the third ligand.

MAGNETIC PROPERTIES OF RARE EARTH ACETYLACETONATES AND ETHYLENEDIAMINETETRAACETATES (WITH JAMES J. FRITZ AND PAUL E. FIELD)*

In the discussion above, no mention was made of the possible participation of electrons in the bonding of ligands to the rare earth ions. In fact, the trend of the results is the reverse of what would be expected of a stabilization due to π-bonding. Nevertheless, it seemed desirable to determine if the magnetic properties of a rare earth ion were influenced by the character of the co-ordinated ligands.

---

*This work was supported by the Office of Naval Research through contract No. Nonr 65624 with, and by, the National Research Foundation, through grant No. 9928 to Pennsylvania State University. A preliminary account of the work is being published in the *Journal of the American Chemical Society*.

EXPERIMENTAL

The magnetic susceptibilities of the acetylacetonates of Pr, Nd, Gd, Tb, Dy, Ho, Er, Tm, and Yb, all of the same general formula $M(acac)_3 \cdot H_2O$ [prepared according to Stites *et al.* (19)], and ethylenediaminetetraacetates of Pr, Nd and Gd of the formula $Na\,[M(EDTA)] \cdot 8\,H_2O$ [obtained from Professor T. Moeller; for preparation see Moeller *et al.* (20)] were measured between 1.3 and 77.2 °K using the same general method as described by Fritz *et al.* (21)

The purity of the specimens was 99.9 per cent or better (with respect to the content of the rare earth), with the exception of the neodymium chelates, which contained 1 per cent impurity (Pr and Sm, both weaker magnetically than the Nd). Carbon-hydrogen analyses showed in all cases excellent agreement with values calculated for the compositions listed. Measurements were made at four temperatures in the liquid helium range (1 to 4 °K), four in the hydrogen range (10 to 20 °K) and two in the liquid nitrogen range (65 to 77 °K). $CuSO_4 \cdot 5\,H_2O$ was used for calibration. (21) In all cases, measurements were made at 400 and 1,000 cycles. Agreement of the "dynamic" susceptibilities obtained at these two frequencies was taken to indicate absence of relaxation effects, and the static susceptibility was then taken as the average of the two results. In the case of $Dy(acac)_3 \cdot H_2O$ alone, relaxation was observed at and below 4.2 °K; for this specimen, measurements were made also at 100, 200, and 2,000 cycles. Even for the lowest susceptibilities obtained, the correction for diamagnetism was estimated to be within the uncertainty of measurement and was not applied. Representative results are shown in Fig. 4 and 5.

DISCUSSION

From 1 to 20 °K the data could be fitted by empirical equations of the form of the Curie-Weiss law within about 3 per cent (the precision of the data was about 1 per cent). The constants of these equations are given in Table III, along with the theoretical Curie constants of Van Vleck and Fowler. (22) The large deviations of the empirical "Curie" constants from the high temperature theoretical values indicate mainly that at these low temperatures only some of the low-lying multiplets are populated. Some interesting facts become apparent when the results in Table III are compared with one another and with earlier measurements on octahydrated sulfates of Pr and Nd (23), Gd (24), Dy, Er and Yb (25, 26).

For praesodymium and neodymium, the temperature dependence of susceptibility is complicated, but in both cases the acetylacetone chelate has a distinctly larger susceptibility than the EDTA complex, and this in

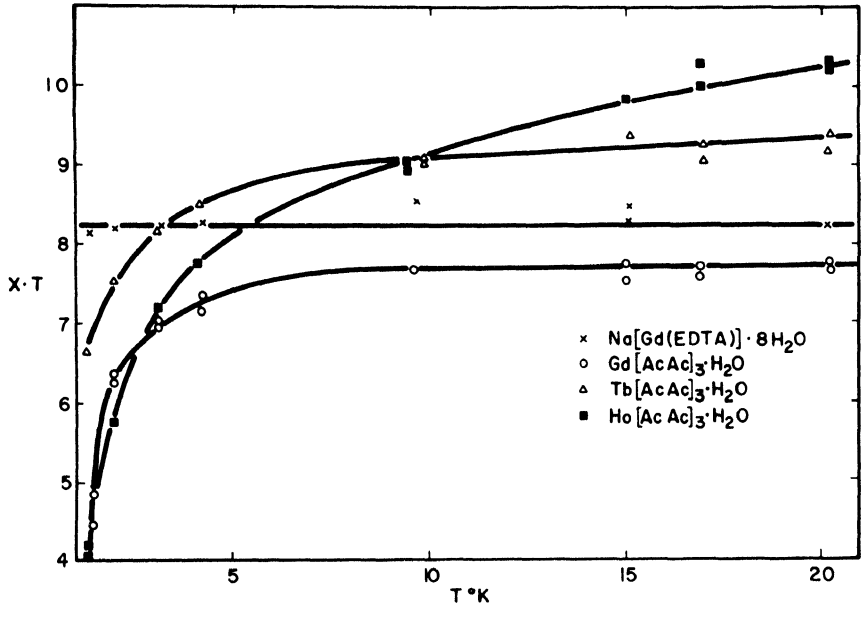


Fig. 4. Magnetic susceptibilities of rare earth complexes.

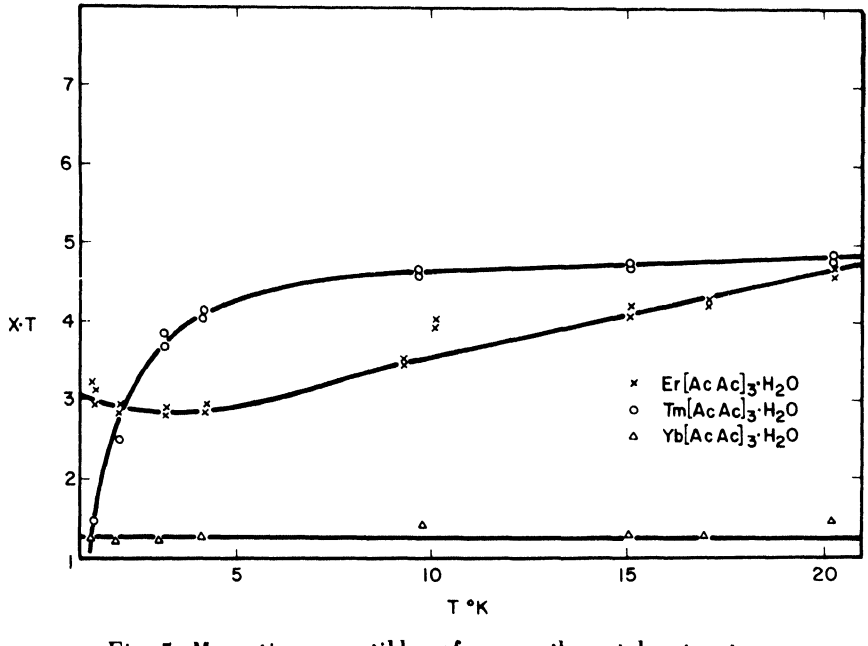


Fig. 5. Magnetic susceptibles of rare earth acetylacetonates.

TABLE III

Range °K	Compound	C (Expt'l)	Δ °K	C (Van Vleck)
20°–1°	$Pr(acac)_3 \cdot H_2O$	1.25	11.3	1.64
	$Nd(acac)_3 \cdot H_2O$	1.04	1.1	1.69
	$Gd(acac)_3 \cdot H_2O$	8.0	0.56	7.87
	$Tb(acac)_3 \cdot H_2O$	9.6	0.67	11.81
	$Dy(acac)_3 \cdot H_2O$*	15.4	1.54	14.0
	$Ho(acac)_3 \cdot H_2O$	10.4	1.67	14.0
20°–4°	$Er(acac)_3 \cdot H_2O$	8.3	1.7	11.5
4°–1°		5.9	0.0	
20°–3°	$Tm(acac)_3 \cdot H_2O$	6.6	0.0	7.2
3°–1°		11.9	3.3	
20°–1°	$Yb(acac)_3 \cdot H_2O$	1.3	0.0	2.53
	$Na[Pr(EDTA)] \cdot 8H_2O$	2.4	0.58	1.64
	$Na[Nd(EDTA)] \cdot 8H_2O$	0.73	0.29	1.69
	$Na[Gd(EDTA)] \cdot 8H_2O$	8.3	0.0	7.87

*Below 10°K, the data are for the static (zero-frequency) susceptibility calculated from the Debye model.

turn larger than the sulfate. For gadolinium, the acetylacetonate, the EDTA complex, and the sulfate are all relatively ideal. For erbium—the only member of the series beyond gadolinium for which detailed information about the sulfate is available—the situation is reversed, with the sulfate showing a larger susceptibility than the acetylacetonate. Dysprosium acetylacetonate, with the observed relaxation effects, is obviously a special case; the data available for ytterbium sulfate do not permit detailed comparison with the chelate. It is clear, however, that in all cases the magnetic behavior of the acetylacetone complex is definitely different from that of an ordinary hydrated salt.

The relaxation phenomena observed for $Dy(acac)_3 \cdot H_2O$ in the helium range could be fitted by a simple Debye model (27) at the low-frequency end (400 cycles and below). The relaxation time obtained from this model was about 10^{-3} sec, and decreased with increasing temperature.

GENERAL REMARKS

The need for further work on both the formation constants and magnetic behavior of the rare earths is very evident. Only occasionally are the formation constants of a given ligand a linear function of atomic number (ionic radius or ionic potential). The differences between the constants for successive rare earths are less for the yttrium earths than for the cerium earths. While there seems to be no reason to feel that the maximum co-ordination number changes across the rare earth series, it would be interesting to check this matter more carefully. A series of ligands whose individual members are very closely related chemically, but differ

in the number of points of attachment (5–8) to the co-ordinated ion, might be studied. While certain halogen ions (ligands) appear to stabilize higher oxidation states, especially Ce (IV), most of the results do not apply to aqueous solutions nor to extractable combinations. The stabilization of lower oxidation states by ligands is an untouched field. While the present results do not indicate any $p_\pi - f_\pi$ types of bonding, there are no data bearing on $d_\pi - f_\pi$ bonding, except an isolated observation that the rare earth complexes of $S(CH_2COO)_2$ appear to be more stable than those of $O(CH_2COO)_2$. It is highly desirable that the structures of a few representative co-ordination compounds of the rare earths be determined.

While it is very desirable to have additional data on the magnetic properties of rare earth complexes, there is also the formidable task of subjecting the present data to detailed theoretical treatment. In view of the complicated multiplet structure of the low-lying spectroscopic states of the rare earth ions, considerable work will be required for a full explanation of the observed magnetic behavior.

REFERENCES

1. R. M. Izatt *et al.*, *J. Phys. Chem.*, 59, 170 (1955); cf. L. G. Van Uitert *et al.*, *J. Am. Chem. Soc.*, 75, 451, 455, 457, 2736, 2739, 3577, 3862 (1953); 76, 5887 (1954); B. B. Martin and W. C. Fernelius, *ibid.*, 81, 2342 (1959); H. Kido and W. C. Fernelius, NYO-8774 (June, 1960).
2. R. M. Tichane and W. E. Bennet, *J. Am. Chem. Soc.*, 79, 1293 (1957).
3. G. Anderegg, *Helv. Chim. Acta*, 43, 414 (1960).
4. J. Bjerrum, *Metal Ammine Formation in Aqueous Solution.* Copenhagen: P. Haase and Son, 1941.
5. I. Leden, *Acta Chem. Scanda.*, 6, 971 (1952); cf. S. Ahrland, J. Chatt, W. R. Davies, and A. A. Williams, *J. Chem. Soc.*, 276 (1958).
6. B. P. Block and G. H. McIntyre, Jr., *J. Am. Chem. Soc.*, 75, 5667 (1953).
7. E. J. Wheelwright, F. H. Spedding, and G. Schwarzenbach, *ibid.*, 75, 4196 (1953).
8. G. Schwarzenbach, R. Gut, and G. Anderegg, *Helv. Chim. Acta*, 32, 937 (1954).
9. G. Schwarzenbach and R. Gut, *ibid.*, 39, 1589 (1956).
10. F. H. Spedding, J. E. Powell, and E. J. Wheelwright, *J. Am. Chem. Soc.*, 78, 34 (1956).
11. R. Harder and S. Chaberek, *J. Inorg. Nucl. Chem.*, 11, 197 (1959).
12. T. Moeller. Private communication.
13. T. Moeller, F. A. J. Moss, and R. H. Marshall, *J. Am. Chem. Soc.*, 77, 3182 (1955).
14. R. H. Betts and O. F. Dahlinger, *Can. J. Sci.*, 37, 91 (1959).

15. A. Sonesson, *Acta Chem. Scand.*, 12, 165, 1937 (1958); 13, 998, 1437 (1959).
16. C. E. Crouthamel and D. S. Martin, *J. Am. Chem. Soc.*, 73, 569 (1951).
17. G. Anderegg, *Helv. Chim. Acta*, 43, 825 (1960).
18. S. Ahrland, J. Chatt, and N. R. Davies, *Quart. Revs.*, 12, 265 (1958).
19. J. G. Stites, C. N. McCarthy, and L. L. Quill, *J. Am. Chem. Soc.*, 70, 3172 (1948).
20. T. Moeller, F. A. J. Moss, and R. H. Marshall, *ibid.*, 77, 3182 (1955).
21. J. J. Fritz, R. V. G. Rao, and S. Seki, *J. Phys. Chem.*, 62, 703 (1958).
22. J. H. Van Vleck, *The Theory of Electric and Magnetic Susceptibilities*. New York: Oxford University Press, Inc., 1932, p. 243.
23. C. J. Gorter and W. J. DeHaas, *Comm. Phys. Lab. University of Leyden*, No. 218b.
24. H. Van Dijk, *ibid.*, No. 267a.
25. W. J. DeHaas, E. C. Wiersma, and W. H. Capel, *ibid.*, No. 201b.
26. L. C. Jackson, *Proc. Roy. Soc.* (London), 48, 741 (1939).
27. C. G. Gorter, *Paramagnetic Relaxation*. Princeton: Elsevier Publishing Company, Inc., 1947.

SOME OBSERVATIONS REGARDING RARE EARTH GLYCOLATES*

J. E. POWELL AND J. L. FARRELL

Institute for Atomic Research and Department of Chemistry
Iowa State University, Ames, Iowa

A number of years ago Jantsch and Grünkraut (1) prepared a few rare earth glycolates and determined their solubilities. They found that lanthanum, cerium, praseodymium, neodymium, and samarium glycolates separated in anhydrous form, but that gadolinium and yttrium glycolates separated as dihydrates. The solubilities observed for lanthanum, cerium, praseodymium and neodymium glycolates were quite similar, but the solubility increased considerably in the case of samarium glycolate and even more in the case of gadolinium glycolate dihydrate. Dihydrated yttrium glycolate was less soluble than the anhydrous light rare earth glycolates.

In recent years, ammonium glycolate has been used as an eluant in the ion-exchange separation of rare earths (2–4). Because of this, it is desirable to obtain further information concerning glycolates of the rare earths. Sonesson (5) has measured the complexity constants of the various species, $Rgly_n^{3-n}$, where R denotes a rare earth, *gly* denotes the glycolate radical, and n is an integer from 1 to 4. The measurements were performed at an ionic strength of $2M$ at 20° C and included all the lanthanons except promethium, europium, terbium, thulium, and lutetium. Yttrium was not included in his investigations. A break was noted in the data at gadolinium. This, of course, coincides with the transition from anhydrous to dihydrated glycolates, in agreement with the data of Jantsch and Grünkraut.

EXPERIMENTAL

The glycolates of all the naturally occurring rare earths, including yttrium, were prepared by combining individual, neutral, rare earth chlorides with a slight excess of ammonium glycolate in aqueous solution. At room temperature, anhydrous glycolates were obtained for the light rare

*Contribution No. 925. Work was performed in the Ames Laboratory of the U.S. Atomic Energy Commission.

earths, lanthanum-europium. The heavy rare earths and yttrium separated as dihydrated glycolates. The formation of light rare earth glycolates was delayed at 25° C, but at higher temperatures they separated in less time. Anhydrous gadolinium glycolate, rather than the dihydrate, was obtained at temperatures above 60° C.

The solubilities of the rare earth glycolates at 20 and 60° C are given in Table I.

TABLE I: SOLUBILITIES OF THE RARE EARTH GLYCOLATES

Compound	Solubility (g cmpd/100 g H_2O)	
	20° C	60° C
La gly_3	0.378	0.462
Ce gly_3	0.381	0.495
Pr gly_3	0.421	0.465
Nd gly_3	0.447	0.449
Sm gly_3	0.823	0.667
Eu gly_3	0.841	0.811
Gd gly_3	1.098	0.997
Gd $gly_3 \cdot 2 H_2O$	1.021	...
Tb $gly_3 \cdot 2 H_2O$	0.552	1.135
Dy $gly_3 \cdot 2 H_2O$	0.323	0.695
Ho $gly_3 \cdot 2 H_2O$	0.230	0.518
Er $gly_3 \cdot 2 H_2O$	0.171	0.375
Tm $gly_3 \cdot 2 H_2O$	0.140	0.322
Yb $gly_3 \cdot 2 H_2O$	0.111	0.234
Lu $gly_3 \cdot 2 H_2O$	0.093	0.225
Y $gly_3 \cdot 2 H_2O$	0.220	0.462

The dihydrated glycolates form a regular series in which the solubility decreases from gadolinium to lutetium (Fig. 1). The compounds in this series are considerably more soluble hot than cold. Yttrium glycolate dihydrate has a molal solubility which places yttrium between dysprosium and holmium, in agreement with atomic radii.

The picture is not nearly so simple in the case of the anhydrous light rare earth glycolates. Except for cerium glycolate, the first four compounds show a gradual rise in the 20 degree solubility and a decline in the 60 degree solubility; these trends terminate at neodymium glycolate, whose solubility is almost the same at 60 as at 20° C. Europium glycolate resembles neodymium glycolate in that its solubility does not change markedly between 20 and 60° C. Samarium and gadolinium glycolates, on the other hand, are notably less soluble hot than cold. It is possible that these anomalies can be explained by differences in crystal structure, but no work has been done to confirm such a hypothesis.

The differences in composition, solubility, rate of formation, and stability of the glycolates of the rare earth series suggested that it should

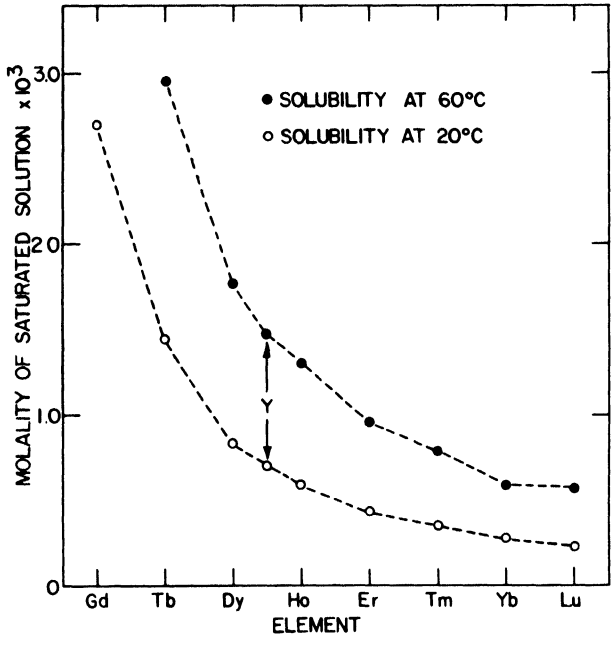


Fig. 1. Solubilities of rare earth glycolates in water at 20 and 60° C. The solid in equilibrium is $Rgly_3 \cdot 2\,H_2O$ in each case.

be feasible to separate members of the cerium-group lanthanons from members of the yttrium-group lanthanons by precipitation with ammonium glycolate. Consequently, some fractional precipitations were carried out.

EXPERIMENT A

Five g each of Pr_6O_{11} and Er_2O_3 were dissolved in a minimum of hydrochloric acid. The nearly neutral solution was diluted to 400 ml and treated with sufficient ammonium glycolate in 150 ml of water to form the triglycolates of both the praseodymium and the erbium. The solution was stirred at 20° C for three hours, and then the precipitate was filtered off, washed with water, and dried. The pink-colored residue comprised 10.444 g of a theoretical 21.976 g. It assayed roughly 95 per cent erbium glycolate and 5 per cent praseodymium glycolate.

EXPERIMENT B

Five g of Sm_2O_3 and 5 g of Dy_2O_3 were dissolved in a minimum of hydrochloric acid and heated with seven-sixths the stoichiometric amount of ammonium glycolate in a total volume of 500 ml. After stirring seven hours at 25° C, the resulting precipitate was filtered off, washed, and

ignited to the oxide. The rare earths in the filtrate and washings were recovered by addition of oxalic acid and converted to the oxide also. The pertinent data are given in Table II.

TABLE II: ANALYSIS OF THE FRACTIONS FROM B

	g oxide	% Sm_2O_3	% Dy_2O_3
Glycolate precipitate	5.1421	16	84
Filtrate	4.9255	85	15

The single-stage separation factor (ratio of dysprosium to samarium in the precipitate/ratio of dysprosium to samarium in filtrate) for this operation was about 30.

EXPERIMENT C

In order to test the process further, 8.5 g of Dy_2O_3 and 1.5 g of Sm_2O_3 were dissolved in a minimum of hydrochloric acid and treated with seven-sixths the stoichiometric amount of ammonium glycolate in a total volume of 850 ml. The mixture was stirred for seven hours at 25° C. Analyses of the oxides obtained from the precipitate and the filtrate are given in Table III.

TABLE III: ANALYSES OF THE FRACTIONS FROM C

	g oxide	% Sm_2O_3	% Dy_2O_3
Glycolate precipitate	7.0080	5	95
Filtrate	3.0053	43	57

The separation factor for this step was 14—about half as big as in experiment B.

EXPERIMENT D

Another experiment was performed in which 1.5 g of Dy_2O_3 and 8.5 g of Sm_2O_3 dissolved in a minimum of hydrochloric acid were treated with seven-sixths the amount of ammonium glycolate required to form $Rgly_3$ in a total volume of 150 ml. The mixture was stirred for seven hours at 25° C. At first only a small amount of precipitate was observed, but after several hours, two-thirds of the total rare earth separated within a short time. It was thought that, due primarily to the small volume used to encourage the precipitation of dysprosium glycolate dihydrate, the formation of anhydrous samarium glycolate was initiated. Anhydrous glycolate, which ordinarily is slow to appear, may have formed initially by

evaporation of water from droplets of solution spattered on the walls of the beaker by the stirrer. Only a very small enrichment was observed in this experiment.

SUMMARY

From the behavior described above, it appears that precipitation as hydrated glycolates would be useful for separating yttrium-group elements from cerium-group rare earths. Light rare earths apparently do not form glycolate dihydrates, but separate instead as anhydrous glycolates, which form more slowly than dihydrated glycolates of the yttrium-group rare earths. The change in hydration occurs at gadolinium, which can form either the anhydrous glycolate or the dihydrate. A change in chelate stability also occurs at gadolinium. It is apparent that these phenomena are related.

REFERENCES

1. G. Jantsch and A. Grünkraut, *Z. anorg. Chem.*, 79, 305 (1913).
2. S. W. Mayer and E. C. Freiling, *J. Am. Chem. Soc.*, 75, 5647 (1953).
3. D. C. Stewart *et al.*, *Proc. Internat. Conf. Peaceful Uses of Atomic Energy*, 7, 321 (1956).
4. D. C. Stewart, *Anal. Chem.*, 27, 1279 (1955).
5. A. Sonesson, *Acta Chem. Scand.*, 13, 998 (1959).

THE USE OF ZINC AND HYDROGEN IONS IN THE DEVELOPMENT COLUMNS IN THE SEPARATION OF CERIUM-GROUP RARE EARTHS BY ION-EXCHANGE ELUTION

JACK E. POWELL

Institute for Atomic Research and Department of Chemistry
Iowa State University, Ames, Iowa

The use of common-metal ions to retain rare earth ions in the elution of mixtures of lanthanons from ion-exchange systems by means of ethylenediamine-*N*,*N*,*N'*,*N'*-tetraacetate (EDTA) solutions was first proposed by Spedding, Powell, and Wheelwright in 1954. They used both ferric (1) and cupric (2) ions and pointed out that the function of a retaining ion is to cause redeposition of the rare earths on the resin bed once they have been dislodged from the resin phase by the eluant, and to permit the chelating agent to leave the system in soluble form. Nickel and lead were also proposed as possible retaining ions. (2)

By using a suitable retaining ion, it is possible to operate the system with a compact band of adsorbed ions under conditions of total reflux and to simulate the banding behavior observed in simple displacement chromatography. In order for the system to perform properly, the complex species formed by the reaction of the eluant with a retaining ion must be sufficiently soluble that no solid phase precipitates from the eluate to clog the interstices of the resin bed. It has been determined that the concentration of EDTA should not exceed 0.015 *M* when copper is the retaining ion (3), due to the limited solubilities of Cu_2 (EDTA)·5 H_2O and the hydrated HR(EDTA) species, particularly HLa(EDTA)·$n H_2O$.

In 1958, Wolf and Massonne (4) adapted the retaining-ion technique of Spedding, Powell, and Wheelwright to the case of nitrilotriacetate (NTA) elutions. Instead of Cu^{+2} they used Zn^{+2}, primarily because the zinc-NTA species appeared to be more soluble than the corresponding copper-EDTA species. They were able to employ 2 per cent (0.105 *M*) NTA at *p*H's of 7 and 8 in the elution of cerium-group rare earths without difficulty. Shortly thereafter, Massonne (5, 6) reported a number of separations of yttrium-group rare earths using zinc as the retaining ion and *p*H 8 NTA eluant at concentrations ranging from 0.079 to 0.158 *M*. Some of his eluant solutions contained ammonium acetate in addition to NTA; but,

aside from increasing the concentrations of rare earths in the eluate, no advantageous effects of buffering with acetate are apparent from Massonne's data.

Fuger (7) proposed the elution of rare earths from Dowex 50 resin saturated with zinc ion, using an eluant containing $Zn(EDTA)^{=}$. His method appears to be most useful when only trace quantities of lanthanons are involved.

Krumholz *et al.* (8) have considered the use of EDTA for the recovery of pure rare earths from Brazilian monazite. It is their opinion that EDTA should be employed after removal of the major constituents, cerium and lanthanum, by other means.*

Instead of copper, Krumholz and co-workers preferred to use zinc as the retaining ion. Although zinc did not actually retain some of the heavier rare earths, these were recovered in partially separated form from the zinc-laden early eluate. Krumholz and his co-workers stated that the use of zinc instead of copper permits the recovery of EDTA by simple acidification and filtration.

DISCUSSION

It is the personal opinion of the author that copper should be used as the retaining ion in elutions with EDTA when yttrium-group elements abound in the mixture to be separated, but there is certainly merit in the proposition that zinc be used as the retaining ion for mixtures containing predominantly cerium-group elements. Concentrates obtained from certain minerals, such as monazite and bastnäsite, contain insignificant amounts of rare earths heavier than dysprosium, and may be resolved by development on columns charged with zinc ion with only minor losses occurring. It is advisable, of course, to remove cerium and lanthanum by conventional means before attempting the EDTA elution of such mixtures, whereupon a neodymium-rich concentrate containing substantial amounts of praseodymium and samarium is obtained. The combined percentages of yttrium and lanthanons heavier than samarium comprise perhaps 5 per cent of the total weight of such mixtures. Since the position of zinc in the rare earth elution sequence falls between ytterbium and thulium when the eluant is *p*H 8.4, 0.015 *M* EDTA, only lutetium and ytterbium are not retained. (9)

Zinc chloride is less expensive than $CuSO_4 \cdot 5\ H_2O$ on a poundage basis and has a smaller equivalent weight. The log stability constants

*The prior removal of cerium and lanthanum is highly advantageous, since hydrated HCe(EDTA) and HLa(EDTA) species tend to precipitate and fill the interstices of the resin bed at eluant concentrations even lower than 0.015 *M*. Precipitation of hydrated HR(EDTA) species does not occur with the other rare earths (Pr–Lu) unless the EDTA concentration is in excess of 0.015 *M* or the *p*H is less than 8.4.

for $Zn(EDTA)^{=}$ and $Cu(EDTA)^{=}$ are 16.50 and 18.80, respectively. (10) Since EDTA is an amino acid it has a minimum solubility around a *p*H of 2 and dissolves to a considerable extent in more acidic solutions. When sufficient acid is added to a 0.015 *M* solution of $Cu(EDTA)^{=}$ to decompose the anionic chelate, the liberated EDTA remains in solution as $H_6(EDTA)SO_4$. In the case of $Zn(EDTA)^{=}$, the chelate decomposes more readily in the presence of acid. This permits the recovery of about 85 per cent of the EDTA as $H_4(EDTA)$ from 0.015 *M* $Zn(EDTA)^{=}$ solutions after addition of 4.5–5.0 ml of concentrated H_2SO_4 per liter of eluate. The rate of precipitation is moderately slow, and maximum yields are approached only after 2–4 hours of stirring. The EDTA that may be recovered from the zinc-laden eluate amounts to about 42 per cent of the total required in the separation of neodymium-rich concentrates. If one cares to heat the rare earth eluate to a temperature between 90–100°C, during the precipitation and recovery of the individual rare earth oxalates, additional $H_4(EDTA)$ can be salvaged from the filtrate upon cooling. It has not been proved, however, whether or not this latter product can be obtained sufficiently free of trace rare earths to allow it to be reused in rare earth separations.

A further saving could be effected when zinc is the retaining ion. As with copper-state resin, it is not necessary that all of the exchange sites in the retaining bed be occupied by zinc. For example, a mixture of ammonium, hydrogen, and zinc ions, containing about 60 per cent zinc on an equivalent basis, will retain rare earths as effectively as zinc ion alone. The acidified zinc eluate after removal of the bulk of the $H_4(EDTA)$ is approximately 0.015-0.020 *M* in Zn^{++}, 0.0023 *M* in $H_4(EDTA)$, 0.01 normal in NH_4^+, 0.12-0.14 normal in H^+, and 0.08-0.09 *M* in $SO_4^{=}$. If this solution is passed through an ammonium-state cation-exchange bed (the columns are in the ammonium state after a previous elution), the zinc will adsorb preferentially, due to its greater charge and consequent greater affinity for the resin. If the equivalent concentration of zinc deposited on the resin after this treatment exceeds 0.6, and the presence of some H_4Ch or H_6Ch^{++} in the retaining bed can be tolerated, the zinc can be used repeatedly. Similar mixed retaining beds containing cupric ion and hydrogen ion have been used to retain rare earths during elution with EDTA on several occasions. (3, 11, 12, 13)

EXPERIMENTAL

A series of elutions was performed in order to prove that the zinc eluate could be reused as retaining ion. In this set of experiments, Sm–Nd–Pr mixtures derived from Lindsay Chemical's Code 630 "neodymium carbonate" were eluted down 4-in. diameter columns. The resin beds were previously prepared by filling 5-ft-long columns with 40–50 mesh,

hydrogen-form, Dowex 50W, cation-exchange resin to a height of 58 in. and backwashing carefully (during backwash operations, an extra five-foot section of four-inch-diameter column was attached to provide sufficient length for bed expansion).

It was the general practice to load one section of bed with rare earth mixture, prepared by dissolving 2 kg of crude "neodymium carbonate" in 2.25 liters of concentrated HCl and 45 liters of water. The excess rare earth was rinsed out with distilled water. The mixture was then eluted down one or more beds of resin which had been converted to the zinc-hydrogen-ammonium state by pretreatment with either a synthetic mixture (0.015 *M* $ZnCl_2$; 0.015 *M* NH_4Cl; 0.06 *M* H_2SO_4) or waste zinc solution recovered from the eluate from previous runs (see prior description). Solutions of such composition provide a retaining bed in which zinc is predominant, comprising 60–65 per cent of the equivalent capacity.

Experiments were performed with 0.015 *M* EDTA at *p*H 8.5 in which the adsorbed mixture was eluted one-and-a-half band lengths. The flow rate was 50 ml per minute. Although eluting an additional half band length decreased the Nd–Pr overlap slightly, the improvement was not sufficient to warrant the extra time and expense. It appeared in these runs that lanthanum and/or cerium, which make up about 1 per cent of the adsorbed mixture, were precipitating to a slight extent at the rear boundary of the band. Subsequent runs were made with 0.015 *M* EDTA at *p*H 8.7 and with 0.0083 *M* EDTA at *p*H 8.5. Neither modification completely eliminated the tendency for precipitation at the rear boundary.

The yield of greater than 99.9 per cent Nd_2O_3 was about the same in all runs—roughly three-quarters of the neodymium oxide available. The samarium and praseodymium bands, however, were not long enough to yield pure Sm_2O_3 and Pr_6O_{11} at the flow rate used in these experiments. Previous experience has shown that the yields of all components can be made to approach the amounts available by merely employing longer bands of adsorbed mixture or reducing the flow rate. Scale-up should present no difficulty and should furnish good yields of high-purity samarium and praseodymium.

It was amply demonstrated in these runs that the zinc recovered from one run would serve as the retaining ion for the next run. It was also confirmed that about 42 per cent of all the EDTA required in the separation of a mixture of this sort could be recovered from the zinc-laden eluate by simple acidification, followed at a suitable interval by filtration.

RECOMMENDED PROCEDURE FOR PROCESSING MIXTURES CONTAINING SUBSTANTIAL AMOUNTS OF HEAVY RARE EARTHS

Although zinc does not retain all the heavy rare earths, it can nevertheless be used to replace copper ion to a considerable extent in the separation of yttrium-earth mixtures derived from xenotime and gadolinite.

When 30-in.-diameter columns, 10 ft long, are used to separate half-ton quantities of such yttrium-rich oxide mixtures, it is practical to work with a total of twelve units. (3) A thousand pounds of oxide concentrate dissolved in sulfuric acid is used to saturate the first four beds of the system, and the fifth column is converted to the cupric state by treatment with excess cupric sulfate solution containing some sulfuric acid. The adsorbed band is then eluted down the fifth column with 0.015 *M* EDTA at *p*H 8.4–8.5 until rare earths appear at the bottom of the fifth column. At this point the front 10 per cent of the adsorbed band is allowed to pass off the main system onto an auxiliary column (usually a 30-in.-diameter section of cupric-state resin bed about 3½ ft long). From this auxiliary column the Lu–Yb–Tm–Er–Ho mixture can be eluted at leisure down a series of 6-in.-diameter, hydrogen-state, resin beds with 0.018 *M* diammonium *N*-hydroxyethylethylenediaminetriacetate (HEDTA) solution to complete the separation of the individual heavy lanthanons.

The mixture remaining on the main resin-bed system must then be eluted down seven additional large units in order to complete the purification of the main constituent yttrium. On the basis of our recent findings, there appears to be no reason why these units could not be used in the zinc-hydrogen cycle rather than the cupric cycle. The use of zinc in place of copper would permit easy recovery of about half of the EDTA required for the run and would allow virtually all the retaining ion to be reused again and again.

The dysprosium-rich, terbium-rich, and light rare earth portions of the band could be diverted to 6-in.-diameter, zinc-hydrogen, resin beds to improve the separation of the minor constituents, or simply stored on auxiliary columns to be recycled on the main system when sufficient mixture of a given kind is accumulated.

REFERENCES

1. F. H. Spedding, J. E. Powell, and E. J. Wheelwright, *J. Am. Chem. Soc.*, 76, 612 (1954).
2. F. H. Spedding, J. E. Powell, and E. J. Wheelwright, *ibid.*, 76, 2557 (1954).
3. J. E. Powell and F. H. Spedding, USAEC report, *ISC-617* (1955) and *Chem. Eng. Progress Symposium Series*, 55, No. 24, 101 (1959).
4. L. Wolf and J. Massonne, *Chemische Technik*, 10, 290 (1958).
5. J. Massonne, *ibid.*, 10, 591 (1958).
6. J. Massonne, *Österreichische Chemiker-Zeitung*, 60, No. 1, 16 (1959).
7. J. Fuger, *Bull. soc. chim. Belges*, 66, 151 (1957).
8. P. Krumholz *et al.*, "Brazilian Practices of Rare Earth Separation," *Proc. Second U.N. Internat. Conf. on Peaceful Uses of Atomic Energy*, A/Conf. 15/P/2491 (1958).

9. Dean B. James. Unpublished Ph.D. dissertation, Iowa State University Library (1960).
10. G. Schwarzenbach, R. Gut, and G. Anderegg, *Helv. Chim. Acta*, 37, 937 (1954).
11. J. K. Marsh, *J. Chem. Soc.*, *1957*, 978.
12. G. Brunisholz, *Helv. Chim. Acta*, 40, 2004 (1957).
13. L. K. Matson. Unpublished Ph.D. dissertation, Iowa State University Library (1959).

LIQUID-LIQUID EXTRACTION OF TRIVALENT RARE EARTHS USING ACIDIC PHOSPHONATES AS EXTRACTANTS*

D. F. PEPPARD AND G. W. MASON

Argonne National Laboratory, Argonne, Illinois

In this presentation, the application of liquid-liquid extraction techniques to the fractionation of mixtures of the trivalent rare earths will be discussed in a general way preliminary to the more detailed discussion of the acidic phosphonate systems, since this technique may be new to some of the symposium attendees. For this reason the terminology is treated in some detail.

In each of the more common techniques investigated for application to the fractionation of mixtures of trivalent rare earths—precipitation (including fractional crystallization and dissolution), ion exchange (both cation and anion exchange variants), volatilization, and liquid-liquid extraction—it is found necessary to exploit small differences in behavior between adjacent members of the rare earth series. From a pragmatic view, this behavior may be either physical or chemical in nature, provided that the differences may be used to effect a slight separation and provided that this separation is readily repeatable.

In considering the partition of trivalent rare earth solutes between two mutually equilibrated, sensibly immiscible, liquid phases—usually organic and aqueous phases—as a fractionation technique, the important factors are (1) the degree of fractionation per stage, (2) the constancy or variance of this degree of fractionation from stage to stage, (3) the ease with which multiplication of stages may be achieved, and (4) the range of partitioning Z-values, i.e., the atomic number, or fictitious atomic number above which all members report preferentially to the organic phase and below which all members report preferentially to the aqueous phase.

The degree of fractionation per equilibrium stage for a given pair of rare earth elements may be calculated from the volume ratio R (volume of equilibrated organic phase divided by the volume of equilibrated aqueous phase per stage) and the K values for each of the rare earths (K = distribution ratio, i.e., the concentration of the given rare earth in the or-

*Based on work performed under the auspices of the U.S. Atomic Energy Commission.

ganic phase divided by the concentration of the same rare earth in the aqueous phase). For example, consider rare earth M distributed at equilibrium between a volume V of aqueous phase and a volume RV of organic phase, where R may have a value on either side of unity or be equal to unity. Thermodynamically,

$$\text{Activity of M(organic)} = \text{Activity of M(aqueous)} \tag{1}$$

By definition of the activity coefficient, γ, it follows that

$$(\gamma_M)_O(C_M)_O = (\gamma_M)_A(C_M)_A \tag{2}$$

where the subscripts O and A refer respectively to equilibrated organic and aqueous phases and C_M represents concentration of M.

Rearrangement of Eq. (2) leads to

$$(C_M)_O/(C_M)_A = (\gamma_M)_A/(\gamma_M)_O \tag{3}$$

By the definition of distribution ratio, K, to be employed throughout this discussion, the left-hand side of Eq. (3) is K. On the assumption that the ratio given by the right-hand side of (3) remains constant throughout the range of investigation, the distribution ratio, K, is truly a constant. This constancy of K is found for all of the systems reported in this paper.

From material balance considerations,

$$(Q_M)_T = (Q_M)_O + (Q_M)_A \tag{4}$$

where Q represents quantity, i.e., the total quantity of M in a given stage is equal to the quantity of M in the equilibrated aqueous phase, plus the quantity of M in the equilibrated organic phase. The fraction, F, of the total M in this stage reporting to the organic phase is thus

$$(F_M)_O = (Q_M)_O/[(Q_M)_O + (Q_M)_A] \tag{5}$$

Substitution of the volume times concentration product for quantity results in

$$(F_M)_O = RV(C_M)_O/[RV(C_M)_O + V(C_M)_A] \tag{6}$$

Cancellation of V's, division of both numerator and denominator of the right side by $(C_M)_A$, followed by substitution of K for its equivalent, $(C_M)_O/(C_M)_A$, results in

$$(F_M)_O = RK_M/(RK_M + 1) \tag{7}$$

It follows, since the fraction of M in the organic phase plus the fraction of M in the aqueous phase is unity, by definition, that

$$(F_M)_A = 1/(RK_M + 1) \tag{8}$$

Analogous expressions for rare earth N may be set up. If we take, as a measure of fractionation, the ratio of the respective fractions of M and N reporting to the organic phase in a one-stage extraction, there results, from Eq. (7):

$$(F_M)_O/(F_N)_O = (K_M/K_N)[(RK_N + 1)/(RK_M + 1)] \tag{9}$$

The ratio, (K_M/K_N), is frequently defined to be the "separation factor," β:

$$\beta = K_M/K_N \tag{10}$$

The "separation factor," β, although a useful criterion of the applicability of a given system is not to be confused with the "decontamination factor," DF:

$$DF = F_M/F_N)_{\text{product phase}} \tag{11}$$

where the expression applies to a product phase, aqueous or organic, following any given number of stages and the F refers to the fraction of M (or N) initially present in the feed which reports to the product phase considered.

It may be noted from simultaneous consideration of Eqs. (9), (10), and (11) that as RK_N and RK_M both approach zero the DF for a single stage approaches β for the organic product phase. It is this fact that has led to so much confusion of these two terms, DF and β.

From Eq. (9) it is evident that satisfactory fractionation of M with respect to N not only requires a β different from unity but also requires that the RK values for M and N respectively be on opposite sides of unity.

For purposes of hasty evaluation of a given system, it is instructive to use the formulas for the fractions of M from a single portion of feed reporting to the organic and aqueous product phases, respectively effluent from a countercurrently operated system of $(2n - 1)$ batch stages, after attainment of steady state, in which the feed enters the nth (center) stage, the barren aqueous scrub enters the first stage, and the barren organic extractant enters the $(2n - 1)$th stage. (1) These expressions are

$$(F_M)_O = (RK_M)^n/[1 + (RK_M)^n] \tag{12}$$

$$(F_M)_A = 1/[1 + (RK_M)^n] \tag{13}$$

It is apparent that for an (RK) value greater than unity, as n increases, $(F_M)_O$ approaches 1 and $(F_M)_A$ approaches 0. Conversely, for an (RK)

value less than unity, as n increases, $(F_M)_O$ approaches 0 and $(F_M)_A$ approaches 1.

From Eqs. (12) and (13) and the corresponding expressions for rare earth N, it follows that rare earth elements M and N may be separated mutually to any desired extent by using a sufficiently large value of n, provided that RK_M and RK_N are on opposite sides of unity. Examination of these expressions shows further that the value of n required for a given degree of mutual separation decreases as β (i.e., K_M/K_N) increases. For example, starting with the defining expression for the DF of element M, with respect to contaminant element N, in the organic product phase,

$$DF = (F_M)_O/(F_N)_O \tag{14}$$

and substituting from Eq. (12), and finally expressing DF in terms of β and the fractional yield, Y, of M in the organic phase, the following is derived:

$$DF = \beta^n(1 - Y) + Y \tag{15}$$

For DF values greatly in excess of unity, this expression reduces to

$$DF = \beta^n(1 - Y) \tag{16}$$

or to the alternative form, expressed in terms of fractional loss, L, of the product considered:

$$DF = \beta^n L \tag{17}$$

Through obvious substitutions, expressions identical to Eqs. (15), (16), and (17) may be derived for the DF of N with respect to contaminant M in the aqueous-product phase. These three expressions are thus directly applicable to the "product" in each of the two effluent phases, i.e., to M in the organic phase and to N in the aqueous phase.

Through combination of these various expressions, the product of the DF of M with respect to contaminant N in the effluent organic phase, and the DF of N with respect to N in the effluent aqueous phase, is shown to be equal to β^n:

$$(DF)_{M(O)} \times (DF)_{N(A)} = \beta^n \tag{18}$$

For the specific set of conditions in which the DF for M with respect to N in the organic effluent, and the DF of N with respect to M in the aqueous effluent, are equal (i.e., identical mutual decontamination), Eq. (15) thus becomes

$$DF = \beta^{n/2} \tag{19}$$

From the foregoing arguments it is apparent that, although a high value of β is desirable, a value in the neighborhood of 2 is sufficiently

large to make fractionation feasible, provided that countercurrent operation of a large number of stages is readily accomplished. For example, application of Eq. (19) to a physical system of 39 stages ($n = 20$, $n/2 = 10$) employing a chemical system with a β of 2.0 predicts a DF of 1,024 for each of the products, M and N, with respect to the other as contaminant. From Eq. (17), the same system will produce a DF of 10^6 L for either product; M, for example, may be obtained in the organic effluent in 90 per cent yield with a DF of 10^5 with respect to contaminant N.

In the chemical system employing tris n butyl orthophosphate, $(n\mathrm{C_4H_9O})_3\mathrm{PO}$, normally called tributyl phosphate, and symbolized as TBP in liquid-liquid extraction and chemical processing literature, in a carrier diluent as the organic phase and an aqueous solution of nitric acid as the opposing aqueous phase, a β of 1.6 between adjacent elements in the region La–Gd is obtained under a variety of conditions. (2) The K values increase with increasing atomic number, and the requirement that the two RK values lie on opposite sides of unity is easily met in the higher Z-range, but not in the lower. In addition β values of 1.6 are not easily obtained under desirable operating conditions for pairs of adjacent elements in the range above atomic number 64.

Nevertheless, this system has been employed in the upgrading of a Gd fraction in the kilogram range (3) and in separation of Pm ($Z = 61$) from its neighboring rare earth radioactive fission products. (4)

The extraction is commonly represented by the reaction:

$$M_A^{+3} + 3\ \mathrm{NO}_{3A}^- + 3\ \mathrm{TBP}_O \rightleftharpoons M(\mathrm{NO_3})_3(\mathrm{TBP})_{3O} \tag{20}$$

the subscripts A and O referring respectively to the mutually equilibrated aqueous and organic phases. On the assumption that no other chemical species are involved, application of the mass law to Eq. (20), followed by substitution of K, the distribution ratio, for its equivalent, leads to

$$K = k[\mathrm{NO_3^-}]_A^3[\mathrm{TBP}]_O^3 \tag{21}$$

where k is the equilibrium constant for the reaction represented by Eq. (20).

The expression for K in Eq. (21) implies a third-power dependence of K upon the $\mathrm{NO_3^-}$ concentration in the aqueous phase and upon the TBP concentration in the organic phase. That is, plots of log K *vs.* $[\mathrm{NO_3^-}]_A$ ($[\mathrm{TBP}]_O$ = constant) and of log K *vs.* $[\mathrm{TBP}]_O$ ($[\mathrm{NO_3^-}]$ = constant) should be straight lines of slope +3.0. This expected third-power TBP dependence has been confirmed for the lower-Z members (toluene diluent) by Peppard *et al.* (1, 5) and for Y and Ce (III) (kerosene diluent) by Scargill, Healy, and McKay *et al.* (6, 7, 8).

Direct evidence for the third-power nitrate dependence is lacking, although a study of the extraction of Am(III), atomic number 95 and considered the actinide analogue of Eu, in the TBP × HNO_3 system shows the nitrate dependency to be essentially third-power, the log K *vs.* $[NO_3^-]$ plot having a slope of 2.9. (9)

Systems involving a number of other examples of $(GO)_3PO$ compounds, as well as a few examples of $(GO)_2(G')PO$ compounds in place of TBP and systems involving NO_3^-, Cl^-, Br^- or CNS^- have been investigated. (2, 10, 11) These have shown no greater promise than has the TBP × HNO_3 system. Consequently, this type of investigation has largely given way (in our group at the Argonne National Laboratory) to investigation of systems involving "organo-inorganic" acids as extractants—the extractant ionizing to furnish the anion of the extracted species. The extraction may be represented in a general way as

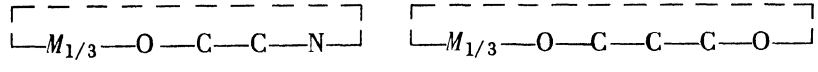
$$M_A^{+3} + 3\ HS_O \rightleftharpoons MS_{3O} + 3\ H_A^+ \tag{22}$$

where HS represents the un-ionized extractant or "solvent." Assuming no other chemical species present, the distribution ratio, K, is thus:

$$K = k[HS]_O^3/[H^+]_A^3 \tag{23}$$

where k is the equilibrium constant for the reaction in Eq. (22). In other words, the K for M is directly third-power dependent upon the concentration of extractant, HS, in the organic phase, and inversely third-power dependent upon the concentration of hydrogen ion in the aqueous phase.

The application of 5,7-dichloro-8-hydroxyquinoline (12) and thenoyltrifluoroacetone (13) as extractants in such systems has been reported. These extractants are considered to ionize as weak monobasic monomeric acids and to function as extractants by chelation of the metal ion by the resulting anion. The essential feature of the resulting chelates might be represented, for these two extractants respectively, as



These systems show considerable promise and merit further study.

The first reported application, known to the present authors, of an organo ortho phosphoric acid to the fractionation of trivalent rare earths is that of Scadden and Ballou (14) in 1953. These workers reported the preferential extraction of the "yttrium-group" rare earths with respect to the lower-Z rare earths into a solution of di n-butyl ortho phosphoric acid, $(n\text{-}C_4H_9O)_2PO(OH)$, in di n-butyl ether as carrier diluent, from an aqueous phase containing mineral acid. The "extractant" as used was reported to be a mixture of the di ester $(n\text{-}C_4H_9O)_2PO(OH)$, and the mono ester,

$(n\text{-}C_4H_9O)PO(OH)_2$, in the respective ratio of 4.5 to 1, on a formula weight basis. (14)

The next reported study of such systems dealt with the application of bis(2-ethyl hexyl) ortho phosphoric acid, $[2\text{-}(C_2H_5)C_6H_{12}O]_2PO(OH)$, frequently referred to as di octyl phosphoric acid and symbolized in various ways—including HDEHP*—to the preferential extraction of the heavier rare earths. (15) The HDEHP (carrier diluent) plus aqueous mineral acid system was found to fractionate radioactive, tracer-level, rare earths in a regular fashion, the degree of extraction increasing with Z. A plot of log K *vs.* Z for this system is an essentially straight line of slope approximately 2.5. Yttrium falls on this curve at a Z-value approximating 67.6.

The mode of extraction was originally postulated (15) as

$$M_A^{+3} + 3\ HDGP_O \rightleftharpoons M(DGP)_{3O} + 3\ H_A^+ \tag{24}$$

as in Eq. (22), since the effects of varying extractant and acid concentrations conformed to Eq. (23).

However, later work proved the extractant dimeric (16) in the carrier diluent, so the expression was modified to (17)

$$M_A^{+3} + 3\ (HDGP)_{2O} \rightleftharpoons M[H(DGP)_2]_{3O} + 3\ H_A^+ \tag{25}$$

on the assumption that the mono-ionized dimer served as a singly charged anion combining with the cation either through covalent bonding or through ion-pair formation, or perhaps through both.

When the rare earth content of the organic phase is in slight excess of 1 mole of M^{+3} per six formula weights (or three dimer weights) of HDGP, gel formation is encountered. This phenomenon severely limits the applicability of HDGP (carrier diluent) plus aqueous mineral acid systems to final purification of a single rare earth, in general, although in specific instances in which the neighboring elements are present in low concentrations relative to the concentration of the desired element, satisfactory operating conditions can be found.

The organo phosphorus work has now been extended to include acidic phosphonates, i.e., (GO) (G′) PO (OH).† These compounds are also, in general, dimeric when in carrier diluent. A detailed study, of the extrac-

*Throughout this discussion, HDGP represents a general orthophosphoric acid di ester, $(GO)_2PO(OH)$, in which G is a generalized organic group, D signifies di and H represents an ionizable hydrogen. (The EH represents the 2-ethyl hexyl group.) The corresponding mono ester $(GO)PO(OH)_2$ is represented as H_2MGP, the M signifying mono and two theoretically ionizable hydrogen atoms being involved per formula weight.

†Both G and G' are generalized organic groups, not necessarily different from each other, and G' is linked to the P by a C—P bond. Since the compounds have one ionizable hydrogen atom per formula weight, they are symbolized as HG(G′P), the parentheses indicating the group bound by a C—P bond.

tion of radioactive La(57), Pm(61), Eu(63), Tb(65), and Tm(69), from aqueous mineral acid phases into these extractants has confirmed the expected third-power extractant and inverse third-power hydrogen ion dependencies:

$$M_A^{+3} + 3\,[HG(G'P)]_{2O} \rightleftharpoons M\,\{H[G(G'P)]_2\}_{3O} + 3\,H_A^+ \tag{26}$$

$$K = k[\{HG(G'P)\}_2]_O^3/[H^+]_A^3 \tag{27}$$

where k is the equilibrium constant for the reaction of Eq. (26). A Z-study shows the plot of log K *vs.* Z to vary considerably as G and G' are varied. For example, although in several systems the plot very closely approximates a single straight line of positive slope of 2.5–2.9—the exact slope being a function of G and G'—in several other systems the plot is represented much better by two straight lines of positive slope joining at the neighborhood of a Z of 62–65. In the latter plots the low-Z portion of the curve is, in general, much flatter than the high-Z portion.

The high-Z portion of such a plot has a slope approximating that of the single straight-line plots. Consequently, it has seemed reasonable to evaluate the effect produced upon the extraction of an element by varying G and G′ at an element contained in this high-Z region. Terbium (65) was chosen as this element, and the comparison made as follows.

By reference to Eq. (27), it is seen that the distribution ratio, K, for a trivalent rare earth in one of these extraction systems should vary with the third-power of the "molar" concentration of the extractant. In this discussion the "molar" concentration is considered to be the number of "molecular weights" of the extractant divided by the number of liters of solution containing the extractant, i.e., molarity, represented by M. In order to facilitate comparison with systems involving extractants of unknown states of aggregation, it has proved helpful to introduce the concept of formality, F, the number of "formula weights" of extractant divided by the number of liters of solution containing the extractant.

For a dimeric extractant $M = F/2$, therefore, $kM^3 = (k/8)F^3$. Substitution of the right-hand side of this expression for its equivalent in Eq. (27) followed by substitution of K_s for $(k/8)$ leads to

$$K = K_s F_s^3/[H^+]_A^3 \tag{28}$$

where F_s represents the "formality" of the "solvent" or extractant, and K_s may be numerically interpreted as the value of K at unity, formality of the extractant in the organic phase and unity formality (as well as molarity) of the hydrogen ion in the aqueous phase.

There exists, therefore, a single value of K_s for each trivalent rare earth in a given system of solvent phase plus aqueous phase. It should

be noted at this point that since concentrations, not activities, are employed, the foregoing statement is approximately correct only for systems employing a given ionic strength of the aqueous phase and a reasonably dilute solvent phase, in general less than 0.6 *F*. It should be noted, further, that the carrier diluent cannot be considered an "inert" diluent, since the K_s may differ by a factor of two or more by changing from benzene to toluene as a diluent, and may change by a factor of 100 or more by changing from a hydrocarbon diluent to an ether diluent. With these qualifications in mind, it is instructive to consider K_s values for a given element as a function of *G* and *G'*.

From the data of Table I, it may be noted:

TABLE I: K_s VALUES FOR EXTRACTION OF Tb(III)
(*Toluene as carrier diluent except as noted. Aqueous phase:* $\mu = 1.0$, $NaClO_4 + HClO_4$)

Extractant	K_s
Hϕ(ΦP),* $\Phi = C_6H_5$	1.1×10^4
HB(BP),* β = *n*-C_4H_9	7.5×10^{-1}
HHx(HxP),* Hx = *n*-C_6H_{13}	4.8×10^{-1}
HEH(EHP), EH = 2-$(C_2H_5)C_6H_{12}$	6.6×10^{-3}
HEH(ΦP)	8.6×10
HEH(ΦP), in hexone diluent	3.5
HEH(ClMP), ClM = $ClCH_2$	1.2×10^3
Hn-O(ΦP), *n*-O = *n*-C_8H_{17}	5.5×10^2
Hn-O(ClMP)	3.1×10^3
HB(ΦP)*	4.6×10^2
HDΦP*	2.8×10^4
HDBP*	3.4×10
HDEHP	3.1×10^{-1}
HDOΦP, OΦ = para octyl phenyl, the octyl being 1,1,3,3-tetramethyl butyl	9.5×10^3

*Data obtained using 0.1–0.3 *F* extractant were used to calculate the K_s values on the *assumption* of third-power extractant and inverse third-power acid dependencies.

(1) A "homogeneous" phosphonate—i.e., HG(GP), *G* = *G'*—is a less effective extractant than the corresponding ortho phosphate, HDGP. For example, the K_s value for HDEHP is approximately fifty times that for HEH(EHP). Other examples are the HDBP comparison with HB(BP) and HDΦP with HΦ(ΦP).

(2) In the (EHO)(G')PO(OH) series, the K_s increases as *G'* becomes successively 2-ethyl-hexyl, phenyl and chloro methyl, the total increase exceeding a factor of 10^5.

(3) In the (GO)(Φ)PO(OH) series, the K_s increases only slightly as *G* becomes successively, *n*-C_4H_9, *n*-C_8H_{17}, and C_6H_5, the total increase approximating a factor of 25.

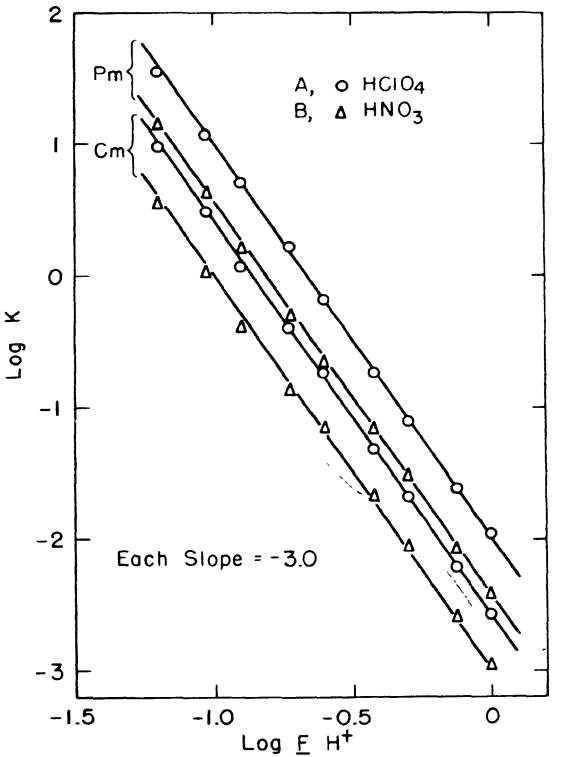


Fig. 1. Hydrogen-ion dependency of the extraction of Pm and Cm into 0.20 *F* HEH(ΦP) in toluene from: (A) $HClO_4 + NaClO_4$, (B) $HNO_3 + NaNO_3$. $\mu = 1.0$.

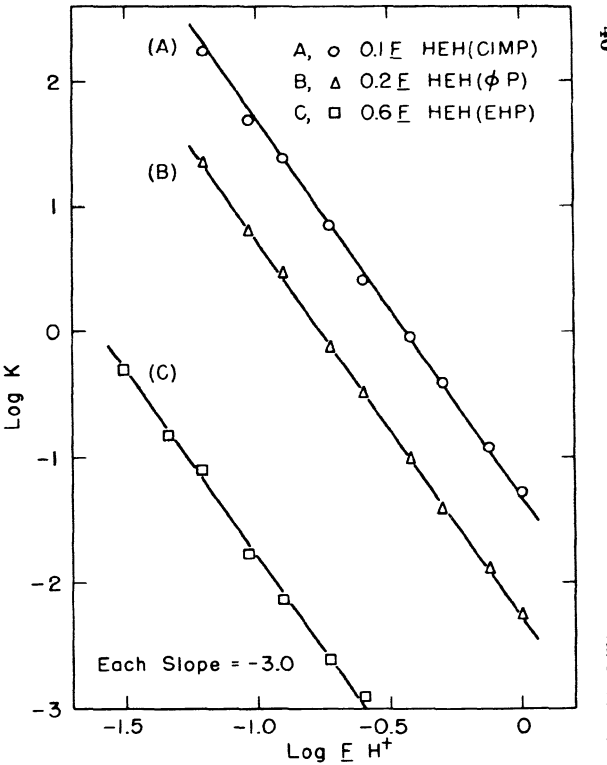


Fig. 2. Hydrogen-ion dependency of the extraction of Pm from HCl + NaCl, $\mu = 1.0$, into: (A) HEH(CIMP), (B) HEH(ΦP), (C) HEH(EHP). Toluene diluent.

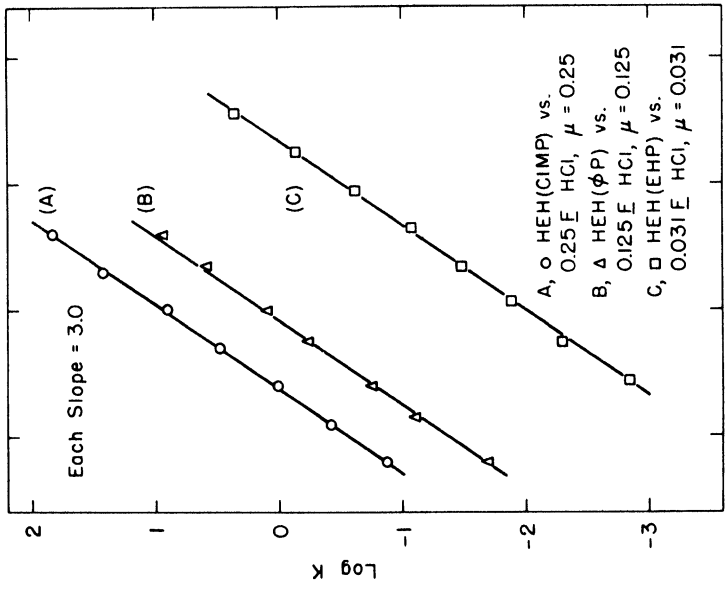


Fig. 4. Solvent dependency of the extraction of Pm from HCl into: (A) HEH(ClMP), (B) HEH(ΦP), (C) HEH(EHP). Toluene diluent.

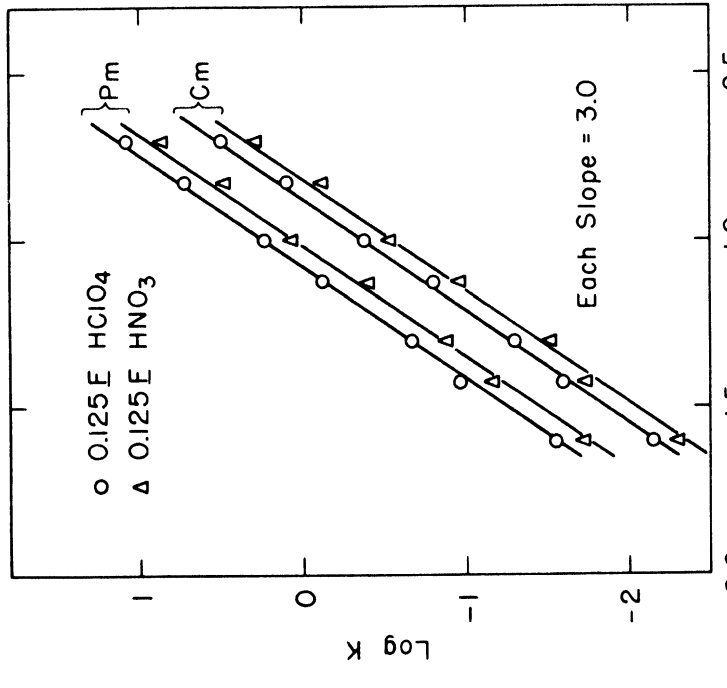


Fig. 3. Solvent dependency of the extraction of Pm and Cm into HEH(ΦP) in toluene from: (A) $HClO_4$, (B) HNO_3. μ = 0.125.

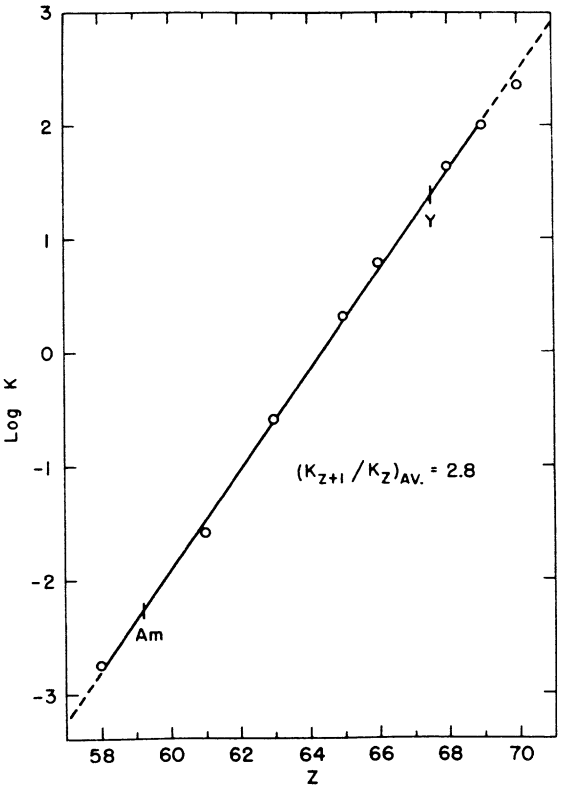
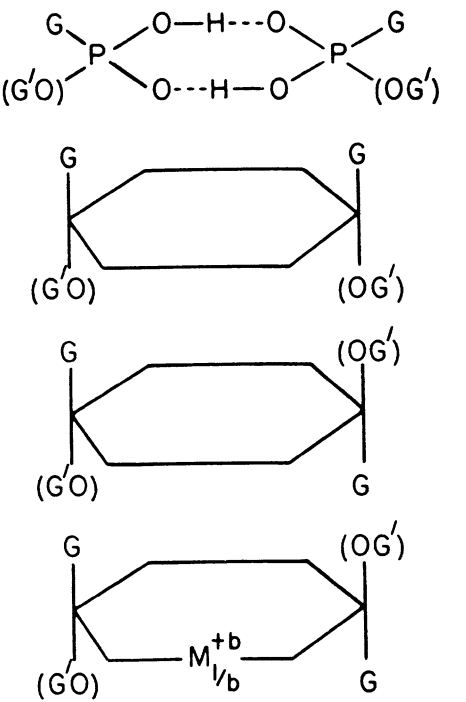


Fig. 5. Variation of log K with Z (lanthanides) in the 1.0 *F* HEH(ΦP) in toluene *vs.* 2.0 *F* HCl system. Placement of Y and Am in-



* Symmetry considerations unaltered by substitution of (OG) or G′ for G or conversely of (OG) or G′ for (OG′).

Fig. 6. Possible isomerism of $\{(G'O)(G)PO(OH)\}_2$ and related molecules.

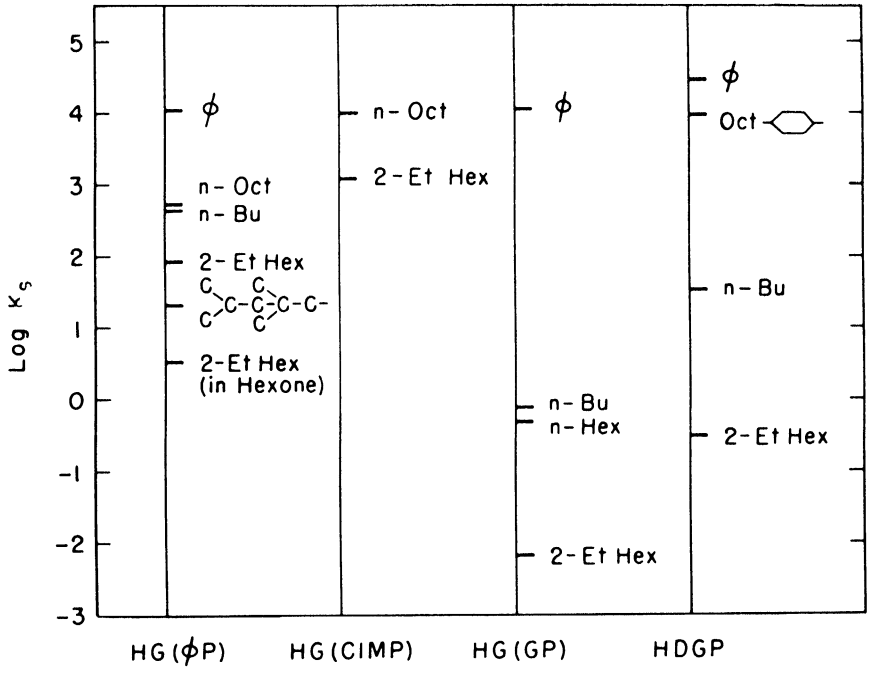


Fig. 7. K_s values of Tb(III) from $HClO_4 + NaClO_4$ ($\mu = 1.0$) into (GO)(G′)PO(OH) and $(GO)_2PO(OH)$ extractants. Toluene diluent, except as noted. (22° C)

(4) In the HEH(ΦP) experiments, the K_s for Tb is lower in hexone (methyl iso butyl ketone) diluent than in toluene diluent by a factor of approximately 25.

(5) In the (octyl O)(Φ)PO(OH) and (octyl O)(ClM)PO(OH) experiments, respectively, involving isomeric octyl groups, the n-C_8H_{17} compound showed a K_s approximately six and three times greater than that shown by the 2-ethyl hexyl compound.

(6) In the experiments mentioned in (5), for a given octyl group, the chloro methyl compound showed a K_s approximately six and fourteen times greater than that shown by the phenyl-compound, for the normal and 2-ethyl hexyl isomers, respectively.

(7) The K_s value for this selection of phosphates and phosphonates ranges from 6.6×10^{-3} to 2.8×10^{4}, the ratio of highest K_s to lowest thus being 4×10^{6}.

Specific "acid-dependency," "extractant-dependency," and log K *vs.* Z data are presented in Fig. 1–5. The spatial relationships involved, including cis-trans and *d-l* isomerism, are shown in Fig. 6. The data of Table I are presented graphically in Fig. 7.

Figures 1-6 are taken from reference (18). Detailed treatment of several other selected systems will be published shortly in the same journal.

REFERENCES

1. D. F. Peppard and M. A. Peppard, *Ind. Eng. Chem.*, 46, 34 (1954).
2. D. F. Peppard *et al.*, *J. Phys. Chem.*, 57, 294 (1953).
3. B. Weaver, F. A. Kappelmann, and A. C. Topp, *J. Am. Chem. Soc.*, 75, 3943 (1953).
4. Oak Ridge National Laboratory. Unclassified annual progress report of the Chemical Technology Division for period ending August 31, 1959, *ORNL-2788.*
5. D. F. Peppard *et al.*, *J. Inorg. Nucl. Chem.*, 4, 326 (1957).
6. T. V. Healy and H. A. C. McKay, *Rec. Trav. Chim.*, 75, 730 (1956).
7. H. A. C. McKay, K. Alcock, and D. Scargill. Unclassified report of the Atomic Energy Research Establishment (England), *A.E.R.E. C/R 1514* (1954).
8. D. Scargill *et al.*, *J. Inorg. Nucl. Chem.*, 4, 304 (1957).
9. K. A. Walsh, *Preprint 270.* Presentation made at the Nuclear Engineering and Science Congress, sponsored by Engineers Joint Council (Cleveland), December 12-16, 1955.
10. D. B. Appleton and P. W. Selwood, *J. Am. Chem. Soc.*, 63, 2029 (1941).
11. G. F. Asselin, L. F. Audrieth, and E. W. Comings, *J. Phys. Colloid. Chem.*, 54, 640 (1950).
12. T. Moeller and D. E. Jackson, *Anal. Chem.*, 22, 1393 (1950).
13. L. B. Magnusson and M. L. Anderson, *J. Am. Chem. Soc.*, 76, 6207 (1954). *Also*, H. J. Bronaugh and J. F. Suttle, Los Alamos Scientific Laboratory unclassified report, *LA-1561* (1953).
14. E. M. Scadden and N. E. Ballou, *Anal. Chem.*, 25, 1602 (1953).
15. D. F. Peppard *et al.*, *J. Inorg. Nucl. Chem.*, 4, 334 (1957).
16. D. F. Peppard, J. R. Ferraro, and G. W. Mason, *ibid.*, 4, 371 (1957); 7, 231 (1958).
17. D. F. Peppard *et al.*, *ibid.*, 7, 276 (1958).
18. D. F. Peppard, G. W. Mason, and I. Hucher. Forthcoming publication in *ibid.*

SOME ELECTROCHEMICAL DIFFERENCES OF THE LANTHANONS AS RELATED TO THEIR SEPARABILITY AT AMALGAM CATHODES*

E. I. ONSTOTT

Los Alamos Scientific Laboratory University of California, Los Alamos, New Mexico

The discussion of electrochemical behavior of the lanthanons will be limited here to valences of (III) or lower, since higher oxidation states are not generally encountered in amalgam cathode separations. The term "lanthanon (III)" is used to describe the lanthanons, including yttrium, which show only (III) or higher valence in compounds. Thus, Sm, Eu, and Yb are not (III) lanthanons. Thulium is designated as a (III) lanthanon, since it shows no tendency to be stable in the (II) state in aqueous and methanol electrolytes or in amalgams.

CLASSIC ELECTRODE POTENTIALS *VS.* ELECTRODE MECHANISMS

The tabulation of electrode potentials of the lanthanons as (O)-(III) oxidations, calculated from thermochemical data (1), are useful for showing the similarities and the strongly electropositive nature of the metals. However, they generally do not give clues to the electrode mechanisms, and some chemists may mistakenly think that the process actually entails simultaneous transfer of three electrons. There is one paper in the literature (2) giving electrochemical data from cell measurements which support the idea of a simultaneous three-electron reduction for cerium. A similar cell with a different reference electrode was investigated by us (3), but the behavior described by Walters and DeVries could not be duplicated. As a matter of fact, the irreversible behavior of this cell gave first clues that hydride is co-transferred with the (III) lanthanons when they are electrolyzed from water and methanol solvents. (3)

The electrostatic charge of the lanthanons in the (III) state is so high, and the solvent molecules are so tightly bound in water solutions, that it is easier for electrons at an electrode surface to break the oxy-

*Work done under the auspices of the Atomic Energy Commission.

gen-hydrogen bonds of ligand water than it is to penetrate the co-ordinated solvent shield to reduce the metal ion by a three-electron reduction. The solvent-destroying reaction is so fast that it swamps or masks other reactions, unless an intermediate oxidation state at an intermediate energy level can be reached. Thus, the electrochemical properties of the lanthanons fall into two groups: those which show an oxidation number intermediate between (O) and (III)—Sm, Eu, and Yb—and the remainder, which show no tendency to go to intermediate oxidation states.

The classic designation of electrode potentials can be descriptive of electrode mechanisms of the lanthanons when describing the (II)-(III) oxidation (reduction) of Sm, Eu, and Yb. It should be pointed out, however, that solvent degradation also takes place at rapid rates at the high potentials of the Yb(II)-Yb(III) and Sm(II)-Sm(III) reactions. Consequently, accurate measurement of these potentials by classical concentration-cell procedures probably is not possible. Latimer's tabulation of the value of E° for the Yb(II)-Yb(III) *vs.* H_2 couple of 0.578 v (1) is low by at least 0.6 v; Laitinen's value of 1.15 v *vs.* H_2 from polarographic measurements (4) appears to be much more nearly correct. The estimate of > 0.9 v by Latimer for the Sm(II)-Sm(III) *vs.* H_2 couple (1) is quite conservative with regard to the reducing character of Sm(II) (5). A value of 1.2 v $< E^\circ <$ 2.0 v *vs.* H_2 should be a better guess.

The potential barrier for reduction of the (III) lanthanons from aqueous electrolytes is so high that the charge on the (III) ions evidently must be lowered before reduction can proceed at measurable rates. It has been proposed that the easy way the charge can be lowered is by co-ordination of a hydride ligand, since hydrogen has been found to be deposited with some of the lanthanons on electrolysis. (3)

The relative heights of the potential barriers for electroreduction at a mercury cathode, indicated by the relative rates of electrolysis of the individual lanthanons, is found to be a function of their ion size. The relative ease of electrolysis is as follows: Eu, Sm, Yb, La...Er, in sequence, Y, Tm, Lu. This series is a little different than the one proposed previously (6), in that Sm and Yb are interchanged. Recent data have been obtained (7) which show that the rates of electrolysis of Yb, like Sm, can vary widely depending on electrolyte *p*H, and that under chosen conditions, the electrolysis rate constant for Sm (8) could be somewhat greater than that for Yb.

The values of the ionic radii of the lanthanons (9) are guides to the relative rates of electrolysis, with the exception of Eu. The fastest rate will be found for the lanthanon with the largest radius: Sm(II) > Yb(II) > La(III), and so forth. The rate for Y also falls where expected on the basis of Templeman and Dauben values for the ionic radii (9), between Er and Tm.

The potential barrier for reduction of the (III) lanthanons is inherently due to the (III) charge, but it evidently shows up in oxygen-hydrogen containing solvents as a metal–oxygen bond of a hydroxide ligand or ligands, and the height of the barrier undoubtedly is related to the bond strength. Thus, the heavy (III) lanthanons are more difficult to electrolyze than the light (III) lanthanons, because more energy is required to displace the hydroxide ligand with a hydride ligand. It must also be inferred from this argument that the difference in bond strength between any two (III) lanthanons is greater for hydroxide ligands than for hydride ligands. That is to say, it would be energetically easier, for example, to replace a hydroxide ligand with a hydride ligand on a La(III) ion than on a Ce (III) ion.

GROUP DIFFERENCES BETWEEN THE (III) LANTHANONS AND Sm, Eu, Yb IN THE METALLIC AMALGAM PHASE

The divalent nature of Sm, Eu, and Yb is carried over to the amalgams of these elements, so that they behave much more like Sr amalgams in being very reactive in the presence of water and other oxidizing agents. By contrast, the (III) lanthanon amalgams are less reactive and can be considered to behave like trivalent metals in mercury.

The reactivity of Sm, Eu, and Yb amalgams is noticed in amalgam cathode separations, where a layer of enriched hydroxides of these elements is invariably found underneath the mercury, due to the back reaction with the electrolyte. Sm, Eu, and Yb can probably be separated from each other by differences in amalgam reactivity and, as a group, can be readily separated from the (III) lanthanons by differences in reactivity of the amalgams. (6)

The (III) lanthanons probably all act as trivalent lanthanons in mercury,* since they do not behave much differently when mixtures in amalgams are oxidized. That is to say, there is little separation between lanthanons as compared to the separations obtained by the reverse procedure of electrolysis. The reason is undoubtedly tied to the mechanism of the (0)–(III) oxidation. The oxidation evidently proceeds by forming a hydrido complex as the first step in polar, hydrogen-containing solvents, and then by loosing electrons and simultaneous solvation as the final steps. However, since there are no hydroxide–metal bonds to break in the metallic phase, the properties of the (III) lanthanons are quite similar, and a leveled group behavior is observed when they are oxidized in the presence of each other.

---

*An interesting ramification of the metallic state is that Sm evidently behaves like a (III) lanthanon in the pure metallic state; yet, it shows a lower valence behavior when diluted with mercury. Tm does not show a similar behavior pattern.

THE AMALGAM CATHODE AS A SEPARATION TOOL

The electrolyte region immediately adjacent to a mercury cathode represents a region where chemical and electrochemical exchange can proceed with great rapidity, with a large steady-state current flowing; the steady-state condition is forced by the dynamic energy transfer. To metal ions at the electrolyte-electrode interface, the cathode presents a plane surface of negative charge, with a compatible metal reservoir on the other side of the charged region. The electrode surface can be very selective to ions of any charge, because it is a singular source of controlled-energy electrons, and true differences in ions can be discriminated under properly chosen conditions.

There are two conditions of interest in operating an amalgam cathode as a separations device. The first condition is that of polarization with a large current flow with respect to the supply of reducible species. Here the electrode is able to reduce ions reaching it by diffusion with 100 per cent current efficiency, *provided the potential is sufficiently high to exceed any potential barrier inherent in the reduction process.*

The second condition of interest is that of limited current flow, with the concentration of reducible species deliberately chosen to be large, so that the rate of reduction then is limited by the current passed—a condition of depolarization. This is often called a saturation condition, since the rate of reduction is essentially independent of the amount of reducible species, because of the very large supply, and the rate is zero order. A saturation condition is discriminatory for different species with inherent differences, because the electrons which traverse the cathode boundary will be divided among the reducible species according to the relative ease of reduction of each, and according to the relative height of the potential barrier for such reduction.

The amalgam-cathode method of separating the lanthanons seems to be the most selective practical means now known, for the reason that inherent differences of lanthanon ions in the same environment can be differentiated by the limited current flow and controlled potential, in a region where all ions are subjected to the same forces. It is fortunate in a practical sense that the condition of saturation which is necessary for the electrode discrimination is also a condition which allows rapid electrolysis of large amounts of mixed lanthanons.

RECENT RESEARCH AT LOS ALAMOS

The method used by the author and co-workers of elucidating some of the electrochemical differences of the lanthanons has been that of studying the steady-state electrolysis of mixtures at a lithium amalgam cathode. Mass transfer into the mercury phase has been followed most

successfully with radioactive tracers, but the spectrophotometric method of analysis is better for complex mixtures when gram quantities are available.

Recently a rather ideal system has been found for study of the electrochemical properties of the heavy lanthanons. (10) Electrolysis rates are sufficiently rapid in methanol containing LiCl so that the kinetics can be studied in some detail. Significant experimental findings (10) on a study of the electrolysis of Tm from a mixture of 1 per cent Tm in Lu are briefly as follows:

(1) The electrolysis of Tm into the cathode is accompanied by a simultaneous Tm precipitation reaction at the cathode. No visible precipitate forms in the electrolyte bulk, but a precipitate appears at the edge of the cathode at the junction of the cathode, the electrolyte, and the vessel. This precipitate probably is formed from residual water or hydroxide in the methanol. Adding water to the electrolyte causes the amount of precipitate to increase.

(2) The electrolysis of Tm proceeds at reasonable rates under limited conditions. The concentration of *total* Tm plus Lu must be in excess of about 0.005 *M* for a current density of 0.02 amp/cm^2. The water content must be kept as low as possible. For example, the rate of electrolysis of Tm is decreased by a factor of at least ten by increasing the water content from $\sim$ 0.06 to $\sim$ 0.25 per cent. The current density must be chosen carefully, since the rate constant for Tm electrolysis is directly proportional to the current density.

(3) The rate of electrolysis of Tm is relatively independent of Tm concentration, which shows that the reaction is zero order and that another parameter limits the rate. However, as mentioned above, the rate constant is directly proportional to the current density, showing that the rate depends on a species generated by the electron current. The species generated is undoubtedly hydride ion, and the amount generated is proportional to the current passed through the cell. Current efficiency for Tm plus Lu electrolysis under optimum conditions is only one-half of 1 per cent.

(4) The rate of precipitate formation is linear with time at constant current density, showing that a species must be formed at the electrode surface which causes the precipitation. The rate constant is relatively independent of current density, indicating that the rate is limited by another parameter—probably diffusion to the electrode surface. However, the rate constant for precipitate formation shows an exponential dependence on the electrolyte

concentration of Tm–Lu. It is believed that the precipitation reaction is caused by electrosolvolytic formation of hydroxide ligand from water ligands on Tm and Lu ions. This reaction can proceed at 100 per cent current efficiency, but is limited by the

TABLE I: EXAMPLES OF AMALGAM-CATHODE ENRICHMENT OF LANTHANONS

(*All separations done in one operation—one continuous electrolysis—except where designated*)

Aqueous Electrolyses					
Lanthanon Mixture	Scale-Grams	Starting % Purity (oxide)	Product* % Purity (oxide)	Yield %	Reference
Sm, Eu	10–15	98.4 Sm	>99.995 Sm	91	8,12
Eu, Sm	10–15	1.6 Eu	17 Eu	~quant.	8,12
Sm, Eu	10–15	99.956 Sm	>99.9997 Sm	90	12
Eu, Sm	10–15	34 Eu	98 Eu	68	8
Eu, Sm	10–15	87 Eu	~99.9 Eu	79	8
Sm, Gd	5	90 Gd	~99.8 Gd	~90	8
Monazite	100		~20 fold enrichment of middle and heavy lanthanons		6
[Ho, Er, Tm, Yb, Lu]	35	31 Yb	~99.9 Yb	quant.	7
Tm, Yb	4	50 Yb	99.96 Yb	98	7

*With respect to other lanthanon impurities specified in mixtures.

TABLE II: EXAMPLES OF AMALGAM-CATHODE ENRICHMENT OF LANTHANONS

(*All separations done in one operation—one continuous electrolysis—except where designated*)

Methanol Electrolyses					
Lanthanon Mixture	Scale-Grams	Starting % Purity (oxide)	Product* % Purity (oxide)	Yield %	Reference
Yttrium earth containing Gd	1200	6.4 Gb	24 Gd	32	6
Yttrium earth containing Tb	1200	2.3 Tb	7.0 Tb	25	6
Yttrium earth containing Y	1200	70 Y	92 Y	65†	6
Ho, Er, Tm, Lu	0.6	60 Lu	87 Lu	49	11
Er, Tm, Lu	0.2	87 Lu	98.9 Lu	20	11
Tm, Yb, Lu	0.2–0.6	68 Lu	99.8–99.9 Lu	24‡	11
Tm, Lu	0.2	99 Lu	99.9 Lu	20	11
Ho, Er, Tm, Lu	12	6.4 Ho	34.5 Ho	40	11

*With respect to other lanthanon impurities specified in mixtures.
†Twelve electrolyses done.
‡Six electrolyses done.

diffusion to Tm and Lu species to the electrode surface. By increasing the current density, the mass transfer of Tm–Lu to the cathode phase can be made to predominate through providing a larger supply of hydrido ligand.

(5) Both Tm and Lu are, of course, simultaneously electrolyzed when present together in the same electrolyte. However, the enrichment of Tm in the mercury phase invariably will be about threefold, *even though the ratio of atoms in the electrolyte is varied between wide limits.* Thus a uniform separation is effected under variable conditions; yet, the yield is critically dependent on a proper choice of electrolysis conditions, because of the degrading precipitation reaction.

REFERENCES

1. W. M. Latimer, *Oxidation Potentials.* Englewood Cliffs: Prentice-Hall, Inc., 1952, p. 286.
2. G. C. Walters and T. DeVries, *J. Am. Chem. Soc.*, 65, 119 (1943).
3. E. I. Onstott and A. N. Syveruda. Paper presented at the San Francisco meeting of the ACS, April, 1958.
4. H. A. Laitinen, *J. Am. Chem. Soc.*, 64, 1133 (1942).
5. T. Moeller, *Inorganic Chemistry.* New York: John Wiley and Sons, Inc., 1952, p. 904.
6. E. I. Onstott, *J. Am. Chem. Soc.*, 81, 4451 (1959).
7. E. I. Onstott. Paper presented at the 138th National Meeting of the ACS, September, 1960; to be published in J. Am. *Chem. Soc.*
8. E. I. Onstott, *J. Am. Chem. Soc.*, 78, 2070 (1956).
9. D. H. Templeton and C. H. Dauber, *ibid.*, 76, 5237 (1954). *Also,* J. Kleinberg, W. J. Argersinger, Jr., and E. Griswold, *Inorganic Chemistry.* Boston: D. C. Heath and Co., 1960, p. 75.
10. E. I. Onstott. Paper presented at the 138th National Meeting of the ACS, New York, September, 1960; submitted to *J. Am. Chem. Soc.* for publication.
11. E. I. Onstott, *J. Am. Chem. Soc.*, 77, 2129 (1955).

TETRAVALENT NEODYMIUM AND DYSPROSIUM*

L. B. ASPREY

Los Alamos Scientific Laboratory
University of California, Los Alamos, New Mexico

Among the lanthanide elements, only cerium, praseodymium, and terbium have been shown to have tetravelent oxidation states. From time to time, claims have been made that tetravalent neodymium and pentavalent praseodymium have been prepared, but such claims, upon re-examination, have not been verified. (1)

This paper presents evidence for the existence of both Nd(IV) and Dy(IV) as double fluorides of cesium or rubidium, with at least two atoms of alkali per lanthanide. The work on this subject is not yet complete; this paper will therefore present only as much evidence as exists at this time. The subject is being actively pursued both at the University of Münster by Dr. Rudolf Hoppe and also here at the Los Alamos Scientific Laboratory, and a collaborative paper will be published. The preliminary results of Dr. Hoppe's investigation are included in this paper.

The compounds containing tetravalent neodymium or dysprosium are prepared by treating mixtures of alkali-lanthanide chlorides with elemental fluorine at temperatures between 100 and 400 °C. Praseodymium and cerium are completely oxidized when sodium, potassium, rubidium, or cesium are used as the alkali metal. With neodymium or dysprosium, however, evidence of oxidation is obtained only with cesium and rubidium, and not with sodium and potassium. Complete oxidation has not yet been achieved, with about 80 per cent as the upper limit thus far obtained. The evidence for the tetravalency of neodymium and dysprosium derives from several different measurements:

(1) The absorption spectrum of the lanthanides in the oxidized compounds. These data are probably the most direct evidence for the existence of Nd(IV) and Dy(IV).

*This work was sponsored by the U. S. Atomic Energy Commission. A study of the sodium-praseodymium fluoride system (5) with Dr. T. K. Keenan led directly to this investigation, and the first preparations of compounds containing Nd(IV) and Dy(IV) were made with his collaboration. Deep appreciation is expressed to Kenneth Vos and Edward Bosier for carrying out much of the laborious experimental work involved. The help of Dr. F. H. Kruse in the X-ray studies is gratefully acknowledged.

(2) The total oxidizing power of the compounds as measured by a combination of iodometry and gas evolution. This measurement shows the presence of an oxidized substance, but does not unequivocally show that this oxidizing power is due to the tetravalent lanthanide.

(3) Measurement of the weight change occurring on fluorination. Since the weight changes are relatively small, this method is rather insensitive.

(4) Magnetic susceptibility of the compounds. This method also provides direct evidence as to the oxidation state of the lanthanide in these compounds. Unfortunately, this test can be employed only in the case of dysprosium, because the difference in magnetic moment between Nd(III) and Nd(IV) is too small.

(5) X-ray structure measurements. Such measurements might prove the existence of tetravalency of the lanthanide in these compounds if sufficient data could be obtained. Unfortunately, no single crystals have been prepared, and all conclusions must be drawn from powder-pattern data.

A complicating factor in this work is the presence of what is presumably an addition compound of fluorine with cesium, the compound approximated by the formula CsF_3. (2) Unmistakable evidence for the existence of this or a similar compound in some of our preparations (at low fluorination temperatures) comes from the analytical measurement of total oxidizing power.

EXPERIMENTAL

MATERIALS

The materials used in this work were of the best quality available. The lanthanides were 99.9 per cent pure. Commercial fluorine gas from pressurized cylinders was used, and was freed from HF by passing it over sodium fluoride. Fluorolube oil* was dried with magnesium perchlorate.

FLUORINE REACTOR

Details of the fluorine reactor have been published elsewhere (3); it consists essentially of a piece of nickel pipe with provisions for evacuating and flushing with helium. Heat was supplied by a Nichrome heating element and the temperature controlled by a Wheelco controller. The temperature was measured by a chromel-alumel thermocouple in good thermal contact with the sample. The fluorine pressure was measured by a Monel Bourdon gauge.

---

*A fully fluorinated fluorocarbon, Grade S-30, sold by the Hooker Electrochemical Co.

PREPARATION OF STARTING MATERIALS

Weighed amounts of freshly ignited lanthanide oxides were added to weighed amounts of CsCl in the appropriate stoichiometric ratios, usually 3 Cs or 2 Cs per lanthanide. The mixture was dissolved in an excess of HCl and evaporated to dryness, followed by heating to ~200 °C in air. Materials prepared in this way agreed with the calculated weights within a few tenths of a per cent or less, when assumed to be Cs_3MCl_6 or Cs_2MCl_5, where *M* is a lanthanide. The dried solids were ground in a mortar, redried, and stored in a dessicator until used.

CONTAINERS

Nickel dishes were found to be unsatisfactory, since the bright red salt, Cs_2NiF_6, was always produced to a variable extent with cesium-containing starting materials. Suitable containers were prepared from single crystal calcium fluoride blanks by use of air-abrasive and wet-grinding techniques. These dishes showed no change in weight under repeated fluorinations at several atmospheres of F_2 and 400 °C temperatures, and did not react with any of the reagents employed in subsequent analyses. However, the dishes do show sensitivity to mechanical and thermal shock and must be handled with reasonable care.

FLUORINATION PROCEDURE

The dried cesium-lanthanide chlorides were weighed into the calcium fluoride containers in air. (The chlorides with 3 Cs are hydroscopic, but pick up moisture rather slowly, so that no appreciable error is introduced from this source. The di-cesium compounds are much more hydroscopic and consequently more difficult to handle.) The container containing the sample was then introduced into the fluorinator, and the system flushed with dry helium gas. The system was evacuated and heated to 100 °C. Fluorine was admitted to the desired pressure (usually 3 atm) and the temperature adjusted. After the appropriate time, the fluorinator was allowed to cool to room temperature under fluorine pressure. The fluorine was removed by displacement with helium, and the reactor was then ready to open.

HANDLING OF REACTIVE FLUORIDES

The fluorination products react very rapidly with water vapor in the air. In order to obtain accurate weights of the products, a procedure using a fully fluorinated oil was developed. The reactor was opened and the sample was withdrawn in a stream of dry helium gas. It was transferred rapidly by tongs to a previously weighed bottle containing Fluorolube oil, and the bottle was then capped. This procedure allowed no more than a few seconds exposure to the air and no evidence of reaction was observed.

Weighing to within a few tenths of a per cent accuracy can be achieved in the overall operation.

ABSORPTION SPECTRUM MEASUREMENTS

Samples treated as described above were transferred to an inert-atmosphere box. In a helium atmosphere, they were ground in Fluorolube oil in a mortar. The resulting slurry was allowed to settle into a calcium fluoride crucible with a flat top. Excess oil was removed and a quartz disc sealed on the crucible with either silicone grease or Kel-F grease. This assembly was placed in a brass cell holder for use in the Cary Model 14 spectrophotometer. Balance of the light path was achieved by use of electro-etched screens in the reference beam; the optical density of the fluorinated samples was from about two to five O.D. units. An evacuated cell holder was used for measurements at liquid nitrogen temperatures. Samples thus prepared showed little or no change over a period of several days.

CHEMICAL ANALYSIS

The analysis of these compounds proved to be difficult due to their strongly oxidizing characteristics. Two results were desired: a measure of the composition of the salt and also its oxidizing power. The weight change from the original chloride to the fluoride provided a rather insensitive measure of the composition. The total change from Cs_3NdCl_6 to Cs_3NdF_7 was about 10 per cent, and the difference between Cs_3NdF_6 and Cs_3NdF_7 was only 2.7 per cent. However, this weight, combined with a measure of oxidizing power, would provide a satisfactory analysis.

A total weight, a measure of evolved gas volume, and a total fluoride were originally chosen as sufficient tests. However, in the dissolution of the compounds with water, an oxidizing gas (starch-iodide test) was evolved, leading to consequent uncertainty both as to the composition of the evolved gas and the total fluoride analysis. Since pyrohydrolysis techniques proved very laborious and not very reproducible, this approach was abandoned.

Compounds containing Pr(IV) have been analyzed iodometrically for oxidizing power. (4) It was found in the case of the neodymium or dysprosium compounds, that it was necessary to increase the concentration and amount of KI solution. This decreased to a minimum ($\sim$ 25 per cent) the amount being reduced by water. The gas produced gave a negative test with starch-iodide paper and was assumed to be oxygen. The procedure was as follows:

The sample in the CaF_2 boat under Fluorolube oil in a weighing bottle is removed and placed in a platinum wire holder, attached to a magnet covered with Teflon. The covered magnet is held (by means of another magnet) inside a cap with a tapered joint; this may be sealed to a lower

tube by an O-ring. The lower tube contains 25 ml of saturated KI solution. When the pressure is equalized, the system is sealed by turning a stopcock. The outer magnet is then removed and the sample allowed to drop to the bottom of the KI solution. A rapid reaction ensues, with production of I_2 and gas. The system is opened after 10 minutes to a gas buret, where the evolved gas is measured and tested with starch-iodide. The KI-I_2 solution is titrated separetely with 0.05 *M* thiosulfate. The oxidizing power of the sample is considered to be the sum of that calculated from each measurement. It is difficult to prepare suitable standards to test the method, because no other available compounds appear to be such violent oxidizing agents. However, results with Pr indicate that this combined method is satisfactory.

One other uncertainty remained, that of whether any chloride ion was left. Although the total weight was an indication, a chloride analysis was carried out, in a number of cases, on the iodide solution after the thiosulfate oxidation. All iodide was oxidized to iodine by nitrite ion and acid. The iodine was removed by filtration and by solvent extraction, and the chloride was precipitated by Ag^+. The AgCl was weighed to determine the Cl^- ion.

MAGNETIC SUSCEPTIBILITY

Measurements of this type have been made in Germany by Dr. Hoppe and co-workers. They report a great deal of trouble in carrying out the measurements, due to the reactivity of the compounds and to the fact that Dy is highly paramagnetic, exceeding the optimum for their apparatus. No details of their measurements have been received. Similar measurements have been made here with an apparatus designed for these strongly paramagnetic materials.

X-RAY

A great number of powder patterns have been obtained both at Münster and in this laboratory. The detailed technique of Dr. Hoppe is not known; ours was as follows:

The samples were ground in Fluorolube oil in an inert atmosphere, the slurry transferred to X-ray capillaries, and the capillaries temporarily sealed with wax. The solids were then centrifuged to the base of the capillary and sealed off with a microtorch. Pictures were taken by means of a Philips 114.6-mm powder camera using filtered radiation with either Ilford or Type-AA Eastman film. Exposures varied from 5 to 30 hours.

RESULTS AND DISCUSSION

A great deal of the work has been carried out on the compounds with three cesiums to one lanthanide. A considerable amount of data has been

accumulated: (1) absorption spectra, (2) chemical analysis, (3) X-ray powder patterns, and (4) magnetic measurements.

(1) Some of the most definite evidence for the existence of a new oxidation state of both Nd and Dy comes from measurements of the absorption spectra of these solid oxidized compounds. While a quantitative explanation of the spectra is impossible, there is no question that *new peaks arise*, and at the same time *diminution* of the characteristic (III) peaks occur. Consideration of these data by C. K. Jørgenson of the Technical University of Denmark results in his conclusion that these peaks are indeed due to (IV) oxidation states and can be explained in no other reasonable way. The maxima and relative intensities of the peaks are tabulated in Table I.

TABLE I: MAIN ABSORPTION MAXIMA OF Nd(IV) AND Dy(IV), 25° C*

Cs_3NdF_7		Cs_3DyF_7	
λ Å	Relative Intensity	λ Å	Relative Intensity
24,000 ±	35	24,240 ± 20	100
[18,700 ± 100]	14	20,775 ± 50	5
16,160 ± 20	100	[18,700 ± 200]	18
[15,375 ± 30]	64	18,270 ± 20	25
[14,600 ± 50]	38	[17,850 ± 200]	14
12,330 ± 30	64	[17,450 ± 200]	13
11,800 ± 50	59	15,660 ± 20	10
10,800 ± 25	19	15,260 ± 40	10
8350 ± 15	14	14,440 ± 50	8
8130 ± 15	20	13,840 ± 30	16
<5200	off-scale	13,420 ± 20	13
		9450 ± 150	1
		9000 ± 20	8
		8785 ± 15	5
		8005 ± 10	7
		7925 ± 10	3
		6000	35
		5600	100
		<5500	off-scale

*[ ] denotes unresolved peaks.

Dr. A. D. Sharp of Imperial College, London, has investigated the infrared spectrum of these compounds. Although the details of his work are not available, the conclusion is reached that tetravalent lanthanides are present in these molecules.

(2) Chemical analyses of a number of these compounds show that oxidation of the lanthanide is incomplete under the various conditions used. As would reasonably be expected, there is less oxidation at the higher temperatures. The results of some typical analyses are given in Table II.

TABLE II: ANALYTICAL DATA

Temperature (°C)	% Deviation* from Calcd. wt.	% Oxidation per mole Dy	% of Original Chloride Remaining
150	+6.5†	248.2	12.2
175	−0.58	75.7	...
200	−1.25	42.7	2
300	−2.02	29.1	2
400	−2.94	21.6	...

*Based on $Cs_3DyCl_6 \xrightarrow{F_2} Cs_3DyF_1$.
†Corrected for residual chloride.

The weight changes on conversion of the chlorides to the fluoride end product are generally in good agreement with the iodine and gas-evolution analysis. At 150°C, it would seem that another phenomenon is occurring. About two and one-half times as much oxidizing power is found as would come from oxidation of (III) to (IV). Considering the behavior of CsCl when fluorinated at this temperature, it seems reasonable to ascribe this extra degree of oxidizing power to the substance CsF_3. The product must then be a mixture approximating CsF_3 and Cs_2MF_6, or possibly a compound with this ratio. Since a relatively large amount of chloride is left after fluorination, the possibility of a chloride-fluorine addition compound exists.

(3) X-ray powder methods have been used to investigate these compounds. Dr. Hoppe and his colleagues have photographed a large number of di- and tri-alkali metal fluorides. Our results agree with his for the cases of Cs_3CeF_7, Cs_3PrF_7, and Cs_3TbF_7. These compounds have the $(NH_4)_3AlF_6$ cubic structure, with lattice constants of about 10. In the case of Cs_3NdF_7 and Cs_3DyF_7, his results indicate a different structure, the $(NH_4)_3ZrF_7$ cubic structure. Our results, however, seem to show the same structure as in the Ce, Pr, and Tb compounds. There is also an appreciable difference in lattice constants between his results and ours. This disagreement may be due to varying amounts of oxidation or may be due in part to the quality of the photographs. The difference in the two structures is relatively subtle, but further work should settle the question.

(4) Magnetic-susceptibility measurements should show directly the oxidation state of the lanthanide atom in the molecule. In the case of dysprosium, Dr. Hoppe reports that he finds μ_B = 10.0-10.1. Dy(III) should have a value of 10.6 and Dy(IV) should have a value of 9.7 Bohr magnetons, indicating oxidation of about one half of the dysprosium. Our results are in agreement with Dr. Hoppe's and indicate that the dysprosium is about 50 per cent oxidized.

In addition to the evidence given above, it should be noted that the marked change in absorption spectra is a phenomenon which apparently

occurs only for the Nd and Dy compounds. Lanthanum under these conditions showed no color. X-ray measurements showed the presence of $CsLaF_4$. No change in the appearance of the cesium-holmium or cesium-gadolinium compounds upon fluorination was observed.

CONCLUSIONS

The weight of the evidence from spectral data, chemical analysis, X-ray, and magnetic measurements strongly indicates that Nd(IV) and Dy(IV) are present in these double salts prepared by fluorination. Further work is being carried out on these compounds and will be published.

REFERENCES

1. D. M. Yost, A. Russell, Jr., and C. S. Garner, *The Rare Earth Elements and Their Compounds.* New York: John Wiley and Sons, Inc., 1947. *Also*, R. C. Vickery, *The Chemistry of the Lanthanons.* New York; Academic Press, Inc., 1953. *Also*, L. B. Asprey and B. B. Cunningham, *Progress in Inorganic Chemistry*, Vol. II, F. A. Cotton (ed.). New York: Interscience Publishers, Inc., 1960.
2. H. Bode and E. Klesper, *Z. anorg. u. allg. Chem.*, 267, 97 (1951).
3. L. B. Asprey, *J. Am. Chem. Soc.*, 76, 2019 (1954).
4. L. B. Asprey and T. K. Keenan, *J. Inorg. Nucl. Chem.* In press.

PART TWO

Oxide Systems and Their Properties

THERMAL AND ELECTRONIC PROPERTIES OF RARE EARTH OXIDES*

EDGAR F. WESTRUM, JR.

Department of Chemistry, The University of Michigan, Ann Arbor, Michigan

Measurement of heat capacities at low temperatures provides one of the most powerful methods for the study of many solid-state phenomena, including energy separation and degeneracy of some of the low-lying energy levels in crystalline substances. The rare earth sesquioxides provide an especially interesting series for investigating heat-capacity anomalies occasioned by the magnetic (electronic) structures of the cations. Although the spectral and magnetic properties of many salts of the rare earth elements have been investigated, and these properties correlated with electronic structures of the rare earth ions, relatively little spectroscopic, magnetic-susceptibility, and crystal-field work has yet been reported on the oxides.

In certain instances, heat-capacity measurements may yield more direct information about electronic levels than magnetic measurements. For example, paramagnetic resonance determinations made on magnetically "concentrated" substances are sometimes difficult to interpret because of the broad absorption lines. Moreover, traces of ferromagnetic impurities do not affect calorimetric measurements in the same degree as they do susceptibility determinations. The advantage of low-temperature heat-capacity measurements in providing an insight into the energetic situation in these oxides is that the contribution of the Schottky anomaly, which accompanies the process of populating the excited energy levels, may be of the same order of magnitude as is the lattice specific heat.

While the determination of the magnetic contribution to the thermodynamics of the rare earth oxides was the prime motivation for this work, an important secondary motivation was that of gaining information concerning the variation of the lattice heat capacity within isostructural series as one lanthanide ion is replaced by another. The resolution of electronic and lattice heat capacities in all regions of the periodic table

*This research was supported in part by the Division of Research of the U.S. Atomic Energy Commission. The cryophysical study described herein has been pursued in collaboration with Bruce H. Justice.

could be aided considerably by a more secure "corresponding states theory for isostructural solids." An enhanced knowledge of the dependence of heat capacity on the atomic weight of the rare earth cations and on variation of the crystalline lattice dimensions (and hence force constants) in this series would facilitate the accurate resolution of contributions other than vibrational to the heat capacity of solids.

SCHOTTKY EFFECT

An important energy contribution in solids results from promotion of electrons to higher levels. The effect of this upon the heat capacity has been discussed by Schottky. (1) The expression for a Schottky effect can be derived from the partition function, Z.

$$Z = \Sigma g_i \exp(-E_i/RT)$$

in which g_i is the degeneracy of the energy level having molal energy E_i. The excess heat capacity associated with these excited levels is given by the expression

$$C_{exc} = \left(\frac{\partial E}{\partial T}\right)_{exc} = RT \frac{\partial^2}{\partial T^2} T \ln Z$$

or, alternatively, in terms of the fluctuation in the energy, simply as

$$C_{exc} = \frac{1}{RT^2}\left(\overline{E^2} - (\bar{E})^2\right)$$

which yields a formulation especially amenable to computer evaluations

$$C_{exc} = \frac{1}{RT^2}\left\{\frac{\Sigma E_i^2 g_i \exp(-E_i/RT)}{\Sigma g_i \exp(-E_i/RT)} - \left(\frac{\Sigma E_i g_i \exp(-E_i/RT}{\Sigma g_i \exp(-E_i/RT)}\right)^2\right\} \quad (1)$$

In the simplest case—that for which only a single excited level exists close to the ground level, and all other levels are at much higher energies—the excess heat capacity is given by

$$C_{exc} = \frac{R(E_1/RT)^2 g_0 g_1 \exp(E_1/RT)}{[g_0 \exp(E_1/RT) + g_1]^2} \quad (2)$$

If $g_0 = g_1$, the Schottky heat capacity has a maximum value of 0.872 cal/(deg mole) at $T = 0.417\ E_1/R$.

In the event that two or more excited levels are involved, the more general formulation, Eq. (1), holds. An IBM 704 digital computer was employed to generate the Schottky function best representing the experimental data.

Although Schottky anomalies are often considered to exist only in dilute paramagnetic salts where the interaction is very weak (2), a

Schottky anomaly has been found in magnetically concentrated UF_4 at 6.4°K. (3)

Schottky anomalies in "magnetically dilute" rare earth salts have already been studied by low-temperature thermal measurements. Heat capacities of three (Sm, Gd, and Nd) octahydrated rare earth sulfates were studied in the 1930's (4, 5), and more recently Meyer and Smith (6) studied the heat capacities of seven hydrated rare earth ethyl sulfates at temperatures in some portions of the range between 0.6 and 20°K.

The rare earth sesquioxides represent a distinct problem because of their more "concentrated" magnetic environment. However, the $4f$ electron shell (which is responsible for the paramagnetism of the lanthanides) remains shielded by the $5s$ and $5p$ shells, even when some valence electrons of the $6s$ and $5d$ shells have been removed in forming ions. Consequently, the effects of change in magnetic concentration and in crystalline fields are less pronounced in the lanthanides than in the magnetic transition elements. The oxides pose an advantage in that their lattice heat capacity is small compared to that of the hydrated salts. Certain properties of the rare earth sesquioxides are summarized in Table I.

TABLE I

RARE EARTH SESQUIOXIDES (M_2O_3)

At. no.	Symbol	At. wt.	Structure type	Density (g/cc)	Cell edge (7) (A)	Ground state (8)	Magn. mom. (8)
39	Y	88.92	Cub.	5.03	10.60		
57	La	138.92	Hex.	6.51		$^1S_6$	0.0
58	Ce	140.13	Hex.			$^2F_{5/2}$	2.6
59	Pr	140.92	Hex.			$^3H_4$	3.6
60	Nd	144.27	Hex.	7.24		$^4I_{9/2}$	3.7
61	Pm	147.00				$^5I_4$	2.8
62	Sm	150.35	Mono.			$^6H_{5/2}$	1.6
63	Eu	152.00	Cub.	7.42	10.84	$^7F_0$	3.4
64	Gd	157.26	Cub.	7.407	10.79	$^8S_{7/2}$	7.9
65	Tb	158.93	Cub.		10.69	$^7F_6$	9.7
66	Dy	162.51	Cub.	7.81	10.63	$^6H_{12/2}$	10.6
67	Ho	164.94	Cub.		10.58	$^5I_8$	10.6
68	Er	167.27	Cub.	8.640	10.51	$^4I_{15/2}$	9.6
69	Tm	168.94	Cub.	8.6	10.52	$^3H_6$	7.6
70	Yb	173.04	Cub.	9.2	10.41	$^2F_{7/2}$	4.5
71	Lu	174.99	Cub.		10.38	$^1S_0$	0.0
			RARE EARTH DIOXIDES				
58	Ce	140.13	Cub.	7.3		$^1S_0$	

RESOLUTION OF LATTICE AND EXCESS HEAT CAPACITY

Among the rare earth sesquioxides, both those of lanthanum and luetium have $^1S_0$ ground states, and hence their total heat capacity should be due entirely to lattice vibrations (phonon excitation). Thus the heat capacity of lanthanum oxide is used to represent the lattice contribution for the neighboring A-type (hexagonal) sesquioxides. Similarly, lutetium sesquioxide, which possesses a C-type (cubic) structure, will ultimately be used to represent a lattice heat capacity of the other rare earth sesquioxides which possess this structure (Eu to Yb). Gadolinium(III) ion has an $^8S_{7/2}$ ground state. Gadolinium sesquioxide also provides a mid-series lattice heat capacity approximation at relatively high temperature, because the crystal field acts mainly upon the orbital angular momentum of the ion and has only a small effect on levels which are compounded purely from electron spins. The heat capacity of ytterbium oxide at present appears to have small if any contribution from electronic states between 8 and 60°K, and provides an estimate of the lattice contribution in the absence of data on lutetium. With data on additional members in this series and further development of the theory of corresponding states of isostructural solids, resolution of lattice and electronic contributions will be improved.

EXPERIMENTAL

Measurements over the range 4 to 350°K were made in a calorimeter of laboratory designation W-16. Mark I helium cryostat—similar in most details to one previously described (9)—was used, and an adiabatic technique of operation was employed. Circuitry of this unit included calibrated standard cells, standard resistors, and an autocalibrated White potentiometer. Duration of the energy input was determined with a calibrated tuning fork. All electrical, mass, and time measurements were referred to standard devices calibrated at the National Bureau of Standards.

The platinum resistance thermometer (laboratory designation A-3) was calibrated above 10°K by the Bureau of Standards. Below this temperature a provisional scale was adopted.

The rare earth oxides were of 99.9 per cent or higher purity, with certified spectrochemical analyses. Calorimetric samples of about 150 to 180 g were used. They were fired to constant weight in air at about 900°C and were loaded into the calorimeter in the anhydrous nitrogen atmosphere of a dry box. Helium gas at a fraction of an atmosphere was added to facilitate achievement of thermal equilibrium. Because the samples were finely divided (200 mesh), they tended to adsorb this conduction helium strongly as the temperature was decreased toward 4°K. This made the time required for the achievement of thermal equilibrium long and precluded heat-capacity determinations much below 8°K.

RESULTS

At the present time, measurements on the heat capacities of neodymium, lanthanum, samarium, gadolinium, dysprosium, holmium, erbium, and ytterbium sesquioxides have been completed by Bruce Justice and the author, at the University of Michigan, over the range 8 to 350°K. Measurements on yttrium, neodymium, and lanthanum oxides over a more limited range have been reported from Ohio State University. (10) Data on lanthanum oxide from the Bureau of Mines experimental station in Berkeley exist. (11) Data on cerium dioxide also exist. (12)

The heat-capacity data of the present investigation are considered to have a probable error less than 0.1 per cent above 15°K. The experimental determinations are presented in Fig. 1, 2, and 3, with the low temperature portions plotted against an expanded scale.

Resolution of the electronic and lattice contributions will be discussed for each lattice type.

HEXAGONAL (A-TYPE) OXIDES

Interest in the neodymium oxide problem was stimulated by the determination of the heat capacity of neodymium oxide from 18 to 300°K by Professor David White *et al.* (10, 13) The trend of the relatively high heat capacity of neodymium oxide below 30°K suggested the possibility of an anomaly at lower temperatures. Re-examination of the heat capacity from 4 to 16°K revealed a distinct Schottky anomaly, with an excess heat-capacity maximum at about 16°K. The experimental results of this investigation are shown in Fig. 1. Our data are at considerable variance with those reported by Goldstein *et al.* (10) over the higher temperature range, and also differ somewhat from those of Kelley *et al.* (11)

Moreover, early attempts to resolve the lattice heat capacity, using the data reported on lanthanum oxide (10), extending down to about 16°K, proved unsatisfactory, and we therefore independently redetermined the heat capacity of lanthanum sesquioxide in order to make a better evaluation of the lattice contribution.

The failure of different laboratories to reproduce heat capacities on a given substance is a well-known phenomenon. Confidence in the reliability of the present results is predicated upon the determination of the heat capacity of the Calorimetry Conference sample of benzoic acid (14) and the comparison of those data with that of other established laboratories. It is to be noted, however, that systematic errors in the evaluation of the electronic heat capacity (ΔC_p) will be very largely minimized by the fact that all of the data compared herein (with a single exception) are on samples of very nearly similar size, in the same cryogenic apparatus, using a single temperature scale and one electrical calibration.

The difference between the heat capacities of Nd_2O_3 and of isostructural La_2O_3, from the present investigation, exclusively yields an electronic heat capacity, shown by the experimental data points in Fig. 4, in calories per gram ion of neodymium. The use of the isostructural, diamagnetic La_2O_3 to represent the lattice heat capacity of Nd_2O_3 involves atomic masses differing by only 4 per cent and interatomic distances differing by only 5 per cent.

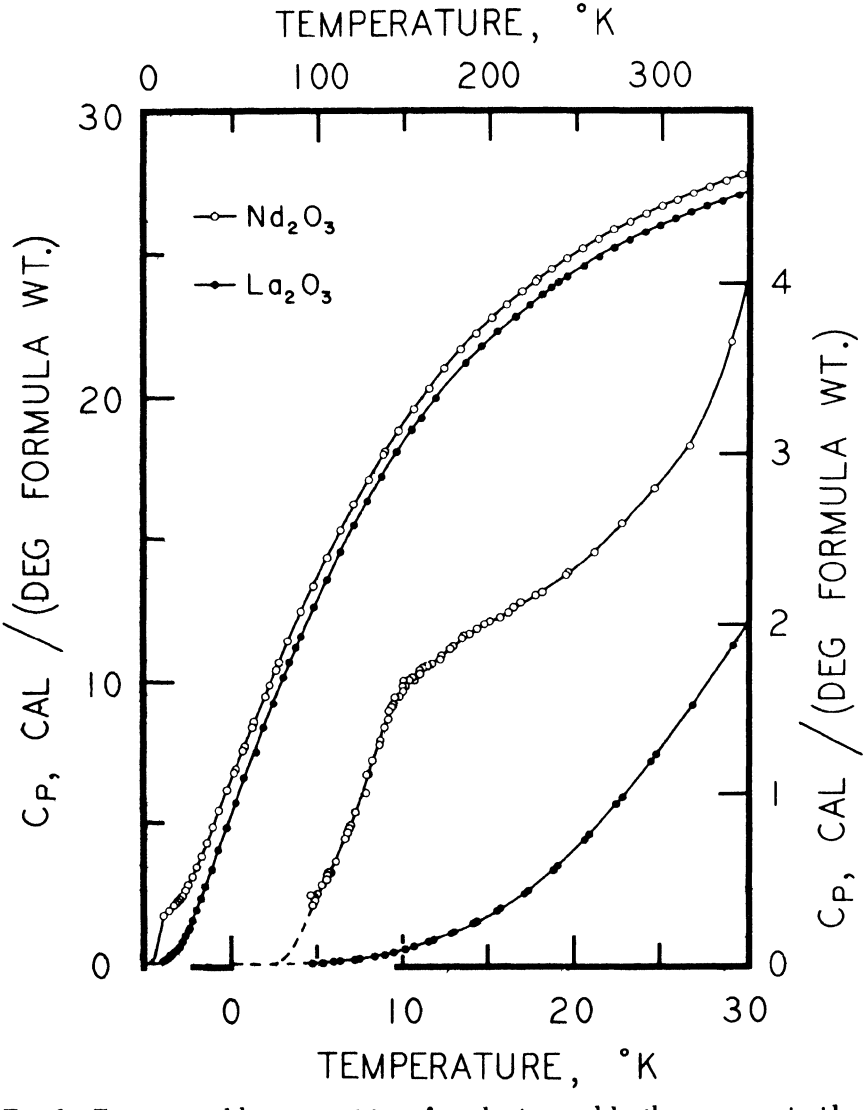


Fig. 1. Experimental heat capacities of neodymium and lanthanum sesquioxides.

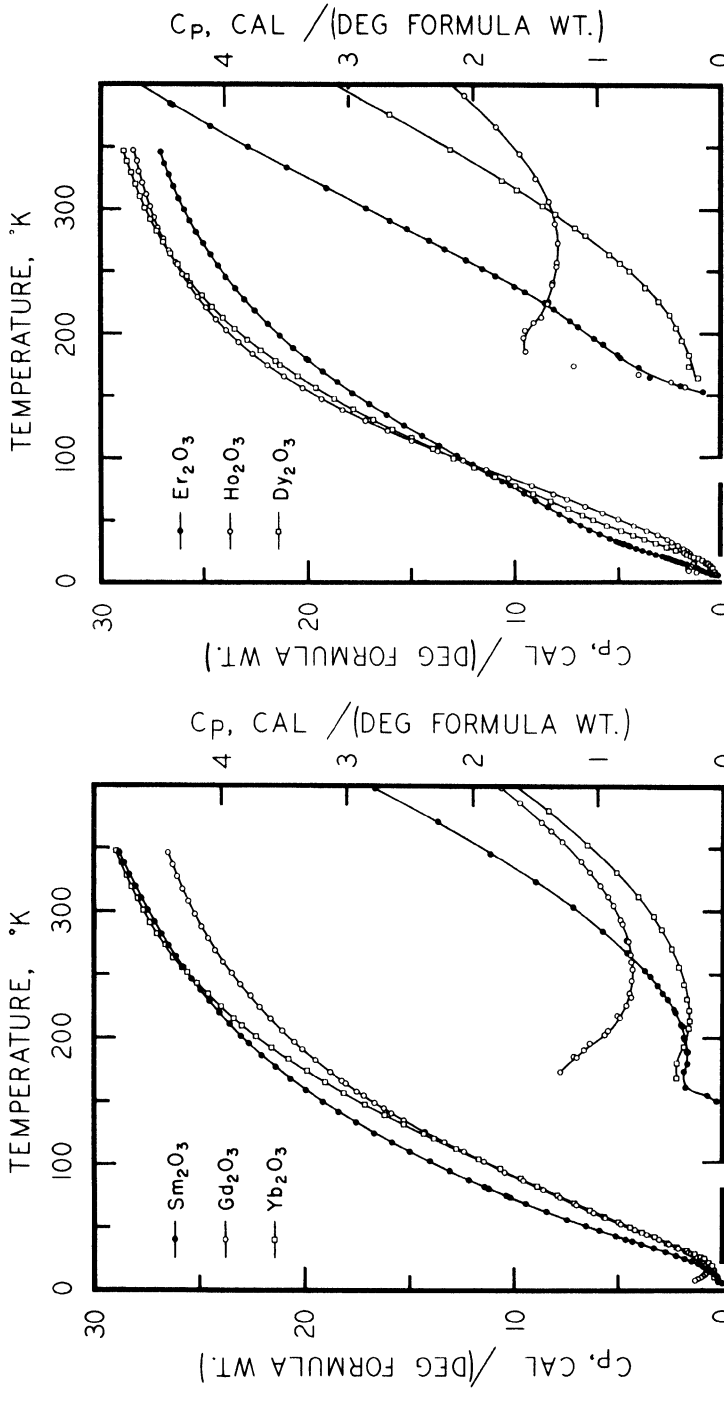


Fig. 2. Experimental heat capacities of samarium, gadolinium, and ytterbium sesquioxides.

Fig. 3. Experimental heat capacities of erbium, holmium, and dysprosium sesquioxides.

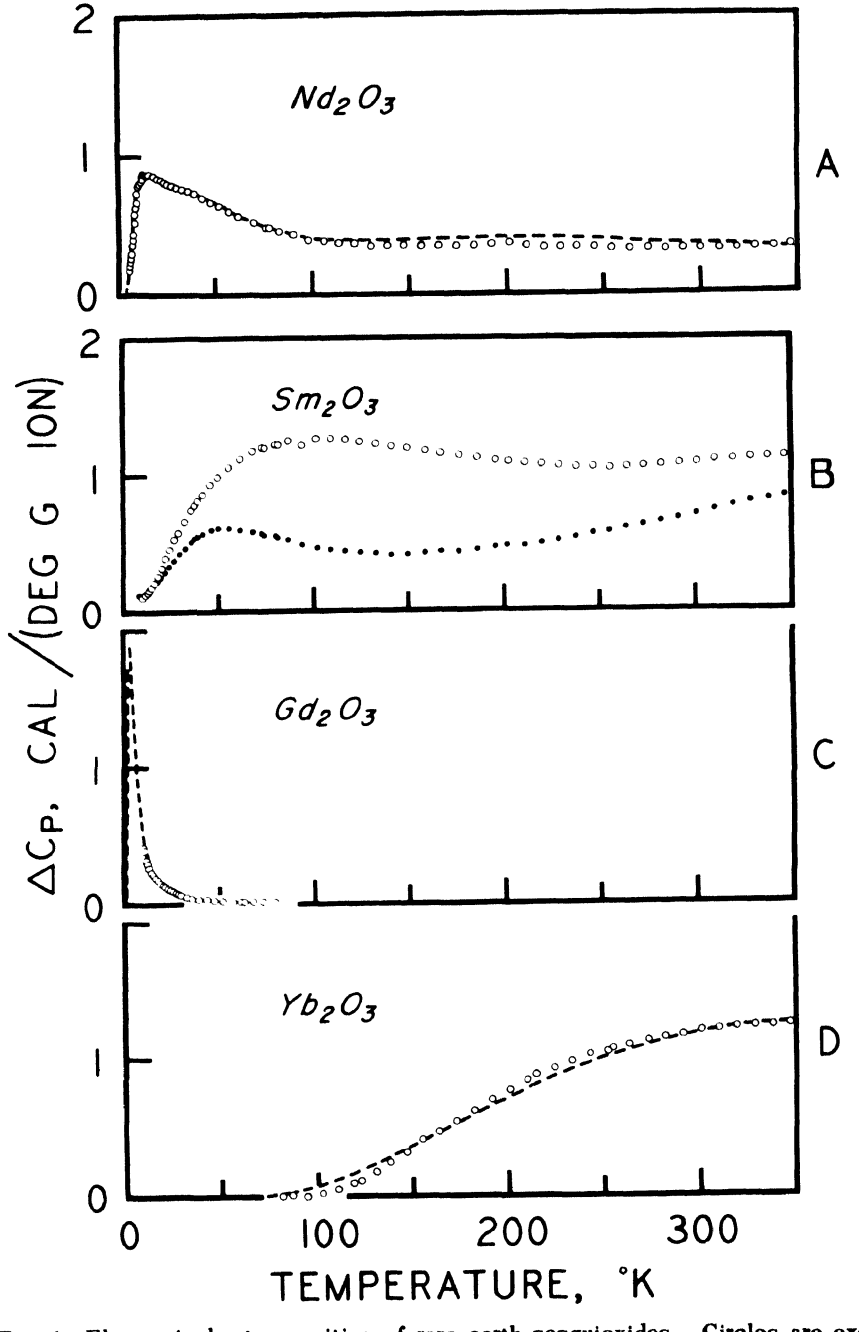


Fig. 4. Electronic heat capacities of rare earth sesquioxides. Circles are experimental determinations; dashed curve represents calculated fit.

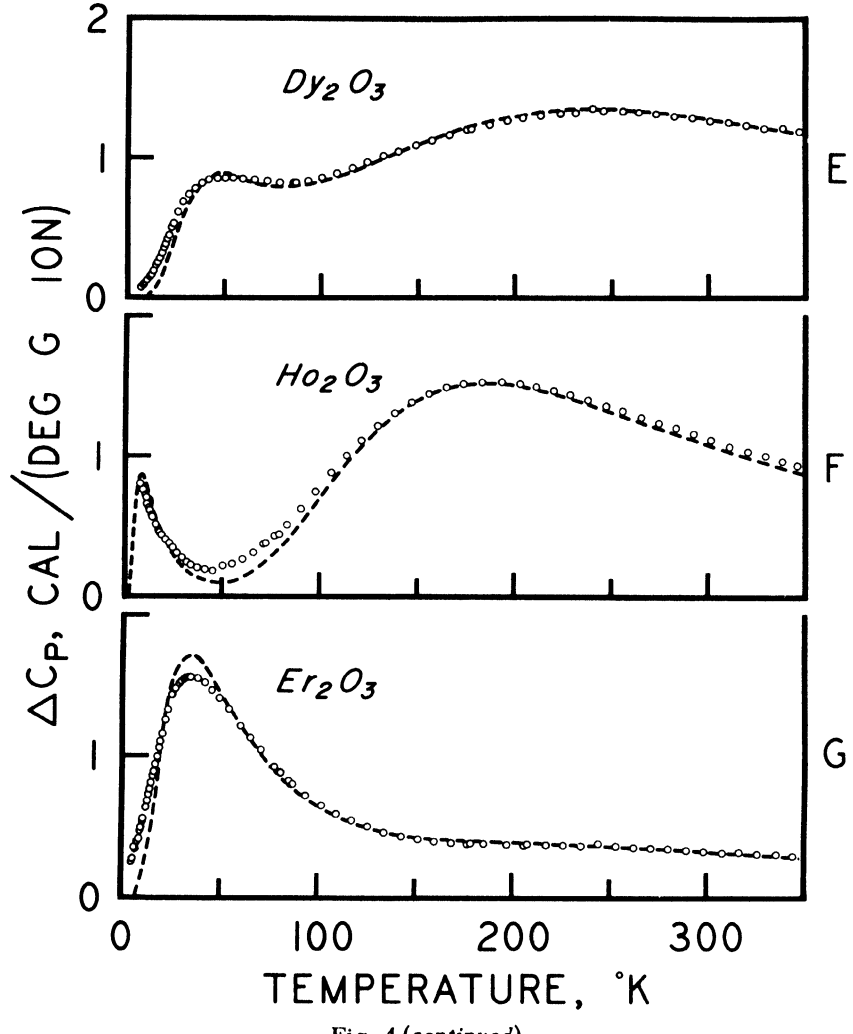


Fig. 4 (*continued*)

Considering the ground state of neodymium (III) to be $^4I_{9/2}$ and Kramer's rule to be operative, one might expect to find four doubly degenerate levels above the crystalline ground state. This has been confirmed in other salts of neodymium (III). In $Nd(BrO_3)_3 \cdot 9\ H_2O$ levels exist at 115, 184, 363, and 382 cm^{-1} (15); likewise, in the octahydrated sulfate, levels exist at 76, 226, 263, and 301 cm^{-1}. (16) The dashed curve represents Schottky effects, with excited levels at 59, 229, and 1150 cal (1 cm^{-1} = 2.86 cal) and all levels (including the ground state) doubly degenerate. The agreement appears to be excellent.

Thermodynamic functions of neodymium sesquioxide (derived from our heat capacity data by an IBM 704 program) at 298.15°K are as follows: entropy increment [$S° - S_5°_K° = 35.05$ cal/(deg mole)], enthalpy increment ($H° - H_5°_K° = 4989$ cal/mole), and free-energy function [$(F° - H_5°_K°)/T = -18.31$ cal/(deg mole)]. The probable error is estimated to be less than 0.1 per cent. The effects of nuclear spin and isotopic mixing are not included in the entropy and free-energy function. The entropy at 298.15°K is 1.7 e.u. lower than the Goldstein *et al.* figure. (10) The molal excess or magnetic entropy over the measured range at 298.15°K is 4.6 e.u. which is still somewhat less than the spin-only value, $2R \ln (2S + 1) = 5.50$ e.u.

The heat capacity of lanthanum sesquioxide is a typically sigmoid curve (as may be seen in Fig. 1), shows no anomalies, and has no electronic contributions.

MONOCLINIC (B-TYPE) SESQUIOXIDES

The heat capacity of samarium sesquioxide has not previously been reported. Accurate heat-capacity measurements could not be made below 8°K because the sample adsorbed the conduction helium gas within the calorimeter. X-ray diffraction on the calorimetric sample confirmed the monoclinic structure of this sample. (17, 18) At the present time no data on the lattice contribution of a B-type structure exist. In Fig. 4, the ΔC_p has been computed by deducting the heat capacity of lanthanum sesquioxide (solid dots) and that of the ytterbium-gadolinium sesquioxide lattice (open circles). Obviously neither is an adequate representation of the contribution of a monoclinic lattice.

CUBIC (C-TYPE) SESQUIOXIDES

Calorimetric samples of gadolinium, dysprosium, holmium, erbium, and ytterbium sesquioxides all revealed cubic (C-type) diffraction patterns. (17) The excess heat capacities are shown in Fig. 4 on the basis previously described. The excess heat capacity may, therefore, be slightly revised when data on lutetium oxide become available. Tentative energy levels and statistical weights for the theoretical (dashed) curves in this figure are collected in Table II.

OTHER RARE EARTH OXIDES

The heat capacity of cerium dioxide has also been measured from 4 to 350°K (12) and found to be typically sigmoid in its heat-capacity behavior. The values of the entropy, enthalpy increment, and free-energy function are 14.73 cal/(deg mole), 2478 cal/mole, and 6.58 cal/(deg mole), respectively, at 298.15°K.

TABLE II. TENTATIVE ENERGY LEVELS FOR CUBIC (C-TYPE) OXIDES

Rare earth ion	Level (i)	Statistical wt. (g_i)	Energy level in cal/(g ion) (E_i)
Gd (III)	0	2	0
	1	4	~17
	2	2	27
Dy (III)	0	2	0
	1	2	215
	2	4	1040
	3	4	2060
Ho (III)	0	1	0
	1	1	40
	2	4	1000
Er (III)	0	2	0
	1	4	165
	2	2	350
	3	2	1400
Yb (III)	0	2	0
	1	2	1450
	2	2	2900

Measurements on five other rare earth sesquioxides (praseodymium, terbium, europium, thulium, and lutetium) over the same temperature range are in progress in this laboratory.

In addition, it is planned to extend the measurements on important rare earth sesquioxides below 4°K by employing flame-fused oxides. Magnetic transitions, some possibly co-operative, have been reported in Er_2O_3 at 4.3°K and Ho_2O_3 at 6°K (19) and in Yb_2O_3 at 3°K. (20)

REFERENCES

1. W. Schottky, *Physik. Z.*, **23**, 448 (1922).
2. For example, K. Mendelssohn, *Cryophysics*. New York: Interscience Publishers, Inc., 1960.
3. J. H. Burns, D. W. Osborne, and E. F. Westrum, Jr., *J. Chem. Phys.*, **33**, 387 (1960).
4. J. E. Ahlberg, E. R. Blanchard, and W. O. Lundberg, *ibid.*, **5**, 539 (1937); *ibid.*, 552.
5. W. F. Giauque and C. W. Clark, *J. Am. Chem. Soc.*, **54**, 3135 (1932); J. E. Ahlberg and C. W. Clark, *ibid.*, **57**, 437 (1935).
6. H. Meyer and P. L. Smith, *J. Phys. Chem. Solids*, **9**, 285 (1959).
7. H. Bommer, *Z. anorg. allgem. Chem.*, **241**, 273 (1939).
8. J. H. Van Vleck, *The Theory of Electric and Magnetic Susceptibilities*. England: Oxford University Press, 1932.

9. E. F. Westrum, Jr., J. B. Hatcher, and D. W. Osborne, *J. Chem. Phys.*, **21**, 419 (1953).
10. H. W. Goldstein *et al.*, *J. Phys. Chem.*, **63**, 1445 (1959).
11. Dr. K. K. Kelley. Private communication.
12. E. F. Westrum, Jr., and A. F. Beale, Jr., *J. Chem. Phys.* (Feb. 1961).
13. Professor D. White. Private communication.
14. G. T. Furukawa, R. E. McCoskey, and G. J. King, *J. Res. Natl. Bur. Stds.*, **47**, 256 (1951).
15. R. A. Satten, *J. Chem. Phys.*, **21**, 639 (1953).
16. R. A. Satten and D. J. Young, *ibid.*, **23**, 404 (1955).
17. R. S. Roth and S. J. Schneider, *J. Res. Natl. Bur. Stds.*, **64**, 309 (1960).
18. R. M. Douglass and E. Staritzky, *Anal. Chem.*, **28**, 552 (1956).
19. Dr. W. C. Koehler. Private communication.
20. Dr. W. E. Henry. Private communication.

STRUCTURE AND MAGNETIC PROPERTIES OF PEROVSKITES

AARON WOLD

*Lincoln Laboratory, Massachusetts Institute of Technology, Cambridge, Massachusetts**

The principal effects responsible for the crystal structure of rare earth-transition-metal perovskites (ABO_3), ionic size and electronic ordering, are discussed. The further relationship between these two effects and the magnetic properties of several perovskite systems is described.

Extreme purity of the rare earth constituents is found to have important effects on the phenomenon of parasitic ferromagnetism in perovskites, which indicates the desirability of re-examination of previous investigations. The perovskite compounds which will be considered in this paper have the chemical formula ABO_3, where A represents a trivalent ion which is co-ordinated with twelve oxygens and B a transition-metal ion co-ordinated to six oxygens. The primarily ionic perovskites exhibit several interesting physical properties, such as ferroelectricity (as in $BaTiO_3$) and ferromagnetism [as in (La, Ca)MnO_3]. Only the ferroelectric properties have been extensively explored for possible practical applications. The relatively large conductivity associated with ferromagnetic perovskites and the lack of long-range ionic order in ferrimagnetic perovskites has discouraged practical exploitation of their magnetic properties. However, the perovskite-type structure is ideal for an investigation of cation-anion-cation interactions, since no other competing interactions are present. The important of these interactions in many magnetic oxides has motivated a number of important studies concerning the influence of chemistry on the magnetic properties of perovskites.

In the discussion of the crystallographic and magnetic properties of ionic perovskites that follows, an attempt will be made to correlate the distortions caused by outer-electron configurations and relative ionic-

*Lincoln Laboratory is operated with support from the U.S. Army, Navy, and Air Force. The author would like to thank Dr. J. B. Goodenough, whose ideas on magnetic interactions have been the basis of our researches on perovskites at Lincoln Laboratory. In addition he would like to acknowledge experimental assistance from R. J. Arnott, R. Germann, and E. Delaney, and helpful discussions with K. Dwight and N. Menyuk.

size effects with the magnetic properties. Although these distortions represent only a perturbation superposed on the ideal structure, they are of sufficient magnitude to be of interest both for the theory of magnetic interactions and for their role in the phenomenon of parasitic ferromagnetism.

IONIC-SIZE EFFECTS

Early investigators have shown that a definite relationship exists between the size of the ionic radii A, B, and O and the formation of the cubic perovskite, or slightly deformed variants. The Goldschmidt (1) formula has been used to determine whether or not an ABO_3 compound is capable of perovskite formation. In order to obtain a perovskite, the relative sizes of the ions have to satisfy the following equation: $R_A + R_O = t\sqrt{2}(R_B + R_O)$ where R equals the ionic radius and $0.8 < t < 1.0$. It has been observed that the ideal perovskite-type structure is seldom realized in nature. Megaw (2) has noted that perovskites having a tolerance factor of $0.8 < t < 0.9$ show a co-operative buckling and enlargement of the unit cell. If $t > 0.9$ there appears to be no enlargement of the unit cell. However, Yakel (3) was unable to find such a convenient correlation among the magnetic perovskites. Wood (4) proposed a method for classifying perovskites in which a graph having R_A as ordinate and R_B as abscissa is plotted. The compounds are then located at points on the graph. Each type of structure appears as an enclosed area on the plot. Most of the compounds considered to have a perovskite-like structure fall within the required range when examined by Wood's method.

The distortions present in rare earth-transition-metal perovskites were classified by Geller and Gilleo (5-10) into two groups. Most of them are orthorhombic and belong to space group $D_{2h}(16)$-$Pbmn$, with four distorted perovskite units in the true crystallographic cell; others are rhombohedral and belong to space group $D_{3d}(5)$-$R\bar{3}m$ with two formula weights per unit cell. Geller has indicated that perovskite oxides containing V^{+3}, Cr^{+3}, Mn^{+3}, and Fe^{+3} are orthorhombic, whereas Co^{+3} and Al^{+3} are rhombohedral. Geller (10) found it necessary to re-estimate the radii of the trivalent A and B ions in perovskite lattices, and there are significant differences between these and sets of radii not so derived. The radii of V^{+3}, Cr^{+3}, Mn^{+3}, and Fe^{+3} range from 0.61 to 0.63, whereas Co^{+3} and Al^{+3} have radii of approximately 0.56 A. Thus it is implied that the difference in distortion is the result of a difference in size of the transition-element cation.

LIGAND-FIELD (JAHN-TELLER) EFFECTS

The orthorhombic distortion from cubic symmetry observed for pure $LaMnO_3$ is larger than that for the other orthorhombic perovskites. The

distinguishing feature of this distortion is that $c/\sqrt{2} < a \leq b$, whereas the compounds isostructural with $GdFeO_3$ have $a < c/\sqrt{2} < b$. Both structures can be indexed with space group $D_{2h}(16)$-*Pbnm*. In order to distinguish between these two types of orthorhombic perovskites, Goodenough (11) has designated them by the symbols O' and O, respectively. The larger distortion observed in pure $LaMnO_3$ is due to superposition of a co-operative electronic ordering of the Mn^{+3} empty $d_{x^2-y^2}$ orbitals (shown in Fig. 1 opposite) on the ionic size distortion responsible for the O structure. This ordering results in the formation of $3d^4$ cations with half-filled e_g orbitals along the z-axis and empty e_g orbitals directed along the x- and y-axis. Therefore, the Mn^{+3}-Mn^{+3} interactions within the c-plane are ferromagnetic; those connecting adjacent planes are antiferromagnetic. The net tetragonal distortion that occurs as a result of this ordering is sufficient to transform a lattice with orthorhombic symmetry $O(a < c/\sqrt{2})$ to $O'(c/\sqrt{2} < a \leq b)$. Wold and Arnott (12) have demonstrated experimentally the relative influence of the ionic-size and ligand-field effects in $LaMnO_{3+\lambda}$.

An examination (13) of the system $(LaM^{+2})MnO_3$ shows that the amount of Mn^{+4} required to eliminate the co-operative distortion decreases as the size of the A cation is increased, or the magnitude of the O "pucker" decreases. This indicates that the O' structure is the result of a superposition of electron-ordering and ionic-size distortions. Em-

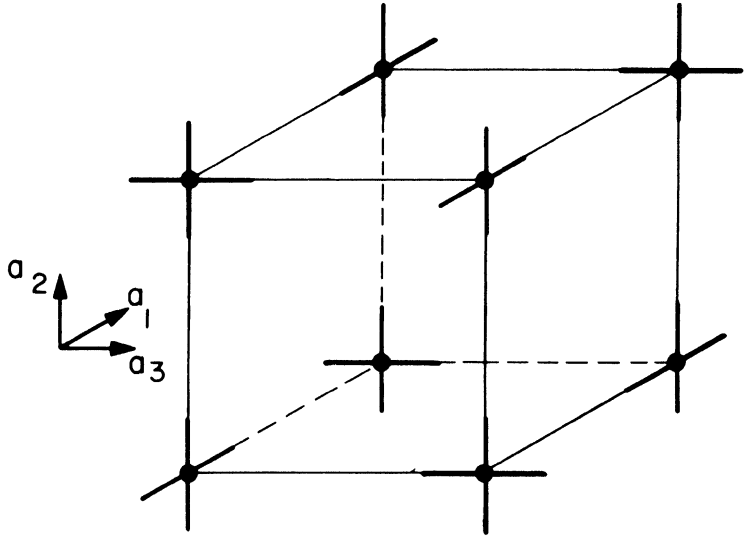


Fig. 1. Simple-cubic array of transition-element ions in perovskite-type lattice showing the orientations of empty $d_{x^2-y^2}$ orbitals responsible for (a) orthorhombic symmetry.

pirically, rhombohedral symmetry seems to inhibit co-operative Jahn-Teller distortions, which is in agreement with experimental evidence.

The introduction of ions such as Mn^{+4}, Cr^{+3}, Co^{+3}, and Ti^{+4}, which have empty d_{z^2} and $d_{x^2-y^2}$ orbitals on octahedral sites, reduces the number of ions which are available to participate in the distorting mechanism. Consequently, the magnitude of the distortion and the temperature of this transition from orthorhombic to rhombohedral symmetry are expected to decrease with increasing concentration of foreign ions, as found experimentally. (12)

In order to interpret the magnetic data for a number of substituted manganese perovskite systems, Goodenough (11) has proposed several rules for the magnetic interactions present. In case one, the cations on opposite sides of the anion each have a half-filled e_g orbital. Maximum stability is achieved if the cations are coupled antiferromagnetically through the pair of electrons present in the anion p orbital. Where the cation on opposite sides of the anion each have empty e_g orbitals, a weak antiferromagnetic coupling results. In case three, the cations on opposite sides of the anion have empty e_g and half-filled e_g orbitals, respectively, so that simultaneous stabilization is achieved by ferromagnetic order.

Mn^{+3}, with an electron configuration of $3d^4$, shows a large Jahn-Teller distortion of its interstice to tetragonal symmetry. Co-operative distortions transform structure O to O'. When the energy involved is large enough to override the thermal energy of lattice vibrations, a long range order of the tetragonal distortion can occur, which induces an ordering of the $x^2 - y^2$ orbitals (effect A). This co-operative electronic ordering results in ferromagnetic $Mn^{+3} - Mn^{+3}$ interactions within the c-plane and antiferromagnetic $Mn^{+3} - Mn^{+3}$ interactions connecting adjacent planes.

Moreover, even when the Jahn-Teller energy is insufficient to override the lattice vibrations, it will significantly favor those vibrational modes of the oxygen ions which preserve tetragonal symmetry around each cation site. As the oxygen ions vibrate, the tetragonal axis will shift back and forth, subject only to the condition that nearest neighbors cannot have paralled c axes. Thus part of the time the instantaneous electron configuration of any two nearest neighbors will be that of case two (empty e_g orbitals on opposite sides of the anion); the rest of the time it will have a configuration corresponding to case three. Since the case three interaction is stronger than that of case two, the time-average interaction between any nearest neighbor pair will be ferromagnetic (effect B). If only one of the two interacting cations is $3d^4$, then there can be no synchronization of orbital occupancies. The Mn^{+3} orbital

involved in the interaction is partially occupied on a time-average basis, and the net interaction corresponds to having the Mn^{+3} orbital occupied because of the relative strength of the possible interactions (effect C).

The introduction of sufficient ions to destroy the O' structure of pure $LaMnO_3$ gives rise to ferromagnetism. Low-spin-state Co^{+3} and Ti^{+4} are diamagnetic, and the ferromagnetism arises from the $Mn^{+3} - Mn^{+3}$ interactions (effect B). In the system (La, Ca)MnO_3 there exists a rhombohedral ferromagnetic phase over the range of compositions 21-50 per cent Mn^{+4}. In this range, $Mn^{+3} - Mn^{+4}$ interactions, as well as the $Mn^{+3} - Mn^{+3}$, are ferromagnetic (effects B, C), and antiferromagnetic $Mn^{+4} - Mn^{+4}$ interactions do not occur. Here, electrostatic forces maintain short-range correlation between the Mn^{+4} ions, so that Mn^{+4} ions are rarely nearest neighbors, and only electronic order being involved.

Examination of the system La(Mn, Cr)O_3, where Cr^{+3} ($3d^3$) has an outer-electron configuration similar to that of Mn^{+4}, gives additional confirmation of these conclusions. The $Mn^{+3} - Cr^{+3}$ and $Mn^{+3} - Mn^{+3}$ interactions are ferromagnetic if there is no e_g electron ordering in Mn^{+3} (effects B, C). The antiferromagnetic $Cr^{+3} - Cr^{+3}$ interactions, which are randomly present throughout the material, give rise to ferrimagnetism without long-range magnetic order. (14)

It is interesting to note that, in contrast to these ferromagnetic or ferrimagnetic systems, La(Mn, Fe)O_3 remains antiferromagnetic. Since Fe^{+3} has the electronic configuration $t_{2g}^3 e_g^2$, it would be expected to couple antiferromagnetically both with Mn^{+3} and with other Fe^{+3} ions. Any tendency to form a ferromagnetic couple would be offset by the stronger antiferromagnetic interactions.

Preliminary measurements (Table I) on the system La(Mn, Ga)O_3 show a net magnetic moment in the highly distorted orthorhombic phase,

TABLE I: SUMMARY OF CRYSTALLOGRAPHIC AND MAGNETIC PROPERTIES OF THE SYSTEM $LaMn_xGa_{1-x}O_3$

	Monoclinic (pseudocubic)					
Composition	μ/metal atom	$a_1 = a_3$	a_2	β	V	$\sqrt[3]{V}$
$LaGaO_3$	0	7.792	7.788	90.3°	472.8	7.760
$LaGa_{0.75}Mn_{0.25}O_3$	0.74				472.2	7.787 ± .01
$LaGa_6Mn_4O_3$	1.27				476.7	7.809 ± .005
$LaGa_{0.5}Mn_{0.5}O_3$	1.55				476.6	7.881 ± .004
$LaGa_{0.4}Mn_6O_3$	1.58	7.845	7.786	90°26'	479.7	7.826
$LaGa_{0.25}Mn_{0.75}O_3$	1.01	7.888	7.749	90°1'	482.1	7.841
$LaGa_{0.1}Mn_{0.9}O_3$	0.42	7.927	7.712	91°30'	484.4	7.854
$LaMnO_3$	0	7.960	7.694	91°56'	487.7	7.869

which extends to approximately 50 atomic per cent gallium. This is equivalent to what would be predicted if the gallium atoms ordered into alternate Mn^{+3} planes of the antiferromagnetic O' structure. The report by Jonker (13) that the system La(Mn, Al)O_3 is nonmagnetic would be consistent with this discussion if the samples investigated had the O' structure and there was no ordering of the Al^{+3} ions.

Available magnetic and neutron diffraction data of $LaNiO_3$ indicate that Ni^{+3} is in a low-spin state. Low-spin-state Ni^{+3} would have one outer e_g electron, and Jahn-Teller stabilizations are anticipated. The one e_g electron of low-spin-state Ni should give rise to ferromagnetic $Ni^{+3} - Mn^{+3}$ and $Ni^{+3} - Ni^{+3}$ interactions (effect B), which is compatible with the ferromagnetism of the system La(Mn, Ni)O_3 reported by Wold, Arnott, and Goodenough. (15) However, stoichiometric $LaNiO_3$ is also rhombohedral, but is not ferromagnetic. This fact indicates that additional factors may be necessary for the interpretation of low-spin-state Ni^{+3} interactions.

PARASITIC FERROMAGNETISM

Parasitic ferromagnetism has been observed in perovskites. Early studies (16) of their magnetic properties established the fact that the magnetization varied for high fields ($H > 6000$ *oe*) according to the expression $\sigma = \sigma_0 + \chi H$. The constant is called the parasitic ferromagnetism, and χ is the susceptibility. The cause of parasitic ferromagnetism in the perovskites has not yet been established. Bozorth (17) has suggested that the parasitic ferromagnetism is caused by small deflections of the *B*-cation moments from a uniaxial direction. This was first proposed by Dzialoshinakii (18) for some antiferromagnetic fluorides. These deflections could be induced in the orthorhombic perovskites by the crystalline fields associated with the puckering of the orthorhombic structure. From a detailed knowledge of that structure, it is possible to write down the direction of the parasitic magnetization to be associated with a given type of magnetic order and spin axis for the nearly antiferromagnetic *B*-cation sublattice. At low temperatures, interactions between paramagnetic rare earth cations and the Fe^{+3} sublattice may induce significant parasitic magnetization. Neel (19) has pointed out that preferential ordering of lattice defects or impurities into one of the magnetic sublattices of an antiferromagnet can give rise to a weak ferrimagnetism.

Wold and Menyuk (20) have observed that the parasitic magnetization found in $LaFeO_3$ can be reduced by two orders of magnitude by careful preparation of stoichiometric, but more completely reacted, materials. Evidently, extreme purity of the rare earth constituent is necessary be-

fore any significant measurements can be made. Furthermore, this fact indicates the desirability of re-examining previous investigations where careful analyses of the reacting materials and end products were not reported.

REFERENCES

1. V. M. Goldschmidt, *Geochem. Verteilungs*, 7, 8 (1927–8).
2. H. D. Megaw, *Proc. Phys. Soc.* (London), **58**, 133 (1946).
3. H. L. Yakel, *Acta Cryst.*, **8**, 394 (1955).
4. E. A. Wood, *ibid.*, **4**, 353 (1951).
5. S. Geller, *J. Chem. Phys.*, **24**, 1236 (1956).
6. S. Geller and E. A. Wood, *Acta Cryst.*, 9, 563 (1956).
7. S. Geller, *ibid.*, **11**, 565 (1956).
8. S. Geller and V. B. Gala, *ibid.*, 9, 1019 (1956).
9. M. A. Gilleo, *ibid.*, **10**, 161 (1957).
10. S. Geller, *ibid.*, **10**, 243 (1957).
11. J. B. Goodenough. To be published.
12. A. Wold and R. J. Arnott, *J. Phys. Chem. Solids*, 9, 176 (1959).
13. G. H. Jonker, *Physica*, 22, 707-722 (1956).
14. U. H. Bents, *Phys. Rev.*, **106**, 225 (1957).
15. A. Wold, R. J. Arnott, and J. B. Goodenough, *J. Appl. Phys.*, 29, 387 (1958).
16. R. Pauthenet and P. Blum, *C. R. Acad. Sci.*, **239**, 33 (1954).
17. R. M. Bozorth, *Phys. Rev. Letters*, **1**, 362 (1958).
18. I. E. Dzialoshinskii, *J. Exptl. Theoret. Phys.* (USSR), 32, 1547 and 33, 1454 (1957) [trans., *Soviet Phys.*, JETP **6**, 1120 and 1259 (1957)].
19. L. Neel, *C. R. Acad. Sci.*, 239, 8 (1954).
20. A. Wold and N. Menyuk. Unpublished research, MIT Lincoln Laboratory.

PHASE-EQUILIBRIA RESEARCH IN SYSTEMS INVOLVING THE RARE EARTH OXIDES

ROBERT S. ROTH

National Bureau of Standards, Washington, D. C.

Phase equilibrium investigations have been conducted at the National Bureau of Standards in the past few years on systems involving many of the rare earth oxides, including the chemically similar La_2O_3, Y_2O_3, Sc_2O_3, and In_2O_3. Two papers on investigations of the rare earth oxides have been previously published under similar title.(1, 2) The first of these is subtitled "Polymorphism of the Oxides of the Trivalent Rare Earth Ions," and the second, "Solid State Reactions in Systems Involving Oxides of the Trivalent Rare Earth Ions." A third paper, "The Eu_2O_3–In_2O_3 System," has been submitted for publication. (3)

The present paper is a review of the unpublished phase-equilibria research at present being conducted at the National Bureau of Standards on systems involving rare earth oxides with (1) oxides of other trivalent ions, (2) Nb_2O_5 or Ta_2O_5, and (3) B_2O_3. More complete experimental details will be published in papers which are being prepared or have been submitted to various journals.

The investigations described in the present discussion are the result of a group effort. S. J. Schneider has conducted most of the work on systems containing only trivalent oxides. The reactions with Nb_2O_5 have been studied by R. S. Roth. P. H. Fang has contributed all of the electrical and magnetic measurements. J. Waring has done much of the specimen preparation and heat treatment in many of the systems, and E. M. Levin has conducted the studies on the borates.

PHASE EQUILIBRIA IN SYSTEMS INVOLVING OXIDES OF THE TRIVALENT RARE EARTH IONS WITH OXIDES OF OTHER TRIVALENT IONS

A considerable amount of data has been accumulated in this laboratory on the phase relations of various systems involving the rare earth oxides and other trivalent oxides. Fig. 1 (*a–e*) summarizes the present state of knowledge of the solid-state phase relationships for binary systems of the oxides of the trivalent rare earth ions and Al_2O_3, Ga_2O_3, Cr_2O_3, Fe_2O_3, Sc_2O_3, and In_2O_3. (4) The diagrams in Fig. 1 are arranged in order of the ionic radii of the constituent cations.

An unexpected result of the present work was to cast doubt on the equilibrium relationships of the Y_2O_3-Al_2O_3 phase diagram. It now appears that the $YAlO_3$ perovskite (and possibly also $HoAlO_3$ and $ErAlO_3$) is actually a stable compound above about 1800°C and has a minimum decomposition temperature below which it transforms to garnet and the 2:1 compound. This interpretation is not inconsistent with any of the published experimental data on the Y_2O_3-Al_2O_3 system. (5, 6, 7) The perovskite $YAlO_3$ can form metastably at relatively low temperatures, but when held for a reasonably long period of time below about 1800°C, and quickly cooled, the perovskite is observed to decompose gradually to the other stable phases. However, when held above about 1800–1850°C and quenched or rapidly cooled, a single-phase perovskite has been observed. If slowly cooled from this temperature range, or reheated and quenched from 1700–1750°C or below, the specimen again shows more than one phase. The Y_2O_3-Al_2O_3 phase diagram is therefore being restudied in detail.

The 3:1 R_2O_3:Ga_2O_3 compounds are apparently isostructural and are reported for the first time. Neither their structure nor their symmetry is known at present. The data—not shown in Fig. 1 (*b*)—indicate that the 3:1 compounds of Y_2O_3, Ho_2O_3, and Er_2O_3 dissociate between 1600 and 1650°C before melting. Solid solutions in the binary R_2O_3-Ga_2O_3 garnet-type structures have been clearly demonstrated by changes in unit-cell dimensions. Apparently, some R^{+3} ions can substitute for Ga^{+3} in the octahedral position of the gallium garnets. The amount of solid solution is dependent on the size of the rare earth ion, and is not dependent on the temperature from which the specimens are quenched. An interesting observation is that, for specimens slowly cooled from high temperatures (below the solidus), the maximum solid solution in the gallium garnets increases from Sm_2O_3 to Tm_2O_3, and then decreases for Yb_2O_3 and Lu_2O_3; however, the Y_2O_3 garnet maximum solid solution has a unit-cell size almost as large as that of the Sm_2O_3 system. Thus it can be seen that the Y^{+3} ion is quite different from the rare earth ions respecting the manner in which it enters into solid solution in the gallium garnets.

PHASE EQUILIBRIA IN SYSTEMS INVOLVING OXIDES OF THE TRIVALENT RARE EARTH IONS AND Nb_2O_5 OR Ta_2O_5

Recently, a series of compositions based on $BaNb_2O_6$ and $R^{+3}Fe^{+3}O_3$ mixtures, having a "bronze" type structure, have been shown to exhibit both ferroelectric and magnetic properties. (8) For this reason a considerable number of systems involving rare earth ions and Nb_2O_5 have been partially investigated in this laboratory.

All of the lanthanides from La^{+3} to Lu^{+3} form a 1:1 compound with both Nb_2O_5 and Ta_2O_5, of the general formula $R^{+3}(Nb, Ta)O_4$. This

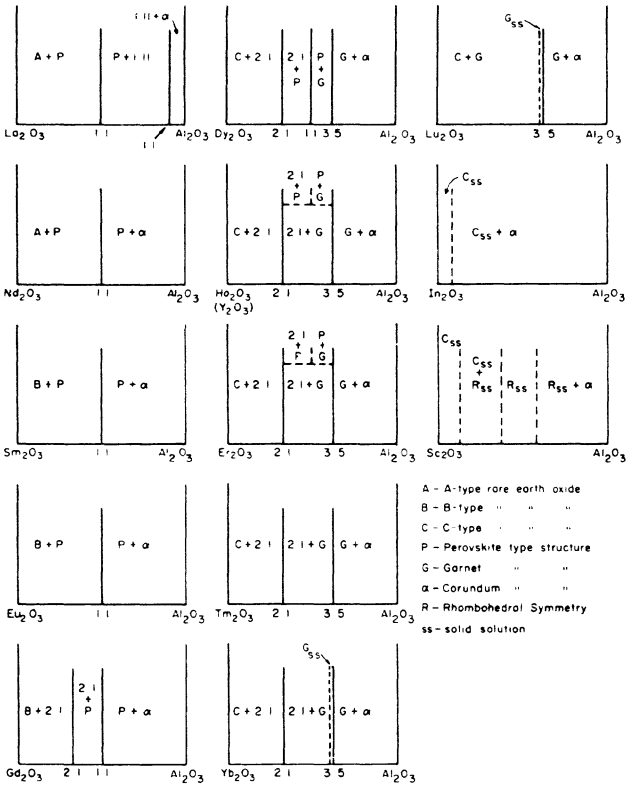


Fig. 1(*a*). Subsolidus phase diagrams for systems containing Al_2O_3 and the oxides of the trivalent rare earth ions (approx. 1650° C).

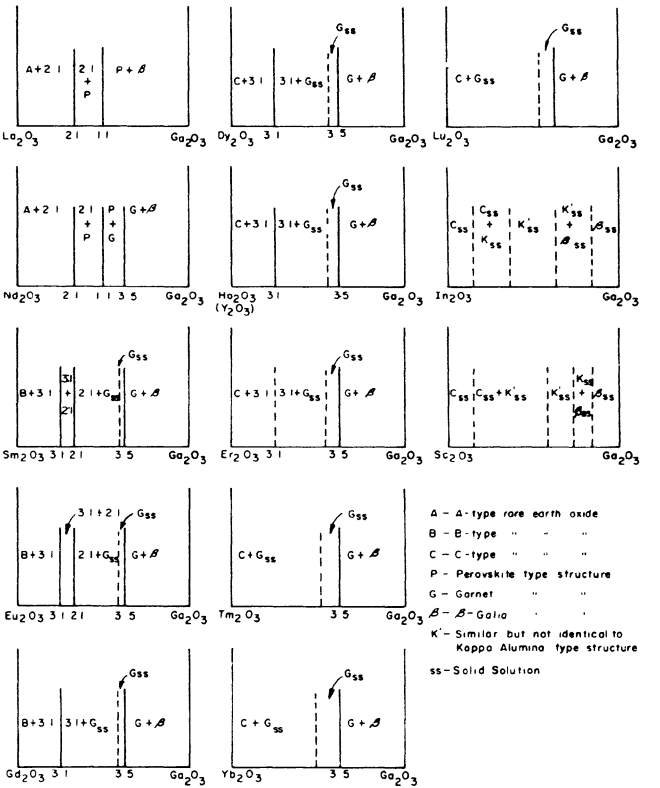


Fig. 1(*b*). Subsolidus phase diagrams for systems containing Ga_2O_3 and the oxides of the trivalent rare earth ions (approx. 1500° C).

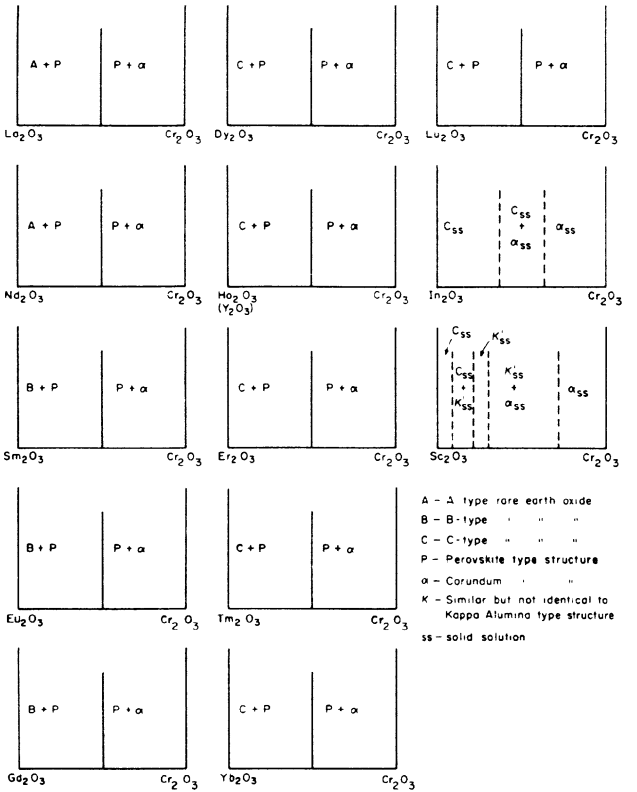


Fig. 1(*c*). Subsolidus phase diagrams for systems containing Cr_2O_3 and the oxides of the trivalent rare earth ions (approx. 1600° C).

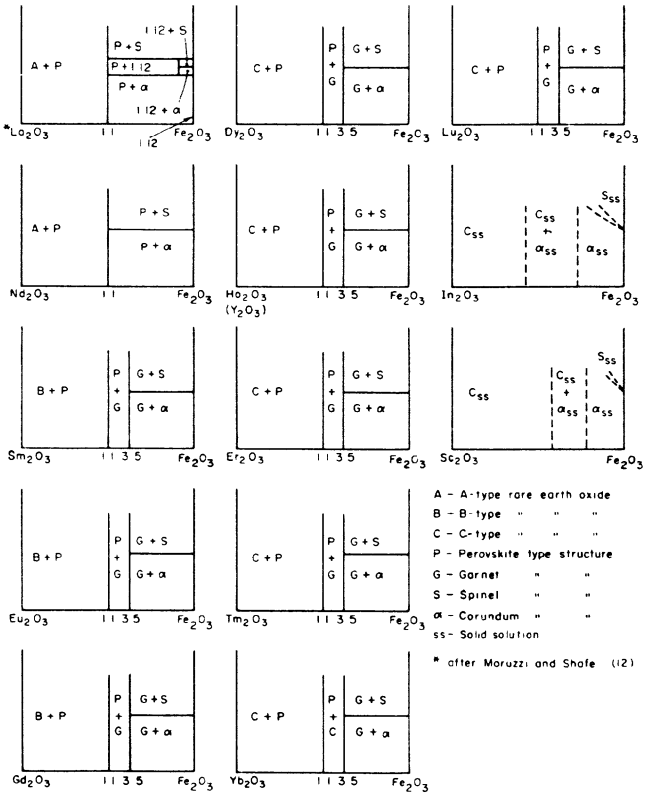


Fig. 1(*d*). Subsolidus phase diagrams for systems containing Fe_2O_3 and the oxides of the trivalent rare earth ions (1300–1500° C).

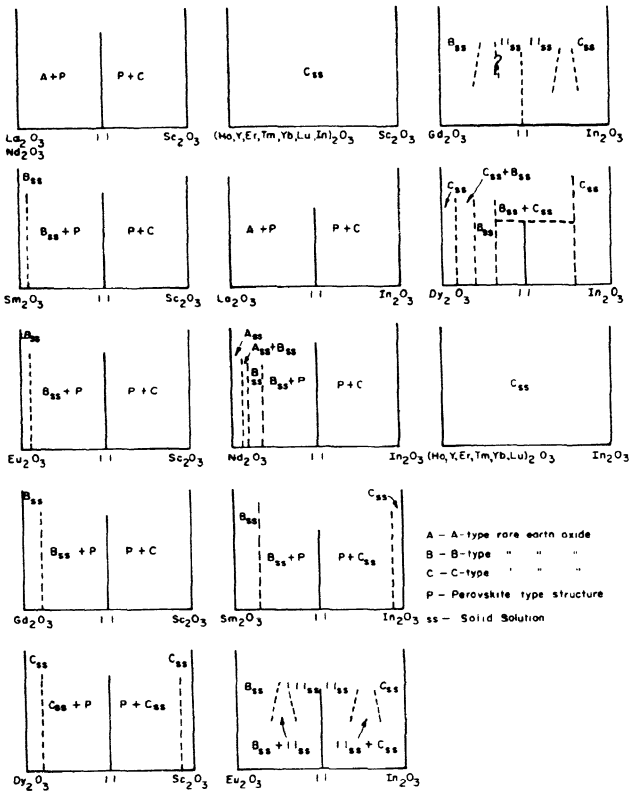


Fig. 1(*e*). Subsolidus phase diagrams for systems containing Sc_2O_3 and In_2O_3 and the oxides of the trivalent rare earth ions (approx. 1650° C).

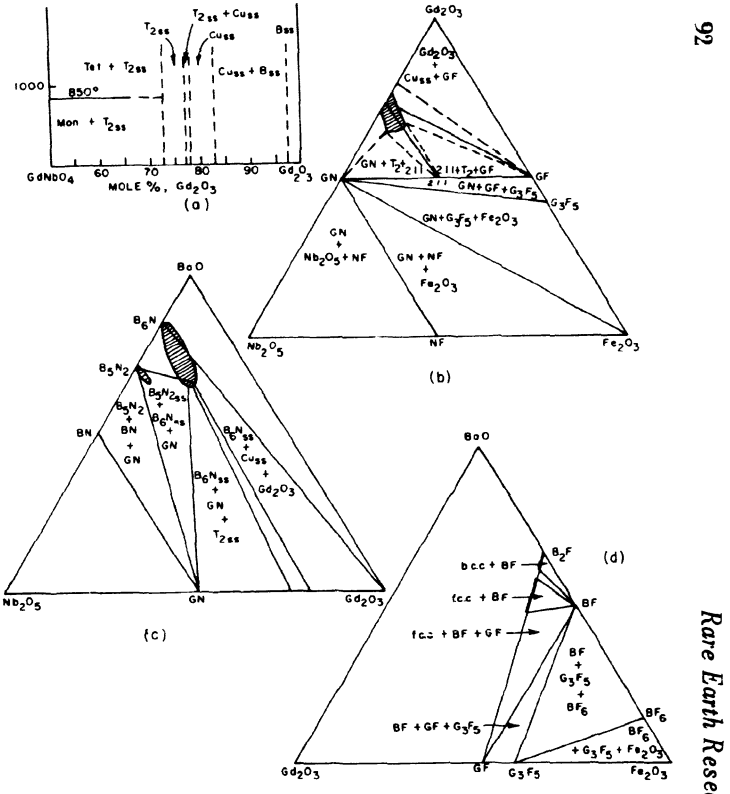


Fig. 2(*a–d*). Subsolidus phase equilibria in portions of the system BaO-Nb_2O_5-Gd_2O_3-Fe_2O_3 (approx. 1400° C).

compound, of fergusonite-type structure, is monoclinic and essentially isostructural at room temperature with pure monoclinic ZrO_2; however, an ordering of the R^{+3} and $(Nb, Ta)^{+5}$ ions results in a superstructure and a doubled b axis. As monoclinic ZrO_2 is known to invert reversibly to a tetragonal form at about 1000–1200 °C, several of these compounds were examined by high-temperature X-ray diffraction techniques. $GdNbO_4$ was found to invert reversibly to a tetragonal form at 850 ± 20 °C, and $YNbO_4$ at 900 ± 20 °C. Unlike the transformation in ZrO_2, there is no appreciable temperature hysteresis involved in this transformation, nor is there any sign of disintegration of the ceramic specimen on heating or cooling through the transformation temperature. This behavior of the niobates is probably due to the smaller monoclinic angle possessed by the rare earth niobates—both at room temperature and at the phase transformation temperature.

A new compound, $La_2O_3 \cdot 3\ Nb_2O_5$, was found to have a distorted perovskite-type structure—orthorhombic, with $a = 3.917$ A, $b = 3.910$ A, $c = 7.91$ A. Single-crystal Weissenberg patterns could not be used to recognize the orthorhombic symmetry, but appeared to show only tetragonal symmetry. At room temperature, the orthorhombic ceramic material showed no sign of ferroelectricity, but was slightly conductive.

Another new phase was found to occur in the Gd_2O_3–Nb_2O_5 binary system (Fig. 2*a*). Although the binary-phase diagram has not yet been completed, a new solid-solution phase appears to exist from about 72 mole per cent Gd_2O_3 to about 82 per cent Gd_2O_3. At 75 mole per cent Gd_2O_3, the phase appears to be just slightly distorted from a cubic fluorite structure (no superstructure), designated as T_2 in Fig. 2. It is probably tetragonal with c/a very close to one. At 80 mole per cent Gd_2O_3, the phase exhibits a good cubic fluorite structure $a = 5.342$ A, designated as Cu in Fig. 2. This is probably the composition of the phase mistakenly reported by Walsh, Goldstein, and White (9) as an ABO_4 compound in studies of vaporization of rare earth oxides in a tantalum cell. This phase probably occurs in many of the other rare earth/Nb_2O_5 and Ta_2O_5 binary systems.

Compositions between 50 and 75 mole per cent Gd_2O_3 show two phases at room temperature. The monoclinic-tetragonal inversion of the fergusonite-type phase in this two-phase region occurs at the same temperature as in the pure $GdNbO_4$, indicating no solid solution of Gd_2O_3 in $GdNbO_4$ up to 1000 °C. All of the specimens in the binary Gd_2O_3–Nb_2O_5 system from $GdNbO_4$ to pure Gd_2O_3 appear to be very strongly paramagnetic, but none has been confirmed to show ferromagnetic properties. No ferroelectricity was observed in the specimens of this binary system.

When Fe_2O_3 is added as a third component, it appears that a solid solution may exist in the "tetragonal" phase within the ternary system. Compatibility relations in the subsolidus are now being studied for this Gd_2O_3-Nb_2O_5-Fe_2O_3 ternary system (Fig. 2*b*), as well as for the BaO-Nb_2O_5-Gd_2O_3 (Fig. 2*c*) and BaO-Gd_2O_3-Fe_2O_3 (Fig. 2*d*) systems as part of the general study of the BaO-Nb_2O_5-R_2O_3-Fe_2O_3 quaternary systems. It should be emphasized that the diagrams in Fig. 2 are of a preliminary nature. They are based on specimens heated to various temperatures and slow-cooled. Accurate quenching data might well change the appearance of some of these solid-state compatability diagrams.

PHASE EQUILIBRIA IN SYSTEMS INVOLVING OXIDES OF THE TRIVALENT RARE EARTH IONS AND B_2O_3

A study of polymorphism in the ABO_3-type rare earth borates has been submitted for publication.(10) This paper shows that $LaBO_3$, and $NdBO_3$ have the aragonite structure; $SmBO_3$, $EuBO_3$, $GdBO_3$, $DyBO_3$, YBO_3, $HoBO_3$, $ErBO_3$, $TmBO_3$, and $YbBO_3$ have the vaterite structure. $LuBO_3$ is the only borate found to have a reversible phase transformation from the calcite-type structure at low temperature to the vaterite-type structure at high temperature. $LaBO_3$ transforms to a high-temperature form, the X-ray pattern of which has not been indexed; $NdBO_3$ and $SmBO_3$ transform to a slightly different high-temperature form. This high-temperature form occurs metastably at temperatures below 1000°C in $SmBO_3$ and $EuBO_3$.

The phase diagram for the system La_2O_3-B_2O_3 has been completed.(11) In addition to the 1:1 compound, 3:1 and 1:3 compounds also exist. The extent of liquid immiscibility in this system was found to correspond closely to the theoretical limit predicted by the Levin and Block theory of liquid immiscibility in glass-forming systems.

Phase-equilibria studies in the Sm_2O_3-B_2O_3 system are now under way.(12) Preliminary evidence indicates the existence of a 1:3 compound essentially the same as that in the La_2O_3-B_2O_3 system. The only other compound found in the system occurs at the 3:1 composition. Its structure appears to be quite different from that observed in the La_2O_3-B_2O_3 system, but the same as that found for the other smaller rare earth ions down through $3Yb_2O_3 \cdot B_2O_3$. The Lu_2O_3-B_2O_3 system apparently does not contain this 3:1 compound. This difference between Yb_2O_3 and Lu_2O_3 is similar to that which occurs in the rare earth aluminate systems, where a 2:1 compound occurs through Yb_2O_3, but does not form in the Lu_2O_3-Al_2O_3 system.

REFERENCES

1. R. S. Roth and S. J. Schneider, *J. Res. Nat. Bur. Stds.*, 64A, 309 (1960).
2. S. J. Schneider and R. S. Roth, *ibid.*, 64A, 317 (1960).
3. S. J. Schneider. Article submitted for publication in *ibid.*
4. S. J. Schneider, R. S. Roth, and J. Waring. Article submitted for publication in *ibid.*
5. M. L. Keith and R. Roy, *Am. Min.*, 39, 1 (1954).
6. R. S. Roth, *J. Res. Nat. Bur. Stds.*, 58, 75 (1957).
7. I. Warshaw and R. Roy, *J. Am. Ceram. Soc.*, 42, 434 (1959).
8. P. H. Fang and R. S. Roth, *J. App. Phys.*, Sup. 31, No. 5, 278S (1960).
9. P. N. Walsh, H. W. Goldstein, and D. White, *J. Am. Ceram. Soc.*, 43, 229 (1960).
10. E. M. Levin, R. S. Roth, and J. B. Martin. Article submitted for publication in *Am. Min.*
11. E. M. Levin, C. R. Robbins, and J. Waring. Article submitted for publication in *J. Am. Ceram. Soc.*
12. E. M. Levin. Unpublished data.

THE INFLUENCE OF TEMPERATURE ON THE CERIUM OXIDE SYSTEM, CeO_2-Ce_2O_3

GEORG BRAUER AND KARL GINGERICH

*Universität Freiburg, Germany; and Pennsylvania State University, University Park, Pennsylvania**

The system of the cerium oxides exhibits a complex crystal-chemical behavior. X-ray investigations of samples cooled to room temperature show the following phase relationships. (1, 2) (See Fig. 6.) The α-phase, cerium dioxide, $CeO_{2.00}$, which has the fluorite-type structure, has a very narrow range of homogeneity. It is followed by a broad two-phase region between the α-phase and the intermediate β-phase, $CeO_{1.81}$. The β-phase, which has a rhombohedral structure very closely related to the cubic fluorite type, is regarded as an ordered structure derived from that of CeO_2 by the introduction of anion vacancies, and it is probable that the ideal formula derived from eight unit cells of the CeO_2 structure by the ordered omission of six O^{2-} ions may be written $Ce_{32}O_{58}$. (2) Similarly the rhombohedral α-phase, $CeO_{1.78}$, and the pseudo-rhombohedral σ-phase, $CeO_{1.72}$, may be considered as the ordered phases $Ce_{32}O_{57}$ and $Ce_{18}O_{31}$, respectively. All three intermediate phases have very narrow ranges of homogeneity. In the region $CeO_{1.69}$-$CeO_{1.67}$, there occurs the cubic C-sesquioxide structure. Then follows a two-phase region in which $CeO_{1.67}$ coexists with the cerium sesquioxide, Ce_2O_3, which is of the hexagonal A-sesquioxide type. The following presentation concerns an investigation of temperature influence on the cerium oxide system by measuring the oxygen dissociation pressures (3) and by high-temperature X-ray powder diffraction analysis. (4, 5)

THERMODYNAMIC PROPERTIES OF THE CERIUM OXIDES

In the temperature range that could be covered with the equipment available, the oxygen dissociation pressures of the cerium oxides are too small for direct measurement; therefore, an indirect method using gaseous hydrogen-water mixtures of known composition was applied to attain equilibrium. The gaseous mixtures were passed over the oxide samples

*The authors wish to thank Dr. D. J. M. Bevan and Dr. J. Kordis for permission to use their results in this presentation.

at a given temperature and constant flow rate, and the attainment of the equilibrium was followed by repeated weighing of the oxide sample, until the weight remained constant. A reversible attainment of equilibrium was verified at temperatures above 600°C. Below this temperature, attainment of the equilibrium was too slow for experimental observation. In one series of experiments the water vapor pressure was held constant, and the relationship between temperature and composition was determined. The experimental curves for the different water vapor partial pressures are shown in Fig. 1. The oxygen dissociation pressures of the cerium oxides—which at equilibrium are identical to the oxygen partial pressures of the gaseous H_2-H_2O mixture—were calculated from the known values for the equilibrium constant of water.

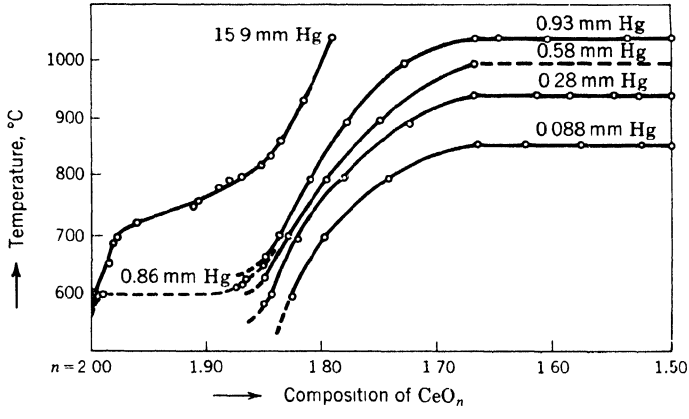


Fig. 1. Temperature *vs.* composition of CeO_n at the indicated water vapor partial pressures.

They were found to be between 10^{-32} and 10^{-17} atm and may be considered as true vapor pressures of the cerium oxides, since the formation of volatile suboxides is to be expected only at considerably higher temperatures (6), and no formation of volatile hydroxides was observed.

From these oxygen partial pressures the partial molar heats of formation ΔH_T^* were calculated for different compositions CeO_n according to the relationship

$$\Delta H_T = RT_1T_2 \frac{\ln Kp_2 - \ln Kp_1}{T_2 - T_1}$$

where $\ln Kp = \ln p_{O2}$. This equation could be applied for the region of composition $CeO_{1.50}$-$CeO_{1.85}$, since there exists in the temperature range of investigation a linear relationship between $\ln Kp$ and $1/T$ for all compositions. The calculated partial molar values ΔH_T^* for the heat of formation are shown in Fig. 2 as a function of composition. An integra-

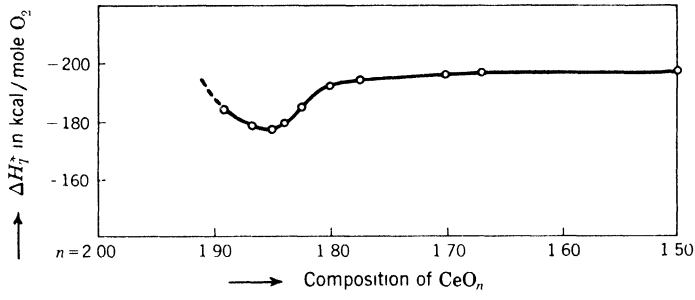


Fig. 2. Partial molar heat of formation of the cerium oxides.

tion over all partial heats of formation can be carried out accurately for the reaction 4 $CeO_{1.50} + 0.7\ O_2 = 4\ CeO_{1.85} - \Delta H_T$ and this results in the value $\Delta H_T = -135 \pm 3$ kcal for an average temperature of 850°C. The uncertainty in the course of the enthalpy curve between $CeO_{1.85}$ and $CeO_{2.00}$ does not as yet allow accurate calculations to be extended to cerium dioxide. As a lower limit, however, the value $\Delta H_T = -188.5$ kcal can be given for the heat of formation of the reaction $2\ Ce_2O_3 + O_2 = 2\ CeO_2 - \Delta H_T$. It is estimated that with a better knowledge of the oxygen-rich oxides this value may be raised by no more than 5 kcal.

In Fig. 3 the partial molar free energies ΔG^*O_2 of oxygen dissociation are plotted against the composition of the cerium oxides for the temperatures 600, 700, 800, 900, and 1000°C. The values were calcu-

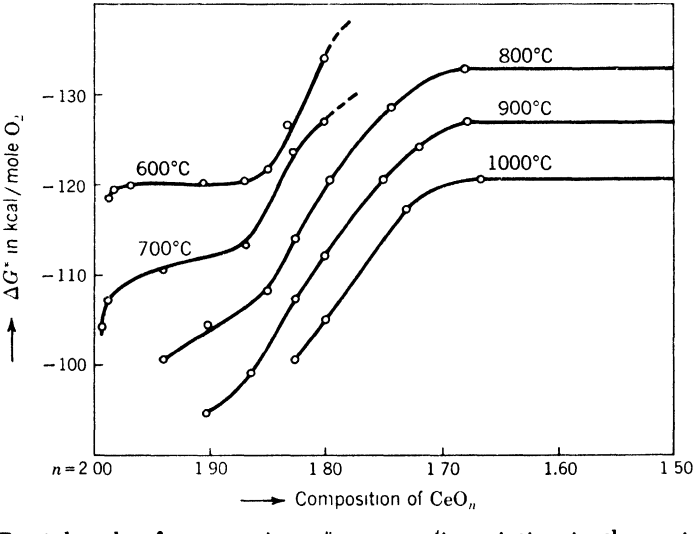


Fig. 3. Partial molar free energies of oxygen dissociation in the cerium oxide system.

lated from the oxygen equilibrium pressures, according to the equation $\Delta G = RT \ln Kp$. The partial molar entropies of formation, shown in Fig. 4, for an average temperature of 1123°K, were calculated from the oxygen dissociation pressures according to the equation $\Delta S_T = R\left(T\frac{\ln Kp_2 - \ln Kp_1}{T_2 - T_1} - \ln Kp\right)$.

HIGH-TEMPERATURE X-RAY STUDY OF THE REGION $CeO_{2.00}$-$CeO_{1.78}$

The evidence from the oxygen dissociation-pressure measurements that, at temperatures above 700°C there exists in the oxygen-rich region of the cerium oxide system a one-phase region, would seem to contradict the previously mentioned phase relationships found at room temperature by X-ray diffraction. This apparent contradiction can only be explained by the assumption that the homogeneous phase which exists above 700°C separates into the different phases observed upon quenching to room temperature. Such behavior would be unusual, since it is generally agreed that in oxide systems high-temperature solid solutions can be preserved upon quenching. It appeared that for the cerium oxides an understanding of the temperature influence upon the phase relationships in the solid could best be obtained by direct observation at higher temperatures.

For this we used a high-temperature X-ray powder-diffraction camera with 12-cm diameter and prevented the chemical composition of the oxide samples from changing during the heat treatments by sealing them into fused silica capillaries under vacuum. For the X-ray exposures, CuKα-radiation filtered through nickel was used. The camera, whose temperature was controlled within ± 10°C, was evacuated to 10^{-1}-10^{-2} mm Hg. From 10 to 35 hours exposure time was required for reduced oxide samples, less for cerium dioxide itself. Annealing times were usually three hours.

On the X-ray patterns of samples in the region $CeO_{2.00}$-$CeO_{1.81}$ taken at room temperature appear the diffraction lines of both the cubic α-

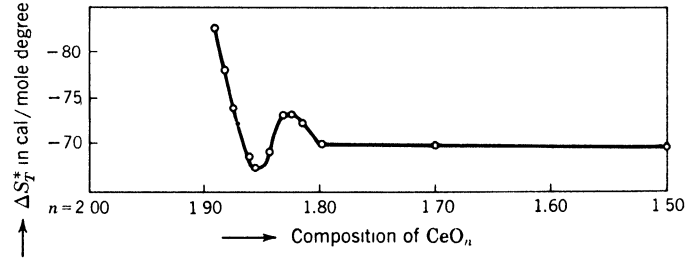


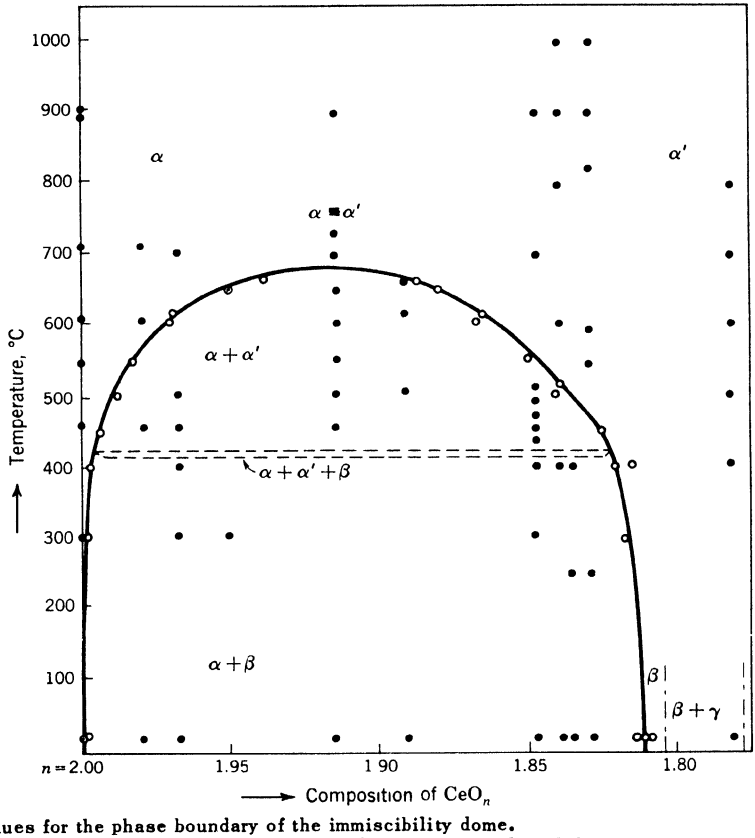
Fig. 4. Partial molar entropy of formation in the cerium oxide system at 1123°K.

phase, $CeO_{2.00}$, and the rhombohedral β-phase, $CeO_{1.81}$. The resolution of the camera was too small to show the splitting of the cubic diffraction lines, due to the distortion of the rhombohedral lattice of the β-phase. Instead, the diffraction lines appeared broad and diffuse. Upon raising the temperature the appearance of the X-ray diffraction patterns does not change markedly, until 400°C is reached. Between 400 and 440°C the rhombohedral lattice of the β-phase transforms into a cubic fluorite-like lattice, which is apparently identical to that of the α-phase, but which has a different lattice parameter. The corresponding phase was therefore called α'. Upon raising the temperature further for a sample $CeO_{1.915}$, the corresponding diffraction lines of the two coexistent cubic phases approach one another until, near 700°C, they become identical. This change in the patterns corresponds to the disappearance of the two-phase region.

The precise determination of the lattice parameters was hampered because the camera construction did not allow asymmetrical patterns to be taken. Pure cerium dioxide was therefore used as a standard. For most of the patterns the parameters were calculated from the reflections with *hkl* values of 620, 533, and 622 which showed α_1-α_2 splitting. The accuracy in the determination of the lattice parameters was then within 0.002-0.003°A. The lattice parameters of the β-phase refer to the pseudocubic indexing of the diffraction lines. In this case the accuracy was within only 0.003-0.005°A.

The change of the lattice parameter with temperature was determined for $CeO_{2.00}$ in the range 20–900°C and for $CeO_{1.848}$ and $CeO_{1.840}$ in the range 500-1000°C, at which temperatures the latter oxides have the cubic structure. Within the accuracy of the measurements for all three samples, a linear relationship $\Delta a/\Delta t$, the value of which is 6.4×1^{-5}Å/deg, was found. From this the average linear coefficient of thermal expansion was calculated to be 11.8×10^{-6} deg^{-1}. This value was used for the conversion of the lattice parameters of the homogeneous cubic high-temperature samples to room temperature. The parameter-composition relationship thus obtained was used to determine the boundaries of the immiscibility dome by applying the parametric and disappearing-phase methods. The maximum of the dome corresponded to a temperature of 685°C and a composition of $CeO_{1.918}$ (Fig. 5).

The resolution of the temperature camera was too small for a detailed investigation of the intermediate region, $CeO_{1.8}$-$CeO_{1.67}$, in which, as previously mentioned, several ordered phases with lower symmetry occur. Therefore, only one sample, $CeO_{1.787}$, which at room temperature consists of a mixture of the β- and γ-phases, was studied. On the film the separation into the lines of the two phases was not clear, but it could be observed that no marked changes in the line pattern occured between room temperature and 600°C. At 700°C, however, there appeared only



O Values for the phase boundary of the immiscibility dome.
● Representative points for the oxide samples investigated, and the temperatures at which they were exposed.

Fig. 5. Phase diagram of the cerium oxide system in the region $CeO_{2.00}$-$CeO_{1.78}$.

one phase with a pattern very similiar to that of the α-phase. The phase changes between 600 and 700 °C were found to be reversible.

The phase relationships found for the region $CeO_{2.00}$-$CeO_{1.78}$ between 20 and 1000 °C are represented in Fig. 5. The existence of a three-phase region, expected for a transition of first degree between the α- and the β-phase, has not yet been detected. It must lie in the temperature range between 400 and 440 °C. Its possible extent has been indicated by dotted lines.

DISCUSSION OF THE CERIUM OXIDE SYSTEM

The investigations described afford an explanation of the peculiar behavior of the cerium oxides. In the region $CeO_{2.00}$-$CeO_{1.78}$, there exists a continuous solid solution of defective fluorite structure and, below 685 °C, a gap of miscibility that broadens upon cooling, until at

room temperature it extends from $CeO_{2.00}$ to $CeO_{1.81}$. The phase changes in this region were found to be "unquenchable" under the experimental conditions applied. This means that they occur in less than the time necessary for quenching the sample from the temperature of investigation to room temperature and for taking the X-ray film patterns at room temperature. The apparent contradiction between the results of earlier X-ray investigations and those of the oxygen dissociation-pressure measurements can thus be understood. The results of the high-temperature X-ray study are in full agreement with the measurements, as can be seen from the partial molar free-energy curves, which require a two-phase region between compositions $CeO_{1.98}$ and $CeO_{1.88}$ for 600 °C, and a one-phase region in the whole range $CeO_{2.00}$–$CeO_{1.81}$ for 700 ° and above (compare Fig. 3 and 5). In addition the changes in the slopes of the free-energy curves indicate that interesting order-disorder phenomena in the "homogeneous" phase may occur. This conclusion is supported by the shape of the entropy curve (Fig. 4). For the intermediate region $CeO_{1.81}$–$CeO_{1.67}$, (Fig. 6), it can be deduced from the free-energy curves (Fig. 3) that only one phase can exist at temperatures above 800 °C. It is therefore assumed that at such temperatures a continuous homogeneous series of the cubic solid solutions extends from CeO_2 to composition $CeO_{1.67}$, thus corresponding to the behavior of analogous systems such as CeO_2–La_2O_3. In the cerium oxide system itself these cubic mixed crystals are stable at room temperature for only a small region near the

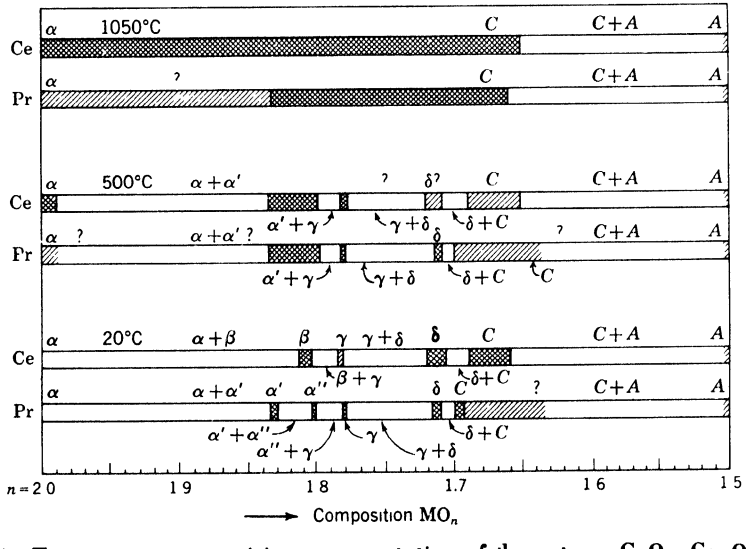


Fig. 6. Temperature-composition representation of the sytems CeO_2–Ce_2O_3 and PrO_2–Pr_2O_3.

composition $CeO_{1.67}$ and for the other compositions disproportionate into the ordered phases previously described upon lowering the temperature (Fig. 6). In the region $CeO_{1.67}$-$CeO_{1.50}$ there exist at all temperatures of observation two phases in agreement with the room temperature X-ray data and the plateau in the free-energy curves. In summary it can be said that at room temperature there exist several ordered phases with lower symmetry; at higher temperatures the trend goes toward higher symmetry in the arrangement of the atoms and a higher degree of disorder of the defective oxygen-lattice sites.

The peculiar temperature behavior in the system CeO_2-Ce_2O_3, compared to that of systems of CeO_2 or ThO_2 with oxides of the other lanthanides, must be caused by the fact that—as has already been pointed out (2) in the case of the cerium oxides—the cation lattice sites are practically equivalent, because the electron transition $Ce^{4+} + e^- \rightleftharpoons Ce^{3+}$ is possible. Because of this reaction no changes of position relative to neighboring ions (which would obviously require a high energy of activation) are necessary between the cations, but only electron transfers. In addition only slight geometric shifts of the ions are necessary in the reversible transitions between the cubic structure and the closely related rhombohedral lattice structures. The cerium oxides thus provide a unique possibility for extensive studies of the stable arrangement of crystal lattices in an oxide system, as a function of temperature and oxygen content, at relatively low temperatures.

That the knowledge which can thus be obtained may have significance beyond the cerium oxide system itself can be seen from the evaluation of investigations (7) which show that the praseodymium oxides PrO_2-Pr_2O_3 exhibit a crystal-chemical behavior of striking similarity to that of the cerium oxides. In Fig. 6 an attempt is made to compare the phase relationships of these two systems at different temperatures. Similar complex behavior at lower temperatures has also been observed in the oxide system of terbium, uranium, titanium, and other metals, but in these latter systems the reactions within the solid state seem to be more sluggish at low temperatures than in the cerium oxide system.

Preliminary investigations of analogous systems, for example, ThO_2-Eu_2O_3, which contain two different metals, showed that a sufficiently high movability of the cations and a rapid attainment of the phase equilibrium occurs at considerably higher temperatures. At 1660°C the time required to attain equilibrium was found to be on the order of minutes, and at 1300°C, of approximately 100 hours. In such oxide systems one apparently has access only to the relatively simple high-temperature phase relationships. It may be that known methods using water vapor as a catalyst under extremely high pressure may be successful in forcing equilibrium between the low-temperature phases in such systems.

SUMMARY

The influence of temperature on the cerium oxide system was investigated by measuring the oxygen dissociation pressures in the region $CeO_{2.0}$-$CeO_{1.5}$, and by high-temperature X-ray powder-diffraction analysis in the region $CeO_{2.0}$-$CeO_{1.8}$ for a temperature range of 20-1050°C. Thermodynamic properties such as partial molar heats, free energies, and entropies of formation were derived from the equilibrium pressures. For the region $CeO_{2.00}$-$CeO_{1.78}$ the phase diagram was determined. All phase changes were found to occur very rapidly. There exists an immiscibility dome which at room temperature extends from $CeO_{2.00}$-$CeO_{1.81}$, narrows with increasing temperatures, and closes at 685°C and a composition of $CeO_{1.92}$. A continuous solid solution with defective fluorite structure such as would be expected for such a system exists at higher temperatures. The influence of temperature upon the crystal-chemical behavior of the entire system was discussed and compared with that of the praseodymium oxides.

SUPPLEMENT

In a private communication in response to the above manuscript, D. J. M. Bevan and J. Kordis have released the results of their measurements of oxygen dissociation pressure above cerium oxides, in the region of composition $CeO_{2.00}$-$CeO_{1.80}$ and temperature range 636-1168.5°C. In their investigation they used a CO_2/CO equilibration. There is substantial agreement with our results in the equilibrium oxygen pressures and partial enthalpies of formation where the measurements overlap. In evaluating the partial enthalpies of formation found by Bevan and Kordis for the region $CeO_{2.00}$-$CeO_{1.85}$, we can now give the value $H_T = -193.5$ kcal for the heat of formation of the reaction $2\ Ce_2O_3 + O_2 = 4\ CeO_2 + \Delta H_T$.

REFERENCES

1. G. Brauer and H. Gradinger, *Z. anorg. allg. Chem.*, 277, 89 (1954).
2. D. J. M. Bevan, *J. Inorg. Nuclear Chem.*, 1, 49 (1955).
3. G. Brauer and K. Gingerich. Article to be published in *ibid.*
4. G. Brauer and K. Gingerich, *Angew. Chem.*, 69, 480 (1957).
5. G. Brauer and K. Gingerich. Article to be published in *J. Inorg. Nuclear Chem.*
6. L. Brewer. Private communication.
7. L. B. Asprey. Doctoral dissertation, University of California (1949); R. E. Ferguson, E. D. Guth, and L. Eyring, *J. Am. Chem. Soc.*, 76, 3890 (1954); E. D. Guth, *et al.*, *ibid*, 76, 5239 (1954); W. Simon and L. Eyring, *ibid.*, 76, 5872 (1954); C. L. Sieglaff and L. Eyring, *ibid.* 79, 3024 (1957).

THE STOICHIOMETRY AND RESISTIVITY OF PrO_x*

A. F. CLIFFORD AND PAUL A. FAETH

Department of Chemistry, Purdue University, Lafayette, Indiana

Praseodymium oxide (PrO_x) is unusual in that it has several stable intermediate compositions between $PrO_{1.50}$ and $PrO_{2.00}$. At constant temperature, the composition may be expressed as a function of the oxygen pressure. In the temperature range 400–1000 °C, and the pressure range 2 to 150 mm, the compositions $PrO_{1.83}$, ($PrO_{1.82}$), $PrO_{1.80}$, $PrO_{1.78}$, ($PrO_{1.72}$), $PrO_{1.71}$, ($PrO_{1.67}$), ($PrO_{1.62}$), and $PrO_{1.50}$ are stable. The direction of approach to equilibrium for certain nonstoichiometric compositions is irrelevent, but it is quite critical for others. In the critical regions, the pressure-ascending isotherms are not superimposable on the pressure-descending isotherms, and a hysteresis is observed between most of the neighboring pairs of compositions mentioned above.

Isotherms have been measured using a quartz-beam microbalance. (1) The microbalance was contained in a glass envelope, and the temperature of the sample and the oxygen pressure were thus easily controlled. Standard auxiliary vacuum equipment was also used. By observing the changes in mass accompanying oxygen pressure changes, the O/Pr ratio was calculated.

A discussion of the hysteresis effects in praseodymium oxide was given in a paper delivered at the one hundred and thirty-eighth national meeting (2) of the American Chemical Society. It was postulated that the PrO_x system is composed of domains of slightly differing energies. The domains may exist in several states, $PrO_{1.83}$, $PrO_{1.80}$, and so forth. In changing from a lower to a higher state, and vice versa, the domains change at slightly different oxygen pressures, depending upon their energies, thus giving rise to hysteresis. Analysis of the experimental curves, according to the general theory proposed by D. H. Everett (3), seems to support this view. Checks of the behavior of the composition versus oxygen-pressure-hysteresis behavior of PrO_x against Everett's theoretical predictions reveals a remarkable degree of correspondence.

*This research was supported by the U.S. Air Force through the Air Force Office of Scientific Research of the Air Research and Development Command, under Contract No. AF 18(603)-45.

As mentioned earlier, several stable composition regions are observed in the PrO_x system. A reasonable scheme to assume is that, as a domain transforms from a lower to a higher state, not only does the O/Pr ratio change but the ratio of Pr^{+3} to Pr^{+n} ($n = 4$ or perhaps 5) changes also. This means that a single domain of PrO_x has a ratio of O/Pr, say, of 1.83 and a Pr^{+4}/Pr^{+3} ratio of 2.00. Reference to Table I shows a scheme relating Pr^{+4} and Pr^{+3} and the appropriate numbers of oxygens. It can be seen that the theoretical x-values compare quite well with the experimental values. Figure 1 shows a plot of the various ratios versus x-values.

It is interesting to note that PrO_x is both an n-type and a p-type semiconductor. At large x-values—$PrO_{1.83}$—PrO_x is n-type, while for low

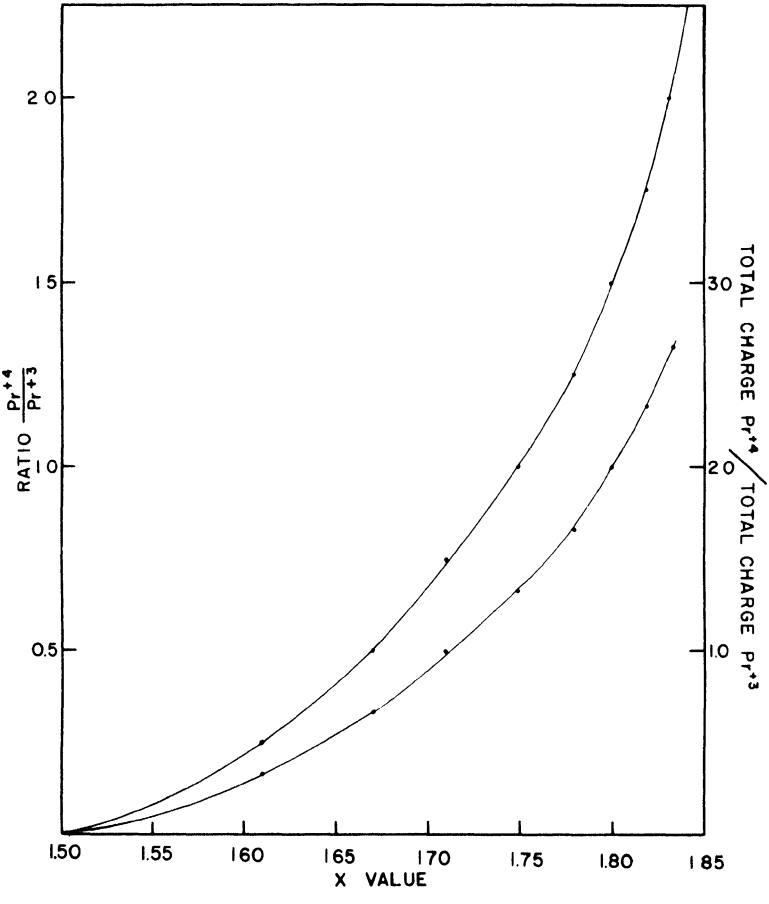


Fig. 1. Praseodymium-Oxygen ratios in PrOx.

x-values—Pr_2O_3—it is p-type. Martin (4) has shown that the change-over from n- to p-type takes place at about 780 °C in air (P_{O_2} = 150 mm). According to the isotherms we have determined, this would correspond to a composition of about $PrO_{1.71}$. The indicative composition ratio suggested in Table I for $PrO_{1.71}$ shows an equivalence in the number of charges for the Pr^{+3} and Pr^{+4} ions in the system, that is,

$$3(Pr^{+4}) = 12^{+} = 4(Pr^{+3})$$

We might therefore have expected a peculiar electrical effect at $PrO_{1.71}$. For $1.50 < x < 1.71$, the system is electron-deficient (p-type), and for $1.71 < x < 1.83$ the system is electron-rich (n-type).

TABLE I: PRASEODYMIUM-OXYGEN RATIOS IN PrO_x

Experimental Regions of Stability	Indicative* Composition Ratio	Theoretical x-value	Simple Ratio PrO_2/Pr_2O_3
1.50	Pr_2O_3	1.500	0 : 1
1.61	$PrO_2 \cdot 2\ Pr_2O_3$	1.600	0.5 : 1
1.67	$2\ PrO_2 \cdot 2\ Pr_2O_3$	1.667	1 : 1
1.71	$3\ PrO_2 \cdot 2\ Pr_2O_3$	1.714	1.5 : 1
not found†	$4\ PrO_2 \cdot 2\ Pr_2O_3$	1.750	2 : 1
1.78	$5\ PrO_2 \cdot 2\ Pr_2O_3$	1.778	2.5 : 1
1.80	$6\ PrO_2 \cdot 2\ Pr_2O_3$	1.800	3 : 1
1.82	$7\ PrO_2 \cdot 2\ Pr_2O_3$	1.818	3.5 : 1
1.83	$8\ PrO_2 \cdot 2\ Pr_2O_3$	1.833	4 : 1

*The symbolism used here is not to be interpreted as a physical mixture of PrO_2 and Pr_2O_3.

†W. D. Kingery, ed., *Kinetics of High Temperature Processes.* Cambridge: Technology Press of Massachusetts Institute of Technology (1959), p. 50.

When the isotherms were determined, it was noticed that oxygen did not immediately react with Pr_2O_3 at high temperatures. However, at a certain critical pressure (at constant temperature) the composition changed rapidly. The break pressure, P_B, was found to increase with temperature; a plot of log P_B *vs.* $\frac{1}{T}$ produced intersecting straight lines (Fig. 2). It was concluded that the point of intersection of the lines represented the cubic to hexagonal phase transition noted in the rare earth oxides of the M_2O_3 type. The transition temperature was 920 °C, and this compares favorably with the temperature at which Foëx (5) noted a large volume change in Pr_2O_3. The energy of the transition was calculated to be about 12 kcal. One experimental point at 485 °C also lies off the line and indicates that another transition occurs in the region of 745 °C.

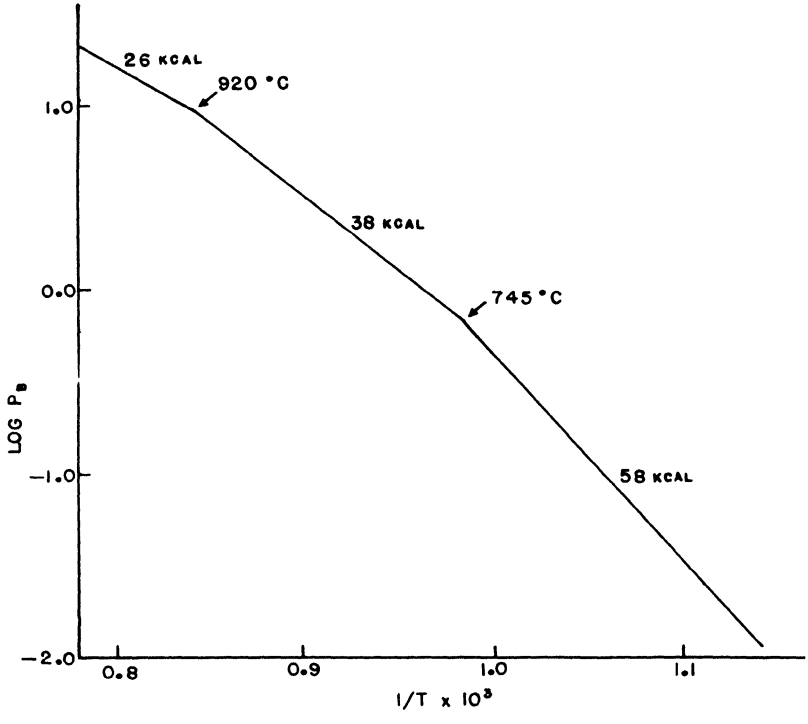


Fig. 2. Temperature *vs.* pressure break curve.

In an effort to obtain a further indication of the phase transition, without resorting to high-temperature X-ray experiments, a thermoelectric power cell (T.E.P.) was constructed for the measurement of thermoelectric power and resistivity. Ideally, such measurements are made on continuous solids, preferably single crystals, and not powders. However, qualitative results should show a break in the resistivity curve at the transition temperature, and semiquantitative results might be expected.

A sample of Pr_6O_{11} was decomposed to Pr_2O_3 *in vacuo* at about 1100 °C. The first experiment consisted of reducing the temperature rapidly to 500 °C, and then measuring the resistance as the sample was cooled to 175 °C (curve 1 of Fig. 3). The temperature was then increased slowly to 1100 °C (curve 2 of Fig. 3). The second experiment was designed to reduce the temperature slowly, and any differences in resistance due to a possible difference in the crystalline form were to be noted (curve 1 of Fig. 4). Curve 2 of Fig. 4 was obtained upon increasing the temperature again to 1100 °C. A third experiment was then run, in which the temperature was reduced quite slowly. It took approximately one week to reduce the temperature from 1000 °C to room temperature (curve 1 of Fig. 5).

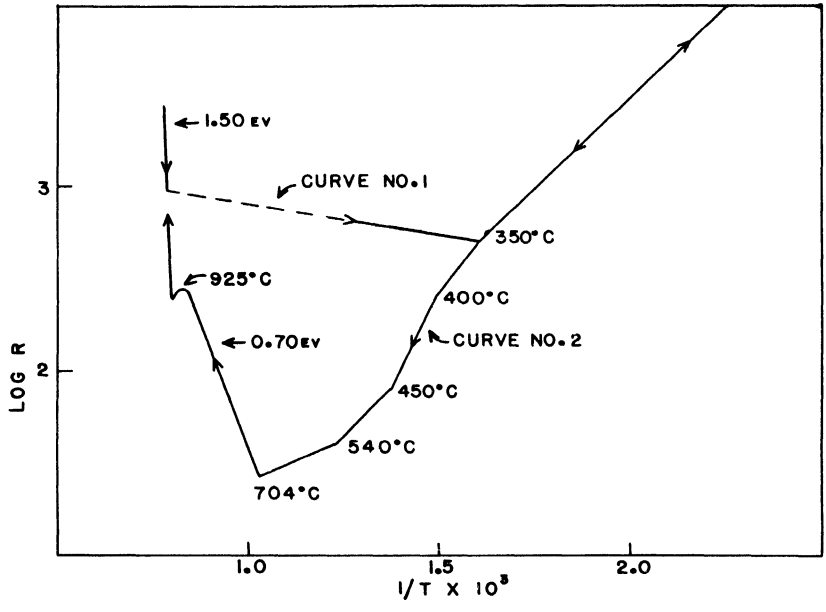


Fig. 3. Temperature *vs.* resistivity curve.

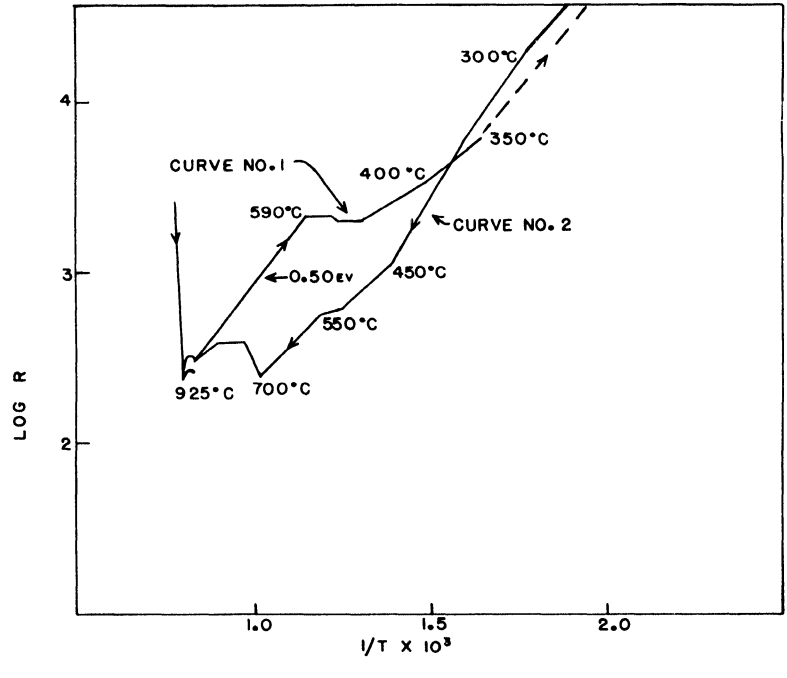


Fig. 4. Temperature *vs.* resistivity curve.

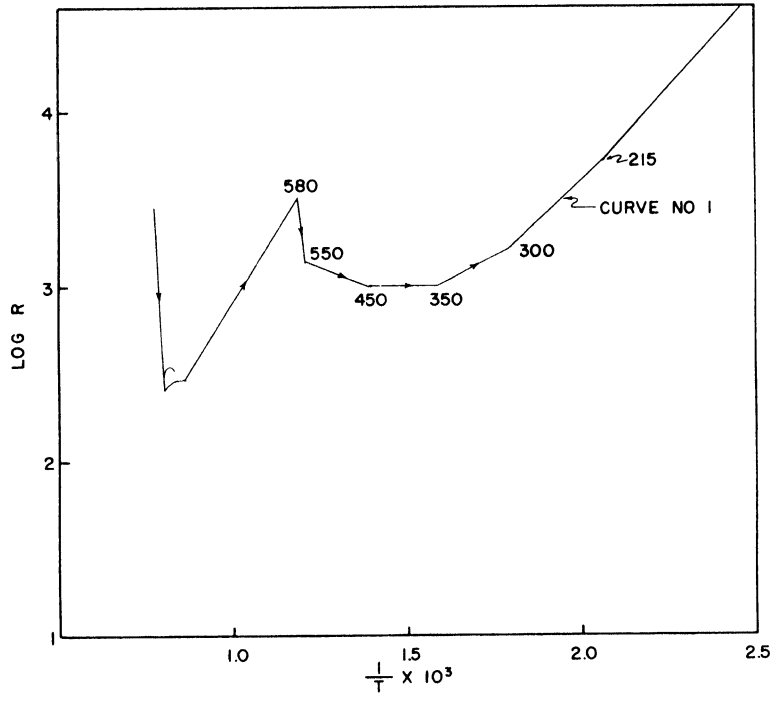


Fig. 5. Temperature *vs.* resistivity curve.

Several important features of the log R (R = resistance) *vs.* $1/T$ plot are worth noting. First, the resistance at about 925 °C appears to be a pivot point, which we interpret as the transition temperature. Second, the vacuum isobars show several linear regions with breaks at significant temperatures. Figure 6 shows a plot of the vacuum decomposition of $PrO_{1.83}$.* It is to be noted that the breaks in the curves of Fig. 3, 4, and 5 for Pr_2O_3 *in vacuo* are (within experimental error) the same as the temperatures at which the stable regions begin to break up when $PrO_{1.83}$ is decomposed *in vacuo*. The break at 550 °C—not evident in Fig. 6—may be due to a composition change between 1.71 and 1.72. Either of two interpretations may be put upon these data:

First, changes in the Pr_2O_3 structure dictate the temperatures at which changes of composition may occur in higher oxides. Perhaps the state of the Pr atom is a determining factor. Possibly the excess oxygen is solvated in the Pr_2O_3 lattice (for $PrO_{1.83}$, say) and there may be a nonequivalence between oxygens.

*We are indebted to Dr. A. W. Czanderna for this measurement.

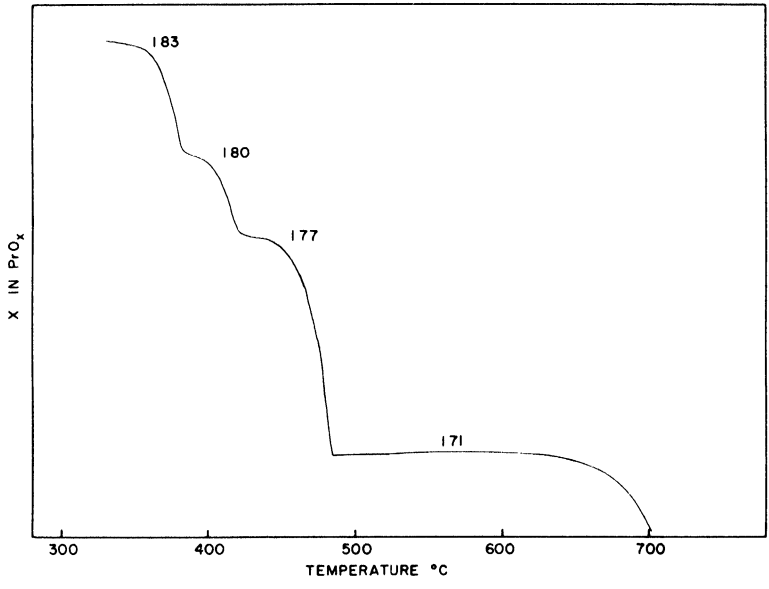


Fig. 6. Decomposition of $PrO_{1.83}$.

Second, despite the fact that the system was maintained at about 10^{-5} mm of pressure by continuous pumping, there was still enough oxygen available to change the surface composition at the appropriate temperatures, giving rise to changes in resistance.

It is interesting to speculate on the significance of the pivot points in the resistance curves. Since various lattice constants and crystal structures have been proposed by Eyring *et al.* (6), we might conclude that the break indicates a phase transition. Comparison of the slopes of the curves at the break points gives values of 12 kcal/mole for the transition at 925 °C (in agreement with the value obtained from the stoichiometry studies) and 20 kcal/mole for the transition at 745 °C. It is postulated that the transition at 925 °C is between A- and B-type oxide and that at 745 °C is between B- and C-type.

The energies calculated from the figures vary between ±0.70 ev. These energies are comparable in magnitude to those cited by Seitz (7) for similar experiments on ZnO. In the case of ZnO the energy was attributed to an ionization process of interstitial metal atoms subject to a homogeneous polarizable medium.

Since the values of the energies associated with the resistance curves are of the order of 15 kcal or less, they are certainly within the region of energies expected for these interpretations. High-temperature vacuum X-ray experiments would be a desirable though difficult measure-

ment. Also, we may expect the oxide to show changing absorption spectra in the infrared region as the temperature is raised.

Curves 1 and 2 of Fig. 3 represent a quenched sample (most likely hexagonal Pr_2O_3). Foëx (5) showed that the C (cubic) to A (hexagonal) transition was irreversible when the temperature was lowered through the transition temperature. It is likely that all resistance experiments were performed on the high-temperature A-form. Note that the quality of the ascending and descending temperature plots, respectively, are all similar even though the curves have been displaced; however, the pivot point at 920 °C remains unaltered. Other experiments along these lines are continuing.

REFERENCES

1. A. W. Czanderna and J. M. Honig, *Anal. Chem.*, 29, 1206 (1957).
2. A. F. Clifford and P. A. Faeth, *Abstracts of Papers*, p. 50S.
3. D. H. Everett, *Trans. Faraday Soc.*, **48**, 749 (1952); **50**, 187, 1077 (1954); **51**, 1551 (1955). *See also* J. A. Enderby, *ibid.*, **51**, 835 (1955); 52, 106 (1956).
4. R. L. Martin, *Nature*, 165, 202 (1950).
5. M. Foëx, *Compt. rend.*, 224, 1717 (1947).
6. L. Eyring *et al.*, *J. Am. Chem. Soc.*, 76, 5238 (1954).
7. F. Seitz, *Modern Theory of Metals*. New York: McGraw-Hill Book Co., 1940, p. 464.

OXYGEN POSITIONS IN RARE EARTH-IRON GARNETS AND THEIR IMPLICATIONS

ERNST R. CZERLINSKY AND FERDINAND EULER*

Electronic Material Sciences Laboratory
Electronics Research Directorate
Air Force Cambridge Research Laboratories
Cambridge, Massachusetts

In recent years, materials with garnet structure have caused considerable interest. The garnet structure has proved suitable for placing rare earth ions in an environment which allows the study of their energy levels by paramagnetic resonance. If iron is placed in this structure, the compounds are usually ferrimagnetic. If both rare earth elements and iron are present, one may study the contributions of the rare earth ions to the ferrimagnetic properties.

Due to the different ionic radii, rare earth and ferric ions are found in different positions in the unit cell. Figure 1 is a representation of these positions. The unit cell may be divided into eight octants, which are exactly alike, except for their orientation. There are three cation positions, called *a*, *c*, and *d*. Position *a* is located at the corners and the center of each octant, *c* and *d* are on the lines bisecting the faces of the octant, as indicated. Positions *a* and *d* are occupied by ferric ions, *c* by rare earth or yttrium ions. There are 16 *a*-, 24 *c*-, and 24 *d*-positions in the unit cell. The co-ordinates of these positions are fixed fractions of the unit-cell edge.

The oxygen ions are located in 96 *h*-positions, with variable co-ordinates which are functions of three parameters, *x*, *y*, and *z*. These positions may be grouped into three characteristic configurations of 4, 6, and 8 nearest neighbors to each *d*-, *a*-, and *c*-position, forming a tetrahedron, octahedron, and dodecahedron. None of these configurations is regular, although certain characteristic symmetries may be observed.

Figure 2 shows the octahedron, respectively tetrahedron, of oxygen ions surrounding the *a*-, respectively *d*-position. Both configurations are shown in projection along their symmetry axes, which are threefold,

*The authors wish to acknowledge the effective assistance of their colleagues Jane A. Bruce, and P. Gielisse and N. Yannoni. The IBM 704 of General Electric Company, Lynn, Massachusetts, was used for the computations.

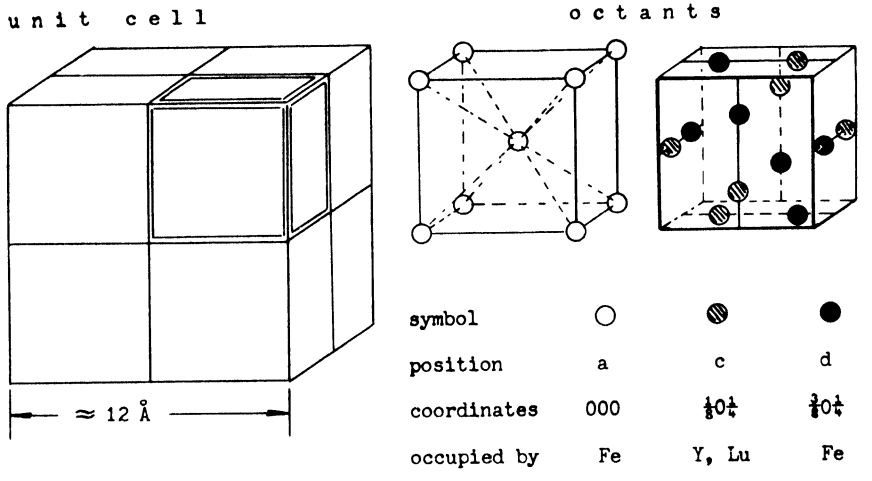


Fig. 1. Cation positions in garnet.

respectively fourfold inversion axes, extending parallel to the body diagonal [111] respectively cube edge [100] of the unit cell. The configurations may be regular, but are in general distorted by squashing or stretching in the direction of the symmetry axes. These distortions are reflected in the O-O interionic distances d_{o1}, d_{o2}, respectively d_{t1}, d_{t2}, and may be expressed by the ratios d_{o1}/d_{o2}, respectively d_{t1}/d_{t2}. If

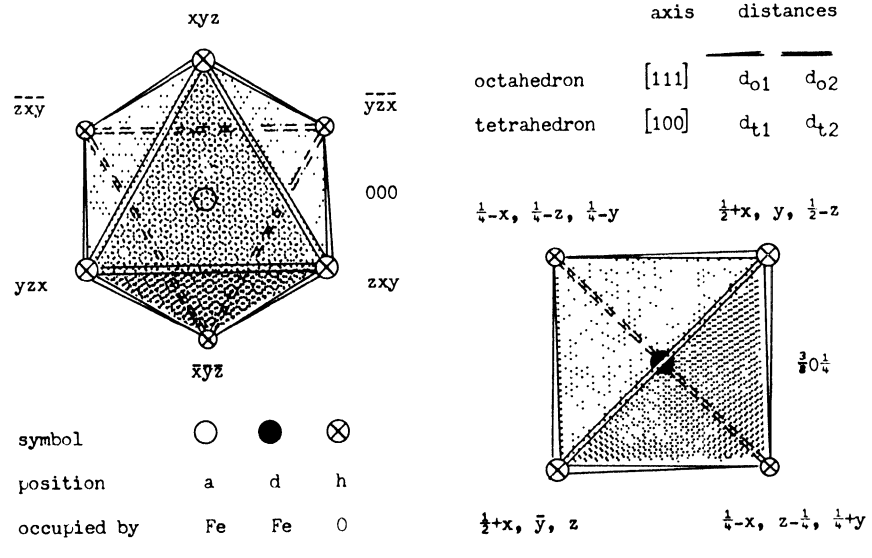


Fig. 2. Oxygen configurations in garnet.

these ratios are smaller than, equal to, or larger than one, the configurations are squashed, regular, or stretched.

In the ferrimagnetic garnets, the strongest magnetic interactions take place between the ferric ions in the *a*- and *d*-positions. The spins of these ions are aligned opposite to each other. The direction of this alignment is determined in general by a magnetic field acting upon the crystal. If there is no field, the spins align along the so-called direction of easy magnetization. One should expect this to be strongly influenced by the shape of the configurations of those oxygen ions which are nearest neighbors to the ferric ions in *a*-, respectively *d*-positions, that is by the octahedron respectively tetrahedron mentioned above.

This influence would be reflected in the magnetic anisotropy which had been studied on single crystals of yttrium-iron garnet (YIG) and several rare earth-iron garnets in these laboratories (1), and elsewhere. (2, 3) The most interesting results had been obtained on lutetium iron garnet (LuIG). Lu^{3+} is, like Y^{3+} diamagnetic, and therefore, in both YIG and LuIG, the ferrimagnetism originates solely from the ferric ions. The magnetization is therefore identical in both materials. The same holds for the magnetic anisotropy, which is, at room temperature, negative, indicating [111] as the direction of easy magnetization. At lower temperatures, however, YIG shows increased negative anisotropy, while with LuIG the anisotropy is positive, indicating that the direction of easy magnetization has changed from [111] at room temperature to [100] at liquid nitrogen temperatures. It would be interesting, therefore, to investigate whether this change is reflected in different oxygen configurations.

This investigation is carried out by a structural refinement of LuIG. Two single crystals of this material had been grown in the laboratory and had been formed into spheres by the familiar cyclone technique. Their orientation was established by Laue patterns. The oriented crystals were transferred to the precisely machined tip of a beryllium cone and mounted there with epoxy. This procedure minimizes irregular absorption effects in the subsequent X-ray diffraction work. The cone with the crystal was attached to the goniometer head of a Weissenberg camera, placed upon a Norelco diffraction unit. As detector, a Geiger-counter attachment was used instead of the usual film camera. Voltage and current of the X-ray tube were stabilized and reflected X-ray quanta counted on a scaler. Iron-filtered cobalt $K\alpha$ radiation was used. Integrated intensities were measured by oscillating the crystal about its [100] axis through the reflecting position.

The nonzero-layer reflections were to be obtained with the crystal in equi-inclination setting. However, many reflections showed a different intensity when examined at settings deviating from equi-inclination. A

survey over a number of reflections, each obtained at several settings ranging from equi-inclination to normal-beam, revealed that the expected "plateau" of constant intensity is frequently interrupted by a distinctly higher "peak." When those "peaks" occurred at the equi-inclination setting, it was decided to use a sufficiently different setting where the intensity proved to be on the "plateau". The "peaks" are due to simultaneous reflections from two or more different sets of lattice planes. (4)

Depending upon its strength, each reflection intensity was determined by oscillating the crystal through a sufficient number of cycles to obtain figures with less than a 3 per cent statistical error. The integrated intensities were modified by applying Lorentz-polarization, Tunell, and absorption corrections. The results, together with the lattice constant obtained from the angular positions and atomic scattering factors were used, as input into the computer program. (5) The trial parameters also required for the input were calculated with the use of the Fe-O and Y-O distances, in YIG (6) the latter being modified to account for the difference in ionic radii (7) between Y^{3+} and Lu^{3+}. Trial temperature and scale factors were obtained graphically.

The computed oxygen co-ordinates x, y, z, and temperature coefficient B are shown in Table I, together with the literature (6) data on YIG for comparison. While the latter were computed from more than seventy film-spot intensities our LuIG data are based on only those twenty two Geiger-counted reflections which are free from cation contributions to the intensity. In spite of this smaller number of used reflections, the discrepancy factor R comes out substantially lower, probably due to the higher accuracy of the counting method. However, the temperature coefficient obtained is rather inaccurate and accounts only for the thermal motion of the oxygen ions. Observed versus calculated structure factors are listed in Table II.

Interatomic distances, calculated from the co-ordinates x, y, and z are presented in Table III where, again, the data for YIG are from the literature. (6) The Fe-O distances are practically the same in YIG and LuIG. The Lu-O distances are 0.06 A smaller than Y-O, due to the difference

TABLE I: OXYGEN PARAMETERS

		YIG	LuIG
co-ordinate	x	−0.0274	−0.0244
	y	0.0572	0.0598
	z	0.1492	0.1532
	error	0.0009	0.0008
temp. coeff.		1.19 Å²	1.04 Å²
	error	...	0.23 Å²
discrepancy R		0.085	0.030

TABLE II: OBSERVED AND CALCULATED STRUCTURE FACTORS IN LuIG

h k l	|*F* (obs.)|	*F* (calc.)	*h k l*	|*F* (obs.)|	*F* (calc.)
4 3 1	155.8	164.0	8 5 3	122.3	− 123.0
5 4 1	39.1	45.0	8 6 0	0	− 34.6
5 4 3	0	6.1	9 4 3	75.0	− 71.8
7 4 1	72.0	70.6	8 7 1	54.6	− 46.1
8 2 0	132.6	131.1	9 5 4	22.9	− 15.8
8 3 1	46.5	− 46.8	11 4 1	45.6	− 37.7
7 4 3	81.8	− 73.5	8 7 5	0	− 0.6
8 5 1	84.4	80.4	10 6 2	87.5	− 87.5
7 5 4	107.3	106.2	9 8 1	82.4	78.0
9 4 1	90.5	78.1	11 4 3	51.6	− 60.4
			9 8 3	0	− 3.8
			12 3 1	64.0	64.3

in ionic radii. These figures confirm the applicability of rare earth ionic radii in calculating interionic distances in rare earth-iron garnets.

The O-O distances are shown together with the octahedral and tetrahedral distortion ratios mentioned above. As demonstrated by these ratios, both configurations are somewhat stretched, the octahedron slightly more than the tetrahedron, and in LuIG slightly more than in YIG.

Direct correlation of these rather small differences in structure with those in magnetic anisotropy is not possible at present. The latter may be due to the different level of impurities in the yttrium respectively lutetium source materials. These impurities may be other rare earth elements that have, in contrast to Lu and Y, a magnetic moment which may affect the magnetic properties of the compound, especially at low temperatures. (8)

A second, far more important, need for determining accurate oxygen positions in the different garnet materials exists if crystal-field theory is

TABLE III: INTERATOMIC DISTANCES (IN Å)

			YIG		LuIG
Fe-O	octahedron		2.00		2.04
	tetrahedron		1.88		1.87
Me-O	(Me = Y, Lu)	I	2.37		2.31
		II	2.43		2.38
	ionic radius	Y	1.05	Lu	0.99
O-O	octahedron	d_{o1}	2.99		3.09
		d_{o2}	2.68		2.68
	tetrahedron	d_{t1}	3.16		3.17
		d_{t2}	2.87		2.80
	ratio	d_{o1}/d_{o2}	1.12		1.15
		d_{t1}/d_{t2}	1.10		1.13

to be applied to magnetic ions in materials with garnet structure. The oxygen ions are the nearest neighbors to the magnetic ions of interest. On the basis of point charges located at the positions of these nearest neighbors, the crystal field existing at the location of the magnetic ions can be estimated. (9) This crystal field not only affects the magnetic anisotropy but also influences the energy levels of the magnetic ions directly, as found by paramagnetic resonance experiments. (10, 11, 12, 13) In this work garnet compounds have been used in which aluminum and gallium occupy the *a*- and *d*-positions. These ions have no magnetic moment. The compounds, therefore, are paramagnetic if the *c*-positions are occupied by rare earth ions like Yb, Er, or Dy.

In these garnets, the geometry of the dodecahedron of oxygen ions about the *c*-position becomes important. This dodecahedron may be described as a somewhat distorted cube. Its symmetry is that of three twofold axes crossing each other under right angles. One of these axes is drawn through two opposite "face centers" of this "distorted cube." The other two axes connect the bisecting points of opposing "cube" edges.

Work is in progress, in these laboratories, on the determination of accurate oxygen positions in yttrium–gallium garnet, yttrium–aluminum garnet, and gadolinium–iron garnet.

REFERENCES

1. E. R. Czerlinsky and W. G. Field. Proceedings of International Conference on Solid State Physics in Electronics and Telecommunications, Brussels, 1958.
2. G. P. Rodrique, H. Meyer, and R. V. Jones, *J. Appl. Phys.*, 31, 376S (1960).
3. S. Geschwind, *Phys. Rev.* To be published.
4. M. Renninger, *Zeits. Physik*, 106, 141 (1937).
5. W. R. Busing and H. A. Levy, *Crystallographic Least Squares Refinement Program for the IBM 704.* Oak Ridge, Tennessee: Oak Ridge National Laboratory, 1959.
6. S. Geller and M. A. Gileo, *J. Phys. Chem. Solids*, 3, 30 (1957); 9, 235 (1959).
7. F. Bertaut and F. Forrat, *Compt. rend.*, 244, 96 (1957).
8. R. F. Pearson and R. W. Cooper. Proceedings of Sixth Conference on Magnetism and Magnetic Materials. To be published in *J. Appl. Phys.*
9. J. C. Phillips, *J. Phys. Chem. Solids*, 11, 296 (1959).
10. J. W. Carson and R. L. White, *J. Appl. Physics*, 31, 53S (1960).
11. D. Boakes *et al.*, *Proc. Phys. Soc.* (London), 74, 663 (1959).
12. W. P. Wolf, *ibid.*, 74, 665 (1959).
13. M. Ball *et al.* Proceedings of the Seventh International Conference on Low Temperature Physics, Toronto, 1960.

HIGH-TEMPERATURE OXIDATION OF RARE EARTH METALS

KARL S. VORRES AND LeROY EYRING

Department of Chemistry, University of Miami, Coral Gables, Florida; and Department of Chemistry, State University of Iowa, Iowa City, Iowa

The study of the kinetics of high-temperature metal oxidation is always a study of a heterogeneous reaction. The reactants are the metal and oxygen, but after the reaction begins, an oxide barrier prevents further reaction unless diffusion of the reactants takes place.

Neglecting thin films, two types of behavior are generally observed, depending on the nature of the oxide film. The film may be either coherent and protective, or contain cracks and pores which would render it non-protective.

For a protective film the reactants must diffuse from one interface to another. Either oxide ions diffuse from the gas-oxide interface to the metal-oxide interface or metal ions diffuse from the metal-oxide to the oxide-gas interface. As the reaction proceeds the film thickness and diffusion path becomes longer. The rate of reaction depends on the rate at which the more mobile species passes between the interfaces. This rate decreases with increasing path length, due to the decreasing value of the concentration gradient. This may be formulated as

$$\frac{dX}{dt} = \frac{k'}{X}$$

where X = the thickness of the oxide or diffusion path, t = the time, and k is a constant dependent on the temperature. For a large sheet of metal it is easily seen that the thickness is proportional to the weight gain, and the expression may be rewritten as

$$\frac{dW}{dt} = \frac{k'}{W}$$

where W is the weight gain per unit of metal area. When integrated this expression is of the form:

$$W^2 = kt$$

Since this is the equation of a parabola, it is known as the parabolic law, and is also associated with diffusion of a reactant as the rate-determining step.

On the other hand, the oxide layer may be porous or cracked. In this case the gas does not encounter any barrier in reaching the metal, and the rate expression does not depend on the oxide thickness. Therefore, it may be written:

$$\frac{dW}{dt} = k$$

When integrated this is the equation of a straight line and is called the linear law.

$$W = kt$$

Thus, the linear law is associated with a porous or cracked coating.

Generally, the oxidation behavior with respect to the applicability of the parabolic or linear law may be predicted according to the Pilling and Bedworth or Tammann rule. This rule makes use of the ratio of the volume of oxide formed from a metal to the volume of metal which produced the oxide. The rule states that if the value of the ratio is greater than one the coating will be protective and coherent. The parabolic law will then be observed. On the other hand, if the ratio is less than one, the coating will be porous or cracked and the linear law will be observed. This rule serves reasonably well to predict behavior in a large number of cases.

Studies of the kinetics of oxidation involve the determination of the type of rate law, the value of the rate constant at different temperatures, and the determination of activation energies for oxidation. Conventionally, this requires the preparation of a metal sample for each measurement at each temperature. Where a large number of measurements are made, this becomes quite repititious and time-consuming. A method of more rapidly determining the rate constant at different temperatures would be advantageous. Two approaches were tried. One approach, called the semiconventional method, may be best understood in terms of the conventional method. Suppose that the rate law is known and the proper function of W (that is, W^n) is plotted versus the time to obtain a straight line. The slope of the line gives the rate constant at the temperature of the experiment. If the data are obtained for a period long enough to get a rate constant at that temperature, and then the temperature is increased to some new value, a new straight line should be obtained whose slope would give the rate constant at the new temperature. This process may be repeated as often as desired and the conditions warrant. The result is a series of straight-line segments, each of which gives a rate constant.

The second approach, called the continuous-temperature-increase (CTI) method is essentially an extension of the semiconventional one. Suppose that a large number of temperature changes are made. As the number increases the plot of the function of W versus time approaches an exponential curve. In the limit it is an exponential curve if the Arrhenius type expression,

$$k = Ae^{-E/RT}$$

is obeyed. Here A is a constant, E is the activation energy, R is the gas constant, and T is the absolute temperature. The large number of temperature increases may most conveniently be carried out by using a linear temperature increase, such that $T = at + T_o$, where a is the heating rate. By extending the reasoning of the semiconventional method, the tangent to the curve of W^n versus time at any time would give a rate constant. This constant is then a rate constant for the temperature at which the tangent was drawn. Thus, in principle with this method, an infinite number of rate constants can be obtained from a single experiment. This indicates the advantage of the CTI method in terms of time. It is also advantageous in that a greater temperature range can be covered than is possible with conventional methods (the oxide serves as a container for the molten metal). More information can be obtained from a single sample—which is advantageous when the supply of material is limited.

The rate constants may be obtained by plotting the data as W^n versus time, drawing curves through the points, and finally drawing the tangents to the curves. The tangents may be drawn visually. A check using four different people beginning with the same raw data showed virtually the same rate constants and activation energies. A mirror may be used to aid in drawing the tangents, or the rate constants may be approximated from

$$\frac{dW^n}{dt} = k = \frac{\Delta W^n}{\Delta t} = \frac{W_1^n - W_2^n}{t_1 - t_2}$$

The latter method was also compared with the tangent method, and gives the same results.

This approach is quite general and merits further study in other systems (homogeneous, and so forth).

The metal samples were small approximate cubes about 6–8 mm on edge. They were sawed from an ingot and polished under mineral oil through 4/0 metallurgical finishing paper. Then they were rinsed in CCl_4, weighed, and placed in an Alundum-lined platinum bucket.

The metals obtained from the Ames Laboratories of the Atomic Energy Commission at Ames, Iowa, were La, Ce, Nd, Sm, Pr, and Yb. Some La and Ce were obtained from the Research Laboratories Company of New-

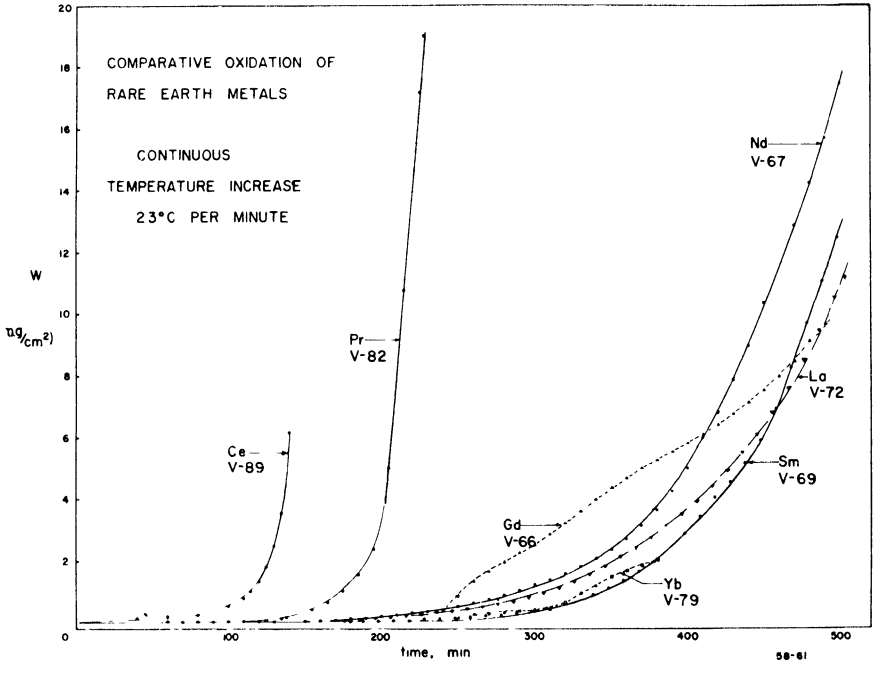
town, Ohio, and from the Heavy Minerals Corporation of Chattanooga, Tennessee. Some Gd was obtained from the Lunex Corporation of Pleasant Valley, Iowa. The metals from the Ames Laboratories were the most pure, stated to be 99.9+ per cent. Those of the Research Laboratories were stated to be 99+ per cent pure, and from the Heavy Minerals and Lunex Corporations, 98+ per cent pure.

The experiments were carried out with these metals in a recording thermobalance with a temperature regulator. This used a continuous stream of oxygen, dried over BaO, at atmospheric pressure.

All of the rare earth metals obeyed a parabolic oxidation law. However, the cerium samples underwent a transition from the parabolic to the linear law after a variable period of time. The transition did not seem to be solely dependent on time or oxide thickness.

The behavior of the metals in the CTI type of oxidation experiment is shown in the figure below. This figure shows that the metals can be divided into two groups. Ce and Pr oxidize much more rapidly than the remainder. The La, Nd, Sm, Gd, and Yb all oxidized at much slower, relatively similar rates.

The anomalous behavior of the Gd shown in the figure can be traced to the presence of impurities in the metal. The impurity—most likely Ta in this case—concentrated in the grain boundaries. On heating, the im-



purity preferentially oxidized leaving a bumpy surface of white oxide on a background of thin transparent Gd_2O_3. The net result was an accelerated oxidation at the early stages.

The Ce and Pr both exhibit a tetravalent, as well as the common trivalent, state. A number of oxide phases are known to occur between the limits of the sesquioxide and the dioxide. It is believed that the rapid rate of oxidation is due to a more rapid rate of diffusion through these phases than through the sesquioxide.

The behavior of the remaining metals may be correlated on the basis of the Pilling and Bedworth ratio. The more the ratio for a metal deviates from one, the more strain is introduced during the formation of the oxide, and the larger the number of defects present. If the ratios are compared, it is observed that the larger they are the more rapidly the metals oxidize. No divalent oxides were observed with Sm or Yb.

The rates and data reproducibility were affected by annealing of the metal and oxide, previous treatment and thermal history of the sample, and the passage of argon over it. Such effects tended to disappear at high temperatures, where bulk diffusion is most important.

Oxygen diffusion though the oxide seems to be the mechanism involved in all of the reactions, with the possible exception of samarium. This might be expected since the structure of the oxides are all related to the fluorite structure, and the migration of the anions seems to take place almost to the exclusion of the cations where this has been studied.

PART THREE

Structure of Metals, Alloys, and Intermetallics

COMPARATIVE CHEMISTRY OF THE LANTHANIDE AND ACTINIDE ELEMENTS

B. B. CUNNINGHAM

Department of Chemistry and Lawrence Radiation Laboratory, University of California, Berkeley, California

It has been recognized for some time that the heavier actinide elements are similar to the rare earths in the sense that they contain various numbers of *f*-electrons in an incomplete inner shell.

The extent to which homologous configurations (same numbers of *d*- and *f*-electrons outside closed shells) actually occur between members of the two series, and the real or expected resemblances in chemical and physical properties of the homologous elements, have been subjects of much interest, considerable experimental investigation, and no little debate.

Comparisons of this kind cannot be made in a meaningful way without accurate and extensive knowledge of the physical and chemical properties of the elements of both series. Such information has been, and still is, rather fragmentary for most of the actinides, and indeed not all members of this series have been discovered as yet.

Recently, however, there has been a rapid accumulation of information about the ground-state configurations of the actinide elements, and comparisons with the lanthanides on this basis may now be made for a number of heavy elements.

While, in general, significant comparisons between the two transition series have been hindered mainly because of lack of information about the actinide elements, interest in such comparisons has stimulated areas of research in rare earth chemistry which have yielded new and interesting results, particularly with respect to multivalency in the 4*f*-series.

The most significant contribution of the study of the actinide elements to rare earth chemistry, however, is that it has shed new light on the kinds of chemical relationships that are possible among numbers of an inner or *f*-transition series.

ELECTRONIC CONFIGURATIONS OF THE LANTHANIDE AND ACTINIDE ELEMENTS AND THEIR POSITIONS IN THE PERIODIC SYSTEM

In the lanthanide-actinide comparison, there has been a major controversy regarding the proper assignment of the actinide elements to positions in the periodic system.

Seaborg (1) and his supporters assign the actinides to the positions of a second rare earth series, immediately below the lanthanides in the conventional long form of the periodic table. This assignment is a logical consequence of the actinide terminology advocated by Seaborg and widely adopted in the United States.

Assignment and terminology both have been criticized (2) by some European and American chemists, most of whom object to the actinide terminology, favor placing thorium and protactinium in groups IVa and Va of the periodic table, and, in general, oppose the positioning of the actinides in a second rare earth grouping.

Logical arguments may be adduced in support of each of these points of view, but there is no intention here to weigh the relative merits of these arguments.

Because of modern tendencies to relate the positions of the elements in the periodic system to their electronic configurations, the ground-state configurations of the actinide elements are highly pertinent to the question of their proper classification.

Ground-state configurations of the neutral gaseous atoms of many actinide and lanthanide elements have been determined recently by W. A. Nierenberg and his associates (3) using the atomic beam resonance method. These data extend considerably the number of lanthanide and actinide configurations which have been determined unambiguously.

Known configurations are summarized in Table I. Similar configurations are exhibited by lanthanum-actinium, samarium-plutonium, europium-americium, and gadolinium-curium. The configuration of thorium is characteristic of the group IVa elements. The remaining actinide configurations are unique.

These and other data show that (1) similar electronic configurations between lanthanide and actinide elements do not necessarily confer marked similarities in chemical properties between the homologous elements, particularly with respect to oxidation-reduction behavior, and (2) the members of an inner or *f*-transition series are not necessarily markedly similar in chemical properties.

TABLE I: KNOWN GROUND-STATE CONFIGURATIONS OF NEUTRAL GASEOUS ATOMS OF SOME LANTHANIDE AND ACTINIDE ELEMENTS

Element	La	Ce	Pr	Nd	Pm	Sm	Eu	Gd	Tb	Dy	Ho	Er
Configuration	$5d$	$4f5d$	$4f^3$	$4f^4$	$4f^5$	$4f^6$	$4f^7$	$4f^75d$	$\left\{\begin{matrix}4f^9\\4f^85d\end{matrix}\right\}$	$4f^{10}$	$4f^{11}$	$4f^{12}$

Element	Tm	Yb	Lu	Ac	Th	Pa	U	Np	Pu	Am	Cm
Configuration	$4f^{13}$	$4f^{14}$	$4f^{14}5d$	$6d$	$6d^2$	$5f^26d$	$5f^36d$	$5f^46d$	$5f^6$	$5f^7$	$5f^76d$

In this connection it must be remembered that at present there is no satisfactory explanation for the remarkable similarity in the chemical properties of the rare earth elements. It would appear to be due to a rather fortuitious balance between ionization potentials on the one hand and crystal and hydration energies on the other. (4) Clearly, however, it is not due per se to the fact that these elements are members of an inner transition series. It is possible that in a more general sense—that is if the periodic system contained several *f*-transition series—the 4*f*-series might be regarded as atypical.

It is a characteristic feature of the atomic beam resonance methods that they yield very accurate values for the Lande factor g_J. For this reason the resonance data are a source of detailed information about the type of interaction between the electrons in the various elements.

In order to achieve satisfactory agreement between observed and calculated g_J values for the lanthanides, Judd and Lindgren (5) recently have shown it is necessary to introduce into the theoretical calculations the Schwinger correction, as well as corrections for relativistic and diamagnetic effects, and for deviations from pure Russell-Saunders coupling.

In the rare earth elements very satisfactory agreement now exists between theory and experiment.

Similar corrections are required to obtain agreement between theory and the resonance experiments on the actinides, but in addition it is found that the electrostatic interaction between the 5*f*- and 6*d*-electrons in unfilled shells is weaker than the spin-orbit interaction, whereas the reverse is true in the lanthanides. In general, however, the interaction of the electrons within the 5*f*-subshell approximates closely to the pure LS limit.

Although there are relatively few cases of homologous configurations between the neutral atoms of the lanthanide and actinide elements, a considerable body of magnetic and spectroscopic evidence indicates that there are many cases of homologous configurations between the ions of these elements. In general, the tripositive ions of the actinide elements have configurations similar to their rare earth homologs. An interesting example is that of Th^{+3}, where spectroscopic evidence shows that the configuration is f^1. This fact can be used as an argument against including thorium with the IVa elements.

Bulk magnetic-susceptibility measurements on various actinide ions in aqueous solution indicate that the heavy element ions through californium have configurations similar to their rare earth homologs in corresponding states of oxidation. However, such data cannot be taken as conclusive, unless the measurements and assignment are in satisfactory agreement with theoretical calculations. Such agreement now exists for

$Pa^{+4}(5f^1)$, $Cm^{+3}(5f^7)$, $PuO_2^{++}(5f^2)$, $NpO_2^{++}(5f^1)$, $U^{+3}(5f^3)$, and $AmO_2^{++}(5f^3)$. Preliminary agreement is found also for $Pu^{+3}(5f^5)$ and $Am^{+3}(5f^6)$, although the theory of these more complicated cases has not been fully developed.

Measurements of the susceptibilities of the hydrated ions Bk^{+3} and Cf^{+3} would appear to confirm the $5f^8$ and $5f^9$ configurations, but these assignments must await the test of full theoretical interpretation.

Experimental studies of the optical absorption and fluorescence spectra of ions in crystal matrices have shown that the positions and even the order of excited levels may be greatly different for homologous lanthanide and actinide ions. Preliminary evidence from comparative studies of the spectra of Eu^{+3} and Am^{+3}, both of which have $^7F_0$ as the ground term, indicates that the splitting between the $J = 0$ and $J = 1$ fine-structure levels is about 2,000 cm^{-1} in Am^{+3} as compared with about 300 cm^{-1} in Eu^{+3}. (6) In americium there is a considerable admixture of higher terms with the ground term.

An interesting result of the current investigation of americium trichloride is that the magnitude of the crystal-field splitting appears to be of the same order of magnitude as that found in rare earth crystals.

Although both the experimental and theoretical investigations of the energy levels of the middle actinide and lanthanide elements present formidable difficulties, progress in this area is now being made at a remarkable rate.

METALS

Some physical properties of the lanthanide and actinide metals are presented for comparison in Fig. 1. (7)

Atomic volumes of the actinide metals are generally smaller than for the corresponding rare earth, reflecting the use of a larger average number of electrons per atom in forming metallic bonds. Heats of vaporization of the actinide metals are correspondingly increased over those of the lanthanides. The lanthanide metals form simple close-packed structures in most cases; however, the room-temperature structures of the actinide metals from protactinium through plutonium are complex, and, in general, the metals exhibit extensive polymorphism. Close-packed structures are encountered in americium, and preliminary evidence indicates that curium is similar in this respect to americium and to the rare earth metals.

A detailed study of the crystallography and magnetic susceptibility of americium metal is now being carried out at the Lawrence Radiation Laboratory at Berkeley. (8) The metal may be obtained as either a double hexagonal close-packed phase, or a face-centered cubic phase, ac-

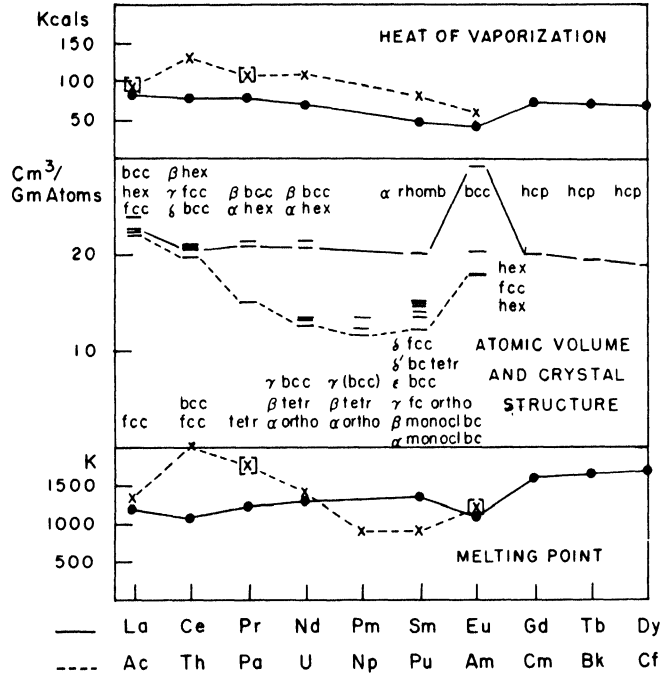


Fig. 1. Some properties of the lanthanide and actinide metals.

cording to the method of preparation. High-temperature distillation yields the cubic phase, while ordinary reduction methods followed by slow cooling produce hexagonal metal. Since the cubic phase transforms fairly rapidly to the hexagonal on cooling at dry ice temperatures, the hexagonal phase appears to be the room-temperature stable modification.

There is evidence that the *dhcp* structure exists in an expanded as well as a collapsed phase, analogous to the expanded and collapsed phases of metallic cerium. A number of preparations of metallic americium have yielded *dhcp* with $a = 3.642 \pm 0.005$A, $c = 11.76 \pm 0.01$; while others have given *dhcp*, $a = 3.474 \pm 0.005$A, $c = 11.25 \pm 0.02$A. Curium also appears to possess a close-packed structure with a lanthanide-like metallic radius, but the investigation of this metal is tentative and very incomplete. The magnetic susceptibility of americium metal (*dhcp* "collapsed") shows a temperature dependence of less than a few per cent over the range of temperature from room temperature to 77 °K.

Thus it appears that metallic americium, and probably curium, resemble rare earth metals, while the lighter actinides possess distinctively different properties.

CRYSTALLOGRAPHY AND THERMOCHEMISTRY OF COMPOUNDS

It has been known for many years that the radii of the lanthanide and actinide ions in corresponding states of oxidation are closely similar, and that there are many examples of isostructuralism and isomorphism between compounds. (9) These cases are too familiar to require extensive illustration here.

Studies of the crystallography of the actinide compounds recently have been extended to the oxide, oxychloride, and trichloride of californium. (10) Although calculations of the lattice parameters of these compounds have not yet been completed, a plot of the lattice parameters *a* and *c* of some lanthanide and actinide trichlorides are presented for comparison (Fig. 2). (11)

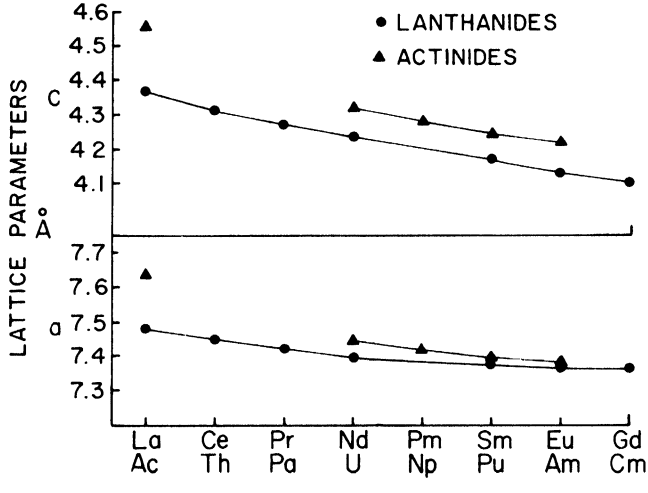


Fig. 2. Lattice parameters for some lanthanide and actinide trichlorides.

For these cases, the actinide contraction is considerably greater for a given range of atomic numbers than the lanthanide contraction, particularly along the *a* axis.

Of more interest with respect to isomorphous compounds of the lanthanides and actinides is the comparison with respect to such properties as melting points, or heats of vaporization or solution (12), since marked differences could be taken as evidence for significant differences in bonding. Comparisons of such properties are presented for a few cases in Table II. The heats of vaporization of the actinide compounds appear to be significantly higher than for similar lanthanide compounds, indicating somewhat stronger bonding.

TABLE II: COMPARISONS OF MELTING POINTS AND HEATS OF VAPORIZATION OF SOME LANTHANIDE AND ACTINIDE TRIHALIDES

Melting Point (°K)		Heat of Vaporization (kcal mole^{-1})	
$CeCl_3$	1075	$CeCl_3$	53
$NdCl_3$	1033	$NdCl_3$	52
$PrCl_3$	1049	$PrCl_3$	52
UCl_3	1108	UCl_3	42
$PuCl_3$	1033	$PuCl_3$	57
$CeBr_3$	1005	$CeBr_3$	47
$PrBr_3$	966	$NdBr_3$	47
$NdBr_3$	957	$SmBr_3$	46
UBr_3	1003	$PuBr_3$	57
$PuBr_3$	954		

Much more pronounced differences in thermochemical properties are found on comparison of the oxidation-reduction behavior of the rare earths and the actinides. This is illustrated in Fig. 3, in which the free energies of formation of the aqueous ions are plotted as a function of atomic number. The free energies of formation of the aqueous tripositive ions of

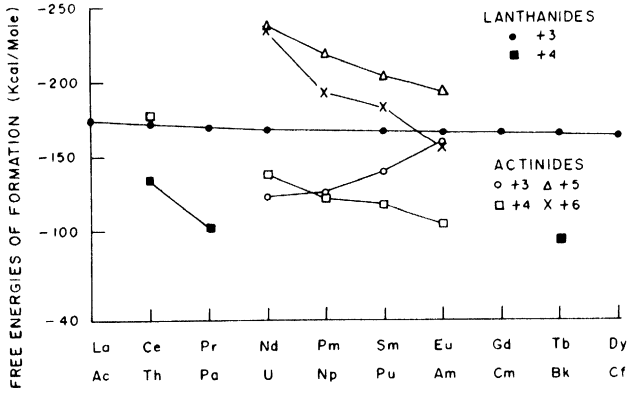


Fig. 3. Free energies of formation of aqueous lanthanide and actinide ions.

the lanthanide elements are seen to be remarkably constant and almost independent of atomic number. The free energies of the tetrapositive ions increase rapidly (toward more positive values).

REFERENCES

1. J. J. Katz and G. T. Seaborg, *The Chemistry of the Actinide Elements*. London: Methuen and Company, Ltd., 1957, Chapter XI.
2. M. Haissinsky, *La Chemie nucleaire et ses applications*, Mason et Cie, Paris. (1957). W. H. Zachariasen in Seaborg and Katz (eds.),

The Actinide Elements "National Nuclear Energy Series," Vol. 14A. New York: McGraw-Hill Book Company, 1954, Chapter 18.

3. J. C. Hubbs, R. Marrus, and J. O. Winocur, *Phys. Rev.*, 114, 586–589 (1959); J. C. Hubbs *et al.*, *ibid.*, 109, 390–398 (1958); R. G. Albridge, J. C. Hubbs, and R. Marrus, *ibid.*, 111, 1137–1139 (1958); Amado Cabezas *et al.*, *ibid.*, 118, 233–234 (1960); Richard Marrus, *UCRL 8547*, Nov. 23, 1958; A. Y. Cabezas *et al.*, *UCRL 9122*, Mar. 16, 1960; Richard Marrus, William A. Nierenberg, and Joseph Winocur, *UCRL 9207*, May, 1960; A. Y. Cabezas and I. P. K. Lindgren, *UCRL 9163*, May 9, 1960; Joseph Winocur, *UCRL 9174*, April 13, 1960.
4. B. B. Cunningham. Proceedings of the Seventeenth International Congress of Pure and Applied Chemistry (Munich, Germany) Sept., 1959. In press.
5. B. R. Judd and I. P. K. Lindgren, *UCRL 9188*, May 9, 1960.
6. J. H. Van Vleck, *Theory of Electric and Magnetic Susceptibilities.* New York: Oxford University Press, 1932, p. 246.
7. F. Spedding and A. Daane, *Progress in Nuclear Energy.* London: Pergamon Press, 1956, Vol. I, Series V.
8. D. B. McWhan, *et al.*, *UCRL 9115*, April, 1960.
9. W. H. Zachariasen, in Seaborg and Katz (eds.), *The Transuranium Elements*, "National Nuclear Energy Series," Vol. 14B. New York: McGraw-Hill Book Company, 1949.
10. B. B. Cunningham and J. C. Wallmann. Unpublished data.
11. W. H. Zachariasen, in Seaborg and Katz (eds.), *The Actinide Elements* "National Nuclear Energy Series," Vol. 14A. New York: McGraw-Hill Book Company, 1954, Chapter 18; D. H. Templeton and C. Dauben, *J. Am. Chem. Soc.*, 76, 5237 (1954).
12. R. C. Vickery, *Chemistry of the Lanthanons.* New York: Academic Press, 1953. W. M. Latimer, *Oxidation Potentials*, 2d ed. Englewood Cliffs, N.J.: Prentice Hall, Inc., 1952; J. J. Katz and G. T. Seaborg, *The Chemistry of the Actinide Elements.* London: Methven and Company, Ltd., 1957.

CELL DIMENSIONS AND MAGNETICAL SUSCEPTIBILITIES OF THE MX COMPOUNDS OF RARE EARTHS WITH P, As, Sb, Bi, S, Se, Te

A. IANDELLI
University of Genoa, Italy

The present work has been carried out in order to complete the existing data on compounds with general formula *MX*, which the rare earths make by reacting with metalloids of the fifth and sixth group of the periodic system.

Such compounds were already known for the elements from La to Sm (1, 2, 3). Here, they have been studied for almost all the others (Gd, Tb, Dy, Ho, Er, Tm, Yb, Y), and examination of the crystal structure and magnetical susceptibilities was directed toward investigating: (1) the variations which result for series of isomorphos compounds of rare earths with ionic-metallic link, (2) the behavior of the elements with a valence other than three, and (3) the possibility that one of these compounds has magnetical anomalies like those observed for some metals (ferromagnetism and antiferromagnetism). Investigations of other properties, such as electrical conductivity, are planned for a further work.

The compounds studied are simplest as to crystal structure (NaCl-type). Others existing in the corresponding systems are known only partially. In systems with S, Se, Te, there are compounds with formula MX, M_3X_4, M_2X_3, and, in some cases, MX_2; in those with P, As, Sb, Bi, certainly, there are several other compounds besides the MX-type studied, but only for La–Sb is the thermal diagram completely known.

PREPARATION

In every case the compounds were prepared by direct reaction between the two elements. As to the metalloids, commercial pure products were used, sometimes with remelting (S, Se, Te) or distilling (As) under vacuum. As to the rare earth metals, the products of the Nuclear Corporation were used. Heretofore, in the case of Sm and Gd, metals were used which were obtained in the laboratory, and these had a lower purity (99.4 per cent Sm; 99.2 per cent Gd).

The reaction was carried out twice. First, turnings of the rare earth metal (about 1 g weight) were set to react in quartz tubes, sealed under

vacuum with the corresponding quantity of metalloid vapor; heating slowly to about 600°C. In this way, brown powders were obtained which were constituted superficially by the phases M_3X_4, and still containing metal inside. Afterward, the powders were pressed in the form of tablets and heated under argon at different temperatures. For the compounds with metalloids of the fifth group (and for the ones of Sm and Yb with S, Se, Te), the final temperature was 1100°C; for the others, it had to be higher. For compounds with S, Se, and Te of the elements from Gd on, in many cases, nonhomogeneous products were obtained, unless a prolonged heating at 1450°C was undertaken.

With such a process, the compounds obtained at 1100°C appear as compact sintered products, of black color—and with an appearance more and more metallic, proceeding from phosphides to bismuthides, and, for Sm and Yb, from sulphides to tellurides. All the others (with S, Se, Te) have a metallic appearance, but they are colored from yellow to red-violet. If the sample is not completely homogeneous, the color is more intense; for example, the sulphides are yellow-gold, but, if the reaction of formation has not been performed, the color appears as red-violet.

Full homogeneousness is the most important result to obtain. Since, in preparation, all reaction with the walls of the container was avoided, the analysis, made only in some cases, did not reveal (within 0.1–0.2 per cent) variations from the initial composition.

STRUCTURE

Structure was determined through use of the powder method, with standard cameras, and with K α radiation of Fe for the compounds of Sm, Gd, Tb, Dy, and of Cu for the others. Tables I and II contain the values of the cell constants; these are also reproduced in Fig. 1.

TABLE I: CELL CONSTANTS OF *MX* COMPOUNDS (NaCl-TYPE) IN Å*

	La	Ce	Pr	Nd	Sm	Eu	Gd
S	5.854	5.777	5.739	5.692	5.970	5.969	5.563
Se	6.063	5.992	5.947	5.909	6.200	6.185	5.781
Te	6.422	6.359	6.322	6.262	6.594	6.585	6.139
P	6.025	5.909	5.872	5.838	5.760	...	5.723
As	6.137	6.072	6.009	5.970	5.921	...	5.862
Sb	6.488	6.412	6.366	6.322	6.271	...	6.217
Bi	6.578	6.500	6.461	6.424	6.362	...	6.316

*For compounds of La, Ce, Pr, Nd with P, As, Sb, Bi, see A. Iandelli and E. Botti, *Atti Accad. Lincei VI*, **26**, 233 (1937); for compounds of La, Ce, Pr, Nd with S, Se, Te, see A. Iandelli, *Gazz. chim. ital.*, **85**, 881 (1955); for compounds of Sm, see A. Iandelli, *Z. anorg. Chem.*, **288**, 81 (1956); for compounds of Eu, see W. Klemm and H. Senff, *Z. anorg. Chem.*, **241**, 259 (1939).

TABLE II: CELL CONSTANTS OF *MX* COMPOUNDS (NaCl-TYPE) IN Å

	Tb	Y	Dy	Ho	Er	Tm	Yb
S	5.517	5.493	5.490	5.465	5.432	5.412	5.677
Se	5.740	5.703	5.711	5.680	5.662	5.640	5.931
Te	6.101	6.080	6.075	6.049	6.021	...	6.361
P	5.686	5.662	5.654	5.626	5.606	5.573	5.554
As	5.827	5.805	5.803	5.771	5.745	5.721	5.702
Sb	6.180	6.165	6.160	6.130	6.107	6.091	6.079
Bi	6.280	6.259	6.251	6.228	6.202	6.192	...

A very important question is whether the compounds form solid solutions. No detailed research has been made on this point; we have merely observed the different behavior of various samples of the same compound. For the compounds with the fifth-group metalloids, the range of homogeneousness seems very small. Differences in cell constants for different samples offer some similarity in the third decimal figure, and the same is true for compounds of Sm and Yb with S, Se, and Te. For those compounds with sixth-group metalloids, nonhomogenized samples give differences of one to two units in the second decimal figure; the values in Tables I and II are for the best (most homogeneous) samples.

In undertaking the present work, we were aware that Professor Flahaut (4) had published a series of works on the sulphides and selenides of the rare earths from La to Gd, also investigating all other compounds of the systems, though with a different method of preparation. The values he published in 1959 for the *MX* compounds are very near mine of 1955–1956 for La, Ce, Pr, and Nd, but are somewhat more inferior for the Sm com-

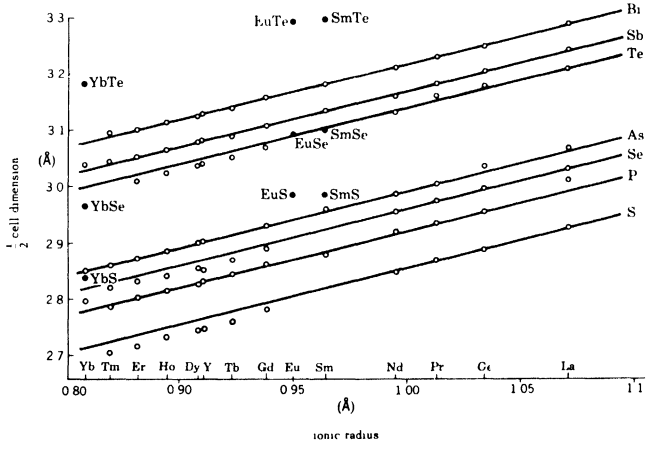


Fig. 1. Approximations of the values of the cell constants.

pounds. Because the values reproduced in Table I have been concordantly obtained on many samples prepared at different times, and with different starting metals, I believe that the present values must be regarded as the most exact.

For a comparison with the obtained values of the cell constants, the graph in Fig. 1 has been constructed with the distances *M-X* a function of the ionic radii of trivalent rare earths. For such radii, the values of Templeton and Dauben (5) have been used (with the exception of La, for which a little higher value has been used—1.071 instead of 1.061 A. It can be seen that the experimental values are well arranged on straight lines at 45-deg angles. (The unit on the two axes is different on Fig. 1, which might be expected when the distances are additive.) It is therefore possible to obtain a series of radii for the metalloids, as discussed hereafter.

An exception is presented by compounds with the metalloids of the sixth group. Up to Gd, behavior is the same as for metalloids of the fifth group; in the case of the following elements, values are more inferior than one might expect, and the reason for this is puzzling.

MAGNETIC SUSCEPTIBILITY

Magnetic susceptibility has been measured for almost all the *MX* compounds from Sm to Yb, and also for metals taking the Foex and Forrer method, modified by Pacault, in a temperature range from −200 to +200–300°C, and with a constant field of 8200 oersteds. The results, to which these explanations may be added, are given in Tables III and IV.

(1) As to the compounds of Y, a slight paramagnetism has been found due to impurities of small quantities of other rare earths. The susceptibility of the others except Sm, follow the Curie-Weiss law and the magnetic moments obtained within the errors of measurements correspond to those for the trivalent ions.

TABLE III: MAGNETIC PROPERTIES OF METALS USED IN THIS STUDY

Metal	$10^6 \chi_A$ (298° K)	μ_B	θ	Temp. Range	
Sm	1367	...	...	...	
Gd	476190	7.91	+289	323–573°K	ferr. at 289°K
Tb	137931	9.45	+217	228–500°K	ferr. at 219°K
Dy	94340	10.31	+158	175–473°K	Néel temp. 175°K
Ho	71942	11.2	+86	208–473°K	Néel temp. 131°K
Er	47619	9.65	+53	203–473°K	slope change between 203 and 100°K
Tm	27027	7.71	+25	90–473°K	
Yb	1161	...	...	...	

TABLE IV: MAGNETIC PROPERTIES OF *MX* COMPOUNDS

MX	$10^6 \chi_M$ (298° K)	μ_B	θ	Temp. Range	
SmS	4717	4.34	−201	123–473° K	
SmSe	4505	4.53	−273.5	148–473° K	
SmTe	4292	4.33	−248	193–473° K	
SmP	1112	...	...	...	
SmAs	1086	...	...	...	
SmSb	1000	...	...	...	
SmBi	1169	...	...	...	
GdS	30300	8.01	−8.6	353–473° K	fast increasing of χ_M be-
GdSe	30300	8.20	−28.5	353–473° K	tween 353 and 263° K
GdTe	26042	7.63	+17.8	203–473° K	
GdP	28450	7.95	+40.5	208–473° K	
GdAs	27548	8.18	+6	192–473° K	
GdSb	25575	7.87	−5.5	233–473° K	
GdBi	24038	8.20	−51.4	90–473° K	
TbS	35088	9.63	−35.5	293–473° K	
TbSe	33755	9.82	−53.5	143–473° K	
TbTe	38760	9.57	+2.7	213–473° K	
TbP	39526	9.56	+9	163–473° K	
TbAs	39033	9.65	+2.2	193–473° K	
TbSb	36232	9.57	−18	163–473° K	
TbBi	38086	9.64	+1	211–473° K	
DyS	40000	10.39	−38.8	177–473° K	
DySe	40984	10.37	−3.0	203–473° K	
DyTe	45977	10.47	−0.5	173–473° K	
DyP	46729	10.34	+12	173–473° K	
DyAs	46948	10.51	+4	163–473° K	
DySb	45558	10.62	−11	161–473° K	
DyBi	44053	10.97	−43	90–473° K	
HoS	41464	10.50	−32	90–473° K	
HoSe	43478	10.62	−26	161–473° K	
HoTe	48780	10.50	+16	108–473° K	
HoP	46083	10.34	+8.6	178–473° K	
HoAs	46080	10.47	+8	174–473° K	
HoSb	44743	10.35	−1.4	169–473° K	
HoBi	44543	10.32	−0.1	185–473° K	
ErS	35088	9.50	−24.3	90–473° K	
ErSe	35635	9.56	−18.4	90–473° K	
ErTe	34965	9.30	−12	153–473° K	
ErP	37523	9.32	+8	197–473° K	
ErAs	37453	9.34	+6	196–473° K	
ErSb	36232	9.36	−4	158–473° K	
ErBi	35714	9.32	−6	143–473° K	
TmS	21505	7.42	−23.8	140–473° K	
TmSe	18180	6.89	−28.5	149–473° K	
TmTe	25641	7.63	+14	158–473° K	
TmP	25316	7.93	−6.5	90–473° K	
TmAs	24390	7.77	−12	90–473° K	
TmSb	26667	8.14	−11	90–473° K	
TmBi	25000	7.63	+12	90–473° K	
YbP	7813	4.5	−26	183–473° K	
YbAs	7825	4.61	−42	90–473° K	
YbSb	5450	3.74	−22	168–473° K	

(2) In the compounds with metalloids of the fifth group, Sm has a low susceptibility which increases with diminishing temperature (as for Sm_2O_3). Its behavior is different, however, in compounds with S, Se, and Te, where it is quite like Eu_2O_3, which has been used for a comparison, pointing out the presence of Sm^{2+} ions. It must be noted that, though the Sm^{2+} and Eu^{3+} ions have a magnetic moment varying with the temperature—according to Van Vleck—it is possible (for the temperature range studied) to apply the Curie-Weiss formula also to these ions, with very high values of θ, and with a formal value of the magnetic moment of about 4, $4\mu_B$.

As for Yb, only the susceptibilities of YbP, YbAs, and YbSb which follow the Curie-Weiss law have been measured, with values of the moment corresponding to Yb^{3+}. However, as shown in Fig. 1, the most metallic compounds (bismutides) among the examined series give the best agreement with the straight line. The ionic radii (mostly from Templeton and Dauben) and the other values here obtained are:

La^{3+}	1.071 A.	Tb^{3+}	0.923	S^2	1.855	for compounds only to Gd
Ce^{3+}	1.034	Dy^{3+}	0.908	Se^2	1.960	
Ce^{4+}	0.941	Ho^{3+}	0.894	Te^2	2.140	
Pr^{3+}	1.013	Er^{3+}	0.881			
Nd^{3+}	0.995	Tm^{3+}	0.869	P^3	1.920	
Sm^{3+}	0.964	Yb^{3+}	0.858	As^3	1.991	
Sm^{2+}	1.143	Yb^{2+}	1.02	Sb^3	2.170	
Eu^{3+}	0.950	Y^{3+}	0.910	Bi^3	2.217	
Eu^{2+}	1.137					
Gd^{3+}	0.938					

The type of valence existing in the compounds examined seems intermediate between ionic and metallic, but with a substantial difference among those compounds with metalloids of the fifth and sixth groups. As to the first, the positive and negative ions should have the same charge of 3; as to the second (except Sm, Eu, and Yb), the charges should be +3 and −2. In the second case, the structure should be formed by ions of different valence, and there should be a metallic electron for every M atom. These differences should agree with the different aspects of the two kinds of compounds and with the deviations in the cell constants of the second.

If the preceding interpretation is right, we may think of transformations in the compounds of Sm, Eu, and Yb as due to a passage of valence from 2 to 3 (similar to the ceriums at low temperature). This supposition will soon be investigated.

(3) The susceptibilities of SmS, SmSe, and SmTe between −80 and −130°C present but minor variations from the straight line $(1/X - T)$ ap-

parent with the antiferromagnetic type. The problem will be examined exactly in the near future.

(4) As to Gd, Tb, Dy, and Ho in compounds with S, Se, and Te, we first obtained some samples which presented magnetic anomalies corresponding to ferromagnetism or antiferromagnetism, at temperatures near the corresponding transformations for the metals. Samples that exhibited such behavior were nonhomogeneous and had slightly lower values for the cell constants. In the case of homogenized samples, the susceptibility varied regularly—with the exception of GdS and GdSe, where it had a very high increase within 353 and 263°K on all samples. The simplest explanation seemed to be that the irregular behavior of the susceptibility was due to metal dispersed in the mass of the compound. This problem will also be examined in the near future.

CONCLUSIONS

Of peculiar interest are those elements which may have the valence of 2 and 3. In the compounds of Sm, Eu, and Yb with S, Se, and Te, valence 2 appears the most stable, while, from the few trials made till now, it seems most difficult to obtain valence 2 with elements of the fifth group. We tried to obtain Sm_3As_2 with no result; X-ray photographs were the same as those of SmAs. We plan to go on with the study of this question in the future.

Finally, the possibility of using ionic radii for compounds with a remarkable metallic character appears quite surprising.

REFERENCES

1. A. Iandelli and E. Botti, *Rend. Lincei VI*, 26, 233 (1937).
2. W. H. Zachariasen, *Acta Crystall.*, 2, 291 (1949).
3. A. Iandelli, *Gazz. chim. ital.*, 85, 881 (1955); *Z. anorg. Chem.*, 288, 81 (1956).
4. J. Flahaut *et al.* Various papers in *Compt. rend.* (1955-1960).
5. D. H. Templeton and C. H. Dauben, *J. Am. Chem. Soc.*, 76, 5237 (1954).

MAGNETIC AND ELECTRICAL PROPERTIES OF RARE EARTH METAL SINGLE CRYSTALS

SAM LEGVOLD

Institute for Atomic Research and Department of Physics, Iowa State University, Ames, Iowa

Various methods have been tried in an effort to obtain rare earth metal single crystals. In early work the Bridgman technique gave crystals of Nd, Dy, Er, and Tb. More recently a strain anneal technique has shown promise. Arc-melted buttons of the metal are polished and annealed for several hours at a temperature about 150 deg below the melting point. There is a big advantage in the latter method in that fewer impurities are introduced in the growing process. The strain anneal method works well on Y, and has been used on alloys of 1 per cent Ho in Y and 0.6 per cent Ho in Y. It has also been used to obtain Ho single crystals.

Magnetic measurements reported below were made using a magnet with a vertical-field gradient and a chemical balance with which to measure the magnetic force on the sample. In the case of Dy, a spherical sample was used, and in other instances rectangular samples $1 \times 1 \times 10$ mm were employed. For the electrical-resistivity measurements, the rectangular samples were used.

RESULTS

DYSPROSIUM

The easy direction of magnetization in Dy (*hcp*) is along an a_0 axis. (1) This can be seen in Fig. 1, which shows the $\frac{1}{\chi}$ *vs.* T plot in the two crystallographic directions. Magnetization curves are shown in Fig. 2, and from these data the curves of Fig. 3 are obtained. The latter show the magnetic moment versus temperature in constant fields. There is an apparent Néel point at 175°K and a ferro-antiferro transition at 85°K. Thus Dy is ferromagnetic below 85°K, antiferromagnetic from 85 to 175°K, and paramagnetic above 175°K. The saturation moment found experimentally is 10.1 which is close to the theoretical g_J value of 10 for the tripositive Dy ion.

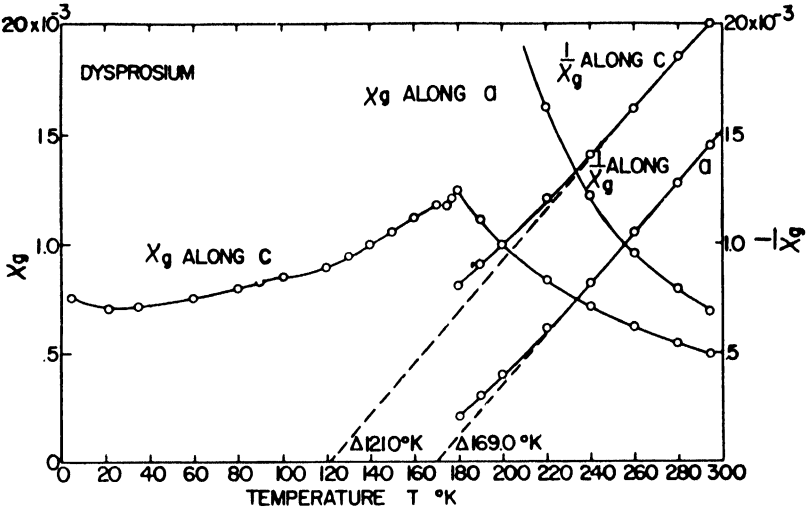


Fig. 1. Magnetic susceptibility of dysprosium.

Electrical-resistivity measurements on two Dy crystals (2) are shown in Fig. 4. From the experimental results the resistivity along c_0 was calculated. This shows a phenomenal peak at or near the Néel point. The a_0 resistivity apparently does not have this peak, although there is a change in the slope of the curve at the Néel point.

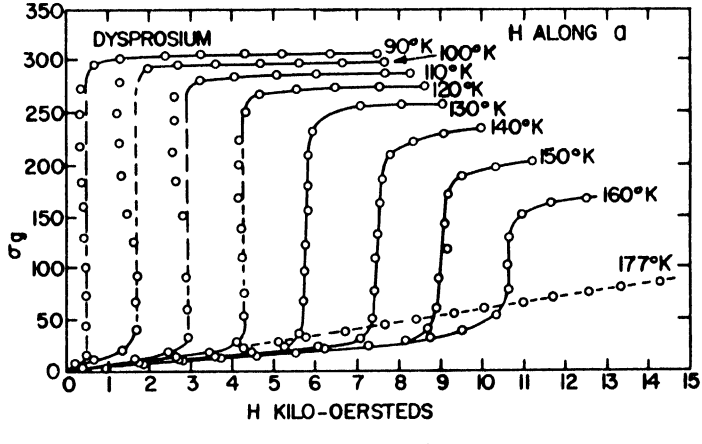


Fig. 2. Magnetization curves for dysprosium along a_0.

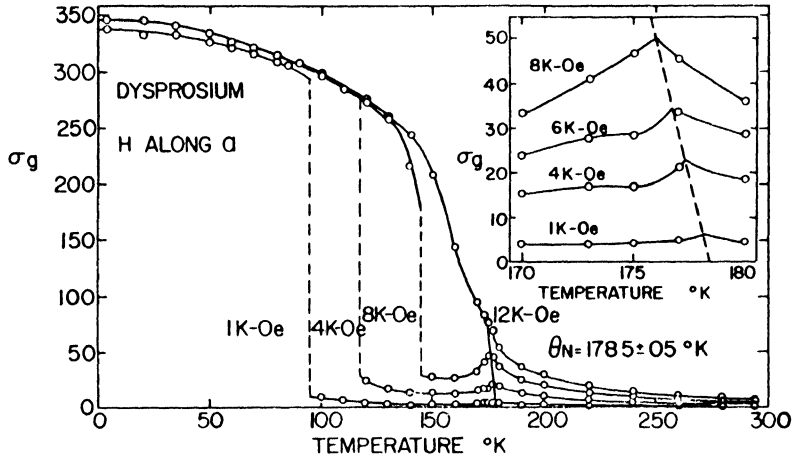


Fig. 3. Isofield magnetic moment *vs.* temperature for dysprosium.

ERBIUM

For Er (*hcp*) the paramagnetic susceptibilities (3) in the different crystallographic directions are shown in Fig. 5. It appears that c_o is the easy direction of magnetization in this metal. The data of Fig. 5 give a paramagnetic Bohr magneton number close to the theoretical value. In

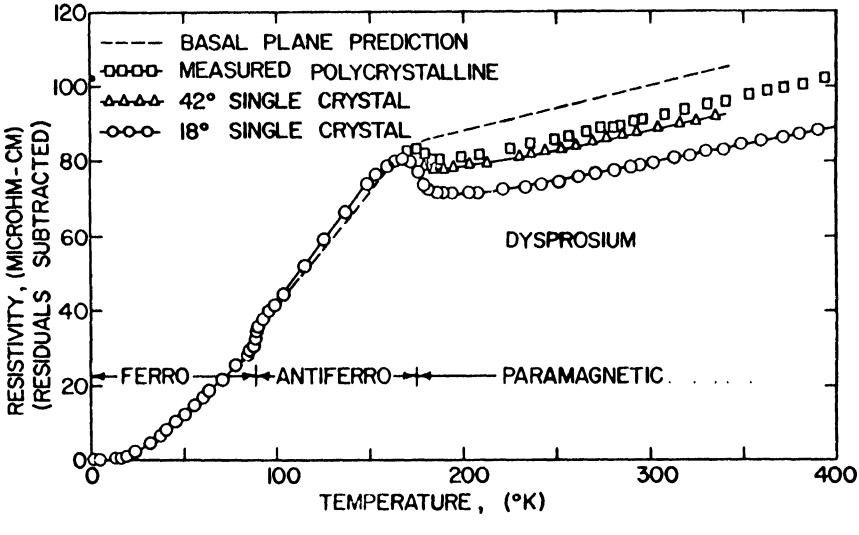


Fig. 4. Electrical resistivity *vs.* temperature for dysprosium.

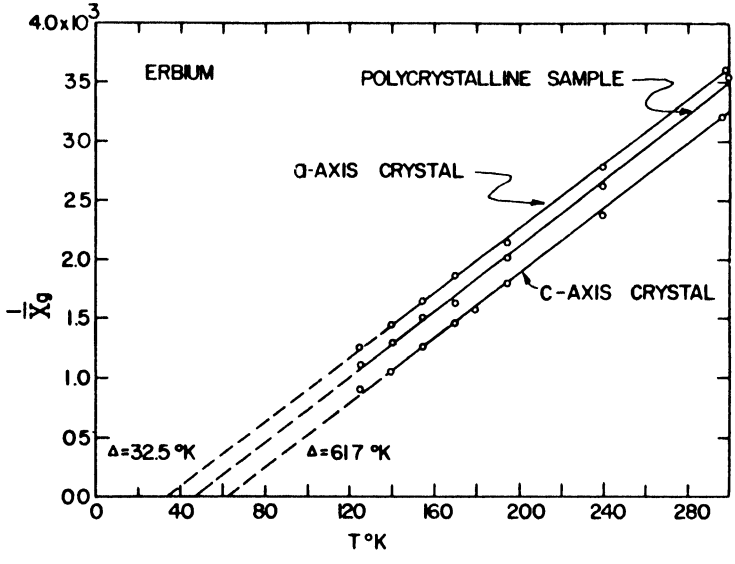


Fig. 5. Inverse magnetic susceptibility *vs.* temperature for erbium.

Fig. 6 curves giving the magnetic moment versus temperature at constant fields are shown. These curves indicate Er is ferromagnetic below 20 °K, antiferromagnetic from 20 to 85 °K, and paramagnetic above 85 °K. Figure 7 shows the magnetization curves at hydrogen and helium temperatures. The saturation moment along c_0, according to Fig. 7, is about 8

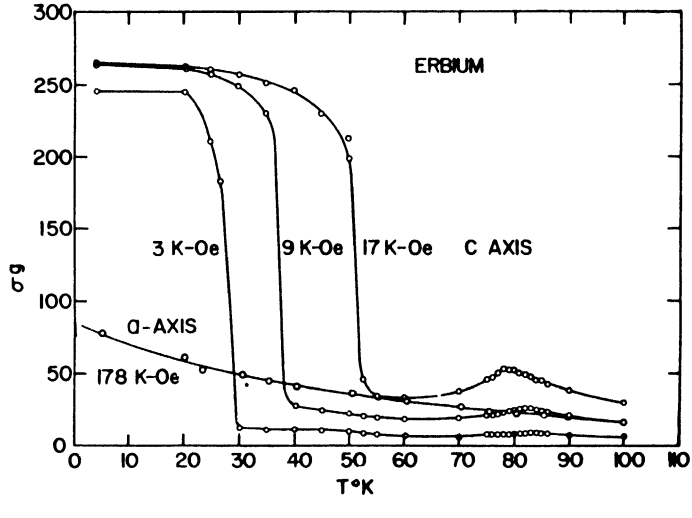


Fig. 6. Isofield magnetic moment *vs.* temperature for erbium.

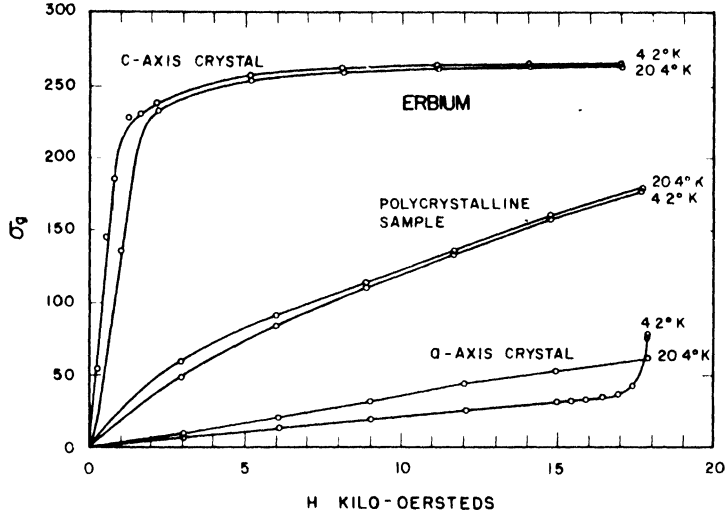


Fig. 7. Magnetization curves for erbium at 20.4°K and 4.2°K.

Bohr magnetons, and the theoretical value is 9 Bohr magnetons. It is interesting to note that along a_0 the 4.2°K curve rises rapidly at fields above 15 kilo-oersteds. Thus it may be possible to get the 9 Bohr magnetons in this direction by going to fields greater than 18 kilo-oersteds or by going to lower temperatures.

Electrical resistivity data (3) for Er are shown in Fig. 8. Again the resistivity along c_0 is particularly interesting and is somewhat different

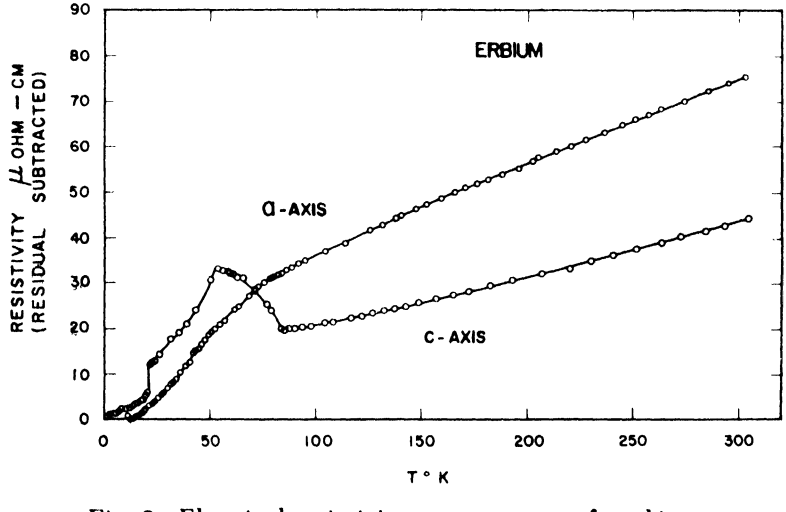


Fig. 8. Electrical resistivity *vs.* temperature for erbium.

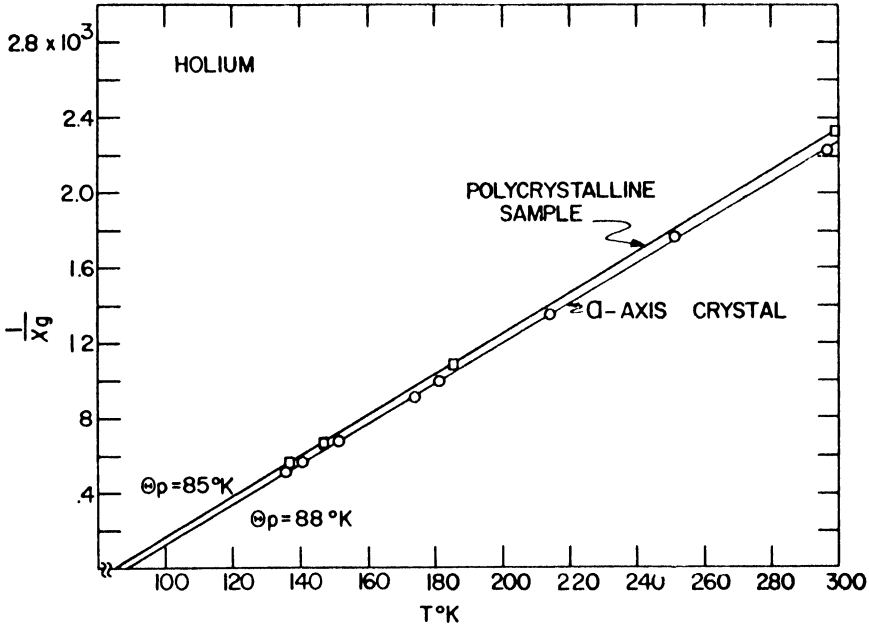


Fig. 9. Inverse magnetic susceptibility *vs*. temperature for holmium.

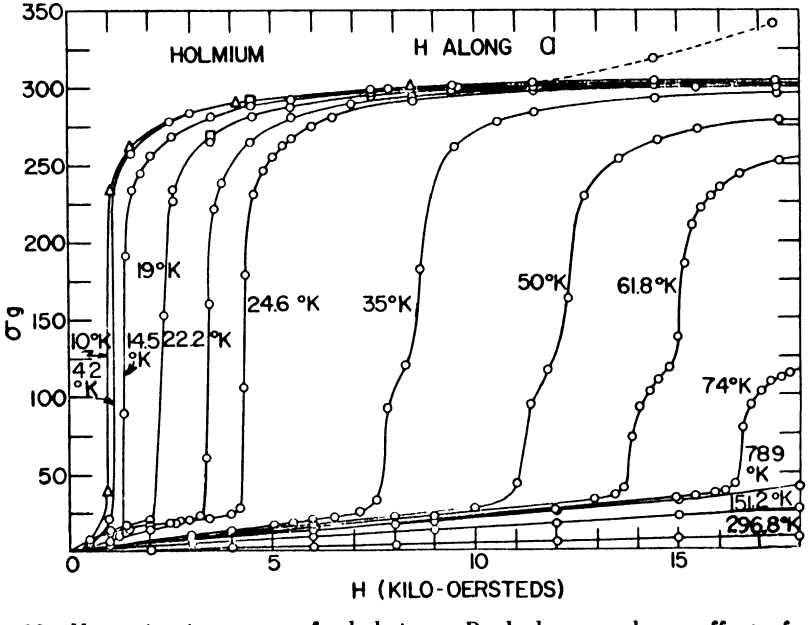


Fig. 10. Magnetization curves for holmium. Dashed curve shows effect of sample turning 30 from a_o in basal plane.

from the curve for Dy. One might surmise that antiferromagnetic ordering takes place over the entire temperature range from 54 to 78°K. It is also interesting to note how sharply the resistivity changes at the 20°K ferroto-antiferromagnetic temperature. No evidence of such a change is detectable in the a_0 resistivity.

HOLMIUM

Very recent measurements (4) on Ho have given the paramagnetic results shown in Fig. 9. It appears that the easy direction of magnetization is the a_0 direction. However, work at helium temperatures (Fig. 10) has shown that in fields greater than 12 kilo-oersteds Ho reaches higher moments when the field is applied between two a_0 axes in the basal plane. Then the saturation moment is very close to the theoretical 10 Bohr magnetons.

The work reported here has been done jointly with Dr. F. H. Spedding.

REFERENCES

1. Behrendt *et al.*, *Phys. Rev.*, **109**, 1544 (1958).
2. Hall *et al.*, *ibid.*, **117**, 971 (1960).
3. R. W. Green. Doctoral dissertation, Iowa State University Library (1960).
4. D. L. Strandburg. Research in progress.

MAGNETIC STRUCTURE PROPERTIES OF RARE EARTH METALS

W. C. KOEHLER, E. O. WOLLAN, M. K. WILKINSON, AND J. W. CABLE*

Oak Ridge National Laboratory Oak Ridge, Tennessee

It is now well known that a number of physical properties of the rare earth metals exhibit anomalous behavior due to the exceptional magnetic properties of these materials. A necessary prerequisite for an understanding of the fundamental processes responsible for these properties is the determination of the magnetic structures of these metals at various temperatures, and under varying conditions of application of an external magnetic field. Let us review the progress made, through neutron diffraction studies carried out at the Oak Ridge National Laboratory, toward the solution of these problems for metals of the second half of the series. We leave out of consideration Gd, because of its prohibitively high-capture cross section for thermal neutrons, and Yb and Lu, because they are diamagnetic.

The five remaining metals, Tb, Dy, Ho, Er, and Tm, all crystallize with the simple hexagonal close-packed structure, and all exhibit similar thermal and magnetic properties. For each of them is observed, at a temperature T_N, a transition from the paramagnetic state to what is generally termed an antiferromagnetic state. At a lower temperature T_C there is an order-order transition to what is usually referred to as a ferromagnetic state. Additional complex behavior in the intermediate-temperature range has been observed in several cases. Neutron diffraction measurements in the various appropriate temperature ranges have been made with polycrystalline specimens of each of these metals, and single crystal specimens of Dy, Ho, and Er have been investigated. We begin our description of results available at this time with those obtained for holmium.

---

*The authors wish to express their gratitude to Dr. F. H. Spedding, who has made available to them single crystal specimens of a number of rare earth metals, without which results reported here would have been impossible to obtain.

HOLMIUM

According to thermal (1) and magnetic (2) measurements, holmium appears to be antiferromagnetic between 20 and 133°K, and ferromagnetic below 20°K. In the ferromagnetic region the measured magnetization approaches $10\mu_B$ per holmium atom.

A typical set of neutron diffraction results in the antiferromagnetic temperature region is represented in Fig. 1, where the data are displayed as a mapping of scattering density in reciprocal space. The full circles represent the nuclear scattering. In the section shown it will be observed that (0001) is absent, and this is due to destructive interference in the scattering by the two holmium atoms in the chemical unit cell. The

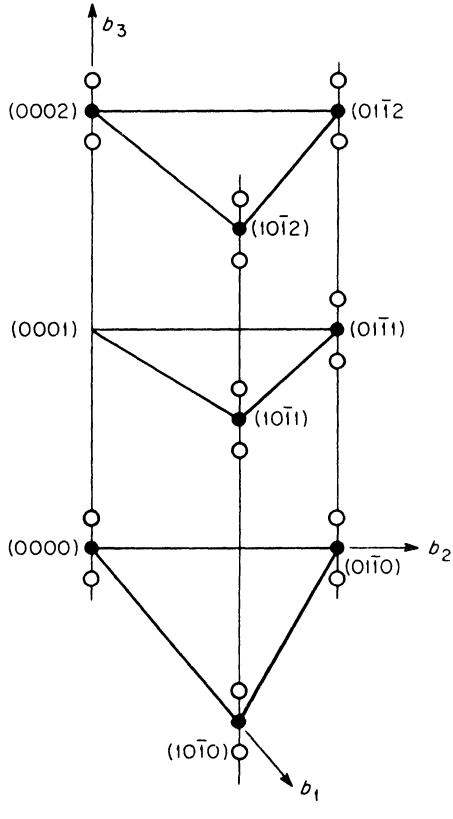


Fig. 1. Scattering density in reciprocal lattice of metallic holmium at 77°K. Full circles represent nuclear scattering; open circles represent magnetic satellites. The line along which the satellites are found determines the direction of the wave vector of the modulation. The separation of a given pair of satellites is a measure of the wavelength of the modulation.

magnetic scattering, represented by the open circles, appears in the form of satellites of the allowed nuclear reflections on lattice rows parallel to b_3. Systematic surveys of reciprocal space in the neighborhood of the origin, of (0001) and of $(10\bar{1}0)$, revealed no additional satellites, nor were magnetic contributions to the normal nuclear reflections detected. The sensitivity of the search for higher-order satellites was such that a secondary satellite 0.01 per cent as intense as the primary satellite of the origin would have been detected.

This general type of scattering-density map is similar to what one encounters in X-ray scattering by crystals with simple disorders (3), and it is possible to apply, with little modification, the theory of X-ray scattering in disordered structures to the diffraction of neutrons by magnetic structures. (4) One can readily show that one is forced by the above-mentioned observations to the conclusion that the magnetic-scattering amplitudes associated with the holmium atoms in the crystal are subject to a sinusoidal modulation. A detailed analysis of the absolute intensities implies that the high-temperature antiferromagnetic structure of holmium is the screw-type, or helical structure, in which the a_3 axis is the screw axis. This structure is illustrated in Fig. 2. The moments are parallel to each other in planes perpendicular to a_3, but between adjacent layers the moment directions differ by a definite angle ω.

The separation of a given pair of satellites is a direct measure of the interlayer turn angle. Measurements of the separation of satellites of (0000) and of $(10\bar{1}0)$ have been made at temperatures ranging from 4.2°K to a few degrees below the Néel point. The corresponding value of ω (Fig. 3) was observed to vary uniformly and linearly with temperature from 36 deg per layer at about 35°K to 49 deg per layer at 120°K.

Below 35°K, the map of scattering density exhibits some distinct changes. One finds, first of all, additional very weak higher-order satellites of the primary $(000H_3)$ satellites. The strongest of these, corresponding to the second and fifth harmonics of $(0000)^+$, have intensities which are about 1 per cent of that of the primary satellite intensity. The temperature variations of the intensities of these additional satellites are illustrated in the upper part of Fig. 3. It will be noted that the temperature at which these intensities are first observed is very close to the temperature at which the interplanar turn angle becomes constant.

In general, the existence of satellites other than the primary satellites of $(000H_3)$ reflections implies a departure from the simple helical arrangement of the components of moments perpendicular to a_3. In the extreme case, for example, of an antiphase domain-type antiferromagnetic structure, odd-order satellites of $(000H_3)$ should be observed, corresponding to the Fourier components of a square wave distribution of moments. For

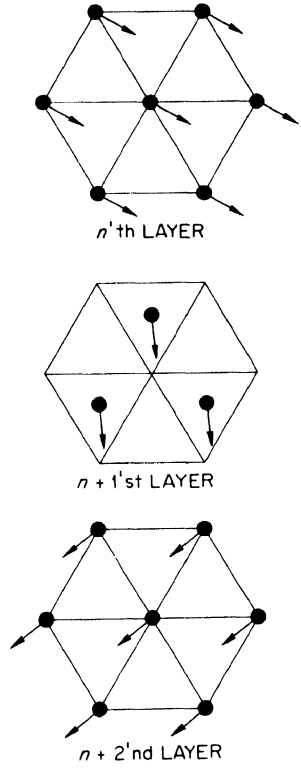


Fig. 2. Screw-type spin structure. Moments of atoms in hexagonal layers are parallel to each other, and perpendicular to the a_3 axis. Spins turn through a definite angle for a unit translation normal to the layers.

the case at hand, the relative intensities of primary to higher-order satellites imply that the distortion of the helix is a relatively minor one, and that to a first approximation the helical arrangement of the basal plane components persists down to 4.2°K. This is further indicated by the temperature variation of the intensity of the $(0002)^-$ and $(10\bar{1}0)^+$ satellites, shown in Fig. 4. Here it will be seen that these quantities follow a smooth curve, and exhibit no anomalies either in the region near 35°K or near 20°K, which temperature is a Curie point according to the macroscopic magnetic measurements.

At the Curie temperature, however, are first observed small but distinct magnetic contributions to the normal nuclear positions, except for reflections $(000H_3)$. Representative measurements of the intensity of the $(11\bar{2}0)$ and $(10\bar{1}0)$ reflections are shown in Fig. 4. The existence of a $(11\bar{2}0)$ magnetic reflection requires that there be a net ferromagnetic moment; the absence of an (0002) magnetic reflection requires that this

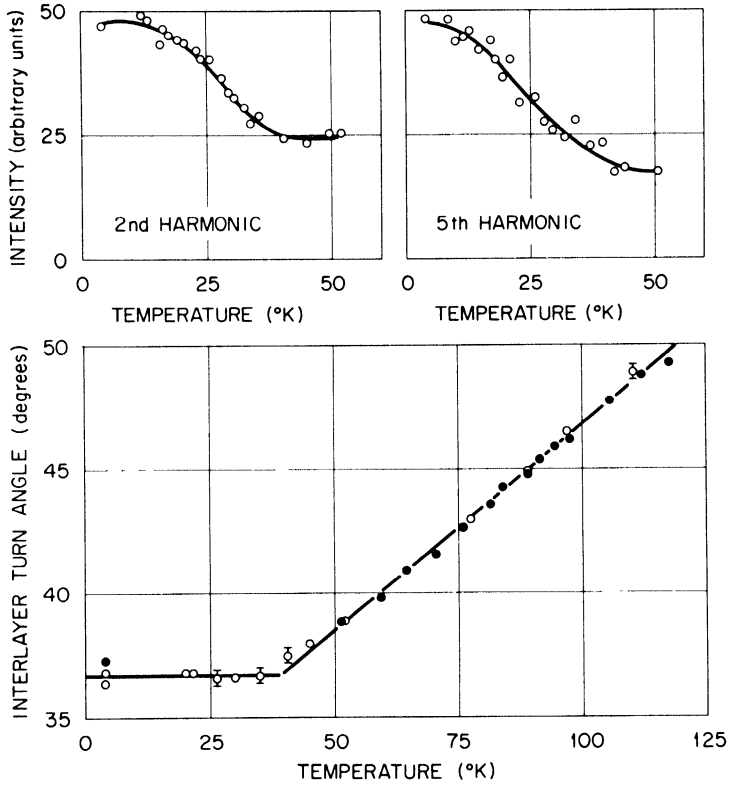


Fig. 3. Temperature variation of interplanar turn angle and of secondary satellite intensities of metallic holmium. Lower curve shows measurements from $(0000)^{\pm}$ satellites (full circles) and $(10\bar{1}0)^{\pm}$ satellites (open circles). The turn angle varies linearly with temperature to about 35°K, and is constant from 35 to 4.2°K. Upper curves show onset of second and fifth harmonics at approximately 35°K.

moment be directed parallel to the a_3 axis. From the interpretation of the absolute intensity data, the magnitude of this ordered z-component was found to be 2.1 μ_B at 4.2°K. Assuming an undistorted helical configuration for the ordered basal plane component, the ordered moment in the basal plane was found to be of magnitude 9.5 μ_B at the same temperature.

It is to be emphasized that the results so far presented are for a virgin magnetic state. The apparent disagreement of these results with those obtained from magnetic measurements is resolved when one studies the effect of an external magnetic field on the diffraction pattern. The application of a magnetic field parallel to the basal plane produces a large net magnetization normal to a_3 which exhibits a high degree of

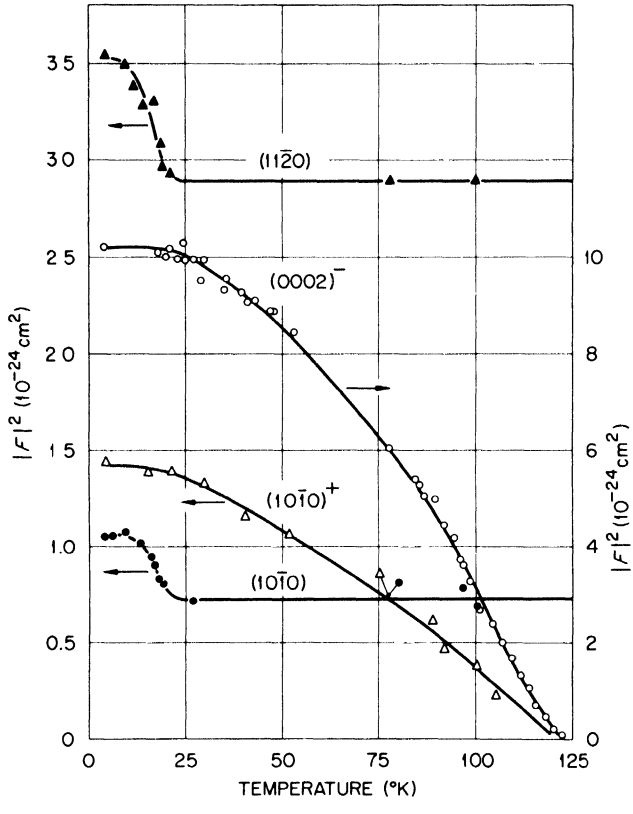


Fig. 4. Temperature variation of intensities of some important reflections of holmium. Scale at right pertains only to $(0002)^-$. Increase of $(11\bar{2}0)$ and $(10\bar{1}0)$ at about 20 °K indicates ferromagnetic ordering of z-component.

remanance. Fields parallel to a_3 produce little or no change in the diffraction pattern when the crystal is in its virgin state. A field of 10 kilogauss suitably applied has been found to produce a remanent magnetization of about 6 μ_B per atom at 4.2 °K.

DYSPROSIUM

Dysprosium appears to be antiferromagnetic between 179 and 87 °K and ferromagnetic below 87 °K. (5,6) The magnetic measurements show that dysprosium is highly anisotropic, with the spontaneous magnetization restricted to the basal planes. In addition there was found an "anisotropy region" below about 110 °K in which was observed a sizable anisotropy of the magnetization within the basal planes.

The single crystal neutron diffraction data obtained for dysprosium in the antiferromagnetic region are analogous to those for holmium, and

the antiferromagnetic structure of dysprosium is helical, with the a_3 axis as the screw axis. The turn angle varies from about 43 deg per layer at the Néel temperature to 26.5 deg per layer at about 90 °K, at which temperature the transformation to a ferromagnetic configuration begins. The variation of the turn angle with decreasing temperature is nearly linear, but there is a definite departure from linearity in the vicinity of 130 °K. As in the case of holmium a minor modification of the helix must exist between 140 °K and the Curie temperature, since in this region additional very weak antiferromagnetic reflections corresponding to second harmonics of the $(000H_3)$ were observed. It is probable that these extra reflections are associated with the anisotropy region below 110 °K, but the exact structural changes involved have not yet been determined.

Below about 87 °K, the slightly distorted helix transforms, in the virgin state, to a classical ferromagnet in which the moments lie in or nearly in the planes of the hexagonal layers. The moment value deduced from data obtained at 4.2 °K is 9.5 μ_B per atom.

TERBIUM

Terbium has been studied thus far only with polycrystalline samples, and, although previous experience with other of these metals has shown that considerable care must be exercised in the interpretation of powder data alone, the data for terbium are reasonably well accounted for on the basis of the metal at low temperatures being a classical ferromagnet with the moments parallel or nearly parallel to the basal planes. The effective ordered moment derived from both the coherent and diffuse scattering data is 9.1 μ_B at 4.2 °K. An attempt was made to study the antiferromagnetic region for this metal, but the range is so narrow—about 10 °K—that the intensities were too weak to be interpretable. The interpretation above is made with some reservation, since there is present in the powder patterns a very pronounced scattering at small angles which increases with decreasing temperature. It has not been possible, even under the best experimental conditions, to rule out the possibility that the scattering is due to a very closely spaced satellite of the origin. Single crystal studies should permit the resolution of this question, as well as the investigation of the antiferromagnetic region.

ERBIUM

The specific heat data for erbium (7) are somewhat more complex than those for any of the preceding metals, in that there are two history-dependent regions, one near 50 °K, and one near 20 °K, in addition to the Néel transition at about 80 °K. In an earlier neutron diffraction study of polycrystalline erbium (8), it was noted that some kind of anti-

ferromagnetic structure set in at 80°K, the data for which could not be satisfactorily interpreted, and that at low temperatures the pattern was characteristic of a normal ferromagnet with moments parallel to the c-axis. It was further noted, however, that at the lowest temperatures studied there remained some weak reflections at positions corresponding to the high-temperature structure. Recently a single crystal of erbium has been under study with an improved goniometer (9) which permits the attainment and control of sample temperatures over the whole range of interest. The results of this study to date may be divided according to these temperature regions: (1) from 80 to 53°K, (2) from 53 to 20°K, and (3) from 20 to 4.2°K. In the first range, the magnetic scattering (Fig. 1) is found in the form of sharp satellites of the nuclear reflections, except that no satellites of the $(000H_3)$ reflection are observed. Surveys of reciprocal space in the neighborhood of the $(10\bar{1}0)$ and $(10\bar{1}1)$ positions revealed no secondary satellites in this temperature region. Further, the satellite spacings remained constant, corresponding to 3.5 a_3 spacings. On the one hand, the lack of any magnetic intensity except that in a single pair of satellites suggests, as before, a modulation of the amplitudes with a single frequency; on the other hand, there is no way in a helical structure to extinguish the magnetic intensities in a given scattering direction completely. As of the present, from purely structural considerations one is led to a model in which the z-component of the moment varies sinusoidally with distance along the a_3 axis, with a period equal to 3.5 a_3 periods. In the third region, below 20°K the structural model which best fits the data is one in which the moments all make a constant projection along the a_3 axis, corresponding to a ferromagnetic moment of 7.3 μ_B—in excellent agreement with 7.2 μ_B obtained from the earlier powder data—and with a component normal to the a_3 axis of 4.2 μ_B, which behaves as a spiral. The interplanar turn angle in the low-temperature range is constant from 20°K, the temperature at which the net moment is observed, to 4.2°K and has the value of 43.4°K per layer. The intermediate range is complicated by the fact that there are simultaneously primary but not secondary satellites of the $(000H_3)$ reflections and secondary satellites of $(10\bar{1}H_3)$ reflections. The spacing of the primary satellites changes continuously from 3.5 to 4.0 a_3 periods over the range from 53 to 20°K. This is the temperature range in which apparently the components of the moments normal to the c-axis are becoming ordered, whereas above 53°K, they are evidently completely disordered.

THULIUM

Magnetic measurements on polycrystalline thulium have been reported recently by three groups of workers. Rhodes, Legvold, and

Spedding (2) found an antiferromagnetic transition near 51 °K and some indications of ferromagnetic behavior between 20 and 4.2 °K. Davis and Bozorth (10) took as an indication of ferromagnetism below 20 °K the existence of hysteresis. The Curie point which they deduced from these measurements was 22 °K. The highest moment per atom which they observed was 0.5 μ_B in a field of 12 Kilo-oersteds. In a much higher field of 70 Kilo-oersteds, Henry (11) observed 3.4 μ_B per atom instead of the expected 7 μ_B for the $4f$ (12) configuration. Davis and Bozorth point out that this result is to be expected if the moments are parallel to the a_3 axis and that the crystalline anisotropy is so great that the moments cannot be appreciably turned out of this direction.

The neutron diffraction data, from polycrystalline samples only, show the onset of a magnetically ordered state at 53 °K. The diffraction patterns obtained at 43 and 4.2 °K are similar to those obtained for erbium in its high-temperature region, and it is probable that thulium exhibits the same type of magnetic structure. At 4.2 °K, well into the so-called ferromagnetic region, the diffraction pattern shows no evidence for a transformation such as is observed at 20 °K in erbium.

From the diffuse scattering data one finds a value for the ordered moment which is equal to 6.7 μ_B, but the net ferromagnetic moment must be less than 0.5 μ_B. Here again single crystal studies will be necessary for an unambiguous solution of the problem.

REFERENCES

1. B. C. Gerstein *et al.*, *J. Chem. Phys.*, 25, 75 (1956).
2. B. L. Rhodes, S. Legvold, and F. H. Spedding, *Phys. Rev.*, 109, 1547 (1958). See also the article in this volume by S. Legvold.
3. See, for example, W. H. Zachariasen, *Theory of X-Ray Diffraction in Crystals*. New York: John Wiley & Sons, 1945.
4. W. C. Koehler, *Acta Cryst.* In press.
5. M. Griffel, R. E. Skochdopole, and F. H. Spedding, *J. Chem. Phys.*, 25, 75 (1956).
6. J. F. Elliott, S. Legvold, and F. H. Spedding, *Phys. Rev.*, 94, 1143 (1954); D. R. Behrendt, S. Legvold, and F. H. Spedding, *ibid.*, 109, 1544 (1958).
7. R. E. Skochdopole, M. Griffel, and F. H. Spedding, *J. Chem. Phys.*, 23, 2258 (1955).
8. W. C. Koehler and E. O. Wollan, *Phys. Rev.*, 97, 1177 (1955).
9. E. O. Wollan. Article to be published.
10. D. D. Davis and R. M. Bozorth, *Phys. Rev.*, 118, 1543 (1960).
11. W. Henry, *J. Appl. Phys.*, Sup. to 31, 323 (1960).

ELECTRICAL AND MAGNETIC PROPERTIES OF THE RARE EARTH METALS AND THEIR ALLOYS AND COMPOUNDS

K. A. GSCHNEIDNER, JR., AND B. T. MATTHIAS*

University of California, Los Alamos Scientific Laboratory, Los Alamos, New Mexico; and Bell Telephone Laboratories, Murray Hill, New Jersey

For many years it has been thought that the rare earths were essentially identical in their chemical and physical nature, except for small variations that were attributed to the differences in the radii of these elements. For example, lanthanum is the most basic rare earth because it has the largest ionic radius, while lutetium is the least basic because it has the smallest. Of course, it was recognized quite early that a few elements, namely cerium, europium, and ytterbium, and possibly praseodymium, samarium, and terbium, could sometimes exhibit a behavior quite different from that of the other rare earths. This difference was easily explained when the ability of these rare earths to form valence states other than the normal +3 state was considered. As more research was performed on the rare earth metals, there was some evidence obtained that this general explanation was not quite true when applied to the pure metals.

Scandium, yttrium, and the rare earths occur in different crystal structures. At room temperature, scandium, yttrium, and the rare earths from gadolinium through thulium and lutetium are hexagonal close-packed; lanthanum, praseodymium, and neodymium are hexagonal with a double c-axis; cerium and ytterbium are face-centered cubic; europium is body-centered cubic; and samarium is rhombohedral. The wide diversity among the crystal structures of these metals (complex metal structures of the light rare earths† and normal structures of the heavy rare earths, scandium and yttrium) may be related to the deviations in their magnetic behavior. However, it is possible, through the formation of compounds, to eliminate these differences. In the following paragraphs we wish to show that once compounds are formed the differences between the elements are no longer observed.

---

*Consultant to the University of California, Los Alamos Scientific Laboratory.

†Cerium forms a normal metallic structure, i.e., face-centered cubic at room temperature, but at slightly lower temperatures—263°K—forms a hexagonal structure isomorphous with lanthanum, praseodymium, and neodymium.

SUPERCONDUCTIVITY

Of all the trivalent transition elements only lanthanum is known to be superconducting. The rare earths from cerium through thulium are not superconducting, presumably because of their magnetic properties, or, more specifically, because of the spins of the unpaired $4f$ electrons. Ytterbium is divalent because the $4f$ shell is filled, and thus should not be compared with the trivalent elements. Experimentally, it has been found that ytterbium is not superconducting down to 1.24°K. (1)

The absence of superconductivity in scandium, yttrium, and lutetium is not as easily explained. We believe, however, that this absence is attributable to the nonisomorphism of these metals with lanthanum. Examination of the two types of crystal structure indicates that hexagonal (α) lanthanum has a stacking arrangement of ABACABAC (I), while that of scandium, yttrium, and lutetium is ABABABAB (II). The only difference between these two types of stacking is that in (I) the second, third, and fourth layers correspond to cubic closest-packing of atoms, but in (II) no such layering is found. Probably it is this face-centered cubic arrangement separated by a stacking fault which accounts for the existence of superconductivity in lanthanum. Indeed, the face-centered cubic modification of lanthanum, β-La, has a transition temperature 1.4°K higher than that of the hexagonal modification of lanthanum, α-La (Table I). That is, proper heat treatment to remove the stacking fault raises the superconducting transition temperature. Examination of Lock's data for the magnetic susceptibility of lanthanum (2) reveals that lanthanum has a magnetic moment of 0.5 Bohr magneton. Scandium, yttrium, and lutetium, however, do not have as high a magnetic moment. It is quite possible that this difference is related to the difference in the

TABLE I: HYPOTHETICAL SUPERCONDUCTING TRANSITION TEMPERATURES FOR SCANDIUM, YTTRIUM, AND LUTETIUM, RELATIVE TO THAT OF LANTHANUM

Metal	Hypothetical Transition Temperature, °K	
	f.c.c.*	hex (2 *c*-axis)*
Sc	2.6	1.9
Y	5.2	4.1
Lu	1.5	1.1
La	6.3†,‡	4.9†

*None of these structures has been observed for scandium, yttrium, and lutetium.
†Observed transition temperatures of pure lanthanum.
‡Recently, we have found that the superconducting transition temperature of β-La is 6.3°K. instead of 5.9°K, as reported by other workers.

crystal structures, the structure of lanthanum being responsible for a large increase in the electron density, which favors superconductivity.

According to the atomic volume and mass-ratio criterion for superconductivity (3), lanthanum would be expected to have the highest superconducting transition temperature, followed closely by yttrium and to a much lesser degree by scandium and lutetium (Table I). This deduction is reasonable only if it is assumed that scandium, yttrium, and lutetium are strictly isomorphous with lanthanum. But since α-La is hexagonal, with a double *c*-axis, and β-La is face-centered cubic, and since scandium, yttrium, and lutetium are not known to exhibit these structures, it is doubtful if this assumption is valid. No further conclusions can be drawn by making comparisons, because there are no hexagonal close-packed trivalent transition elements known to become superconducting above 0.1°K. It is possible to estimate the superconducting transition temperatures of scandium, yttrium, and lutetium by dissolving these elements in a superconducting metal and extrapolating the transition-temperature versus composition curve to pure scandium, yttrium, or lutetium. Data for some thorium-yttrium alloys are given in Fig. 1. The extrapolated value of the superconducting transition temperature of yttrium for a face-centered cubic lattice is 0.2°K. Similarly, the data of Anderson *et al.* (4) for lanthanum-yttrium and lanthanum-lutetium alloys give extrapolated values of −1.8°K for yttrium and 0.7°K for lutetium for a hexagonal (double *c*-axis, La-type) structure. The extrapolated values of the superconducting transition temperature of yttrium for the face-centered cubic and for the hexagonal structures are in the right direction; that is, the transition temperature for the cubic lattice is higher than the one for the hexagonal lattice (+0.2, and −1.8°K, respectively). These ex-

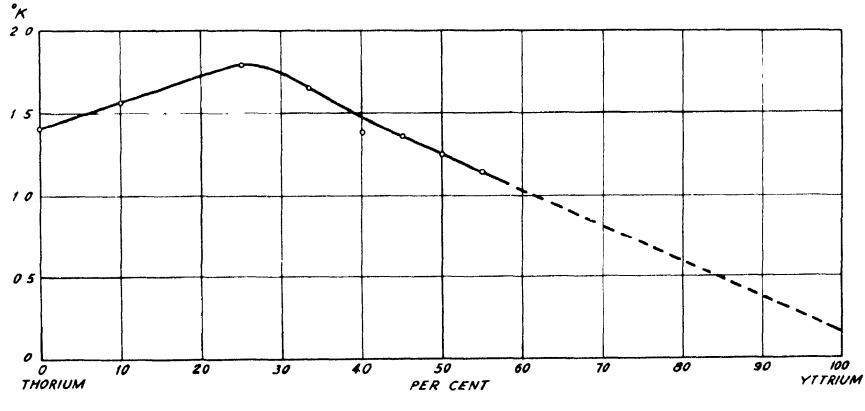


Fig. 1. Superconducting transition temperature as a function of the composition for some thorium-yttrium alloys.

trapolated values are not considered to be accurate, especially since the extrapolations were made from 40 to 55 a_0 yttrium or lutetium. Thus it would appear from these data that yttrium and lutetium would be superconducting if they possessed a favorable crystal structure. Further experiments of alloying scandium with lanthanum and thorium, and of lutetium with thorium, would be very illuminating.

Compounds containing scandium, yttrium, lanthanum, and lutetium show many similarities that are not observed for the pure metals; that is, in their AB_2 compounds with the noble metals and germanium, they behave as if they were closely related elements. The germanium compounds of scandium, yttrium, and lanthanum; the ruthenium compounds of scandium, yttrium, and lanthanum; the osmium compounds of scandium, yttrium, lanthanum, and lutetium; and the iridium compounds of scandium and yttrium are superconducting. The transition temperatures are given in Table II. Thus it is seen that the addition of a second element to these rare earths eliminates the anomalous differences in their superconducting properties.

TABLE II: SUPERCONDUCTING TRANSITION TEMPERATURES OF SOME AB_2 COMPOUNDS OF SCANDIUM, YTTRIUM, LANTHANUM, AND LUTETIUM

	A-element			
B-element	Sc	Y	La	Lu
Ge	1.30	3.8	1.49	...
Ru	1.67	1.52	1.63	...
Os	4.6	4.7	6.5	3.49
Ir	1.03	2.18	...	...

FERROMAGNETISM

The correlation between the crystal structure of the trivalent transition metals and the presence, or absence, of ferromagnetism* is surprisingly good. Scandium, yttrium, lanthanum, ytterbium, and lutetium are not expected to be ferromagnetic, because they do not have any unpaired $4f$ electrons, while all of the other metals do. The light rare earths, all of which have complex structures, are not ferromagnetic, but the heavy rare earths, which have the normal hexagonal close-packed structure, are ferromagnetic (Fig. 2). The ferromagnetic Curie temperatures have been shown by de Gennes (5) to be proportional to $J(J+1)(g-1)^2$ (Fig. 2), where J is equal to $L+S$ for the rare earths beyond gadolinium, and g is

*We are using the term *ferromagnetism* in the restricted sense, that is, where there is a net spontaneous polarization.

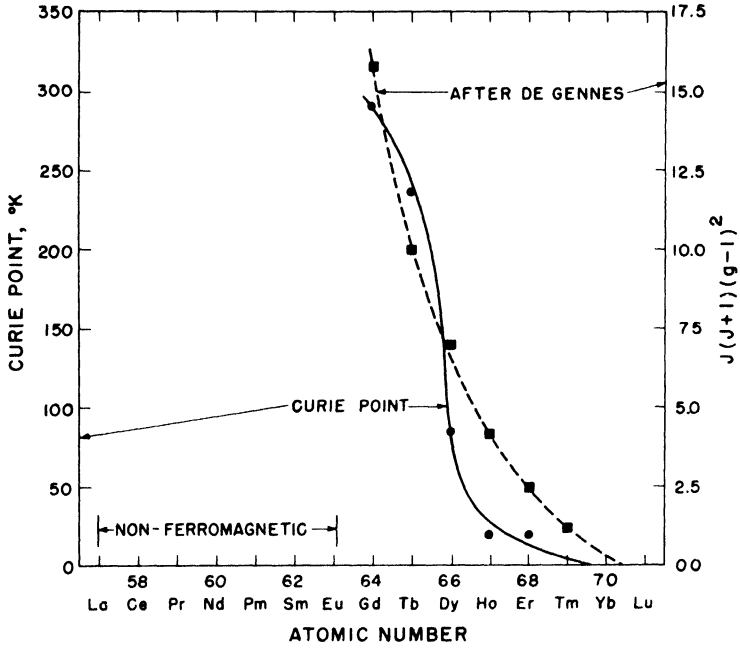


Fig. 2. Ferromagnetic transition temperatures of the rare earth metals, and their proportionality to the de Gennes factor, $J(J+1)(g-1)^2$.

the spectroscopic splitting factor, defined as

$$1 + \frac{S(S+1) + J(J+1) - L(L+1)}{2J(J+1)}$$

The light rare earths, as well as the heavy rare earths (cerium through ytterbium), form ferromagnetic AB_2 compounds with ruthenium, osmium, and iridium (Fig. 3). Initially, we thought that the Curie temperatures of these compounds were related to the spin of the rare earth metal, $S(S+1)$; however, a more detailed analysis (6) indicated that they are more likely to be proportional to $J(J+1)(g-1)^2$.

We (7) have noted that both the superconducting and ferromagnetic transition temperatures of the rare earth RB_2 compounds are dependent upon the electron concentration. For example, the $R\text{Os}_2$ compounds, as compared with the corresponding $R\text{Ir}_2$ or $R\text{Pt}_2$ compounds, have high ferromagnetic transition temperatures (if R has $4f$ electrons) or high superconducting transition temperatures (if R has no $4f$ electrons). These observations are reasonable, since certain electron densities favor both superconduction and spin-spin exchange of the $4f$ electrons via the conduction electrons. The latter is the dominant mechanism in

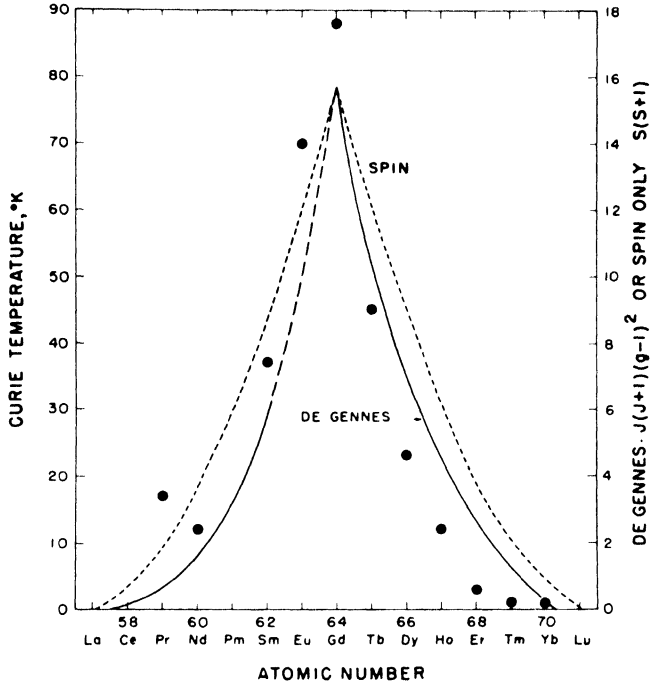


Fig. 3. Ferromagnetic transition temperatures of the RIr_2 laves phase compounds, where R = the rare earths from Ce through Yb.

rare earth ferromagnetism. This is yet another illustration of how the differences among the rare earth metals can be eliminated by compound formation.

CONCLUSION

It would appear that the existence of ferromagnetism and of superconductivity in the pure Group IIIA metals is related to the crystal structures of the metals. The superconducting and ferromagnetic behavior of any one of these metals as compared with another becomes predictable when the differences in crystal structure are eliminated by alloying or by forming compounds.

REFERENCES

1. J. M. Lock, *Proc. Phys. Soc.* (London) 70B, 476 (1957).
2. J. M. Lock, *ibid.*, 566 (1957).
3. C. J. Gorter (ed.), *Progress in Low Temperature Physics.* Amsterdam: North-Holland Publishing Company, 1957, Vol. II, Chap. 5, p. 140.

4. G. S. Anderson, S. Legvold, and F. H. Spedding, *Phys. Rev.*, **109**, 243 (1958).
5. P. G. de Gennes, *Compt. rend.*, **247**, 1836 (1958).
6. R. M. Bozorth *et al.*, *Phys. Rev.*, **115**, 1595 (1959).
7. H. Suhl, B. T. Matthias, and E. Corenzwit, *J. Phys. Chem. Solids*, **11**, 346 (1959).

SATURATION MAGNETIZATION, INTERATOMIC INTERACTIONS AND REMANENCE OF SOME RARE EARTH METALS AND COMPOUNDS

WARREN E. HENRY

Lockheed Missiles and Space Division, Palo Alto, California

A report is here given of experimental results obtained from the study of some rare earth metals and compounds containing $4f$ and $5f$ unpaired electrons, and especially about magnetization data obtained in temperatures down to 1.3°K and in applied fields up to 80,000 gauss. The results include saturation magnetization, molecular fields and exchange integrals, and remanence and general properties resulting from antiferromagnetic, ferromagnetic, and crystalline-field interactions. The metals studied include Ce, Pr, Nd, Gd, Tb, Dy, Ho, and Tm. The compounds include Yb_2O_3, Nd_2O_3, $Gd_2(SO_4)_3 \cdot 8H_2O$, UH_3, UD_3, and UO_2. Except for Gd, which gives the expected 7 Bohr magnetons per atom for the measured saturation, there is an apparent reduction in the saturation magnetization, as measured in fields up to 80,000 gauss and at 1.3°K. This reduction in the magnetization under these conditions probably arises from antiferromagnetic interaction and/or lifting of orbital degeneracy by the combined effect of the crystalline electric field and spin-orbit coupling, in which the Pauli principle comes into play. The measurement was by a sample displacement ballistic method. Calibration was with iron and nickel.

INTRODUCTION

The study of the approach to saturation takes a natural impetus from the circumstance that it has been of interest in the study of unpaired f-electrons to ascertain the magnetic atomic constants and interatomic interactions in solids. Since the atomic structure of magnetic materials is important in determining the macroscopic magnetic properties, it has been important to compare the results which one would expect from the models based on spectroscopically determined magnetic atomic constants with results actually obtained from magnetic experiments. These magnetic results are of two general types. First, there are low field results

depending on the Curie law, in which

$$\mu = A\sqrt{\chi T} \tag{1}$$

$g^2 J(J+1)$ being obtained from the susceptibility. This scheme is not valid if there are interactions, because the susceptibility will be raised or lowered as the interaction becomes important, being raised if the interaction is ferromagnetic, and lowered if the interaction is antiferromagnetic. The interaction is usually recognized by use of the Curie-Weiss law,

$$\mu = A\sqrt{\chi(T+\Delta)} \tag{2}$$

where A is an empirical interaction term. This approach for determining magnetic atomic constants—where there are interactions—is risky, since the apparent Δ can change with temperature.

The second approach, through the direct measurement of g_J and the exchange interaction at low temperature and high magnetic field, is more suitable for the assessment of certain fundamental quantities from which the structure and behavior of magnetic materials can be learned.

The method of high-field, low-temperature evaluation of magnetic atomic constants has been tested by measurement and analysis of saturation magnetization (1) of paramagnetic substances, in which the paramagnetic ions are simple and the interaction negligible for the liquid helium temperature range. With this verification of the applicability of the Brillouin function (space quantization of magnetic dipoles) in the saturation range, it has been possible to use high-field, low-temperature studies of magnetization for the evaluation of the type and magnitude of interaction (2) in solids, as well as the magnetic atomic constants of paramagnetic atoms and ions. The crystalline electric-field effect on the lifting of orbital degeneracy has been studied through the measurement of saturation magnetization of assemblies of paramagnetic ions (3), in which the ion is relatively free on the one hand and under rather severe crystalline-field constraint on the other. In this case (potassium ferricyanide) the crystalline-field constraint was great enough to lift the degeneracy of the ground state of the tripositive iron ion completely, so that the Pauli principle was operable at low temperatures with a consequent reduction in the saturation magnetization. (3, 4) Thus, for the $3d$ unfilled shells, the studies of magnetization as a function of field and temperature have (1) established the applicability of the Brillouin function up to saturation for noninteracting assemblies of paramagnetic ions, (2) used departures from the Brillouin function to study the nature and magnitude of magnetic interactions, and (3) used saturation magnetization to assess the effect of the lifting of orbital degeneracy by the crystalline electric field.

The above approach has been applied to the study of the contribution of $4f$ and $5f$ electrons to the magnetic properties of lanthanide and actinide elements and compounds.

EXPERIMENTAL METHOD

The magnetization measurements were made using a ballistic sample displacement technique. (5) A sample, generally spherical, is moved from the center of one coil to the center of another coil, the coils being equal and oppositely wound, and in series with a ballistic galvanometer, the deflection of which is proportional to the magnetic moment of the sample. The system was calibrated with iron and nickel of high purity, and the displacement was effected by a magnetic moment lift. (6) The temperature was controlled by means of a liquid helium metal dewar (7), and was determined from vapor pressures and a carbon resistance thermometer. (8) The high magnetic fields were produced with a Bitter magnet.

DISCUSSION OF EXPERIMENTAL RESULTS

GADOLINIUM ION AND ATOM

Figure 1 shows a plot of magnetization versus H/T for gadolinium tripositive ion in gadolinium sulphate octahydrate. The curve follows a

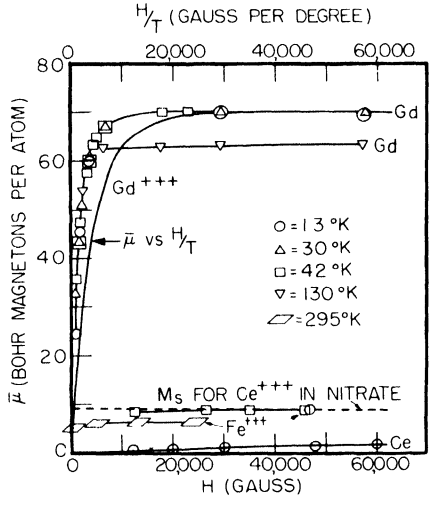


Fig. 1. Plot of average magnetization μ as a function of H at various temperatures. The top scale is in H/T and applies to Gd^{+++} in gadolinium sulfate octahydrate (W. E. Henry, *J. Appl. Phys.*, 29, 524, 1958).

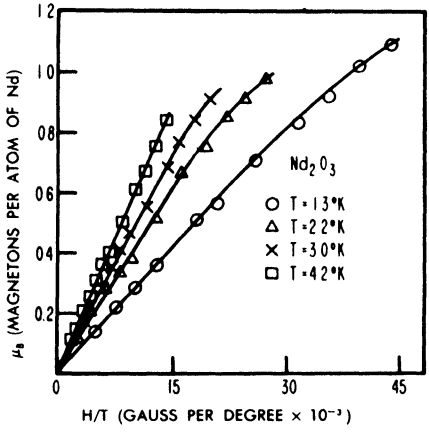


Fig. 2. Plot of magnetization *vs.* H/T for Nd_2O_3 (W. E. Henry, Conference de Physique de basses temperatures, Paris, 2–8 Sept., 1955).

Brillouin function for $g = 2$ and $J = S = 7/2$. The interaction is negligible for this case. The saturation magnetization is 7 Bohr magnetons per ion of gadolinium, in keeping with what is expected for a half-filled *f*-shell. The plot of magnetization versus magnetic field for gadolinium atoms (metal) shows an absolute saturation magnetization of about 7 Bohr magnetons per atom. The magnetization curve at 1.3°K shows a magnetization at low applied magnetic field greater than could be expected from the Brillouin function, indicating a ferromagnetic interaction. Comparison—using the methods of (2)—of the saturation value for complete domain, but incomplete intradomain, alignment for gadolinium at 130°K with a Brillouin value yields a molecular field of 1.3 megagauss.

CERIUM IONS AND CERIUM METAL

Lower curves in Fig. 1 show magnetization results for cerium and cerium ions in cerous nitrate hexahydrate, respectively. Although a cerous ion (Ce^{+++}) shows a magnetization approaching 1 Bohr magneton per atom (J effective $= 1/2$ and $g = 1.9$) at 1.3°K and 60,000 gauss, cerium metal under the same conditions shows only 0.17 Bohr magneton per atom. This low value for cerium metal suggests an antiferromagnetic arrangement, which is also suggested by neutron diffraction data.

NEODYMIUM OXIDE (Nd_2O_3) AND NEODYMIUM METAL

Figure 2 shows a plot of magnetization of Nd^{+++} in Nd_2O_3 as a function of H/T. The nonsuperposition of the magnetic moment isotherms is suggestive of an antiferromagnetic interaction by analogy to the results for antiferromagnetic manganese chloride tetrahydrate. (2) Neutron diffraction work by Koehler, Wilkinson, and Wollan indicate antiferromagnetism in Nd_2O_3. The magnetization is not approaching the theoretical value for $g_J = 3.3$, even at 1.3°K and 60,000 gauss. Figure 3 shows a plot of magnetization of neodymium metal against magnetic field in the liquid helium range. The magnetization shows saturation effects at the high fields at low temperatures. However, the approach to saturation seems headed more toward 1.65 Bohr magnetons per atom of neodymium than toward 3.3, the theoretical value calculated from the spectroscopically determined values of g and J. The remanence for neodymium is 0.006 Bohr magneton per atom at 4.2°K and 0.009 at 1.3°K.

PRASEODYMIUM

Magnetization studies of praseodymium have been carried out at 295°K, 100°K, and in the liquid helium range. At 295°K, $\left(\frac{\partial M}{\partial H}\right)_T =$ 1×10^{-6} Bohr magneton per gauss per atom. At 100°K, this slope is

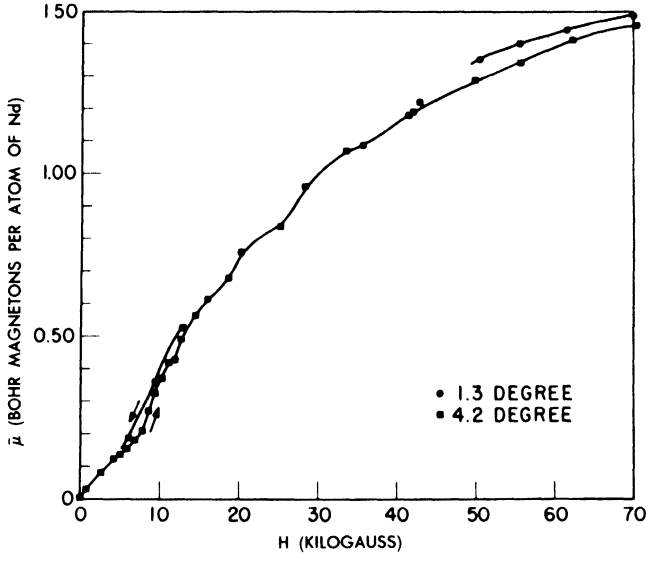


Fig. 3. Plot of magnetization of neodymium metal *vs.* magnetic field for 4.2 and 1.3°K (W. E. Henry, *J. de Physique et le radium*, 20, 192, 1959).

tripled. At 67,000 gauss and 1.3°K, the magnetization is 1.04 Bohr magnetons per atom of praseodymium. This is small compared with the value (3.58 Bohr magnetons per atom) which would be inferred from the high-temperature susceptibility data of Charlotte Henry la Blanchetais on the metal. Calculations of Van Vleck and Frank (not considering crystalline electric-field effects) for the tripositive ion give 3.62 Bohr magnetons per ion. A small remanence is observed. The reluctance to saturate at 67,000 gauss and 1.3°K is probably due either to antiferromagnetism or crystalline-field-induced anisotropy. A full publication of this work is forthcoming.

TERBIUM METAL

Figure 4 shows magnetization results for terbium metal. It is to be noted that the magnetization at 295°K is higher than would be expected from a Brillouin function for $S = 3$, $L = 3$, and $J = 6$ in a $^7F_6$ ground state. Determination of the Van Vleck exchange coefficient $\gamma = 80{,}000$ gauss per Bohr magneton per atom, by a method previously described (2), leads to a value for the molecular field, H_m, of 700,000 gauss. This corresponds to an exchange integral of 120 cm^{-1}. If one uses a $g_{J'}$ value of 7, the value of the molecular field is 540,000 gauss, corresponding to an exchange integral of 96 cm^{-1}.

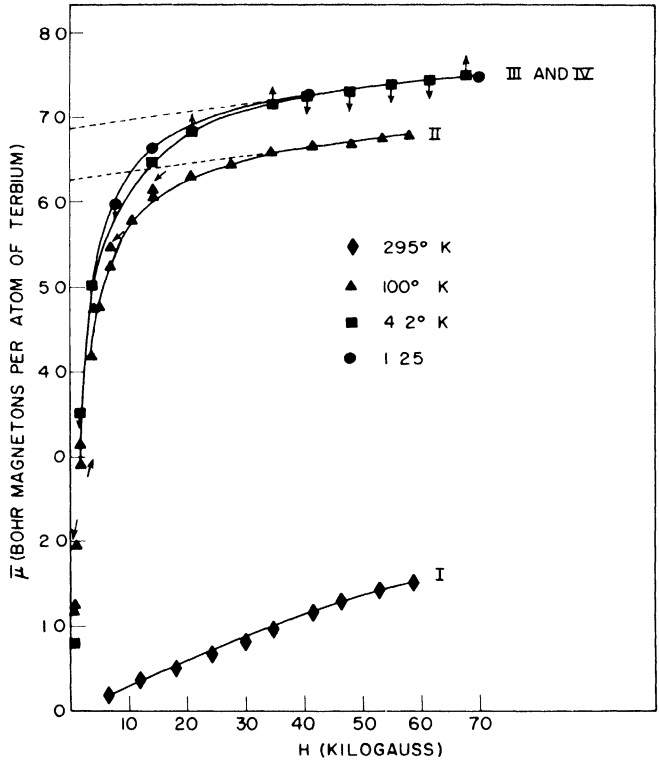


Fig. 4. Plot of magnetization *vs.* magnetic field for terbium metal for 1.25, 4.2, 100 and 295°K (W. E. Henry, *J. Appl. Phys.*, 30, 99S, 1959).

It is to be noticed that in the ferromagnetic range including 100°K and the liquid helium range, the magnetization is increasing rapidly at the low fields, suggesting a rapid approach to what would be a normal saturation. Thus, since the rate of increase of magnetization with magnetic field from 35,000 gauss to 70,000 gauss is temperature-independent it is reasonable to treat this increasing magnetization as a Van Vleck-type temperature-independent magnetization, due to the mixing of states. The slope of the curves in the high field range (1.04×10^{-5} Bohr magneton per atom per gauss) may result from a Paschen-Bach effect in which the nondiagonal matrix component of energy is not negligible. This extra contribution is of the form $\alpha\beta^2 H/\Delta E$, where α is a constant, β the Bohr magneton, H the applied field, and ΔE the splitting. $\alpha/\Delta E$ is determined to be 1.16×10^{35} Bohr magneton^{-1} gauss^{-1}. The extra contribution has the form of the Van Vleck temperature-independent paramagnetism, where $\alpha\beta^2 H$ is the square of the matrix

element $(n|\mu_z|0)$, of the magnetic moment operator connecting the ground state with the excited state arising from the crystalline-field splitting.

The remanence in terbium is 0.1, 0.13, and 0.23 Bohr magneton per atom of terbium at 100, 4.2, and 1.3°K, respectively. The magnetization at 1.3°K and 70,000 gauss is 7.5 Bohr magnetons per atom of terbium. If the temperature-independent part is removed, the remaining magnetization is 7 Bohr magnetons per atom of terbium.

DYSPROSIUM METAL

Figure 5 shows magnetization results for dysprosium metal at low temperatures and at fields up to 80,000 gauss. The magnetization rises rapidly with the field up to about 10,000 gauss, and then saturation effects set in. However, at all temperatures here represented, there seems to be a sluggish approach to saturation, with the value approached—even at 1.3°K and 80,000 gauss, namely, 7.6 Bohr magnetons per atom—to being far less than the Bohr magnetons per atom calculated in the conventional manner. This result probably arises from anisotropy, which in turn arises from the combined effect of the spin-orbit coupling and the crystalline

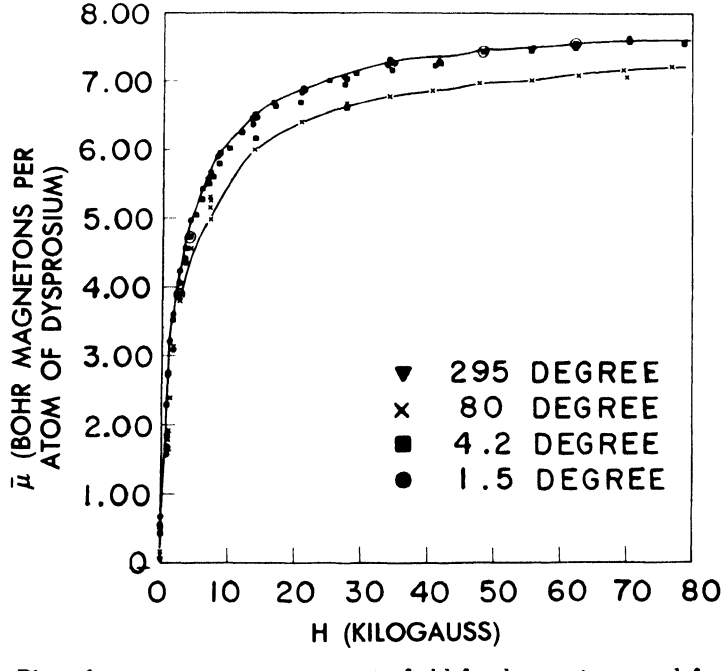


Fig. 5. Plot of magnetization *vs.* magnetic field for dysprosium metal for 140°K and for the liquid helium range (W. E. Henry, *J. de Physique et le radium*, 20, 192, 1959).

electric-field interaction. Anisotropy in dysprosium has been established by Spedding *et al.* The remanence of dysprosium is 0.04 Bohr magneton per atom at 140°K, 0.16 at 80°K, 0.51 at 4.2°K, and 0.67 at 1.3°K.

HOLMIUM METAL

Figure 6 shows average magnetization data for holmium in fields up to 70,000 gauss. The curve for 295°K is linear and higher than would be given by a Brillouin function, using the applied field as the effective field. It is seen that the magnetization at 1.3°K and 70,000 gauss is

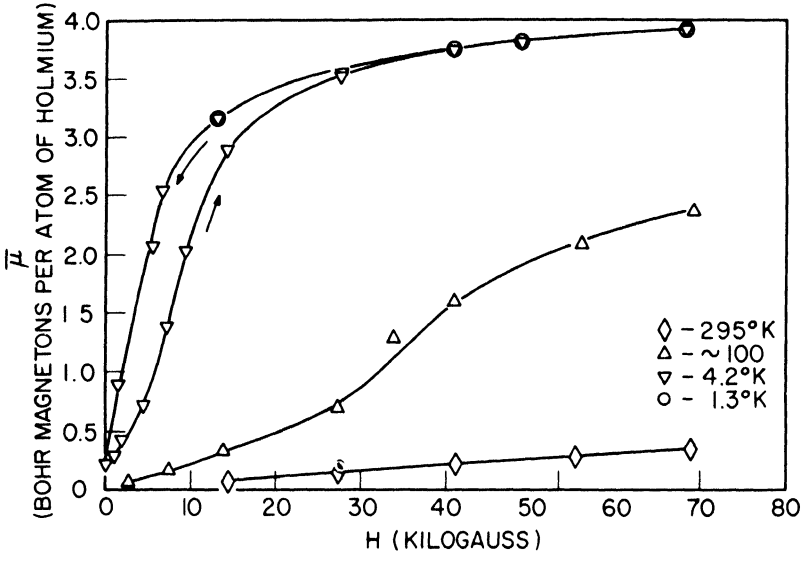


Fig. 6. Plot of magnetization *vs.* magnetic field for holmium metal at 295, 100, 4.2 and 1.3°K (W. E. Henry, *Phys. Rev.*, 117, 89, 1960).

approaching 4.0 Bohr magnetons per atom. It has been established by spectral analysis (9) that holmium metal has a $^4I_{15/2}$ ground state, although high-temperature suspectibility data (10) with Eq. (1) suggests a $^5I_8$ ground state, the same as for the tripositive holmium ion, with $J = 8$ and $g = 1.25$. This leads to a calculation of 10 Bohr magnetons per atom of holmium. Under these circumstances, application of the Brillouin function gives an average magnetization,

$$\bar{\mu} = \frac{g\mu_\beta}{2}\left[(2J+1)\coth\frac{(2J+1)g\mu_\beta H}{2KT} - \coth\frac{g\mu_\beta H}{2KT}\right] \qquad (3)$$

where g is the Landé splitting factor, J the total magnetic quantum number, K the Boltzmann constant, μ_β the Bohr magneton, and H the effective field. Now, it has been demonstrated that the saturation magnetization can be drastically reduced (3) by a lifting of the orbital degeneracy (11) of the ground state. Thus, in the case of iron ammonium alum, the saturation magnetization is 5 Bohr magnetons per atom of iron, whereas in potassium ferricyanide, the saturation magnetization is reduced to 1 Bohr magneton per atom of iron.

To give one possible explanation of the low value of the magnetization of holmium at 1.3°K and 70,000 gauss, we can assume the following: (1) lifting of the orbital degeneracy of the ground state of holmium, (2) nonisotropic combined action of the crystalline electric field and spin-orbit coupling, and (3) application of the Pauli principle.

The achievement of the first assumption is shown by the solid-state spectroscopic studies of holmium by Belianin. (12) The plausibility of the second has been shown in the measured anisotropy of dysprosium (13) and recently of the marked anisotropy of holmium (14) itself. Thus, assuming a normal parallel moment, $\mu_\parallel$, and a Pauli perpendicular moment, $\mu_\perp$ (with $J' = 1/2$),

$$\bar{\mu} = 1/3\,(\mu_\parallel + 2\,\mu_\perp) \tag{4}$$

$$\bar{\mu} = 1/3\left\{0.625\,\mu_\beta\left[17\coth\left(\frac{17\times 0.625\,\mu_\beta H}{KT}\right) - \coth\left(\frac{0.625\,\mu_\beta H}{KT}\right)\right] + 2\tanh\frac{\mu_\beta H}{KT}\right\} \tag{5}$$

the limiting value of which, for H/T large, is 4.0 Bohr magnetons per atom of holmium. The departure of the magnetization from the Brillouin function of high temperatures yields a molecular field of 550,000 gauss.

The remanence is 0.22 Bohr magneton per atom of holmium at 4.2°K and 0.42 at 1.3°K. This high remanence is in keeping with ferromagnetic exchange interaction, with crystalline electric-field anisotropy, and spin-orbit coupling. There is a pronounced hysteresis in the liquid helium range.

THULIUM METAL

Figure 7 shows results for the magnetization of thulium in fields up to 70,000 gauss and in temperatures of 100, 4.2, and 1.3°K. The 100°K curve is linear and reaches 0.8 Bohr magneton per atom of thulium at 70,000 gauss. At 4.2°K the magnetization changes direction of con-

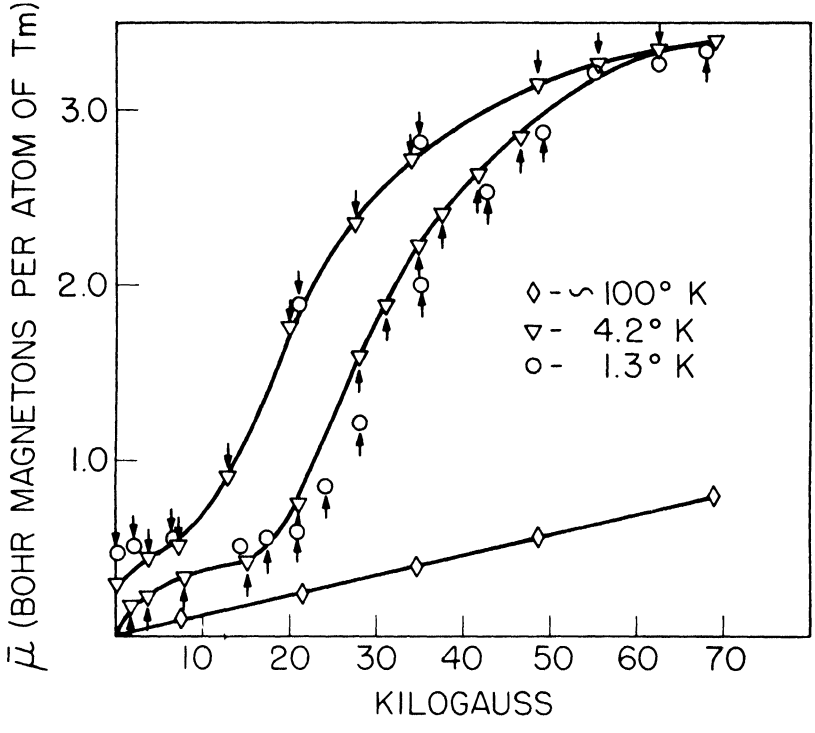


Fig. 7. Plot of magnetization *vs.* magnetic field for thulium metal at 100, 4.2 and 1.3°K (W. E. Henry, *J. Appl. Phys.*, 31, 323S, 1960).

cavity twice. In the high field range, $\left(\frac{\partial M}{\partial H}\right)_T$ is decreasing and between 60,000 gauss and 70,000 gauss it is very small. The magnetization at 4.2°K is in agreement with that produced by Rhodes, Legvold, and Spedding (15) as far as they went, namely, to 18,000 gauss, where they obtained a result of 0.8 Bohr magneton per atom of thulium. At this point the slope is very steep. Beyond 18,000 gauss we applied a magnetic field up to 70,000 and observed strong saturation effects. The magnetization is 3.4 Bohr magnetons per atom of thulium at 1.3°K and 70,000 gauss. The shape of the magnetization curve at 4.2°K, for example, indicates a possible mixture of ferromagnetic and antiferromagnetic interactions. That is, $\left(\frac{\partial^2 M}{\partial H^2}\right)_T$ changes signs twice and would behave in this way in a system of mixed interactions.

If it is assumed that the ground state for the thulium atom is the same as for the trivalent thulium ion, namely $^3H_6$, the g_J or saturation mag-

netization would be 7 Bohr magnetons per atom. However, certain spectroscopic data (16) indicate a $^2F_{7/2}$ ground state for the thulium atom in the metal. This leads to a g_J product of 4.0 Bohr magnetons per atom. The high field results here, where the extrapolated value is slightly less than 4.0 Bohr magnetons per atom, are in keeping with a $^2F_{7/2}$ ground state for the $4f^{13}6s^2$ configuration for thulium metal. This leads to a g_J product of 4.0 Bohr magnetons per atom. The remanence is 0.3 Bohr magneton per atom of thulium at 4.2°K and 0.4 at 1.3°K. A pronounced hysteresis is observed in the liquid helium range.

YTTERBIUM OXIDE

Figure 8 shows magnetization as a function of H/T for Yb_2O_3 for various temperatures in the liquid helium range. The nonsuperposition of magnetic moment isotherms indicates an interaction. The positioning of the isotherms indicates an antiferromagnetic interaction. The shift in $\left(\frac{\partial^2 M}{\partial H^2}\right)_T$ at the low temperatures is also suggestive of an antiferromag-

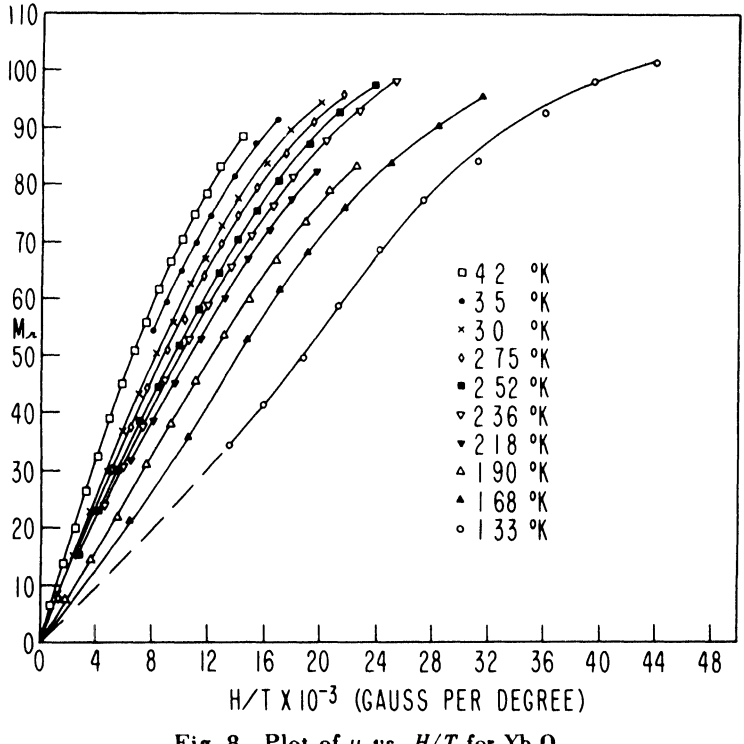


Fig. 8. Plot of μ *vs.* H/T for Yb_2O_3.

netic interaction. The antiferromagnetic transition temperature is 3°K and the apparent molecular field is 35,000 gauss.

URANIUM HYDRIDE, URANIUM DEUTERIDE, AND URANIUM DIOXIDE

Figure 9 shows a plot of magnetization versus magnetic field for UH_3, UD_3, and UO_2. The UH_3 is approaching a value of 1.2 Bohr magnetons per atom at 60,000 gauss and 1.3°K. This value is in keeping with neutron diffraction results of Koehler, Wilkinson, and Shull. (17) The UO_2 shows a linear dependence of magnetization on magnetic field of $M = 7 \times 10^{-7} H$ Bohr magnetons per atom of uranium. This small value is suggestive of an antiferromagnetic ordering.

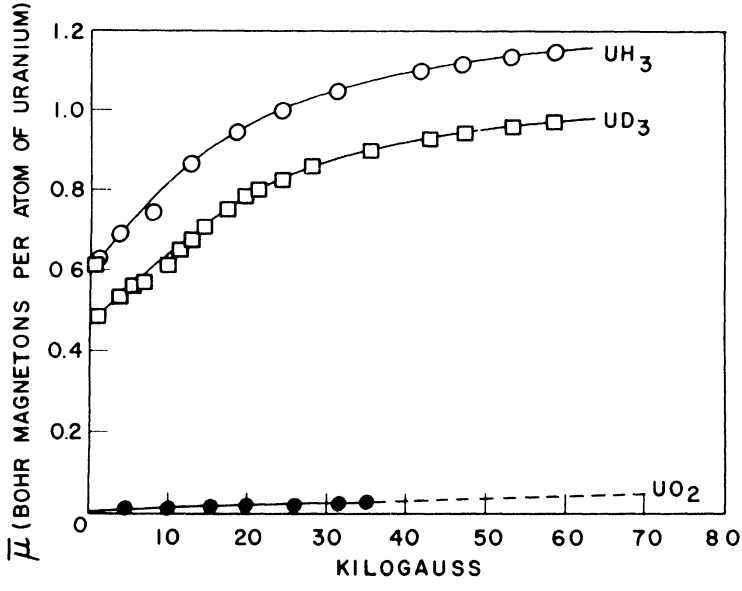


Fig. 9. Plot of magnetization *vs.* magnetic field for UH_3, UD_3, and UO_2 at 1.3°K (W. E. Henry, *Phys. Rev.*, 109, 1976, 1958).

SUMMARY

Analysis of the experimental studies of magnetization of rare earth metals and compounds indicates that the magnetization, as a function of field and temperature, can be predicted on the basis of spectroscopically determined magnetic atomic constants for the *S*-states and for magnetically dilute assemblies. The saturation magnetization can be predicted for the *S*-state even if there is ferromagnetic interaction. Any prediction of magnetization for rare earth materials with orbital contributions must

take into account the anisotropy, the crystalline-field interaction and spin-orbit coupling, and the subsequent lifting of orbital degeneracy of the ground state. Because of these circumstances, the saturation magnetization which is being approached at high fields and low temperatures is less than the values predicted on the basis of simple theory. It is of interest to contemplate high field measurements on the hard direction of single crystals of rare earth materials, in view of the results obtained for hexagonal, magnetically hard barium ferrate, in which the polycrystalline material has been magnetized up to saturation. (18) Plans are under way to carry out these measurements of high field magnetization on single crystals of rare earth metals when they are available.

REFERENCES

1. W. E. Henry, *Phys. Rev.*, 88, 559 (1952).
2. W. E. Henry, *ibid.*, 94, 1146 (1954).
3. W. E. Henry, *ibid.*, 106, 465 (1957).
4. W. C. Koehler, M. K. Wilkinson, and E. O. Wollan: Private communication. *Also*, J. H. Van Vleck: Private communication.
5. W. E. Henry, *Phys. Rev.*, 85, 487L (1952).
6. W. E. Henry, *Low Temperature Physics*, National Bureau of Standards Circular 519, (1952) p. 237.
7. W. E. Henry, *J. Appl. Phys.*, 22, 1439 (1951).
8. J. R. Clement and E. H. Quinnell, *Rev. Sci. Instr.*,23, 213 (1952).
9. V. B. Belianin, *Optika i Spectroskopiya*, 3, 322 (1957).
10. J. F. Elliott, S. Legvold, and F. H. Spedding, *Phys. Rev.*, 91, 28 (1953).
11. J. H. Van Vleck: Private communication. *Also*, M. H. L. Pryce: Private Communication.
12. V. B. Belianin, *Optika i Spectroskopiya*, 5, 236 (1958).
13. D. R. Behrendt, S. Legvold, and F. H. Spedding, *Phys. Rev.*, 109, 1544 (1958).
14. S. Legvold. Private communication.
15. B. L. Rhodes, S. Legvold, and F. H. Spedding, *Phys. Rev.*, 109, 1547 (1958).
16. M. A. Eliashevich, *Spektry Redkikh Zemel' GTTI 1953* (USSR, 1953), p. 8.
17. W. C. Koehler, M. K. Wilkinson, and C. G. Shull: Private communication.
18. W. E. Henry, *Phys. Rev.*, 112, 326 (1958).

PARAMAGNETISM OF POLYCRYSTALLINE RARE EARTH METALS

SIGURDS ARAJS AND R. V. COLVIN*

Edgar C. Bain Laboratory for Fundamental Research, United States Steel Corporation Research Center, Monroeville, Pennsylvania

Much experimental work has been done on the magnetic properties of the rare earth metals from 1 to 300°K. Only in a few cases, however, has the magnetic behavior of these metals been studied above 300°K. Such studies would be of considerable value in understanding their electronic structures. Recently, we studied the magnetic behavior of these metals at elevated temperatures by measuring the magnetic susceptibility. Measurements on cerium, praseodymium, neodymium, samarium, europium, gadolinium, terbium, dysprosium, holmium, erbium, and thulium have been partially described elsewhere. (1-5) In this paper we discuss the experimentally observed paramagnetism of the rare earth metals from a more unified viewpoint, based on the localized $4f$-electron model and the Van Vleck theory of paramagnetism, as has been done before.

FINE STRUCTURE OF GROUND MULTIPLETS

We may look at any one of the rare earth metals as a collection of weakly interacting positive ions imbedded in a sea of electrons. This electron sea is by no means a simple free-electron gas. Fortunately, for understanding the paramagnetism of the rare earth metals, these electrons are of secondary importance only because the localized $4f$-electrons in these metals are the main source for their paramagnetic behavior.

Since most of the rare earth metals are tripositive, we shall discuss the fine structure of the ground multiplets of the tripositive rare earth ions. Also, we shall assume that there are no appreciable crystalline fields present, so that the ions can be considered to be free.

The electronic configurations of the tripositive rare earth ions, their ground states, and the quantum numbers J, L, S are given in Table I.

*The authors are grateful to the following members of this laboratory for their helpfulness: D. S. Miller, for numerous discussions; R. W. Whitmore, for computational aid; and J. M. Peck and R. C. Peck, for technical assistance. Appreciation is also extended to S. Legvold of the Iowa State University for valuable conversations on the rare earth metals.

TABLE I: DATA ON TRIPOSITIVE RARE EARTH IONS*

Rare Earth Ion	Electronic Configuration			Ground State	J	L	S
La^{+++}	Pd core		$5s^25p^6$	$^1S_0$	0	0	0
Ce^{+++}	"	$4f$	"	$^2F_{5/2}$	5/2	3	1/2
Pr^{+++}	"	$4f^2$	"	$^3H_4$	4	5	1
Nd^{+++}	"	$4f^3$	"	$^4I_{9/2}$	9/2	6	3/2
Pm^{+++}	"	$4f^4$	"	$^5I_4$	4	6	2
Sm^{+++}	"	$4f^5$	"	$^6H_{5/2}$	5/2	5	5/2
Eu^{+++}	"	$4f^6$	"	$^7F_0$	0	3	3
Gd^{+++}	"	$4f^7$	"	$^8S_{7/2}$	7/2	0	7/2
Tb^{+++}	"	$4f^8$	"	$^7F_6$	6	3	3
Dy^{+++}	"	$4f^9$	"	$^6H_{15/2}$	15/2	5	5/2
Ho^{+++}	"	$4f^{10}$	"	$^5I_8$	8	6	2
Er^{+++}	"	$4f^{11}$	"	$^4I_{15/2}$	15/2	6	3/2
Tm^{+++}	"	$4f^{12}$	"	$^3H_6$	6	5	1
Yb^{+++}	"	$4f^{13}$	"	$^2F_{7/2}$	7/2	3	1/2
Lu^{+++}	"	$4f^{14}$	"	$^1S_0$	0	0	0

*Pd core $\equiv 1s^2$, $2s^22p^6$, $3s^23p^63d^{10}$, $4s^24p^64d^{10}$.

It should be noticed that the $4f$-shell of Ce^{+++} is empty and that of Lu^{+++} is completely full. As one progresses from Ce^{+++} to Lu^{+++} there is a gradual increase in the number of $4f$-electrons. This is the only change in the electronic configuration, since the outer electron shell $5s^25p^5$ of the tripositive ions remains unchanged. Since the $5s$- and $5p$-subshells are full, they do not contribute to the total angular momentum of the ion. The angular momentum of the particular rare earth ion is completely determined by the number of $4f$-electrons.

Since the arrangement of the lowest energy multiplet of the particular rare earth ion determines its magnetic behavior, a detailed knowledge of this distribution is of great significance. This information in principle can be obtained from the fluorescence spectra and infrared absorption. The positions of the energy levels of the ground multiplets have indeed been determined for various rare earths using these methods. However, the structure of the multiplets can also be approximately calculated using the modified Goudsmit formula and the Landé interval rule. The modified Goudsmit formula (2, 6, 7) is

$$\Delta E = \frac{8\pi^4 me^2}{c^3h^5} \frac{2l+1}{n^3 l(l+1)(2l+1)} (Z-\sigma)^4 \qquad (1)$$

where ΔE is the width of the multiplet in cm^{-1}, m the mass of an electron, e the electronic charge, c the velocity of light, h the Planck constant, n the principal quantum number of an electron, l the orbital quantum number for the whole electronic unit (which for the rare earths is the

incomplete $4f$-shell), Z the atomic number, and σ the nuclear screening constant. This constant has to be introduced because of the nonhydrogenic nature of the rare earth ions. Knowing the over-all width of the multiplet, its detailed structure can be approximately calculated assuming the existence of the Russell-Saunders coupling which leads to the Landé interval rule (8),

$$E_{J-1} - E_J = AJ \tag{2}$$

where E_J is the energy level associated with the total angular-momentum quantum number J, and A is a constant.

The energy levels calculated from Eqs. 1 and 2, using $\sigma = 32, 33, 34, 35, 36$ as a parameter, are summarized in Table II. This table also gives some of the experimentally determined energy levels of the tripositive rare earth ions. These levels have been measured by spectroscopically studying various rare earth salts. The references for these experimental investigations are given at the end of Table II. It should be mentioned that the problem of the electronic spectra of ions in crystals has been reviewed by McClure. (9) Additional references regarding the spectra of the rare earth ions can be found in his article.

Table II also gives the energy-level separations for most of the free tripositive rare earth ions obtained by more refined calculations. The theoretical work of Judd (10) on Sm^{+++}, Eu^{+++}, Tb^{+++}, Dy^{+++}, and Ho^{+++} is particularly noteworthy. He examined the departures from the Landé interval rule in the ground multiplets of the above-mentioned rare earth ions. He found that the magnetic spin-spin interactions between the $4f$-electrons are much too small to account for the apparent distortions from the Landé interval rule, but that, by allowing for the partial breakdown of the Russell-Saunders coupling, it is possible to obtain good agreement between experimental observations and theory. According to Judd, the energy-level separations in the multiplet are given by the formula,

$$E_{J-1} - E_J = aJ + bJ^3 \tag{3}$$

where a and b are constants.

The energy-level calculations by Elliott and Stevens (11) of the ground multiplets of free tripositive rare earth ions, shown in Table II, were based on the assumption of Russell-Saunders coupling, and that

$$\xi = 200\,(Z - 55) \tag{4}$$

where ξ, expressed in cm^{-1}, is the spin-orbit interaction constant.

Runciman and Wybourne (12) have calculated the spectra of trivalent praseodymium and thulium ions with and without orbit-orbit interaction. The results for the ground multiplets are given in Table II. Further de-

Table II: Energy Levels of the Lowest Multiplet of Tripositive Rare Earth Ions

Ce^{+++}

E_J [cm^{-1}]

Term	$\sigma = 32$	$\sigma = 33$	$\sigma = 34$	$\sigma = 35$	$\sigma = 36$	*Elliott and Stevens*	*Experimental*
$^2F_{7/2}$	3476	2972	2524	2129	1782	2100	2253[a]
$^2F_{5/2}$			0			0	0

Pr^{+++}

E_J [cm^{-1}]

Term	$\sigma = 32$	$\sigma = 33$	$\sigma = 34$	$\sigma = 35$	$\sigma = 36$	*Elliott and Stevens*	*Runciman and Wybourne*	*Experimental*	
$^3H_6$	6353	5463	4670	3966	3345	4400	4212 4477	4274[b]	~ 5200[c]
$^3H_5$	2888	2483	2123	1803	1521	2000	2050 2190	2171[b]	
$^3H_4$			0			0	0	0	

Nd^{+++}

E_J [cm^{-1}]

Term	$\sigma = 32$	$\sigma = 33$	$\sigma = 34$	$\sigma = 35$	$\sigma = 36$	*Elliott and Stevens*	*Wybourne*	*Experimental*	
$^4I_{15/2}$	8684	7508	6456	5519	4687	6500	6099		5200[e]
$^4I_{13/2}$	5644	4620	3973	3396	2882		3976	3990[d]	
$^4I_{11/2}$	2449	2118	1821	1557	1322	1800	1928	2028	
$^4I_{9/2}$			0			0	0	0	

Pm^{+++}

E_J [cm^{-1}]

Term	$\sigma = 32$	$\sigma = 33$	$\sigma = 34$	$\sigma = 35$	$\sigma = 36$
$^5I_8$	9992	8684	7508	6456	5519
$^5I_7$	6918	6012	5198	4470	3821
$^5I_6$	4228	3674	3176	2731	2335
$^5I_5$	1922	1670	1444	1242	1061
$^5I_4$			0		

Sm^{+++}

E_J [cm^{-1}]

Term	$\sigma = 32$	$\sigma = 33$	$\sigma = 34$	$\sigma = 35$	$\sigma = 36$	*Judd*	*Elliott and Stevens*	*Experimental*	
$^6H_{15/2}$	9683	8455	7348	6353	5463	6650		6600[f]	6500[h]
$^6H_{13/2}$	7042	6149	5344	4621	3973	5160		5000[g]	4920[h]
$^6H_{11/2}$	4754	4151	3607	3119	2682	3670		3600[g]	
$^6H_{9/2}$	2817	2460	2138	1848	1589	2270		2300[g]	
$^6H_{7/2}$	1232	1076	935	809	695	1030	980	1100[g]	
$^6H_{5/2}$			0			0	0	0	

Table II (*continued*)

Eu^{+++}

E_J [cm^{-1}]

Term	$\sigma = 32$	$\sigma = 33$	$\sigma = 34$	$\sigma = 35$	$\sigma = 36$	*Judd*	*Elliott and Stevens*	*Experimental*	
$^7F_6$	7026	6162	5381	4676	4043	5100		5100[f]	
$^7F_5$	5018	4402	3843	3340	2888	3990		3900[g]	
$^7F_4$	3346	2934	2562	2227	1925	2850		2900[g]	
$^7F_3$	2007	1761	1537	1336	1155	1800		1900[g]	
$^7F_2$	1004	880	769	668	578	940		1100[g]	1000[i]
$^7F_1$	335	293	256	223	192	320	270	300[g]	350[i]
$^7F_0$			0			0	0	0	

Tb^{+++}

E_J [cm^{-1}]

Term	$\sigma = 32$	$\sigma = 33$	$\sigma = 34$	$\sigma = 35$	$\sigma = 36$	*Judd*	*Experimental*		
$^7F_0$	9022	7977	7026	6162	5381	5470	5660[j]	5765[k]	5800[g]
$^7F_1$	8592	7601	6691	5869	5124	5340	5430[j]	5525[k]	5600[g]
$^7F_2$	7733	6515	6022	5282	4612	5020	4975[j]	5018[k]	5100[g]
$^7F_3$	6444	5698	5018	4402	3843	4460	4325[j]	4347[k]	4400[g]
$^7H_4$	4726	4178	3680	3228	2818	3540	3330[j]	3472[k]	3400[g]
$^7F_5$	2578	2279	2007	1761	1537	2120	2080[j]	2101[k]	2100[g]
$^7F_6$			0			0		0	

Dy^{+++}

E_J [cm^{-1}]

Term	$\sigma = 32$	$\sigma = 33$	$\sigma = 34$	$\sigma = 35$	$\sigma = 36$	*Judd*	*Elliott and Stevens*	*Experimental*		
$^6H_{5/2}$	15976	14177	12535	11040	9683	10200		10200[h]	10200[f]	
$^6H_{7/2}$	13942	12373	10940	9635	8451	9320		9340[h]	9200[f]	
$^6H_{9/2}$	11328	10053	8889	7828	6866	8010	8600	8032[h]	7800[f]	8800[e]
$^6H_{11/2}$	8133	7218	6382	5621	4930	6140	6100	6078[h]	6000[f]	6000[e]
$^6H_{13/2}$	4357	3867	3419	3011	2641	3530	3300	3200[g]		
$^6H_{15/2}$			0			0	0		0	

Ho^{+++}

E_J [cm^{-1}]

Term	$\sigma = 32$	$\sigma = 33$	$\sigma = 34$	$\sigma = 35$	$\sigma = 36$	*Judd*	*Elliott and Stevens*	*Experimental*		
$^5I_4$	21201	18880	16755	14814	13047	13270		13330[f]		
$^4I_5$	17214	15249	13533	11965	10538	11440		11200[f]		
$^5I_6$	12231	10892	9666	8547	7527	8790		8500[f]	8470[h]	8747[h]
$^5I_7$	6523	5809	5155	4558	4015	5070	4800	5050[e,f]	5090[h]	
$^5I_8$			0			0	0		0	

Table II (*continued*)

Er^{+++}

E_J [cm^{-1}]

Term	$\sigma = 32$	$\sigma = 33$	$\sigma = 34$	$\sigma = 35$	$\sigma = 36$	*Elliott and Stevens*	*Wybourne*	*Experimental*
$^4I_{9/2}$	23730	21201	18880	16755	14814		15449	15290[d]
$^4I_{11/2}$	17037	15221	13555	12029	10636		10415	10191[d]
$^4I_{13/2}$	9127	8154	7261	6444	5698	6500	6775	8000[e]
$^4I_{15/2}$			0			0	0	0

Tm^{+++}

E_J [cm^{-1}]

Term	$\sigma = 32$	$\sigma = 33$	$\sigma = 34$	$\sigma = 35$	$\sigma = 36$	*Elliott and Stevens*	*Runciman and Wybourne*		*Experimental*
$^3H_4$	22405	20029	17940	15976	14177				
$^3H_5$	12221	10952	9785	8714	7733	8400	8605	8461	8250[l,b]
$^3H_6$			0			0	0		0

Yb^{+++}

E_J [cm^{-1}]

Term	$\sigma = 32$	$\sigma = 33$	$\sigma = 34$	$\sigma = 35$	$\sigma = 36$	*Elliott and Stevens*	*Experimental*
$^2F_{5/2}$	15863	14258	12778	11416	10166	10500	10300[e]
$^2F_{7/2}$			0			0	0

[a] R. J. Lang, *Canad. J. Res.*, **14**, 127 (1936).
[b] From W. A. Runciman and B. G. Wybourne (Ref. 12).
[c] F. H. Spedding, *Phys. Rev.*, **58**, 255 (1940).
[d] From B. G. Wybourne (Ref. 13).
[e] H. Gobrecht, *Ann. Physik*, **31**, 300 (1938).
[f] H. Gobrecht, *ibid.*, **31**, 755 (1938).
[g] H. Gobrecht, *ibid.*, **28**, 673 (1937). Interpreted by B. R. Judd, *Proc. Phys. Soc.*, A69, 157 (1956).
[h] G. Rosenthal, *Physik. Z.*, **40**, 508 (1939).
[i] K. H. Hellwege and H. G. Kahle, *Z. Physik*, **129**, 62 (1951).
[j] H. F. Geisler and K. H. Hellwege, *ibid.*, **136**, 293 (1953).
[k] Zaidel, Larionov, and Philippov, *Zhur. Eksp. i Theoret. Fiz.*, **9**, 17 (1939).
[l] H. A. Bethe and F. M. Spedding, *Phys. Rev.*, **52**, 454 (1937).

tails on the method used for these computations can be found in their original paper. The most recent contribution to the spectra of trivalent rare earth ions is the work of Wybourne. (13) He has diagonalized the complete spin-orbit matrices, with the addition of the electrostatic interaction energies, corresponding to the f^3 and f^{11} configurations, and hence determined the energy level schemes for Nd^{+++} and Er^{+++} ions. These ground state levels are reproduced in Table II.

Figure 1 shows the energy levels of the lowest multiplets of free Ce^{+++}, Pr^{+++},..., Yb^{+++} ions. This plot has been constructed using the above-described calculations of Judd (Sm^{+++}, Eu^{+++}, Tb^{+++}, Dy^{+++}, and Ho^{+++}), Elliott and Stevens (Ce^{+++} and Yb^{+++}), Runciman and Wybourne (Pr^{+++} and Tm^{+++}; second column associated with Runciman and Wybourne in Table II of this paper), Wybourne (Nd^{+++} and Er^{+++}), and ours (Pm^{+++}, $\sigma = 34$). It should be remarked that the multiplets are normal from Ce^{+++} up to Gd^{+++}, whose lowest multiplet is a single energy level $^8S_{7/2}$. Above Gd^{+++} the energy levels are inverted, that is, the

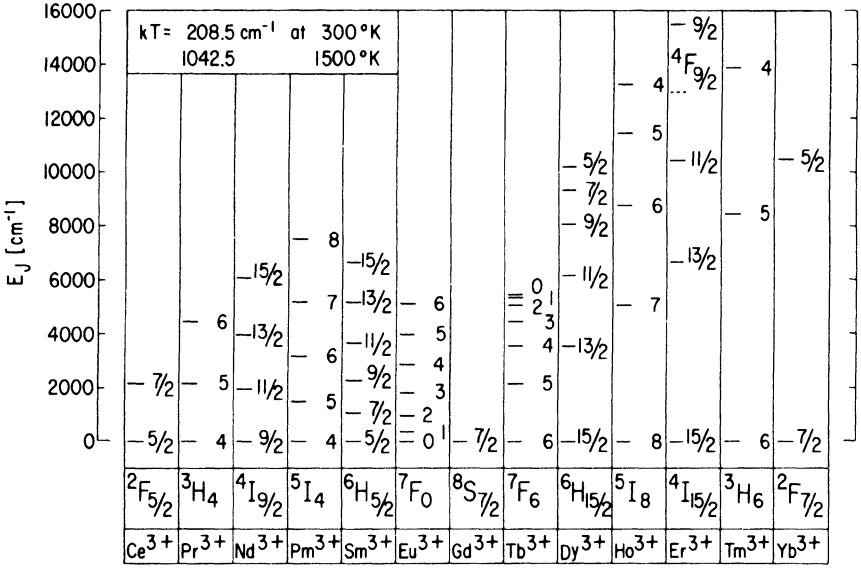


Fig. 1. Energy levels of the lowest multiplets of the tripositive rare earth ions.

energy values increase with decreasing J values. Another important observation should be made about the magnitude of energy-level separations in relation to kT, which at 300 and 1500°K is 208.5 cm^{-1} and 1042.25 cm^{-1}, respectively. It can be expected that at elevated temperatures the energy levels above the ground state will play some role in determining the various magnetic properties resulting from the localized $4f$-electrons for most of the possible electronic configurations.

THE VAN VLECK THEORY OF PARAMAGNETISM

Knowing the energy levels E_J, the paramagnetic susceptibility can be evaluated numerically using the Van Vleck theory. (7) When the thermal energy kT is comparable with the energy intervals of the lowest multiplet, the paramagnetic susceptibility per gram can be written as

$$\chi = \frac{N}{M} \frac{\sum_J \left[\frac{g^2\beta^2 J(J+1)}{3kT} + \alpha\right](2J+1)e^{-\frac{E_J}{kT}}}{\sum_J (2J+1)e^{-\frac{E_J}{kT}}} \tag{5}$$

where N is the Avogadro number, M the atomic weight of the particular rare earth metal, k the Boltzmann constant, T the absolute temperature, β the Bohr magneton, and

$$\alpha = \frac{\beta^2}{6(2J+1)}\left[\frac{f_{J+1}}{E_{J+1}-E_J} - \frac{F_J}{E_J - E_{J-1}}\right] \tag{6}$$

with

$$F_J = \frac{1}{J}[(S+L+1)^2 - J^2][J^2 - (S-L)^2] \tag{7}$$

The quantity g is the Landé splitting factor,

$$g = 1 + \frac{S(S+1) + J(J+1) - L(L+1)}{2J(J+1)} \tag{8}$$

When the energy intervals of the multiplet are large in comparison with kT, Eq. (5) reduces to

$$\chi = \frac{N}{M}\frac{g^2\beta^2 J(J+1)}{3kT} + \frac{N\alpha}{M} \tag{9}$$

It should be mentioned that Eq. (9) is equivalent, except for the term $N\alpha/M$, to that derived by Hund (14), assuming infinite multiplet width and neglecting the second-order Zeeman term in the energy equation. The Van Vleck theory includes this second term, and it gives rise to the expression $N\alpha/M$, which is especially important for tripositive samarium and europium ions, but is negligible for the last half of the rare earth group.

It is often advantageous to express the magnetization in Bohr magnetons. For a substance whose magnetic behavior follows the Curie law, the number of effective Bohr magnetons is given by

$$\mu_{eff} = \left(\frac{3kTM\chi}{N\beta^2}\right)^{1/2} \tag{10}$$

This equation is equivalent to

$$\mu_{eff} = \frac{1}{\beta}\left(\frac{3k}{N}\right)^{1/2}(MC)^{1/2} = 2.827\,(MC)^{1/2} \tag{11}$$

where C is the Curie constant per gram,

$$C = \chi T \tag{12}$$

The preceding considerations were based on an assumption that there are no interactions between the rare earth ions. Although this is almost so for some rare earth metals (for example neodymium, praseodymium, and samarium) as far as the paramagnetic behavior is concerned, the noninteracting approximation definitely is not applicable to other rare earth elements. A convenient and simple way for taking care of the interactions is by use of the paramagnetic Curie temperature θ. Then, instead of the Curie law, we have the Curie-Weiss law

$$\chi = \frac{C}{T - \theta} \tag{13}$$

Effectively, this shifts the 1 χ *vs.* T curves with respect to the temperature axis by θ, leaving the features of the curves unchanged.

EXPERIMENTAL CONSIDERATIONS

The magnetic susceptibilities of the rare earth metals were determined by a modification of the Faraday method, using a magnetic balance described earlier. (15, 16) Forces acting on samples placed in the nonhomogeneous magnetic field produced by two coaxial solenoids were measured with a Mettler type B-5 standard balance capable of detecting, during short time intervals, weight changes of 0.05 mg. The maximum magnetic field obtained at the location of the specimen was about 1200 oersteds and the gradient of the magnetic field was about 130 oersteds/cm^{-1}.

The samples were wrapped in a tantalum foil and were enclosed in silica capsules, either under vacuum or in helium or argon gas at about 20 cm Hg, at room temperature. All the steps of preparing cerium and europium samples for the magnetic-susceptibility studies were done in an argon atmosphere. During these operations the cerium and europium samples maintained bright surfaces.

The temperatures up to 1500 °K were obtained with a platinum furnace. The silica capsule containing the sample was located in the uniform-temperature zone of the furnace. The temperatures of the sample were measured with a platinum and platinum–10% rhodium thermocouple whose junction was also placed in the uniform-temperature zone of the furnace, between the silica capsule and the wall of the furnace. This thermocouple was calibrated at the melting points of tin and gold.

The magnetic contributions of the silica capsule, the silica rods connecting the capsule to the pan of the balance, and the tantalum foil were taken into account for the magnetic-susceptibility calculations of the rare earth metals.

Table III gives the sources of the polycrystalline rare earth metals used in this investigation and the purity of these metals.

TABLE III: SOURCES AND PURITY OF THE RARE EARTH METALS USED IN THIS INVESTIGATION

Metal	Source	Impurities [wt. %]
Ce	St. Eloi Corporation	< 0.5% according to the supplier.
Pr Sample 1	Research Chemicals	La (0.1); O_2 (0.06); Mg (0.05) Fe (0.01); Ta (not detected).
Sample 2	St. Eloi Corporation	< 0.5% according to the supplier.
Nd Samples 1, 2	Lindsay Chemical Div.	< 0.1% rare earth elements; Mo (0.43); O_2 (0.12); Fe (0.02); N_2 (0.01).
Sm Samples 1-3	Lindsay Chemical Div.	Mg (0.1); Nd (0.07); Ca (0.05); Eu (0.03); Gd (< 0.02); Fe (< 0.005); Ti (trace); Cu (faint trace); Al, Ce, Co, Cr, Hf, La, Mo, Nd, Ni, Pr, Si, Ta, Tb, V, Y, Zr (not detected).
Eu	Lindsay Chemical Div.	< 0.1% rare earth elements, O_2 (0.3); Ca, Ta (traces).
Gd Sample 1	Research Chemicals	O_2 (0.08); Fe (0.03); Ca (0.02); Eu (0.01); Ta (0.01).
Sample 2	Research Chemicals	Tb (0.1); Y (0.1); Fe (0.03); O_2 (0.03); Ta (not detected).
Sample 3	Lindsay Chemical Div.	Mo (1.2); O_2 (0.15); N_2 (0.03); Fe (0.02).
Sample 4	St. Eloi Corporation	Ta (2); Fe (0.06); Sm (0.05); Y (0.05); Ca (0.05); Tb (0.02); Eu (0.01); Mg (0.01); Ni (very weak); Cu (trace); Co, Cr, La, Mo, Ti, V, W, Yb, Zr (not detected).
Tb	St. Eloi Corporation	< 0.5% according to the supplier.
Dy	St. Eloi Corporation	Ta (0.2); Tb (0.1); Ca (0.05); Ho (0.05), Er (0.02); Si (0.02); Y (0.02); Fe (0.01); Mg (0.01); Cu, La (traces); Ce, Co, Cr, Mo, Ti, V, W. Yb, Zr (not detected).
Ho	Lindsay Chemical Div.	< 0.1% rare earth elements; Fe (<0.05); O_2 + Ca + Ta (< 0.3).
Er	Lindsay Chemical Div.	< 0.1% rare earth elements; O_2 (0.5); Ta (0.2); Fe (not detected).
Tm Samples 1-4	Lindsay Chemical Div.	< 0.1% rare earth elements; Ta (0.3); Ca (0.3); Mg (0.1); O_2 (0.25); Fe (not detected).

RESULTS AND DISCUSSION

Figures 2 through 6 and 8 through 16 show our paramagnetic-susceptibility measurements on polycrystalline cerium, praseodymium, neodymium, samarium, europium, gadolinium, terbium, dysprosium, holmium, erbium, and thulium. These Figures also present most of the known previous studies of the magnetic behavior of these metals above room temperatures. It should be mentioned that all our magnetic-susceptibility measurements, except those done on europium, have been corrected for the diamagnetism of the tripositive rare earth ions, using the values tabulated by Landolt-Börnstein. (17)

CERIUM

The inverse paramagnetic susceptibility of metallic cerium as a function of temperature is shown in Fig. 2. Our room-temperature meas-

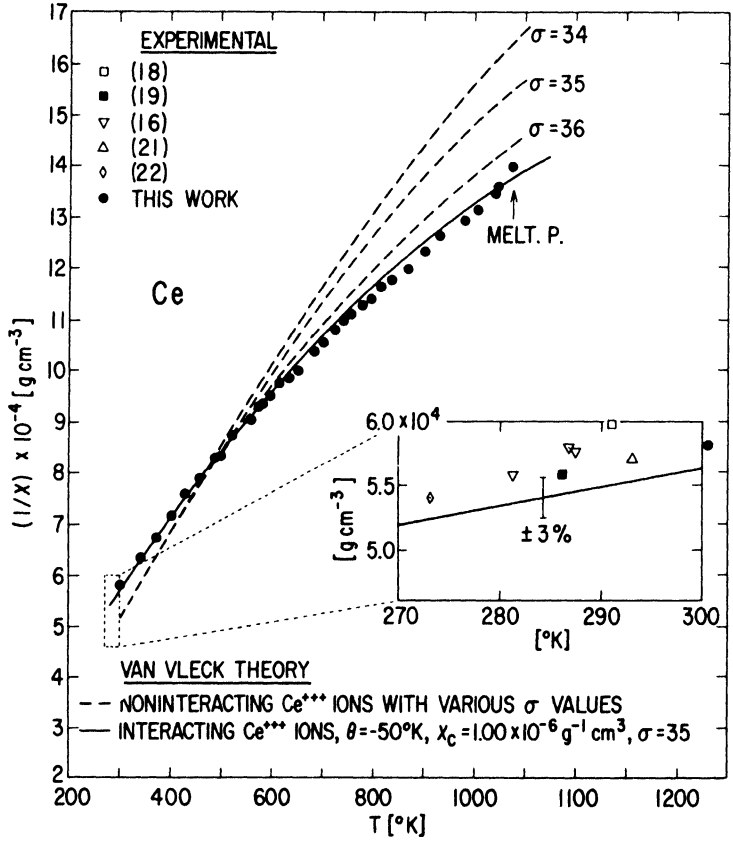


Fig. 2. Inverse paramagnetic susceptibility of Ce as a function of temperature.

urement is in fair agreement with those of other investigators (18-26) in this temperature range. The results of some of the previous studies (18-22), where the authors have provided numerical susceptibility data, are also shown in Fig. 2. Our high-temperature magnetic-susceptibility measurements are also in fair agreement with the earlier studies by Henry La Blanchetais (23) and Bates *et al.* (21) Figure 2 also shows the theoretical curves for noninteracting Ce^{+++} ions with various screening constants. It is obvious that calculations of this type can provide only an order of magnitude agreement with the experimental data. The reason for the imperfect agreement between the simple theory and the experimental observations is due to the interactions between the Ce^{+++} ions and the contribution of conduction electrons to the observed paramagnetism of cerium metal. This latter contribution, which we designated by χ_c, is particularly important for cerium, since at high temperatures it is comparable with the paramagnetism of the localized *f*-electrons of Ce^{+++} ions.

The solid curve shown in Fig. 2 represents the paramagnetic behavior of interacting Ce^{+++}, with $\theta = -50^{\circ}K$, $\sigma = 35$, and $\chi_c = 1.0 \times 10^{-6}\ g^{-1}\ cm^3$. The agreement with the measurements of the paramagnetic susceptibility of metallic cerium is satisfactory. It should be mentioned that the choice of value of θ is very reasonable in light of the experimental work by Bates *et al.* (21) and Lock (25) who have determined the paramagnetic Curie temperatures to be $-42^{\circ}K$ and approximately $-46^{\circ}K$, respectively. The value of the paramagnetic susceptibility of lanthanum, which does not have any *f*-electrons, measured by Trombe (27), Bommer (28), and Lock (25) are 1.19×10^{-6}, 0.99×10^{-6}, and $0.74 \times 10^{-6}\ g^{-1}\ cm^3$, respectively.

PRASEODYMIUM

The inverse susceptibility versus temperature behavior of praseodymium metal is shown in Fig. 3, together with all the known previous investigations. (22, 25, 29-32) It should be noted that our room-temperature measurements are in satisfactory agreement with those of Spedding *et al.* (32), Lock (25), and Leipfinger. (22) The only known previous work on the paramagnetic behavior of praseodymium at high temperatures is that due to Henry La Blanchetais. (31) However, her data do not agree with our measurements, as can be seen in Fig. 3. It is suspected that the differences are due to impurities in the sample used by Henry La Blanchetais.

It is known that praseodymium metal, which has a hexagonal crystal structure at room temperatures, changes to a body-centered cubic structure at $1071^{\circ}K$. (33) The melting point of praseodymium is at $1208^{\circ}K$. (32) Our magnetic studies show a very slight anomaly in the plot of the

inverse paramagnetic susceptibility versus temperature at the *hcp-bcc* transition and a considerably larger anomaly at the melting point. It is significant that there are no finite discontinuities in susceptibility at these phase transformations, indicating that the interactions between Pr^{+++} ions are indeed small. The idea of weak interactions is also supported by the quite satisfactory agreement between the theoretical calculations and the experimental observations on the magnetic behavior of praseodymium, as shown in Fig. 3. If the

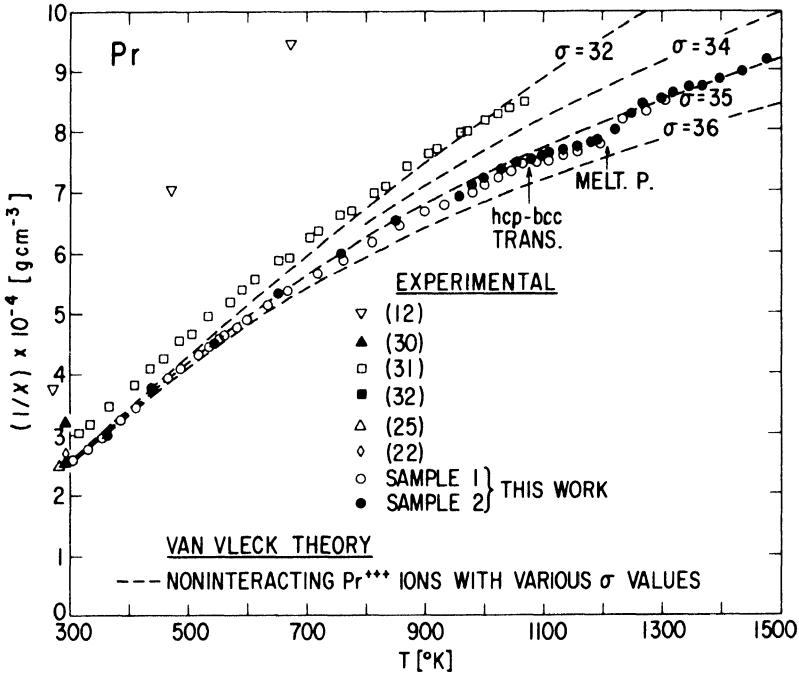


Fig. 3. Inverse paramagnetic susceptibility of Pr as a function of temperature.

contribution χ_c is neglected, the experimental paramagnetic-susceptibility data agree with the theoretical curve associated with $\sigma = 35$. However, assuming $\chi_c = 1.0 \times 10^{-6}\ g^{-1}\ cm^3$, the measured inverse paramagnetic-susceptibility versus temperature curve would approximately agree with the theoretical curve associated with $\sigma = 34$. Such a correction provides even better agreement between the theory and the measurements, because the spectroscopically determined energy levels of Pr^{+++} ions given in Table II are in closer agreement with the calculated levels obtained by using $\sigma = 34$ instead of $\sigma = 35$.

NEODYMIUM

Our paramagnetic-susceptibility measurements on polycrystalline neodymium are shown in Fig. 4. These data are identical with those described elsewhere (1), except that the experimental points presented in Fig. 4 have been corrected for the diamagnetism of Nd^{+++} ions. It is of interest to note that our susceptibility values at room temperature are in approximate agreement (within ± 5%) with the room-temperature data obtained by other investigators. (19, 22, 25, 29, 30, 34-36) The only known high-temperature studies on the magnetic behavior of neodymium are due to Owen (29) and Bates *et al.* (35), extending to about 800 and 700 °C, respectively. Our measurements are in fair agreement with those of Bates *et al.*, but not with Owen's results (obtained in 1912), as can be seen in Fig. 4. Hanak (33) found that at 1141 °K neodymium changes its crystal structure from *hcp* form to *bcc* structure. The melting point of neodymium is at 1297 °K. (32) Our magnetic measurements show slight anomalies, similar to those observed in praseodymium, at these temperatures.

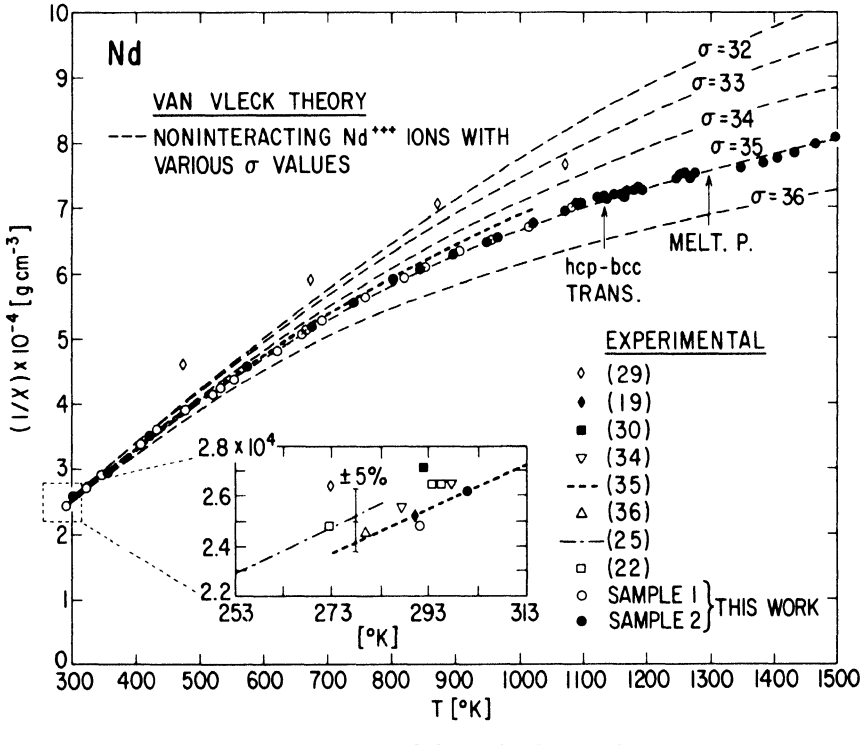


Fig. 4. Inverse paramagnetic susceptibility of Nd as a function of temperature.

Figure 4 also shows the theoretical $1/\chi$ *vs.* T curves for noninteracting Nd^{+++} ions. Our data fit the theoretical curve associated with $\sigma = 35$ if the conduction-electron contribution to the total paramagnetism is neglected. Assuming $\chi_c = 1.0 \times 10^{-6}$ g^{-1} cm^3, the experimental points would fit the theoretical curve, $\sigma = 34$, which is associated with energy-level separations in fair agreement with the spectroscopic determinations, as can be seen from Table II.

SAMARIUM

The paramagnetic behavior of samarium as a function of temperature is presented in Fig. 5, which also shows all the known previous investigations (18, 32, 25, 22) on metallic samarium at room temperatures. The present measurements, in the neighborhood of 300 °K, agree satisfactorily with the room-temperature value determined by Spedding *et al.* (32) The deviations of Lock's (25) and Leipfinger's (22) values

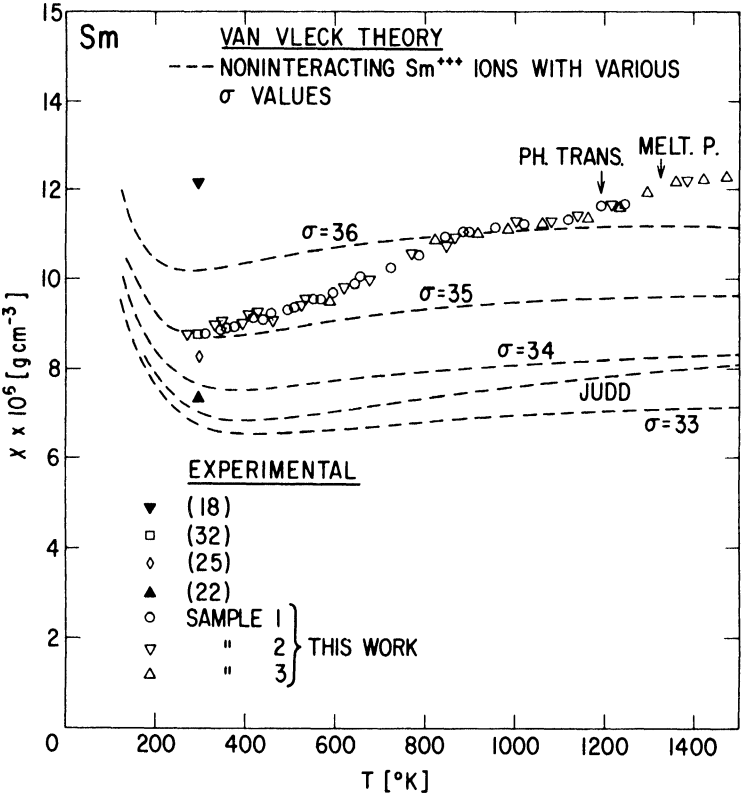


Fig. 5. Paramagnetic susceptibility of Sm as a function of temperature.

from the present investigation are very possibly due to larger impurity contents in their samples. The point shown as Lock's result in Fig. 5 is only approximately correct, since it was obtained from the χ *vs.* T graph of his paper. The magnetic susceptibility of samarium measured by Klemm and Bommer (18) at room temperatures is considerably larger than those of all the other investigators. It can be expected that the cause for this difference is due to impurities. Also, it should be mentioned that Klemm and Bommer used a mixture of powdered samarium and potassium chloride for their magnetic investigations. Similarly, Leipfinger's work was done with a powdered samarium.

The present investigation on samarium shows that the paramagnetic susceptibility does not change appreciably as the crystal structure changes at 1190°K. (32) Also, there is no discontinuity in the χ *vs.* T curve at the melting point of samarium, 1325°K. (32) These facts may be explained as a result of weak interactions between the tripositive ions at elevated temperatures.

Our paramagnetic-susceptibility measurements at and slightly above room temperatures agree satisfactory with the theoretical calculations associated with $\sigma = 35$. However, the measured temperature variation of χ for samarium is considerably larger than the simple theory predicts. It appears that these deviations result mainly from the energy-level distributions used in the susceptibility calculations, although the conduction-electron contribution may also be partially responsible. It is interesting to note that the more refined theory of Judd (10) for finding the energy levels of the tripositive samarium ion does not help to explain the observed temperature dependence of the paramagnetic susceptibility for samarium metal. Thus, it is possible that the breakdown of the Russell-Saunders coupling in metallic samarium is larger than that used in Judd's theory, although it seems to satisfy the observed spectroscopic results in various samarium salts, as indicated in Table II. Finally, it should also be emphasized that the Van Vleck theory does not include any interactions between the rare earth ions; that is, the theoretical curves in Fig. 5 represent the magnetic behavior of systems consisting of noninteracting tripositive samarium ions with various distributions of the energy levels.

EUROPIUM

The magnetic behavior of metallic europium from 300 to 1400°K, as determined in this investigation, is shown in Fig. 6. This graph also gives all the known previous measurements (18, 37, 38) of the magnetic susceptibility between the Néel temperature (about 90°K) and 300°K. The agreement between the data of Bozorth and Van Vleck (38) and

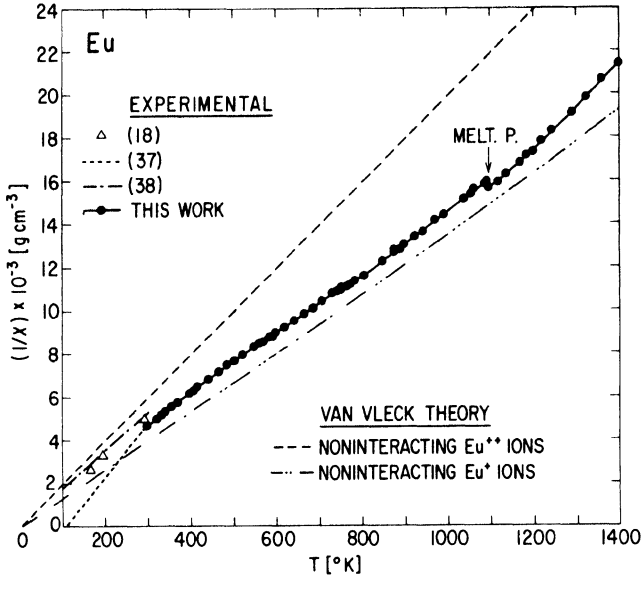


Fig. 6. Inverse magnetic susceptibility of Eu as a function of temperature.

those of Klemm and Bommer (18) is fairly satisfactory. It should be mentioned that Klemm and Bommer studied a powdered mixture of Eu + KCl, while Bozorth and Van Vleck made their measurements on a polycrystalline metallic europium. The results of the investigation by Henry La Blanchetais and Trombe (37) deviate considerably from those of Bozorth and Van Vleck, and Klemm and Bommer. Our value of the magnetic susceptibility of europium at 300 °K is about 10 per cent larger than that measured by Bozorth and Van Vleck. It is very possible that this discrepancy is due to different amounts of impurities in the samples.

Comparing the measured inverse magnetic-susceptibility curve shown in Fig. 3 with the theoretical curves given in Fig. 7 immediately reveals that the Eu^{+++} model cannot explain the observed magnetic susceptibility of metallic europium. It has been suggested that europium metal should be considered to be made up of Eu^{++} ions imbedded in a sea of electrons. (32, 38) Although this model can approximately account for the magnetic susceptibility from the Néel temperature to room temperature, our high-temperature measurements of the magnetic behavior of solid europium clearly show that the Eu^{++} model is not a satisfactory approximation in this range. In fact, it appears that at high temperatures, say between 800 °K and the melting point of europium (1099 °K) (32), the magnetic-susceptibility values are quite close to those resulting from noninteracting Eu^{+} ions. The Bohr magneton number in this

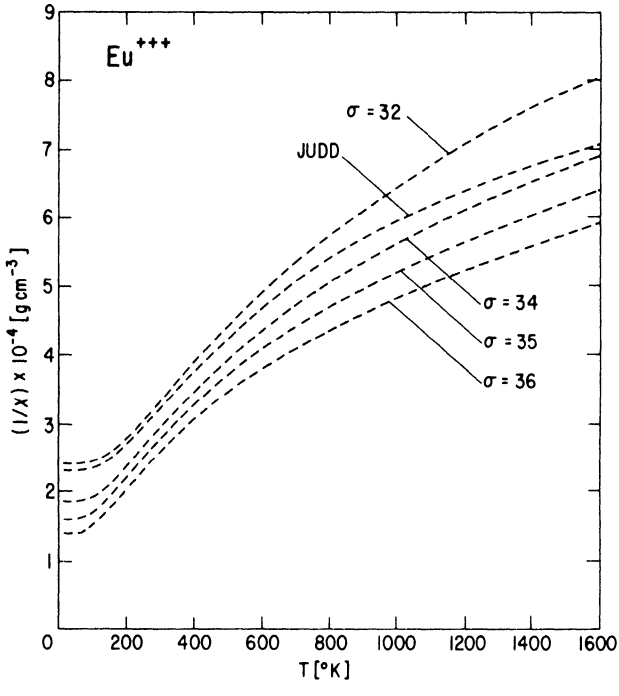


Fig. 7. Inverse paramagnetic susceptibility of noninteracting Eu^{+++} ions.

range is equivalent to that of the Eu^{+} ion in its ground state $^7F_6$. The melting process produces a small anomaly in the plot of $1/\chi$ *vs.* T, as can be seen in Fig. 6. Liquid europium metal approximately follows the Curie-Weiss law. The magnetic moment in this state is very close to that expected from the Eu^{++} system. These observations indicate that metallic europium has unusual magnetic properties, and that europium is not a well-behaved rare earth metal. This supports some previous studies on the crystal structure, density, compressibility, thermal expansion, electrical resistivity, and so forth (32, 33, 39, 40) which are out of line with the corresponding behavior for most of the rare earth elements. At the present time we are unable to provide a theoretical justification for the possible change of valency of europium ions with respect to the temperature.

GADOLINIUM

Figures 8 through 11 show the inverse paramagnetic susceptibility of the gadolinium samples with respect to temperature. Figure 8, representing the paramagnetic behavior of the purest polycrystalline gadolinium sample used in this investigation, shows a very slight anomaly

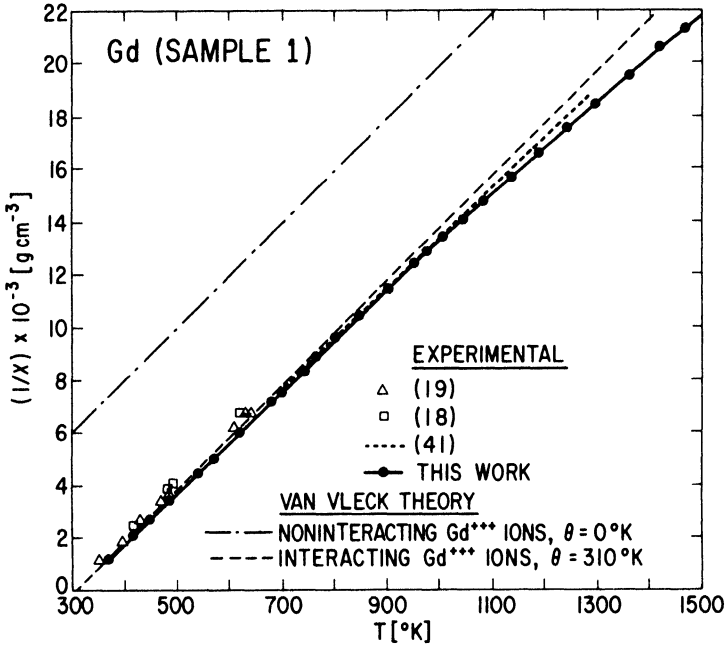


Fig. 8. Inverse paramagnetic susceptibility of Gd as a function of temperature.

at about 750 °K. This anomaly is increasingly noticeable in samples 2, 3, and 4, with the larger impurity concentrations, as can be seen from Fig. 9, 10, and 11. It should be mentioned that the observed behaviors are completely reproducible with respect to slow warming and cooling processes (about 50 °K per hour). The origin of these observations is not understood at the present time.

Gadolinium has been assumed to be a metal with very simple paramagnetic behavior, due to the fact that the lowest multiplet consists of a single energy level. It was expected that the paramagnetic-susceptibility measurements on gadolinium would provide some estimate of the conduction-electron contribution χ_c to the total paramagnetic susceptibility of the rare earth metals. It was hoped that the inverse paramagnetic susceptibility versus temperature plot, instead of being a straight line, would have a small downward curvature at high temperatures. The high-temperature portions of the $1/\chi$ *vs.* T curves given in Fig. 8 through 11 clearly show a curvature of the expected type. However, due to the slight anomaly at about 750 °K, we did not try to determine the quantity χ_c for the gadolinium metal.

Figures 8 through 11, in addition to giving our measurements, also show the known previous investigations (18, 19, 41) on the paramagnetic

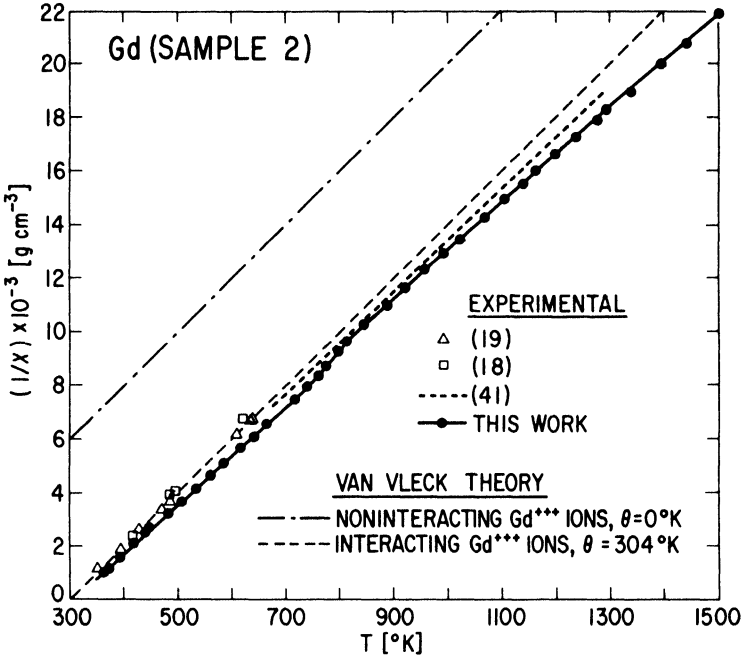


Fig. 9. Inverse paramagnetic susceptibility of Gd as a function of temperature.

behavior of gadolinium. Trombe's results (19) agree very well with the theoretical predictions based on the interacting Gd^{+++} ion model. Also, the study of Klemm and Bommer (18) on a powdered mixture of Gd + KCl is in fair agreement with the theoretical predictions. The study of Kriessman and McGuire (41) between 400 to 1000 °C indicates that the Curie-Weiss law is obeyed in this range.

The effective Bohr magneton numbers and the paramagnetic Curie temperatures of gadolinium metal, determined by the previous investigators and by us, are summarized in Table IV. The theoretical value of the effective Bohr magneton number for Gd^{+++} system is 7.94. Our measurements on the purest gadolinium sample give $\mu_{eff} = 8.07 \pm 0.05$, in satisfactory agreement with the theoretical predictions, and very close to the value reported by Kriessman and McGuire. (41)

TERBIUM

The inverse paramagnetic-susceptibility versus temperature data on metallic terbium are shown in Fig. 12. Our measurements are in good agreement with those of Spedding *et al.* (32) and Thoburn *et al.* (42) as illustrated there. Klemm and Bommer's (18) studies of the paramagnetic susceptibility of powdered Tb + KCl mixture deviate considerably in

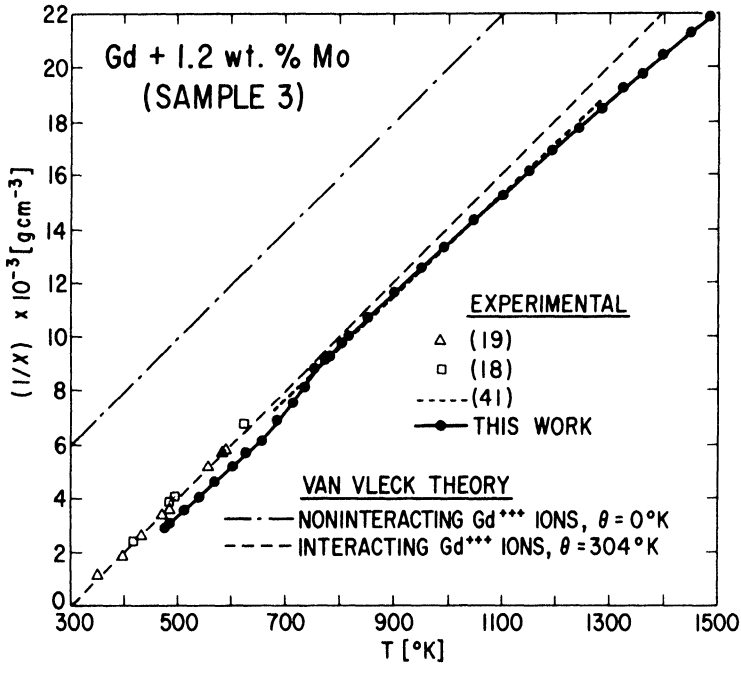


Fig. 10. Inverse paramagnetic susceptibility of Gd + 1.2 wt. % Mo as a function of temperature.

absolute value from the present investigation. The Bohr magneton numbers and the paramagnetic Curie points of terbium obtained by various investigators are given in Table V. The theoretical value of μ_{eff} for a Tb^{+++} system in the ground state $^7F_6$ is 9.72. The work of Thoburn

TABLE IV: COMPARISON OF THE RESULTS ON GADOLINIUM OF THIS STUDY WITH PARAMAGNETIC-SUSCEPTIBILITY DATA OF OTHER INVESTIGATORS

Investigator	Temperature Range [°K]	μ_{eff}* [Bohr Magnetons]	θ_p [°K]
Trombe (19)	360–640	7.97	302.7
Klemm and Bommer (18)	420–620	7.8	302
Kriessman and McGuire (41)	670–1270	8.10	298.2
This investigation:			
Gd (Sample 1)	370–740	8.07 ± 0.05	310 ± 3
Gd (Sample 2)	360–660	8.35 ± 0.05	304 ± 3
	850–1160	8.35 ± 0.05	276 ± 3
Gd + 1.2 wt. % Mo	470–650	8.38 ± 0.05	312 ± 3
Gd + 2 wt. % Ta	440–660	9.05 ± 0.05	281 ± 3

*Theoretical value of μ_{eff} for the state $^8S_{7/2}$ is 7.94.

TABLE V: COMPARISON OF THE RESULTS ON TERBIUM OF THIS STUDY WITH PARAMAGNETIC-SUSCEPTIBILITY DATA OF OTHER INVESTIGATORS

Investigator	Temperature Range [°K]	μ_{eff}* [Bohr Magnetons]	θ_p [°K]
Klemm and Bommer (18)	273–555	9.0	205
Thoburn, Legvold, and Spedding (42)	275–375	9.7	237 ± 2
This investigation	300–800	9.62 ± 0.05	236 ± 2

*Theoretical value of μ_{eff} for the state $^7F_6$ is 9.72.

et al. and our investigation give $\mu_{eff} = 9.7$ and $\mu_{eff} = 9.62 \pm 0.05$, respectively. Thus, the experimental evidence favors the localized *f*-electron model for metallic terbium. There is, however, a slight discrepancy between the theoretical predictions based on the interacting Tb^{+++} model and the experimental behavior. The theory predicts a very slight upward curvature in the $1/\chi$ *vs.* T plot, as shown in Fig. 12. The experimental data, however, indicate that metallic terbium obeys the Curie-Weiss law up to the highest temperatures used in this investi-

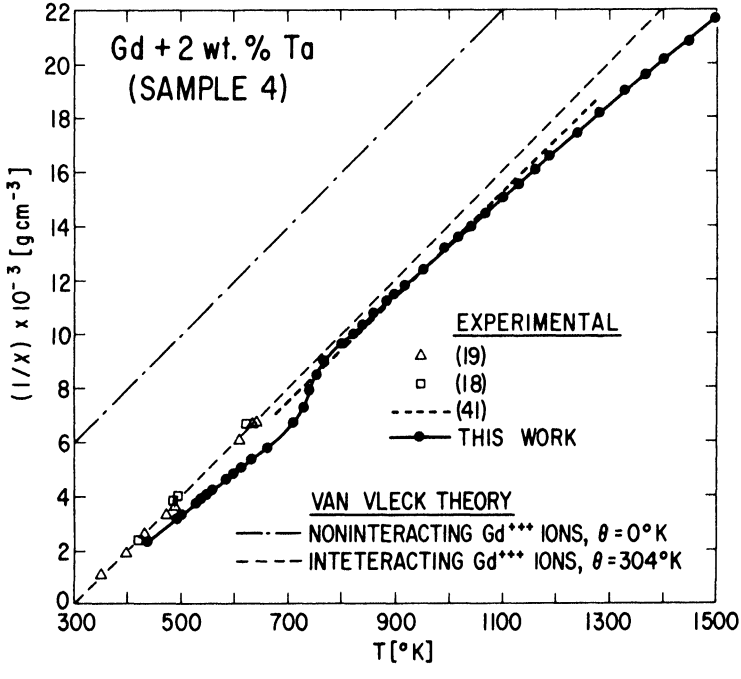


Fig. 11. Inverse paramagnetic susceptibility of Gd + 2 wt. % Ta as a function of temperature.

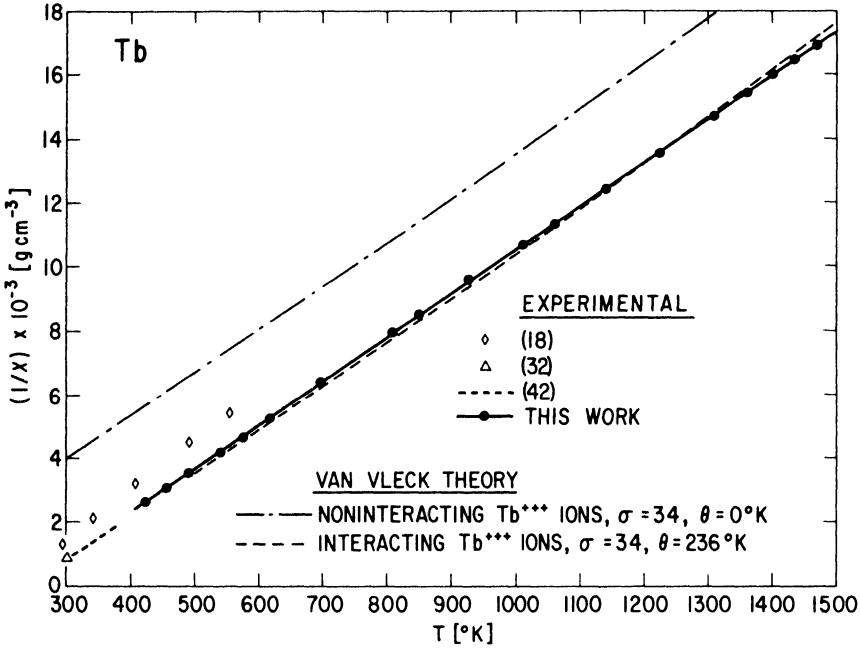


Fig. 12. Inverse paramagnetic susceptibility of Tb as a function of temperature.

gation. We think that this small deviation from the simple theory is due to the conduction-electron contribution to the total paramagnetism in the terbium metal. Due to the slight disagreement between the theoretical μ_{eff} and our experimental μ_{eff} values, no attempt was made to calculate the quantity χ_c.

DYSPROSIUM

The inverse paramagnetic-susceptibility versus temperature data are shown in Fig. 13, in comparison with other investigations (18, 22, 32, 43, 44) and theoretical predictions (see also Table VI). Our measurements are in very good agreement with those of Trombe (43), Spedding *et al.* (32), and Behrendt *et al.* (44), as can be seen. Leipfinger's work (22) was performed with a powdered dysprosium metal, and his data seem to be in good agreement with the predictions of the noninteracting Dy^{+++} ion model. However, the study of Klemm and Bommer (18) on a powdered mixture of Dy + KCl is in fair agreement with the experimental paramagnetic susceptibility measurements of solid dysprosium metal. Our susceptibility data are in good agreement with the predictions of the interacting Dy^{+++} ion theory up to about 900°K. Above this temperature a small deviation from the theory occurs. Since the experimental

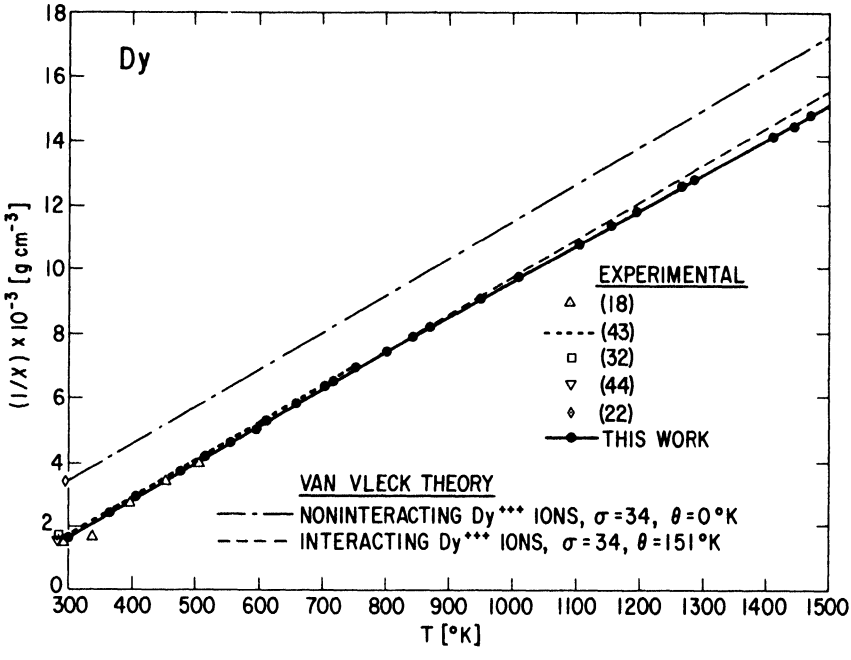


Fig. 13. Inverse paramagnetic susceptibility of Dy as a function of temperature.

value of μ_{eff} is in very good agreement with the theoretical value, as can be seen in Table VI, we attempted to calculate χ_c for this metal. The result $\chi_c = 1.15 \times 10^{-6}$ g^{-1} cm^3 is interpreted as a measure of the

TABLE VI: COMPARISON OF THE RESULTS ON DYSPROSIUM OF THIS STUDY WITH PARAMAGNETIC-SUSCEPTIBILITY DATA OF OTHER INVESTIGATORS

Investigator	Temperature Range [°K]	μ_{eff}* [Bohr Magnetons]	θ [°K]
Klemm and Bommer (18)	290–510	10.9	150
Trombe (43)	250–730	10.64	157
Spedding, Legvold, Daane, and Jennings (32)	250–300	10.2	154.0
Behrendt, Legvold, and Spedding (44)			
H parallel c_0 axis	260–300	10.64	121
H perpendicular c_0 axis	230–300	10.65	169
Calculated polycrystalline behavior	230–300	10.64	153
Leipfinger (22)‡		10.45 ± 0.30	−0.5
This investigation	300–700	10.67 ± 0.05	151 ± 1

*Theoretical value of μ_{eff} for the state $^6H_{15/2}$ is 10.64.
†Dysprosium powder.

conduction-electron contribution to the paramagnetism of the dysprosium metal. The quantity χ_c appears to be independent of temperature, as could be expected.

HOLMIUM

The inverse paramagnetic-susceptibility versus temperature data for holmium obtained in this investigation are shown in Fig. 14. Our data are in fair agreement with the previous investigations of Bommer (45) and Rhodes *et al.* (46). (See also Table VII.)

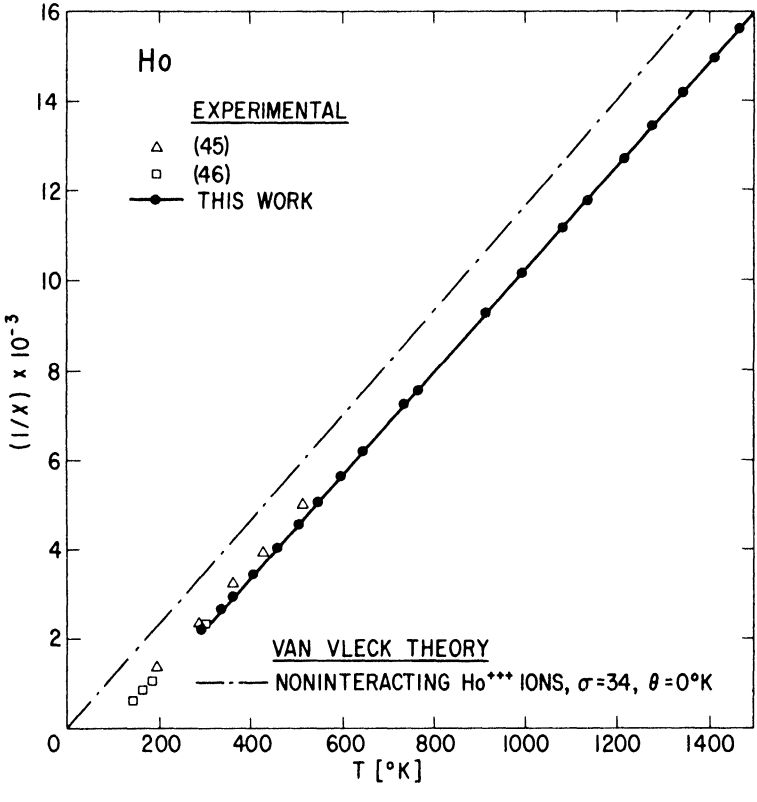


Fig. 14. Inverse paramagnetic susceptibility of Ho as a function of temperature.

Our measurements of the paramagnetic susceptibility of holmium from 300 to 1500 °K can be described by the Curie-Weiss law, $\chi = 8.97 \times 10^{-2}/(T - 87.7)\,g^{-1}\,cm^3$. The effective Bohr magneton number from these data is 10.8, which is in approximate agreement with the theoretical value 10.60 for the spectroscopic state $^5I_8$.

TABLE VII: COMPARISON OF THE RESULTS ON HOLMIUM OF THIS STUDY WITH PARAMAGNETIC-SUSCEPTIBILITY DATA OF OTHER INVESTIGATORS

Investigator	Temperature Range [°K]	μ_{eff}* [Bohr Magnetons]	θ_p [°K]
Bommer (45)	195–515	10.6	87
Rhodes, Legvold and Spedding (46)	140–300	10.9	87
This investigation	300–1500	10.8 ± 0.2	88 ± 3

*Theoretical value of μ_{eff} for the state $^5I_8$ is 10.60.

ERBIUM

The inverse paramagnetic susceptibility of erbium as a function of temperature is given in Fig. 15. The data satisfy the Curie-Weiss law, $\chi = 7.16 \times 10^{-2}/(T - 47.2)\,g^{-1}\,cm^3$. The experimental Bohr magneton number is 9.79, which should be compared with the theoretical value 9.58 resulting from the ground state $^4I_{15/2}$.

The only known previous paramagnetic measurements on metallic erbium are due to Owen (29) and Spedding *et al.* (32). Owen's work was done on powdered metallic erbium. His results, shown in Fig. 15 in

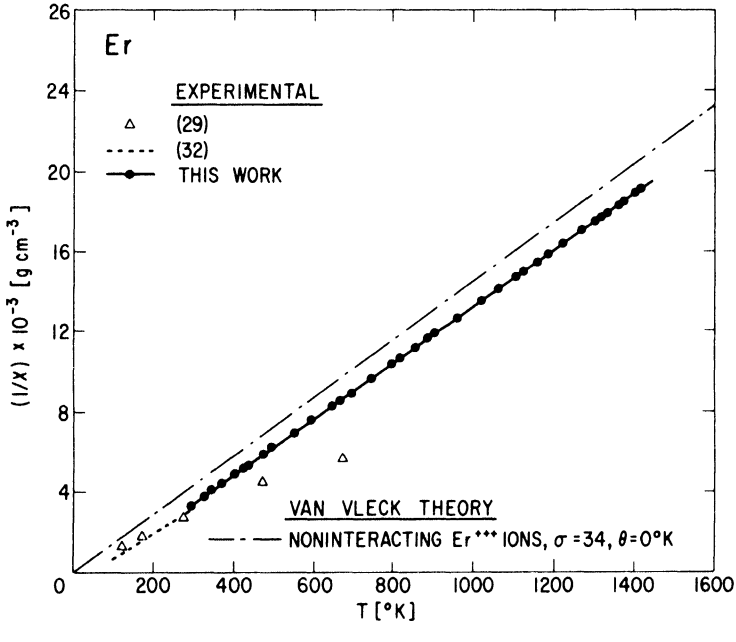


Fig. 15. Inverse paramagnetic susceptibility of Er as a function of temperature.

comparison with the more recent measurements, including ours, strongly suggest that the material was not sufficiently pure, even for studies of this type. Spedding *et al.* report that for polycrystalline erbium the paramagnetic susceptbility satisfies the Curie-Weiss law, $\chi = 7.53 \times 10^{-2}/(T - 41.6)\,g^{-1}\,cm^3$, from about 90 to 300 °K. The corresponding effective Bohr magneton number is 10.0, slightly higher than ours.

THULIUM

The experimentally observed paramagnetic behavior of thulium is shown in Fig. 16. Our data can be described by the Curie-Weiss law, $\chi = 4.37 \times 10^{-2}/(T - 17.4)\,g^{-1}\,cm^3$. The effective Bohr magneton number from these measurements is 7.68, which is in approximate agreement with the theoretical value 7.56 from the ground state $^3H_6$.

The only known previous paramagnetic studies on thulium are those of Klemm and Bommer (18), Rhodes *et al.* (46), and Davis and Bozorth (47).

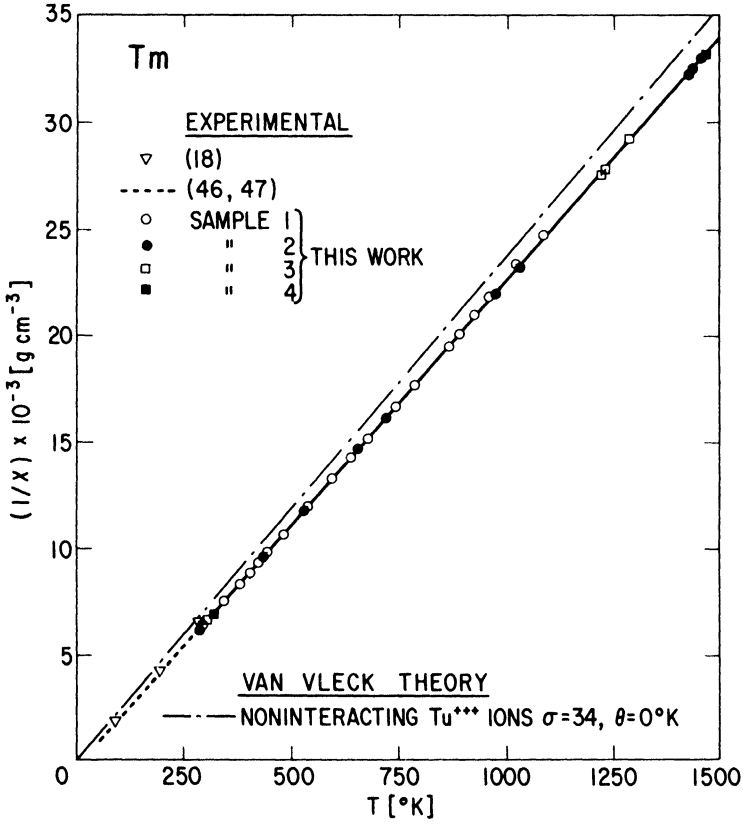


Fig. 16. Inverse paramagnetic susceptibility of Tm as a function of temperature.

Their measurements are shown in Fig. 16 and summarized in Table VIII. The agreement between these investigations is quite satisfactory.

It should be emphasized that the paramagnetic behavior of thulium, just as that of holmium and erbium, follows the Curie-Weiss law, because the separations between the ground state and the first level above the ground state are too large in comparison with the thermal energy, even at high temperatures. Also, the conduction-electron contribution to the total paramagnetism of these metals is almost negligible in relation to the paramagnetism resulting from the localized $4f$-electrons.

TABLE VIII: COMPARISON OF THE RESULTS ON THULIUM OF THIS STUDY WITH PARAMAGNETIC-SUSCEPTIBILITY DATA OF OTHER INVESTIGATORS

Investigator	Temperature Range [°K]	μ_{eff}* [Bohr Magnetons]	θ_p [°K]
Klemm and Bommer (18) (18)	90–291	7.6	10
Rhodes, Legvold and Spedding (46)	60–300	7.6	20
Davis and Bozorth (47)	70–300	7.6	20
This investigation	300–1500	7.68 ± 0.10	17.4 ± 0.5

*Theoretical value of μ_{eff} for the state $^3H_6$ is 7.56.

CONCLUSIONS

The paramagnetic behavior of polycrystalline cerium, praseodymium, neodymium, samarium, europium, gadolinium, terbium, dysprosium, holmium, erbium, and thulium have been studied above room temperatures. All these measurements—except those done on europium—can be interpreted by using the tripositive ion model based on the localized $4f$-electron approximation and the Van Vleck theory of paramagnetism. It has been found that, besides the $4f$-electron contribution to the total paramagnetism of any one of the rare earth metals—except, possibly, europium—a small, approximately temperature-independent paramagnetic susceptibility of magnitude 1×10^{-6} g^{-1} cm^3 exists, and this originates from the conduction electrons.

Our paramagnetic-susceptibility measurements on polycrystalline europium clearly indicate that this metal is not a well-behaved rare earth element. A tripositive europium ion model can possibly be used only below the Néel temperature (90 °K). Above this the magnetic behavior of europium can be described by the Eu^{++} approximation, which gradually changes to the Eu^{+} model. Metallic europium in liquid state behaves magnetically as a collection of intersecting Eu^{+++} ions.

REFERENCES

1. S. Arajs, *J. Chem. Phys.*, 32, 951 (1960) (Tm); S. Arajs and D. S. Miller, *J. Appl. Phys.*, sup. to 31, 325S (1960) (Nd, Ho, and Er).
2. S. Arajs, *Phys. Rev.*, 120, 986 (1960) (Sm).
3. S. Arajs and R. V. Colvin. Sixth Annual Conference on Magnetism and Magnetic Materials, New York, Nov. 16-19, 1960 (Gd, Tb, and Dy).
4. S. Arajs and R. V. Colvin. Article submitted to *J. Chem. Phys.* (pr).
5. S. Arajs and R. V. Colvin. Article submitted to *Phys. Rev.* (Ce and Eu).
6. S. Goudsmit, *Phys. Rev.*, 31, 946 (1928).
7. J. H. Van Vleck, *Theory of Electric and Magnetic Susceptibilities.* London: Oxford University Press, 1932, p. 226.
8. E. U. Condon and G. M. Shortley, *The Theory of Atomic Spectra.* New York: The Macmillan Company, 1935, p. 193.
9. D. S. McClure, in F. Seitz and D. Turnbull (eds.), *Solid State Physics.* New York: Academic Press, 1959, Vol. 9, p. 399.
10. B. R. Judd, *Proc. Phys. Soc.* (London), A69, 157 (1956).
11. R. J. Elliott and K. W. H. Stevens, *Proc. Roy. Soc.* (London), A218, 553 (1953).
12. W. A. Runciman and B. G. Wybourne, *J. Chem. Phys.*, 29, 1149(1959).
13. B. G. Wybourne, *ibid.* 32, 639 (1960).
14. F. Hund, *Z. Physik*, 33, 855 (1925).
15. R. B. Sosman and J. B. Austin, *J. Wash. Acad. Sci.*, 25, 15 (1935).
16. S. Arajs and D. S. Miller, *J. Appl. Phys.*, 31, 986 (1960).
17. Landolt-Börnstein, *Zahlenwerte und Funktionen aus Physik, Chemie, Astronomie, Geophysik, Technik.* Berlin: Springer Verlag (1950), Vol. I, Part I, p. 398.
18. W. Klemm and H. Bommer, *Z. anorg. Chem.*, 231, 138 (1937).
19. F. Trombe, *Ann. phys.*, 7, 383 (1937).
20. Ch. Henry La Blanchetais, *Compt. rend.*, 220, 392 (1945).
21. L. F. Bates, S. J. Leach, and R. G. Loasby, *Proc. Phys. Soc.* (London), B68, 859 (1955).
22. H. Leipfinger, "Magnetic Properties of Rare Earth Metals at Very Low Temperatures" (Physikalisches Institut der Technischen Hochschuhle München, 1957), Technical Report, Contract No. AF(514)-941; *Z. Physik*, 150, 415 (1958).
23. Ch. Henry La Blanchetais, in *Colloque National de Magnetisme*, Centre National de la Recherche Scientifique, Paris (1958), p. 205.
24. F. Trombe, *Compt. rend.*, 198, 1591 (1934); *ibid.*, 219, 90 (1944); F. Trombe and M. Foëx, *Ann. chim.*, 19, 417 (1944).
25. J. M. Lock, *Proc. Phys. Soc.* (London), 870, 566 (1957).
26. L. M. Roberts and J. M. Lock, *Phil. Mag.*, 2, 811 (1957).
27. F. Trombe, *Compt. rend.*, 201, 652 (1934).
28. H. Bommer, *Electrochem.*, 45, 357 (1939).
29. M. Owen, *Ann. Physik*, 37, 657 (1912).
30. W. Klemm and H. Bommer, *Z. anorg. Chem.*, 241, 264 (1939).

31. Ch. Henry La Blanchetais, *Comp. rend.*, **234**, 1353 (1952); *J. des Recherches du C.N.R.S.*, 28, 32 (1954); *ibid.*, 29, 103 (1954).
32. F. H. Spedding, S. Legvold, A. H. Daane, and L. D. Jennings, in C. J. Gorter (ed.), *Progress in Low Temperature Physics.* Amsterdam: North-Holland Publishing Company, 1957, Vol. II, p. 368.
33. J. J. Hanak, "High Temperature Allotropy of the Rare-Earth Elements." Doctoral dissertation, Iowa State University, Ames, Iowa, 1959.
34. J. F. Elliott, S. Legvold, and F. H. Spedding, *Phys. Rev.*, **94**, 50 (1954).
35. Bates, Leach, Losby, and Stevens, *Proc. Phys. Soc.* (London), B68, 181 (1955).
36. D. R. Behrendt, S. Legvold, and F. H. Spedding, *Phys. Rev.*, **106**, 723 (1957).
37. Ch. Henry La Blanchetais and F. Trombe, *Compt. rend.*, 243, 707 (1956).
38. R. M. Bozorth and J. H. Van Vleck, *Phys. Rev.*, **118**, 1493 (1960).
39. F. H. Spedding and A. H. Daane, in H. M. Finniston and J. P. Howe (eds.), *Progress in Nuclear Energy.* New York: Pergamon Press, 1956, Vol. I, Series V, p. 413.
40. F. H. Spedding, J. J. Hanak, and A. H. Daane, *Trans. Am. Inst. Mining, Met. Engrs.*, 212, 379 (1958).
41. C. J. Kriessman and T. R. McGuire, *Phys. Rev.*, **90**, 374 (1953).
42. W. C. Thoburn, S. Legvold, and F. H. Spedding, *ibid.*, 112, 56(1958).
43. F. Trombe, *Compt. rend.*, 221, 19 (1945).
44. D. R. Behrendt, S. Legvold, and F. H. Spedding, *Phys. Rev.*, **109**, 1544 (1958).
45. H. Bommer, *Z. anorg. Chem.*, 242, 277 (1939).
46. B. L. Rhodes, S. Legvold, and F. H. Spedding, *Phys. Rev.*, **109**, 1547 (1958); B. L. Rhodes, "Magnetic Properties of Holmium and Thulium," U.S. Atomic Energy Comm. Report ISC-701 (1955).
47. D. D. Davis and R. M. Bozorth, *Phys. Rev.*, **118**, 1543 (1960).

PART FOUR

Physical Properties of Metals, Alloys, and Intermetallics

STUDIES OF INTERMETALLIC COMPOUNDS BETWEEN THE LANTHANIDE METALS AND IRON, COBALT, NICKEL AND MANGANESE

W. E. WALLACE AND L. V. CHERRY*

Department of Chemistry,
University of Pittsburgh,
Pittsburgh, Pennsylvania

A large number of new intermetallic compounds have been prepared with stoichiometries represented by the formulas AB_2 and AB_5, in which A is a lanthanide or Y, and B is Fe, Co, Ni, or Mn. The AB_2 compounds almost always occur in the $MgCu_2$ structure. Twenty-nine of the AB_5 compounds exist in the $CaCu_5$ structure, and seven, in all of which B is Mn, crystallize in an as yet unsolved orthorhombic structure. Magnetic work shows that in 50 out of 69 compounds examined the moments are spontaneously coupled at room temperature. In a detailed study of the ACo_5 series, YCo_5, $CeCo_5$, and $SmCo_5$ appear to be Néel type-Q ferrimagnetic and $GdCo_5$, $HoCo_5$ and $ErCo_5$ appear to be Néel type-P ferrimagnetic. The other four compounds—$PrCo_5$, $NdCo_5$, $DyCo_5$, and $TbCo_5$—do not appear to fall into any of the categories recognized to date. Their magnetization-temperature curves suggest some unusual kind of magnetic alteration at a temperature characteristic of the individual compounds. Heat-capacity data for $DyCo_5$ reveals an accompanying specific-heat anomaly, which is of an unusual shape.

INTRODUCTION

Constitution diagrams have been established for a number of binary alloy systems in which one component is a lanthanide metal and the other is iron, cobalt, or nickel. In the course of this work, which was carried out mainly by German investigators (1), evidence was adduced which suggested the existence of intermediate phases—or intermetallic com-

*The authors would like to acknowledge the assistance provided by the Davison Chemical Division of the W. R. Grace Company in supporting the present work through a contract with the University of Pittsburgh. They also wish to express appreciation to Professor R. S. Craig, Dr. K. Nassau, and Mr. R. A. Butera for help in designing and constructing much of the equipment used in the present work, and to Dr. Nassau, Mr. S. Weinstein, and Mr. E. A. Skrabek for their generous assistance with some portions of the experimental work.

pounds—in a number of instances. The initial indications of compound formation were based on conventional thermal analysis, but confirmation was provided either at the time or later in many cases by means of X-ray diffraction techniques. (2–10)

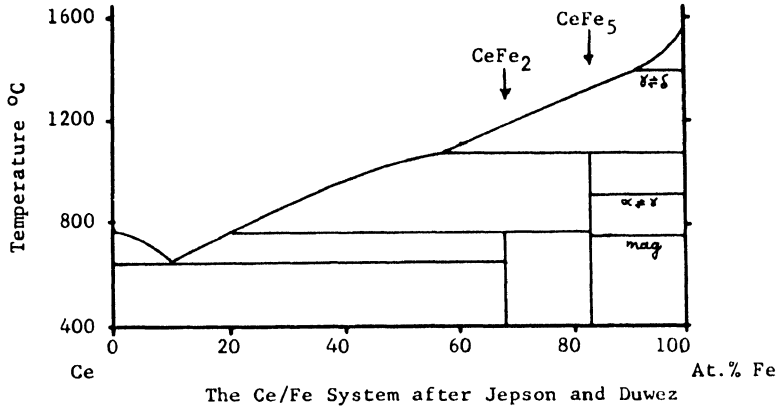
The diagrams for the Ce-Fe, Ce-Co, and Ce-Ni systems, sketched in Fig. 1, exemplify the kind of results which originally suggested the occurrence of compounds in these systems. As is indicated, the data imply the existence of compounds with stoichiometries represented by the formulas AB_2 and AB_5, in which A denotes a lanthanide element and B is Fe, Co, or Ni.* Crystal-structure studies showed that the AB_2 alloys were indeed compounds possessing the $MgCu_2$ structure (cubic Laves phase), and the AB_5 alloys were also compounds, existing in the $CaCu_5$ structure (Haucke phase).

The $MgCu_2$ structure occurs widely in binary metallic systems and has been extensively studied. It is generally agreed that this, and also the hexagonal Laves phases ($MgZn_2$ and $MgNi_2$), owe their stability to a favorable ratio of sizes of the component atoms, which permits very efficient packing. (11) Compounds which adopt one of the Laves-phase type structures are hence termed "size-stabilized" compounds. Haucke-phase compounds have not been extensively studied, and the factors responsible for their stability remain to be clarified. It seems likely, however, that they too are size-stabilized. If so, since the lanthanides do not differ greatly in size, it seemed when studies of these compounds were begun in this laboratory some months ago that it should be possible to replace Ce with other lanthanides in the AB_2 and AB_5 compounds. Furthermore, for the same reason it appeared that one ought to be able to use other metals in the First Long Period as the B component. The chances seemed fairly good that all the AB_2 compounds would be isomorphous, and that the AB_5 compounds would comprise another isomorphous group. If so, since there are a dozen or more possible A's and at least five possible B's (Mn, Fe, Co, Ni, and Cu), an extensive series of isomorphous substances would be available, which would be of considerable interest for systematic study.

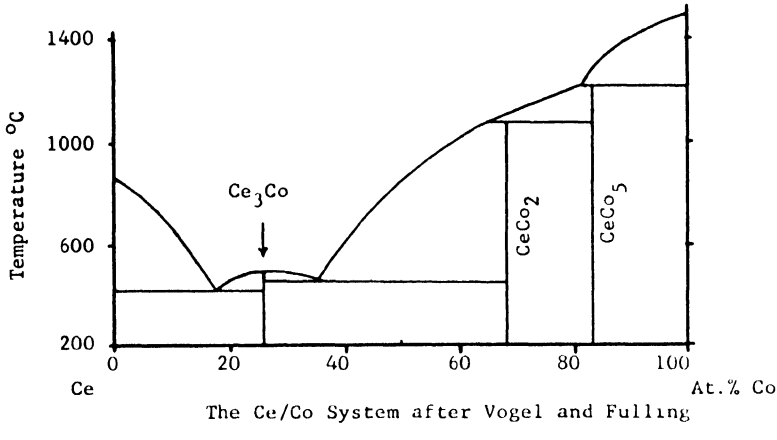
In the last two years considerable work has been carried out in this laboratory and elsewhere for the purpose (in part) of ascertaining whether the above-mentioned expectations are realized in practice. Presentation of the results of these studies forms a portion of the present paper. In addition, the magnetic properties of the AB_2 and AB_5 alloys are being intensively studied to see what, if any, new phenomena develop when the lanthanides are brought into chemical union with the common ferromagnetic

---

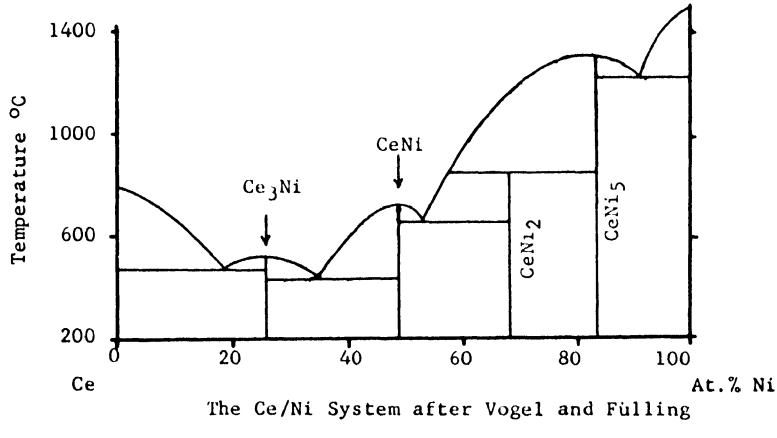
*A_3B and AB compounds are also suggested from the diagram for the Ce-Ni system. Alloys with these formulas have received comparatively little attention to date, and will not be discussed further.



The Ce/Fe System after Jepson and Duwez



The Ce/Co System after Vogel and Fulling



The Ce/Ni System after Vogel and Fülling

Fig. 1. Phase relationships in the cerium-iron, cerium-cobalt, and cerium-nickel systems.

elements and their neighbors in the periodic table. It is of interest to determine whether there will be two essentially independent systems of atomic moments, or whether significant interactions will occur. If the latter, the question arises—how strong are the interactions and what kinds of couplings occur? It has seemed that studies designed to answer these questions will in time lead to improved understanding of the interactions involving *f*-electrons in the metallic state. Presentation of the magnetic results forms the second part of the present paper. The third part, and the least complete by far, has to do with the thermal properties of the substances in question. This work—heat-capacity determinations over an extended range of temperature—was undertaken in part because such measurements are of interest in themselves, but mainly to facilitate interpretation of the results of the magnetic studies.

EXPERIMENTAL RESULTS

The samples investigated were prepared by melting the components together and allowing the melt to solidify. To avoid the possibility of contamination by the crucible, the technique of "levitation melting" was employed. This is a procedure in which, by use of a suitably shaped induction coil, the sample is suspended, or levitated, electromagnetically. While molten, it is in contact only with argon, except for the brief instant when it is cast into a massive copper mold.

CONSTITUTION ANALYSIS AND STRUCTURE DETERMINATION

The general features of the results which have emerged from the work on these compounds are given in Table I. It can be seen that isomorphism is, as anticipated, quite extensive. However, it does not extend throughout the whole body of compounds investigated. For example, the $A\mathrm{Mn}_5$ compounds possess a different structure than their Fe, Co, or Ni analogs. Attempts in this laboratory to prepare the $A\mathrm{Cr}_5$ and $A\mathrm{Cr}_2$ compounds have been uniformly unsuccessful. This together with the results shown in Table I for the Mn alloys indicates that the compounds tend to become unstable when the *B* component is below iron* in the periodic table. The limit of stability occurs at about Ce for the *A* component, probably because of the increase of size of the lanthanides with decreasing atomic number.

It is to be noted that most of the compounds occur in either the MgCu_2 or CaCu_5 structure. Hence a remark or two about these structures seems in order. The former is cubic, with twenty-four atoms per unit cell. The

*The upper limit for *B* lies above Ni, since $A\mathrm{Cu}_5$ compounds have been found with *A* = Y, Nd, Sm, Gd, and Tb (Ref. 9, and unpublished measurements by S. E. Haszko).

TABLE I: RESULTS OF CONSTITUTION ANALYSIS AND STRUCTURE DETERMINATION

	AB_2 Alloys															
	Y	*La*	*Ce*	*Pr*	*Nd*	*Pm*	*Sm*	*Eu*	*Gd*	*Td*	*Dy*	*Ho*	*Er*	*Tm*	*Yb*	*Lu*
Manganese	A*	N	N		?				A*	A*	A*	A*				
Iron	A*	N	A*	?	?		A*		A*		A*	A*	A*			
Cobalt	A*	?	A*	A*	A*		A*	?	A*	A*	A*	A*	A*			
Nickel	A*	A,N*	A*	A*	A*		A*	?	A*	A*	A*	A*	A*			
	AB_5 Alloys															
	Y	*La*	*Ce*	*Pr*	*Nd*	*Pm*	*Sm*	*Eu*	*Gd*	*Td*	*Dy*	*Ho*	*Er*	*Tm*	*Yb*	*Lu*
Manganese	C*	N	N	N	?		C*		C*	C*	C*	C*	C*			
Iron	B*	N	B*				B*		B*		B*	B*				
Cobalt	B*	?	B*	B*	B*		B*		B*	B*	B*	B*	B*			?
Nickel	B*	B*	B*	B*	B*		B*		B*	B*	B*	B*	B*		B	B*

A—$MgCu_2$ structure; *B*—$CaCu_5$ structure; *C*—incompletely solved orthorhombic structure.

Blank—Not investigated.

N—No compound; diffraction pattern indicates mixture of components.

?—Diffraction pattern not interpreted as yet.

A,N (for $LaNi_2$)—Contradictory results from independent studies.

*—Samples which have been studied magnetically.

Source: Studies of Wernick and Geller (Ref. 8 and 9) and Nassau, Cherry and Wallace (Ref. 10).

A's are arranged on a diamond lattice; the *B*'s are packed in to fill the intervening space. The $CaCu_5$ is hexagonal, with six atoms per unit cell. (The *C* structure is orthorhombic, also with six atoms per cell, and may be a distorted version of the $CaCu_5$ structure.)

The lattice parameters range from 7.12 to 7.73 A for the AB_2 compounds. For the AB_5 compounds the ranges are *a*; 4.83 to 5.00 A and *c*; 3.93 to 4.10 A. Above Sm the trend of interatomic distances is consistent with the lanthanide contraction. Distances are anomalously small for the lower lanthanides, however, suggesting that in these the lanthanides are probably ionized beyond the tripositive state (for further details, see Ref. 8, 9, and 10).

MAGNETIC BEHAVIOR

The objectives of this phase of the work were threefold: (1) to determine whether or not the moments of the components are sufficiently strongly coupled to produce spontaneous alignment, (2) to assess the strength of the coupling, and (3) to ascertain if possible the nature of the coupling—whether ferromagnetic, ferrimagnetic, or angular. Toward these ends some examination has been made of the magnetic behavior of all the sixty-nine compounds which have been marked with an asterisk in

Table I. It has been found that nineteen are paramagnetic at room temperature. The rest exhibit spontaneous alignment of the moments at ordinary temperatures and hence are either ferromagnetic or (more likely) ferrimagnetic.

The only detailed study carried out in this laboratory that is even reasonably complete is that dealing with the ACo_5 series in which A is Y, Ce, Pr, Nd, Sm, Gd, Tb, Dy, Ho, and Er. A portion of this work is in press. (12) Two types of measurements were made: (1) determination of the saturation magnetization at room temperature and at the temperature of liquid nitrogen, and (2) determination of the moment as a function of temperature at constant field strength. The latter is usually termed thermomagnetic analysis (TMA).

Since the lanthanides are chemically similar, one would have expected similar behavior for all the ten ACo_5 compounds. Instead one finds on the basis of the TMA results that the compounds divide into three classes—the YCo_5, the $NdCo_5$ and the $GdCo_5$. Data for YCo_5 are shown in Fig. 2. The results for $CeCo_5$ and the $SmCo_5$ are in general similar, and on this basis these three compounds are grouped together as the YCo_5 class. Results of TMA here indicate either a normal ferromagnetic or a

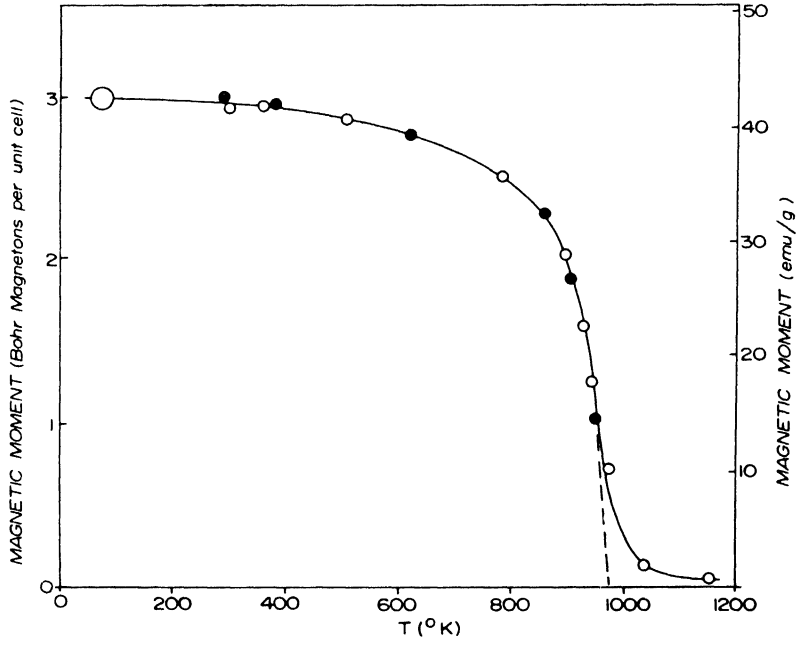


Fig. 2. Magnetic moment of YCo_5 *vs.* temperature at 1910 Oe. Results obtained on heating are indicated by ○, on cooling by ●.

ferrimagnetic material similar to a type-Q ferrite, according to the classification of Néel. (13)

Thermomagnetic-analysis results for $GdCo_5$ are shown in Fig. 3. $HoCo_5$ and $ErCo_5$ exhibit similar behavior and comprise the other two members of this class. The principal difference between the $GdCo_5$ and YCo_5 classes is the reduction in moment with decreasing temperature at low temperatures. This behavior has been shown both by theoretical (13) and experimental (14) work to be characteristic of some types of ferrimagnetic materials (Néel type-P ferrites).

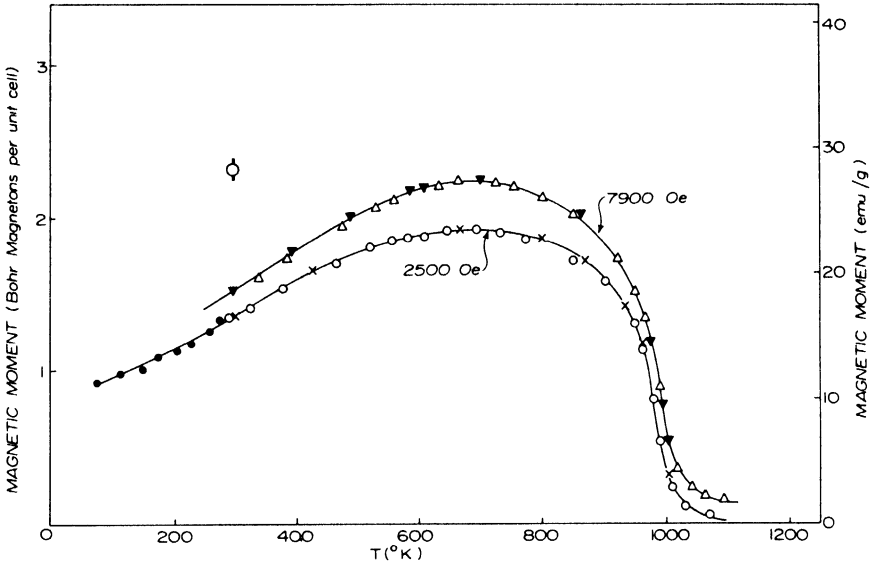


Fig. 3. Magnetic moment of $GdCo_5$ *vs.* temperature. Results obtained with rising temperature: ● indicates 2310 Oe.; O, 2500 Oe.; △, 7900 Oe. Results obtained with falling temperature: x indicates 2500 Oe.; ▲, 7900 Oe. Saturation moment is indicated by ϕ.

Data for all but $DyCo_5$ of the $NdCo_5$ class are shown in Fig. 4, 5 and 6. These curves are unlike any that have been observed before or are expected from theory. (13) The TMA curves for these compounds, it will be noted, are characterized not only by reduced moments at low temperatures but also by a peak in the curve.* Results for $DyCo_5$ closely resemble those for $TbCo_5$, except that the peak occurs about 50 °C lower for the former compound.

*Data for $PrCo_5$ shows only a portion of what may be a peak. It is believed that when measurements are extended to lower temperatures a curve like that for $NdCo_5$ will result.

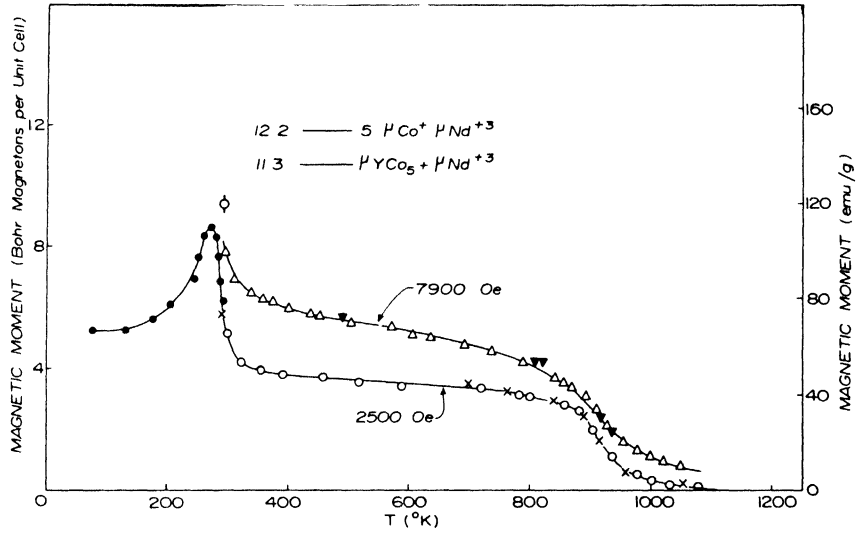


Fig. 4. Magnetic moment of $NdCo_5$ *vs.* temperature. Results obtained with rising temperature: ● indicates 2310 Oe.; ○, 2500 Oe.; and △, 7900 Oe. Results obtained with falling temperature: x indicates 2500 Oe.; ▲, 7900 Oe. ϕ indicates saturation moment

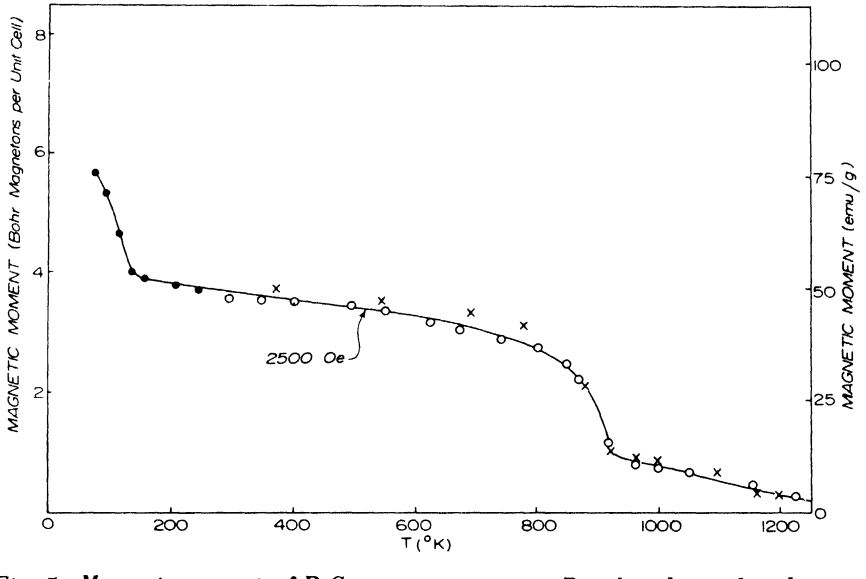


Fig. 5. Magnetic moment of $PrCo_5$ *vs.* temperature. Results obtained with rising temperature: ● indicates 2310 Oe.; ○, 2500 Oe. Results obtained with falling temperature: x indicates 2500 Oe.

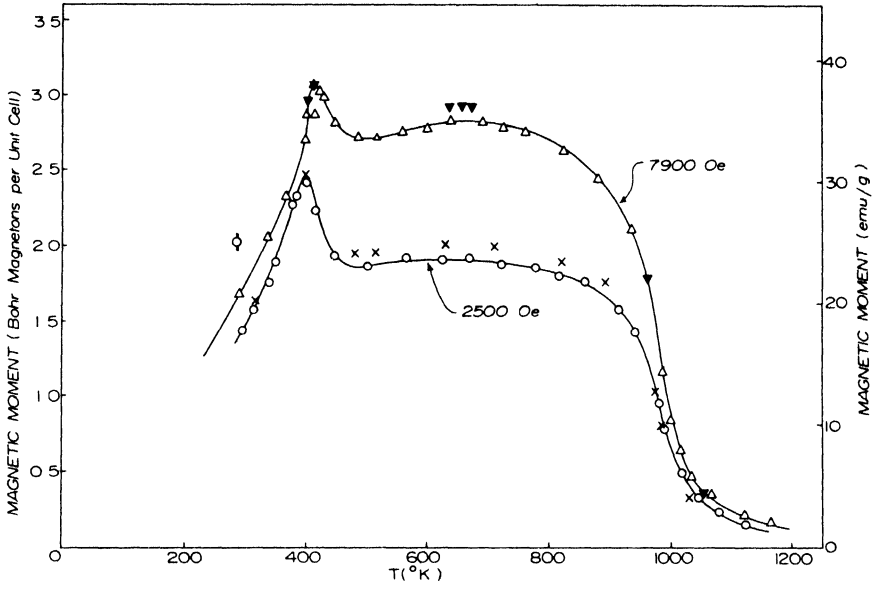


Fig. 6. Magnetic moment of $TbCo_5$ *vs.* temperature. Results obtained with rising temperature: o indicates 2500 Oe.; △, 7900 Oe. Results obtained with falling temperature: x indicates 2500 Oe.; ▼, 7900 Oe. ϕ indicates saturation moment.

The saturation magnetizations which have been obtained to date are given in Table II together with the moments expected if the cobalt moments are all ferromagnetically coupled and the resultant moment is first coupled ferromagnetically and then antiferromagnetically with that of the lanthanide.* The moments assumed are for Co $1.72\mu_B$, the value for elemental cobalt, and for the lanthanide, the value calculated for the tripositive gas ion, except, as noted, for Y. These data seem to indicate, as has been pointed out previously (12), that the coupling is antiferromagnetic in character at low temperatures in all cases except for $NdCo_5$ and $PrCo_5$. In these two compounds the lanthanide moments appear to be coupled ferromagnetically.

In all, the results for the YCo_5 and $GdCo_5$ classes are more or less in keeping with expectation. The TMA curves for the latter materials are somewhat out of the ordinary; however, similar curves have been obtained for some types of ferrites, and hence the behavior observed is not unique. The Curie points for both of these classes are high, indicating reasonably strong coupling of the moments. The saturation moments indicate, as

*There are other types of antiferromagnetic coupling which merit consideration. These have been discussed in (12).

TABLE II: CURIE TEMPERATURES AND SATURATION MOMENT FOR ACo_5 COMPOUNDS

A	Curie Temp. (°C)	Saturation Moment in Bohr Magnetons per Unit Cell*			
		Experimental		Computed†	
		25°C	*78°K*	*Ferromagnetic Coupling*	*Antiferromagnetic Coupling*
Y	700	7.6	7.6	9.3	7.9
Ce	410	5.1	5.2	10.7	6.5
Pr	635	9.1	10.0	11.8	5.4
Nd	650	9.5	9.7	11.9	5.3
Sm	740	7.5	8.0	10.0	7.2
Gd	700	2.8	2.0	15.6	1.6
Tb	710	2.0	0.5	17.6	0.4
Dy	850	3.5	1.1	18.5	1.3
Ho	750	3.9	1.3	18.6	1.4
Er	900	4.3	0.2	17.6	0.4

*The unit cell contains 1*A* and 5 Co's.

†The cobalt moments (taken as 1.72 μ_B per atom) are assumed to couple always ferromagnetically and the resultant is coupled either ferromagnetically or antiferromagnetically with that of the *A*-component. The moment of *A* is taken to be that of the tripositive gaseous ion with a fixed axis, except in the case of Y, where the experimental value of 0.7 μ_B is used. (15)

pointed out above, that the lanthanide moments are coupled antiferromagnetically to the moments of the cobalts, all of which are aligned ferromagnetically. Such deviations as there are between computed and observed results can readily be attributed to the likelihood that the properties of the lanthanide ion in these compounds differ somewhat from those of the free gaseous ion.

It should be noted that Nesbitt, Wernick, and Corenzwit recently reached (15) a similar conclusion concerning the coupling in one of the ACo_5 compounds, $GdCo_5$. They determined moments for this material and for $GdFe_5$ at field strengths up to 9800 oersteds. Even though this field strength was insufficient to saturate these materials, their measurements give some indication of the saturation moments. They observed that their measured moments were far less than the values expected if all the moments present were coupled ferromagnetically. They also noted the rise in moment with increasing temperature at low temperature in the case of $GdCo_5$, which, together with the observed magnitude of its moment, led them to conclude that this substance is not ferromagnetic, but ferrimagnetic.

Results obtained in this laboratory for the $NdCo_5$ class are more interesting and very much more puzzling. Some kind of change—which is rather striking in nature—clearly occurs in the temperature range around the peak in the TMA curves. At this time it is not at all clear what the

change is. One possibility is that there is merely a change from one type of magnetic alignment to another, analogous to the change from antiferromagnetic to ferromagnetic coupling in elemental dysprosium. This may be the case—or something subtler may be involved, such as an alteration in the number of 4*f*-electrons, or a rearrangement of these brought on by crystal field splitting of the *f*-states. Either of these could result in an alteration of moment of the lanthanide and might produce the observed effects. These effects for the present, therefore, remain to be clarified. It appears unlikely that this can be done, however, without supplemental information—for example, neutron-diffraction data.

Very recent measurements in this laboratory indicate that the TMA curve passes through a minimum for four of the ACo_5 compounds studied—$GdCo_5$, $TbCo_5$, $DyCo_5$, and $HoCo_5$. The minima occur at temperatures of 120 °K or below and could, at least in some instances, be due to compensation of magnetic moments. (13) However, definite conclusions concerning this point must await measurements below 60 to 80 °K, which are currently under way in this laboratory.

THERMAL PROPERTIES

The only compound which has been investigated to date is $DyCo_5$. Very recently precision heat-capacity measurements have been completed on it covering the temperature range extending from 10 to 51.5 °K. This work was undertaken in part to establish its third law entropy, but mainly to ascertain whether there is a thermal anomaly in the region of the peak in the TMA curves. The results do show (16) a pronounced, and decidedly unusual, thermal anomaly. The excess heat capacity does not show the sharp spike usually found for second order transitions. Rather, over about a 40-deg interval, the data show what might be described as a "bulge" superimposed on the normal curve. At its maximum the excess heat capacity is about 5 per cent of the total (which is about 50 times the scatter of the data and hence unquestionably real). The "bulge" is nearly symmetrical about its midpoint. It is not clear at this time what could produce such an unusual thermal anomaly. Its unusual character implies that the magnetic transformation which gives rise to it may be equally unusual.

REFERENCES

1. For detailed references consult M. Hansen and K. Anderko, *Constitution of Binary Alloys.* New York: McGraw-Hill Book Co., Inc., 1958. Or K. Gschneidner, Jr., *A Critical Review of the Alloy Systems of the Rare Earth, Scandium, and Yttrium Metals.* To be published.
2. R. Vogel and W. Fülling, *Z. Metallk.*, 38, 47 (1947).

3. W. Fülling *et al.*, *ibid.*, 34, 253 (1942).
4. H. Nowotny, *ibid.*, 34, 247 (1942).
5. F. Endter and W. Klemm, *Z. Anorg. Chem.*, 252, 64 (1943).
6. J. O. Jepson and P. Duwez, *Trans. Am. Soc. Metals*, 47, 543 (1955).
7. T. Heumann, *Nachr. Wiss. Göttingen*, 1, 21 (1948).
8. J. H. Wernick and S. Geller, *Acta Cryst.*, 12, 662 (1959).
9. J. H. Wernick and S. Geller, *Trans. AIMME*. In press.
10. K. Nassau, L. V. Cherry, and W. E. Wallace, I, *J. Phys. and Chem. Solids*. In press.
11. G. V. Raynor, *Progr. in Metal Phys.*, 1, 1 (1949).
12. K. Nassau, L. V. Cherry, and W. E. Wallace, II, *J. Phys. and Chem. Solids*. In press.
13. L. Néel, *Ann. Phys.*, 3, 137 (1948).
14. E. W. Gorter, *Philip Res. Rep.*, 9, 403 (1954).
15. E. A. Nesbitt, J. H. Wernick, and E. Corenzwit, *J. App. Phys.*, 30, 365 (1959).
16. W. G. Saba and W. E. Wallace. Unpublished measurements.

OBSERVATIONS ON SOME GADOLINIUM-SELENIUM COMPOUNDS*

R. C. VICKERY AND H. M. MUIR

Research Chemicals, Division of Nuclear Corporation of America, Burbank, California

Studies in progress in these laboratories on the properties of some gadolinium intermetallic compounds have necessitated delineation of their phase parameters and magnetic and electrical properties. Presented here are preliminary data, resulting from this work, on that portion of the gadolinium-selenium system between 50 and 70 atomic per cent selenium, that is, corresponding to the region of GdSe, Gd_2Se_3 and $GdSe_2$ intermetallic compound formation.

EXPERIMENTAL

The compositions reported here have been synthesized by a two-stage technique. An initial vapor-phase reaction is effected between appropriate amounts of gadolinium and selenium. Gadolinium metal (99.8 per cent purity) is introduced in the form of chips into a Vycor tube; a constriction is then drawn by melting the tube above the metal chips. After cooling, selenium metal (99.99 per cent grade) pellets are introduced above the constriction. Direct solid contact of the reactants is thus prevented. After evacuating the system under argon to 10^{-4} mm of mercury, the open end of the tube is sealed off, and the whole is inserted into a two-zone-tube combustion furnace. The furnace zone adjacent to that part of the ampoule containing gadolinium is heated to 900 °C at approximately 300 °C per hour. After establishing equilibrium, the temperature of the second zone (adjacent to the selenium charge) is raised to 450 °C at approximately 100 °C per hour. Temperatures of the two zones are maintained at these levels for eight hours, when the system is allowed to cool at a rate approximating 200 °C per hour. Direct reaction between gadolinium metal and selenium normally becomes explosively exothermic at *ca.* 500 °C; by using the two-zone heating tech-

*This report is contribution RC 154 from the laboratories of Research Chemicals, Division of Nuclear Corporation of America. This work was supported in part by the Bureau of Ships, U.S. Navy, under Contract NObs 77145.

nique indicated, however, sufficient selenium appears to be absorbed by the gadolinium before this point is reached, and the reaction then becomes controllable.

From this reaction, the compositions are obtained as powders. These are consolidated by pressing into pellets, which are then either sintered in a vacuum induction furnace at 1650–1700 °C, or arc-melted under argon with a nonconsumable tungsten electrode against a water-cooled copper hearth.

Using −200 mesh powders of the materials prepared, X-ray diffractograms have been obtained through a General Electric XRD-5 diffractometer employing nickel-filtered copper $K\alpha$-radiation. All materials prepared were friable and annealing, after comminution for relief of stresses was found to be unnecessary.

In later work, single crystals of the Gd_2Se_3 compound were obtained, and their structure determined, by Laue, Weissenberg, and rotation X-ray photographs.

Electrical-resistivity values have been obtained on all materials prepared by the four-probe technique (1) and accuracy of ±5 per cent is felt to be obtained.

For measurements at elevated temperatures, an argon-purged, noninductive Kanthal wire heater has been used as the heat source, controlled to ±1 °C over the entire heating range through a Wheelco unit.

Magnetic susceptibilities have been determined using equipment previously described (2) in which a transducer measures the force exerted on the sample by a known magnetic field.

Standard techniques have been used for chemical analysis (3), and materials prepared have also been examined metallographically. Direct observations have also been made of such properties as melting point, chemical stability, and so forth.

DATA OBTAINED

STRUCTURAL

GdSe: Within the range of compositions studied, this compound is that of lowest selenium content and appears to melt at 2160 °C with no black-body correction. Metallographic observations on an arc-melted material containing 67.6 per cent gadolinium and 32.3 per cent selenium, showed it to be essentially monophase. The compound was brassy in color, and powder X-ray diffractometry showed it to be isomorphous with the other rare earth monoselenides examined by Klemm and Koczy (4), the probable structure being:

$B1$ (NaCl) type structure

Cubic: $O_h^5 - Fm3m$

a_o = 5.758A; X-ray density = 8.2 g/cm^3

Unit Volume = 190.0A^3; Z = 4

Each selenium atom is surrounded by six gadolinium atoms at the vertices of a regular octahedron and at a distance of $a_o/2$ = 2.879 A. Each gadolinium atom is also surrounded by six selenium atoms, but no contact exists between the gadolinium atoms. It is to be noted that Cd–Se distance is somewhat less than the sum of the C.N. 6 radii of the atoms.

Gd_2Se_3: All preparations containing more than 50 per cent selenium, after the vapor-phase reaction, liberated selenium vapor upon subsequent heating, and resolved to the 2 : 3 composition at temperatures *ca.* 1000 °C. The crystal structure assigned to Gd_2Se_3 (below) did not appear in X-ray diffractograms of materials prepared below about 800 °C. When once the structure had been established, however, it persisted at low temperatures and showed no signs of disruption after several thermal cyclings. The compound melts conguently at 1750 ±25 °C.

Metallographic observations of arc-melted specimens containing 57.3 per cent gadolinium and 42.5 per cent selenium showed the material to be largely monophase, but with a trace of eutectic component. The amount of eutectic in similar specimens increased with slight increase in gadolinium content. As prepared in massive form the compound is black; some single crystals, grown by zone-refining techniques exhibited, however, a reddish tinge and black material—shown by metallography to contain approximately 15 per cent eutectic—and became red upon powdering. Powder X-ray diffractometry of the arc-melted material has been supplemented by single crystal investigations. Work in this area is continuing, but results thus far obtained present the following parameters:

$D7_3$ (Th_3P_4) type structure

bcc, T_6^d–$I\bar{4}3d$

a_o = 8.72 ± 0.005A; X-ray density = 7.36 g/cm^3

Volume = 664.2A^3

The unit cell contains $26\frac{2}{3}$ atoms, of which $10\frac{2}{3}$ gadolinium atoms randomly occupy the metal positions giving a disordered, or defect structure. An ordered system would contain 28 atoms per unit cell, i.e., 12 gadolinium and 16 selenium atoms, stoichiometrically equivalent to Gd_3Se_4. Existence of the 3 : 4 compound has indeed been claimed by Benacerraf *et al.* (5), but we have been unable to verify the data presented; relationships between Gd_2Se_3 and the prognosticated Gd_3Se_4 will be discussed later. At this point, it is sufficient to note that a

preparation, slightly on the gadolinium-rich side of Gd_2Se_3, heated at 1380 ±25°C for a short period, exuded a liquid material shown metallographically to be a eutectic and chemically to contain 61 per cent gadolinium. (The theoretical composition of Gd_3Se_4 contains 60 per cent gadolinium.)

$GdSe_2$: The least stable of the compounds found in the region examined, this decomposes above 300°C and gradually loses selenium. If maintained at a temperature of *ca.* 1000 C for a prolonged period, resolution to GdSe and selenium vapor is complete. If, on heating, the temperature is raised rapidly to *ca.* 1200°C, Gd_2Se_3 is formed with selenium vapor.

Although the data obtained are not conclusive, powder diffractograms of the compound prepared at low temperatures suggest it to have an orthorhombic structure with a_o, 7.27A; b_o, 4.03A; c_o, 8.30A. Isomorphism for this structure is believed to agree with that reported (6) for $ThSe_2$-*C*23-type (D_{2h}^{16}-*pnma*), and attempts are now being made to prepare this compound in single crystal form for closer examination.

ELECTRICAL

Resistivity values, obtained through the compositional sequence, are shown in Fig. 1, and can be seen to cover a wide range. As far as has been elicited, only the 2:3 compound possesses semiconductor characteristics (Fig. 2). This behavior is in keeping with the defect structure of this compound and partially confirms indications previously given of the semiconductive nature of rare earth chalcogenides. (7) It is to be expected that, in the defect structure established by Gd_2Se_3, extrinsic conductance will develop, and preliminary measurements of Hall effect show *n*-type conductivity for this compound, with mobilities similar to those previously reported. (7) The exceptionally high room-temperature resistivities of Gd_2Se_3 and low resistivities of the other compounds in this series indicate that only in the 2:3 compound does bonding become potentially ionic—in other compounds covalent attachment would seem to be the rule. However, because ρ values, even for Gd_2Se_3, do drop significantly at temperatures far below the melting point, we should consider that even in this compound a degree of covalent-bonding character occurs. Some confirmation of this can be evinced from the high stability of the compound and the contraction noted in its lattice.

MAGNETIC

Susceptibilities for the compositions studied are shown in Fig. 3. Table I compares theoretical and observed moments on a molecular basis, in terms of Bohr magnetons, for the compounds found.

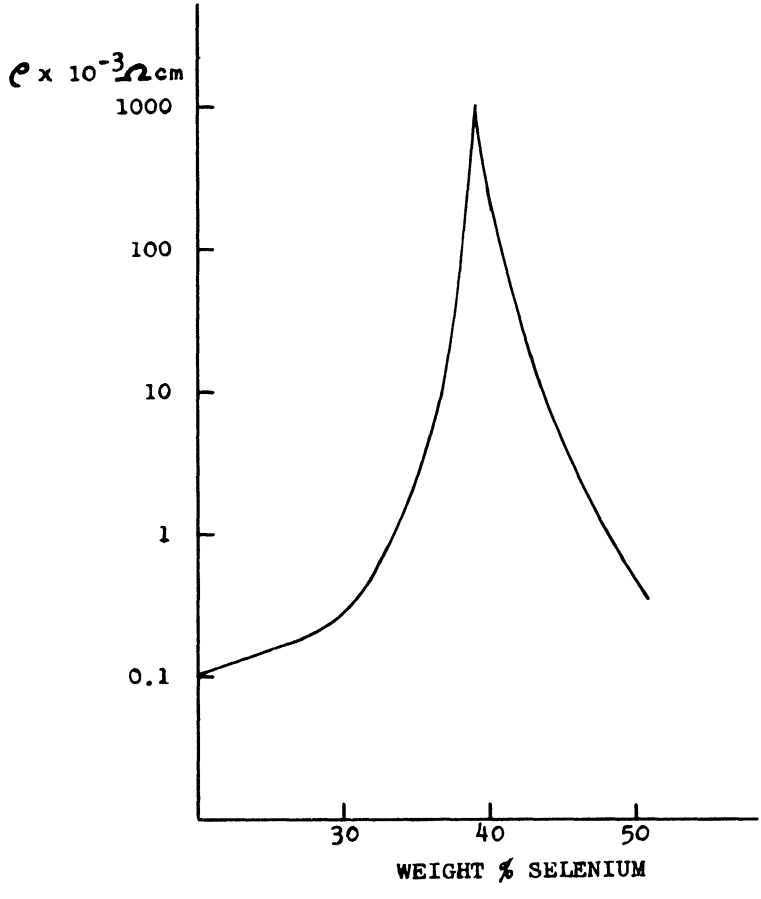


Fig. 1. ρ *vs.* composition gadolinium-selenium system.

In no instance has ferromagnetism been found to develop in this system, and magnetic data of the type obtained do not permit distinguishing between ionic and covalent compounds of gadolinium, because the metal does not adopt 2^+ or 4^+ states. Bonding therefore will not otherwise effect the $4f$-electron level, which is largely respon-

TABLE I: $\Delta\theta$ VALUES IN GADOLINIUM-SELENIUM COMPOUNDS

	μ		
Compound	Observed	Theory	$\Delta\theta^\circ$C
GdSe	4.0	3.6	32
Gd_2Se_3	2.78	2.88	26
$GdSe_2$	2.8	2.60	30

sible for its moment. It has frequently been shown in magnetic studies on the rare earth elements that the Weiss constant, θ, in $\chi = C/(T\theta)$, does not live up to its name; however, Selwood (8) has pointed out that the value of $\Delta\theta$ does bear a relationship to the distances between gadolinium atoms. $\Delta\theta$ values—also shown in Table I—suggest that the gadolinium-gadolinium interatomic distance in the gadolinium-selenium

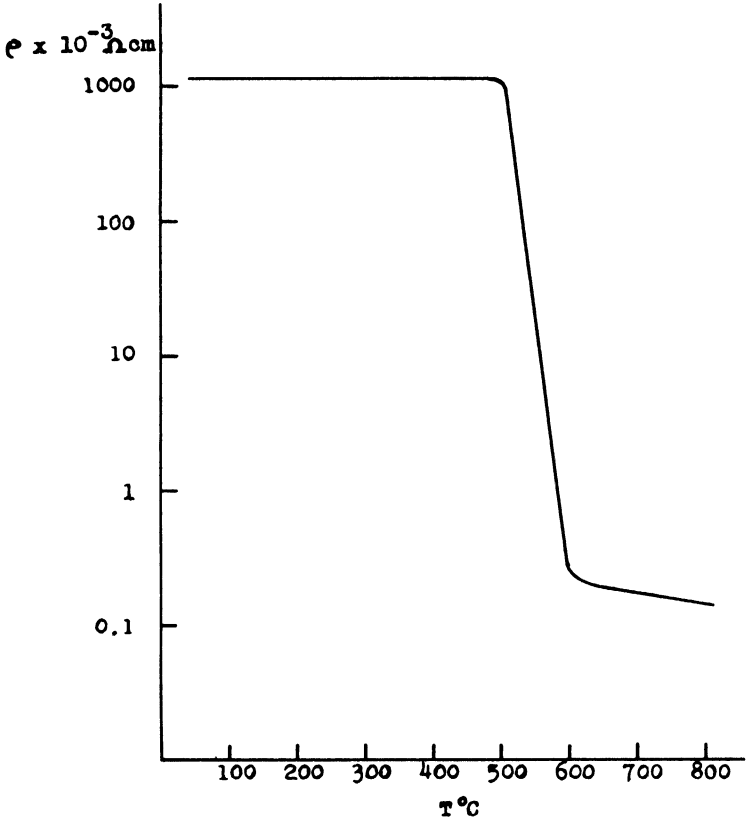


Fig. 2. ρ *vs.* T for Gd_2Se_3.

compounds is less than that in the oxide ($\theta = 12\,^{\circ}C$). It can be shown, moreover, that the differential increase in θ-values is greater than would be expected for the different atomic radii of selenium and oxygen. This can be construed as indicating closer approximation of gadolinium atoms (compare X-ray data), and hence, the development of covalent bonding, or, as Burstall and Nyholm (9) express it, utilization of "lower" covalent orbitals.

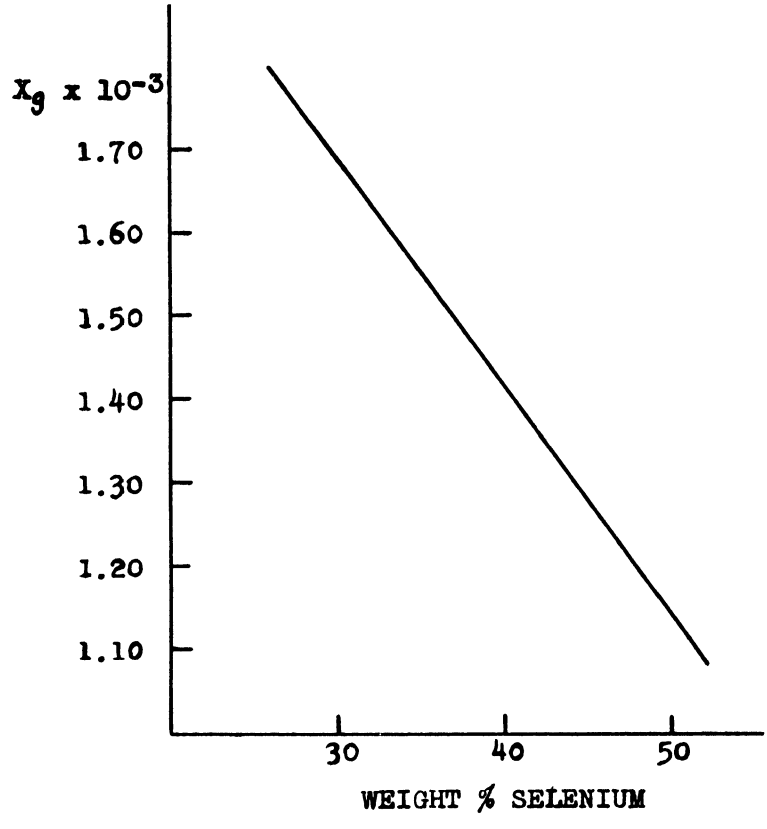


Fig. 3. Magnetic susceptibility of gadolinium-selenium compounds.

CHEMICAL CHARACTERISTICS

All compositions examined in this system are soluble in dilute hydrochloric acid with evolution of hydrogen selenide. All compounds except Gd_2Se_3 and closely approximating compositions hydrolyze in humid air; a similar degree of affinity is also found with carbon. Only the Gd_2Se_3 compound can be melted in graphite without carburization. This is a further distinction from the work of Benacerraf *et al.* (5), who claim carburization at temperatures below 1700 °C.

DISCUSSION

Sufficient information is not yet considered available to warrant the construction of even a partial phase diagram for this system, but our observations would seem to permit the following rationalizations.

Our data on gadolinium monoselenide appear to agree with those given in the referenced work. Low-temperature addition of selenium to the GdSe compound produces only mildly progressive structural changes, until a composition equivalent to Gd_3Se_4 is reached, when the orthorhombic structure of $GdSe_2$ becomes apparent in powder X-ray diffraction patterns.

The proximity of this lattice-change point to the Gd_3Se_4 composition may account for previous assumptions of the existence of such a compound having a *maille lacunaire* structure. (5) The presence of a high temperature eutectic at 61 weight per cent gadolinium is considered further evidence against the existence of a 3:4 compound in this system.

Since the 2:3 compound has a defect structure, it is felt that the ordered 3:4 compound claimed by Benacerraf *et al.* (5) may represent a 2:3 compound in which available lattice sites are occupied by oxygen atoms derived through their mode of preparation (Gd_2O_3 + Se). Such vacancy-fulfillment would not affect magnetic properties—for which the French work and ours are in good agreement. Comparison of observed and X-ray determined densities would permit distinction of species, but the data reported by Benacerraf *et al.* are somewhat ambiguous in this respect. The existence of three temperature-dependent crystal modifications of Gd_2Se_3 has also been suggested. In one instance only, in these laboratories, differential thermal analysis of Gd_2Se_3 has shown an endothermic transition at 1070 °C.

In general, recent studies on rare earth–selenium compounds have been interpreted from the standpoint of ionic stoichiometry. (5–10) However, the semiconductor nature of gadolinium sesquiselenide reported here and contemporary studies, together with the rather small gadolinium-selenium distances noted, would seem to suggest that the selenides are not wholly ionic entities, but are probably intermetallic in nature, possessing partially covalent bond characteristics. It has indeed been found possible on the basis of such a hypothesis to establish a rationale of electronic properties resulting from lattice interpenetration of such covalent-ionic-covalent structures. This thesis will shortly be presented elsewhere.

It is possible, in the present context, to suggest that covalency in the compounds now studied might involve hybridization of Gd 5*d*- and 6*s*- and Se 4*p*-electron levels. Magnetic-resonance studies may confirm this. Again, the resistivity of GdSe finds a counterpart in that of ErSe (7) which has been interpreted by Iandelli (11) as indicating the presence of only one conduction electron in compounds of this form.

Summarizing data specifically, it is felt that the definitive phenomena exhibited by the compounds GdSe, Gd_2Se_3 and $GdSe_2$ may be interpreted,

with Welker (12), in terms of ionic covalent resonance in the gadolinium-selenium bond.

Acknowledgments are made of the assistance of E. Avis and W. C. Sexton in making electrical and magnetic measurements on the materials prepared, and of S. Samson and V. Novy for assistance in interpretation of X-ray data.

REFERENCES

1. L. B. Valdes, *Proc. IRE.*, 42, 420 (1954).
2. R. C. Vickery and W. C. Sexton, *Rev. Sci. Instr.*, 31, 647 (1960).
3. R. C. Vickery, *Analytical Chemistry of the Rare Earths*. New York: Pergamon Press, 1960.
4. W. Klemm and A. Koczy, *Z. anorg. Chem.*, 233, 84 (1937).
5. A. Benacerraf *et al.*, *Compt. rend.*, 248, 1672, 2012, (1959).
6. R. W. M. D'eye *et al.*, *J. Chem. Soc.* (London), 1952, 2555; 1953, 1670.
7. J. F. Miller *et al.*, *J. Electrochem. Soc.*, 106, 1043 (1959).
8. P. W. Selwood, *J. Am. Chem. Soc.*, 55, 3161, 4869 (1933).
9. F. H. Burstall, and R. S. Nyholm, *J. Chem. Soc.* (London), 1952, 3570.
10. A. A. Menkov *et al.*, *Doklady Akad. Nauk. SSSR*, 128, 92, (1959).
11. A. Iandelli, *Gazzeta Chem.*, 85, 881 (1955).
12. G. Welker, *Physica*, 20, 893 (1954).

RARE EARTH INTERMETALLIC COMPOUNDS WITH ELEMENTS OF GROUPS V AND VI*

J. F. MILLER AND R. C. HIMES

Battelle Memorial Institute,
Columbus, Ohio

In the past, rare earth intermetallic compounds have received relatively little attention. Earlier publications relating to these compounds deal almost exclusively with elucidation of crystal structure (1-10) and describe studies which were made of the materials in powder form.

Recent and current work at Battelle has been concerned with preparation of bulk specimens of some of the rare-earth intermetallic compounds, and with study of their bulk physical properties. Primary interest lies in the study of electrical properties.

The potential value of III-V compound semiconductors (made from elements in groups IIIB and VB of the periodic table) and of semiconducting selenides and tellurides (containing common metallic elements) has long been widely recognized. Recent research at Battelle (11) indicates that analogous rare earth compounds (IIIA-VB, selenides, tellurides) are also semiconductors.

The development of rare earth semiconductors to a useful state would greatly increase the catalogue of semiconductors which electronic technology has at its disposal. Consider that in a single class of compounds, for example, the sesquitellurides, there are sixteen possibilities.† Further, it is hypothesized that the gradation in chemical properties and atom sizes, from element to element in the rare earth series, should lead to a similar gradation in electrical properties within a given class of compounds. This hypothesis has been borne out by experimental results obtained to date. Thus, rather broad ranges of semiconducting properties may be covered in many small steps, making these rare earth compounds an especially valuable group for both theoretical study and practical application.

---

*This paper is based on results of investigations supported by Wright Air Development Division, Wright-Patterson Air Force Base, and by the Rare Earth Research Group.

†Inclusion of yttrium, which is geologically, chemically, and physically closely related to the lanthanons, is considered appropriate.

In this paper, results of exploratory work with some rare earth compounds containing elements of chemical groups V and VI, specifically antimony, bismuth, selenium, and tellurium, are discussed. Work is continuing in all areas.

PREPARATION

VAPOR-SOLID REACTION

In the most successful method developed to date for the preparation of bulk specimens, the compound is first prepared in powder or granular form. The granular material is then melted down and cast into an ingot, from which bulk specimens suitable for evaluation can be obtained.

The compounds are prepared in granular form by reacting vapor of the group V or group VI element with filings of the rare earth metal at moderate temperatures. Some contaminants are probably introduced in producing the filings. However, the increased reaction rate obtained thereby is believed to outweigh the contamination effects, at least in an exploratory program.

The vapor-solid reactions are carried out in sealed, evacuated Vycor tubes, which are designed so as to maintain physical separation of the rare earth metal and the group V or VI element in the condensed state. Maintaining this physical separation precludes the possibility of the rapid, violent reaction which tends to take place on direct contact of the condensed phases. For example, the reaction between dysprosium and selenium has been observed to reach explosive proportions at about 400 °C.

To carry out the desired reaction, vapor of the group V or VI metal is distilled over rare earth metal filings at temperatures in the range 450–950 °C. The reaction conditions are varied somewhat, depending on the specific reaction being carried out. In general, temperature is increased slowly to 450–950 °C in a period of 4–24 hours, and is held at the selected level for an additional 16–100 hours. Periodic inspection is made to follow progress of the reaction. The reaction is considered to be complete when (1) a condensate of the volatile constituent fails to form on the reaction-tube wall as it cools after being removed from the furnace, and (2) the product has a homogeneous appearance. Longer reaction times and higher temperatures are usually required for preparing the antimony and bismuth compounds. For example, the reaction between yttrium and bismuth required 140 hours at 800–900 °C, while that between dysprosium and selenium, to form the sesquiselenide, appeared to be complete in 6 hours at 400 °C.

The granular reaction product is then melted down, by use of induction heating, and cast into an ingot in a tantalum or graphite container under argon at 1 atm pressure. Although the compounds melt at relatively high

temperatures, in the simple melting process, times at temperature are short, and under these conditions, there is little evidence of reaction between the compounds and the tantalum containers. Graphite also appears to be satisfactory as a container material for this purpose.

In the course of the melting, some of the compounds show a tendency to decompose, and hence the final composition may deviate from the stoichiometric, synthetic composition. In the exploratory work, which is to be discussed, the final compositions were generally not determined. However, for the sake of simplicity, the materials are referred to as discrete compounds in the ensuing discussions, even though such designation may not ultimately prove to be technically exact. In general, decomposition is relatively heavy for the bismuthides and antimonides, and moderate to light for the sesquiselenides and sesquitellurides. To obtain stoichiometric samples of these compounds, the melting must be done in an atmosphere of the vapor of the volatile constituent. However, the monoselenides and monotellurides appear to melt with little or no decomposition.

VAPOR-LIQUID REACTION

A number of the selenides, tellurides, antimonides, and bismuthides have also been prepared by reacting vapor of the group V or VI metal with the molten rare earth metal. These reactions are carried out in evacuated, sealed quartz or Vycor tubes. Induction heating is used to melt the rare earth metal, which is placed in a tantalum or graphite boat within the sealed quartz envelope. The remainder of the quartz envelope is heated, usually with electric furnaces, so as to create and maintain a suitable concentration of vapor of the group V or VI metal.

The vapor-liquid reaction has been carried out in two different ways, both of which yield bulk specimens of the compounds. In both of the methods, an excess of the group V or VI metal is used, and vapor pressure of this component is controlled by controlling minimum temperature of the condensed excess. In the first, the ingot of rare earth metal is melted and maintained at a temperature just above its melting point. Minimum temperature of the quartz envelope is then gradually increased so as to increase concentration of the vapor of the group V or VI metal slowly. As concentration of the vapor is increased, the intermetallic compound crystallizes first in the cooler regions of the inductively heated melt and, under proper conditions, the solid-liquid interface progresses gradually toward the high-temperature regions. (12) In the second method, the ingot of rare earth metal is melted and maintained at a temperature just above the melting point of the intermetallic compound being synthesized. Pressure of the vapor of the group V or VI metal is then made equal to decomposition pressure of the compound (at its melting point) by

raising minimum temperature of the quartz envelope to a suitable value. Progressive crystallization of the compound is accomplished by withdrawing the (molten) ingot laterally from the induction coil.

In carrying out the vapor-liquid reactions, a container problem was encountered. Whereas tantalum apparently is a satisfactory container for simple melting of the compounds, the tantalum boats are severely attacked during prolonged periods of exposure to selenium, tellurium, or antimony vapor. Graphite containers, which are not noticeably attacked by group V or VI metal vapors or by the molten intermetallic compounds, are attacked by the molten rare earth metals. In current work on preparative methods, use of other container materials such as MgO and BN is being investigated, and other techniques are being sought which would eliminate or minimize contamination from container materials.

One such preparative technique, which has been used for the synthesis of Dy_2Se_3, can be outlined as follows:

$$Dy_2O_3 \xrightarrow[550\,^\circ C]{CCl_4\,(vap)} 2DyCl_3 \qquad (1)$$

$$2DyCl_3 + 2H_2Se \xrightarrow{800\,^\circ C} Dy_2Se_3 + 6HCl \qquad (2)$$

The preparation of the anhydrous chloride (step 1) has been described in a previous publication.(13) Dry H_2Se used in the second reaction was generated by heating a suspension of powdered amorphous selenium in high-boiling mineral oil. Treatment of the chloride with hydrogen selenide for 36 hours at 800° C yielded the Dy_2Se_3, mostly in the form of small acicular single crystals. In this, or other processes, it may be desirable to use high-purity rare earth chlorides. In another investigation at Battelle, it was shown that zone-refining could be used to purify the individual rare earth chlorides. For example, in recrystallization by zone-melting, significant segregation of $DyCl_3$ in $HoCl_3$ was observed. With a ten-pass program the concentration of $GdCl_3$ in YCl_3 was reduced from an initial value of 1 per cent to a value below the detection limit of 0.3 per cent.

MELTING POINTS

Reasonably accurate melting points have been determined for three compounds, Er_2Se_3, Gd_2Te_3, and Y_2Te_3 (Table I). In making the determinations, specimens were placed in a horizontal cylindrical cavity at a depth equal to twelve times the diameter of the cavity, so as to obtain near black-body conditions.(14) The specimens were of triangular cross section and were supported by contact of the edges with the wall of the cavity. Incipient melting at the edges produced readily detectable move-

TABLE I: MELTING POINT DATA FOR SOME RARE EARTH INTERMETALLIC COMPOUNDS

Compound	Melting Point, °C
Sm_2Se_3	est. > 1540
SmSe	est. > 2100
Er_2Se_3	1520*
ErSe	est.~ 1800
Y_2Se_3	est. > 1800
Yb_2Se_3	est. > 1665
YbSe	est. > 1940
Sm_2Te_3	est. > 1440, < 1550
Gd_2Te_3	1420*
Y_2Te_3	1525*
YbTe	est. 1720-1760
LaSb	1540†
ErSb	< 1900
YSb	est. > 1850, < 2200
GdAs	> 2270

*Temperature read by optical pyrometer—accuracy ± 25 °C.
†Vogel and Kloso (Ref. 16).

ment of the specimens. Temperatures were measured with an optical pyrometer, and are estimated to have an accuracy of ± 25 ° C.

Observations made in the course of the preparative work, that is, compaction of powders by melting, yielded estimates of melting points for a number of additional compounds. Melting was detected by (1) visual observation of the sample surface, and (2) by the acceleration in rate of temperature increase which resulted when the sample densified and became a better susceptor for the r-f radiation. Temperatures were again monitored with an optical pyrometer. These estimates—which are also presented in Table I—may be seriously in error. However, the data indicate that all of the compounds prepared possess high melting points, and that melting points of some of the more refractory compounds of this class may be well above 2000 ° C.

CRYSTAL STRUCTURES

Only a limited amount of study of crystal structures of the rare earth intermetallic compounds has been done to date at Battelle. X-ray diffraction patterns for specimens from the "crude" polycrystalline ingots are consistent with the structure data given in Table II. It is anticipated that more thorough study of crystal structure will be made to aid in analysis of transport processes in these compounds.

ELECTRICAL PROPERTIES

Electrical properties observed at room temperature for some of the compounds in their initial preparations as polycrystalline, cast ingots

TABLE II: DATA ON CRYSTAL STRUCTURES OF SOME RARE EARTH INTERMETALLIC COMPOUNDS

Compound	Structure	Lattice Parameters		
		a, A	*b*, A	*c*, A
Dy_2Se_3*	Orthorhombic or pseudotetragonal	3.69	10.85	11.0
Gd_2Te_3†				
La_2Se_3	*bcc*, isomorphous with Ce_2Se_3	9.05		
La_2Te_3	"	9.62		
ErSb	*fcc*	6.07		

*Single crystal specimen.

†Two structures have been observed—one tetragonal, and the other a structure of lower symmetry which has not been satisfactorily indexed.

are given in Table III. It will be noted that the resistivities for the selenides and tellurides generally fall in the semiconducting range. Variations of Hall coefficient, resistivity, and charge-carrier mobility with temperature for Gd_2Te_3 specimens, which have been investigated (11), show behavior typical of an impure semiconductor. Similar studies, now in progress, on the other compounds show very sharp temperature dependencies of resistivity and point up the fact that the room-temperature values given in Table III, while useful for comparison among the com-

TABLE III: OBSERVED ELECTRICAL PROPERTIES (MEASURED AT ROOM TEMPERATURE) OF SOME RARE EARTH INTERMETALLICS

Synthetic Composition	Hall Coefficient, R_H, $cm^3\ coul^{-1}$	Resistivity, ρ, ohm-cm	Mobility, μ, $cm^2\ v^{-1}\ sec^{-1}$	Seebeck Coefficient, S, $\mu v\ °K^{-1}$	Carrier Concentration n, cm^{-3}
La_2Se_3	Negative	0.024	...	...	$\sim 3 \times 10^{19}$
Er_2Se_3	Positive	7.9	...	...	...
ErSe	Negative	1.7×10^{-4}	...	...	$\sim 10^{20}$
Y_2Se_3			(Insulator)		
La_2Te_3	Negative	1.9×10^{-4}	...	−30	$\sim 10^{20}$
Sm_2Te_3	Negative	0.85	...	...	...
Gd_2Te_3	−3.25	0.019	170	−26	2×10^{18}
Gd_2Te_3	+3.3	0.2	17	>+200	2×10^{18}
Er_2Te_3	Negative	1.1×10^{-3}	...	...	$\sim 10^{19}$
YbTe	...	340	...	...	...
Y_2Te_3	−1400	10.0	140	...	4×10^{15}
LaSb	Negative	1.2×10^{-4}	...	~−40	...
ErSb	Negative	4.7×10^{-5}	...	~−10	...
YSb	Negative	6.5×10^{-5}	...	−40 at 100°C	...
YBi	Negative	1.96×10^{-4}	...	...	est. 9×10^{20}

pounds, should not be given great weight in assaying the nature or the potential of these semiconductors.

Room-temperature resistivities for the sesquiselenides are somewhat higher than those for the corresponding tellurides. In general, resistivities in both classes of compounds, increase with progression through the rare earth series, the yttrium compounds falling at the end. The Ce, Sm, and Yb compounds may not, because of the several stable valence states of these elements, fit into such a picture.

The room temperature resisitivity of Y_2Se_3 appears to be in the insulator range. In attempts to eliminate possible high contact resistance, a number of different methods of contacting specimens of this compound were used. Various techniques explored utilized pressure contacts with probes of Pt, W, Mo, Cu, Fe, Al; contacts of conducting silver paint; leads of Cu, W, and Fe applied by spot welding; solder contacts of Pb-Sn, In, Al, and Ga applied with various fluxes, by both normal and ultrasonic soldering techniques. However, under applied potentials up to 60 v, there was in no instance a detectable current through the sample.

At the other extreme, resistivity for the monoselenide of erbium was found to be quite low at room temperature. Low resistivities would be expected for the 1:1 compounds if only two of the valence electrons of the rare earth atom were involved in the chemical bonds, leaving the third free to act as a charge carrier with rather low activation energy. Iandelli (15) also concluded that this was the case through analysis of structures and interatomic spacings for the cerium-group compounds. Here again, the Ce, Sm, and Yb compounds may be exceptions, as the data for YbTe suggest.

Data on the antimonides and bismuthides do not clearly indicate whether these are impure specimens of semiconductors or whether the compounds are nearly metallic in nature. Considerable difficulty was experienced in attempting to prepare satisfactory specimens of these compounds. The difficulty may be partially attributable to the phase relationships existing in the *RE*-Sb and *RE*-Bi systems. In the one case which has been studied, the 1:1 compound, LaSb, incongruent melting is reported. (16) Attempts to crystallize this compound from solution in excess antimony yielded specimens with electrical properties similar to those given in the table. Future work on these groups of compounds must, of necessity, initially deal with development of better preparative techniques.

THERMOELECTRIC PROPERTIES

Seebeck coefficients have been measured for a number of the compounds, and are given in Table III. These coefficients were measured over a range of temperatures for specimens of Gd_2Te_3 and La_2Te_3 and

were found to remain constant up to 450 and 525 °C, respectively, the highest temperature to which measurements were extended.

Thermal conductivity of Gd_2Te_3 has been determined at room temperature by use of the "Z-meter." (17, 18) Values for *n*- and *p*-type specimens were found to be 0.026 and 0.023 watt-cm^{-1}-deg^{-1}, respectively. Since the lattice component of thermal conductivity usually predominates at room temperature for materials of this type, the nearly identical values are to be expected.

High-temperature thermoelectric properties of the refractory rare earth intermetallic compounds may prove to be of practical interest and are to be investigated.

PURITY

It will be noted in Table III that carrier concentrations for most of the specimens are high. In synthesizing the compounds, high-purity (better than 99.99 per cent) selenium, tellurium, antimony, and bismuth were used. However, purity of available rare earth metals has been relatively low (about 99 per cent). It is therefore probable that carriers, other than those resulting from excess of one of the component elements, were introduced principally as impurities present in the rare earth metals, or as contaminants incorporated during synthesis of the compounds. Spectrographic analyses of specimens of Gd_2Te_3, for example, show that relatively high concentrations of Ca, Mg, Fe, Ni, Ta, Si, and Al are present in the material.* Such high impurity concentrations seriously interfere with study of basic properties of the compounds. The desirability of efforts to improve purity is evident.

In current work at Battelle, higher purity is being sought in three ways: (1) by purification of rare earth metals which are to be used in preparing the compounds, (2) by elimination or minimization of sources of contamination associated with synthetic processes, and (3) by purification of the compounds themselves. In attempting purification of the elements and compounds, emphasis is being placed on the use of zone-refining processes, which have been applied successfully in refining other semiconductor materials. Normal zone-refining and float-zone refining, utilizing both electron-beam and induction heating, are being investigated. To eliminate or minimize sources of contamination, use of various container materials (for example, BN, MgO, ThO_2) and various synthetic processes are being investigated. Preliminary results indicate that, under proper conditions, significant purification of the metals may be attained by the floating-zone process.

---

*Per cent by weight detected: 0:01 Ca, 0.05 Mg, 0.01 Fe, 0.001 Ni, < 0.05-5.0 Ta, 0.001 Si, 0.005-0.01Al.

REFERENCES

1. A. Iandelli and E. Botti, *Atti accad. nazl. Lincei*, 25, 498 (1937).
2. A. Iandelli and E. Botti, *Gazz. chim. ital.*, 67, 638 (1937).
3. A. Iandelli, *Z. anorg. Chem.*, 288, 81 (1956).
4. A. Iandelli and E. Botti, *Atti accad. nazl. Lincei*, 25, 233 (1937).
5. A. Iandelli and E. Botti, *ibid.*, 24, 459 (1936).
6. A. Iandelli and E. Botti, *ibid.*, 25, 638 (1937).
7. W. Klemm and A. Koczy, *Z. anorg. Chem.*, 233, 84 (1937).
8. W. Klemm and H. Senff, *ibid.*, 241, 259 (1939).
9. W. Nowacki, *Z. Krist.*, 99A, 339 (1938).
10. H. Senff and W. Klemm, *Z. anorg. Chem.*, 242, 92 (1939).
11. J. F. Miller, F. J. Reid, and R. C. Himes, *J. Electrochem. Soc.*, 106, 1043 (1959).
12. Stambaugh, Miller, and Himes, "Growth of Refractory III-V Compounds and Alloys from Solution." Paper presented at AIME Technical Conference on Metallurgy of Elemental and Compound Semiconductors in Boston, August 29, 1960.
13. J. F. Miller, S. E. Miller, and R. C. Himes, *J. Am. Chem. Soc.*, 81, 4449 (1959).
14. I. E. Campbell, *High Temperature Technology*. New York: John Wiley & Sons, Inc., 1956.
15. A. Iandelli, *Gazz. chem. ital.*, 85, 881 (1955).
16. R. Vogel and H. Kloso, *Z. Metallkunde*, 45, 633 (1954).
17. T. C. Harman, *J. Appl. Phys.*, 29, 1373 (1958).
18. T. C. Harman, J. H. Cahn, and M. J. Logan, *ibid.*, 30, 1351 (1959).

HIGH-TEMPERATURE SEMICONDUCTORS FOR THERMOELECTRIC CONVERSION*

S. W. KURNICK, M. CUTLER, R. L. FITZPATRICK, AND J. F. LEAVY

General Atomic, Division of General Dynamics Corporation, John Jay Hopkins Laboratory for Pure and Applied Science, San Diego, California

The rapidly developing field of semiconductors for direct conversion includes those which differ from the known semiconductors (Ge, InSb, PbS and Bi_2Te_3) with controlled impurities. At the high end of the temperature scale (800–1600° K), new semiconductors are receiving emphasis in development. $CeS_{1.33-1.50}$ is such a semiconductor, and at present the material is sufficiently optimized to give zT's of 0.1 and above. The study of this semiconductor (n-type) is implemented by the study of a p-type semiconductor $ThS_{1.71-1.76}$. Progress to date on these materials is discussed. The measurement of the thermal conductivity of Ce–S at high temperatures, usually very difficult to make, is made by a small-area-contact technique developed at General Atomic.

INTRODUCTION

The Ce–S and Th–S† semiconductor materials are being intensively studied because of their low-lattice thermal conductivities and chemical stability at high temperatures (800–1600° K) which makes them promising materials for thermoelectric conversion. An important part of the intensive study of these compounds is the determination of the nature of their electric and thermal transport phenomena, parameters which are relatively unknown compared to those of semiconductor materials such as germanium, silicon, and lead telluride.

One of the most significant aspects of this program is the measurement of thermal conductivity by a small-area-contact technique being developed at General Atomic. In this technique, measurements of thermal

---

*Some of the work described in this paper was done under Bureau of Ships, U. S. Navy, Contract NObs-77144.

†The designation Ce–S is used to indicate the Ce–S phase $Ce–S_{1.33-1.50}$. Similarly, the term Th–S indicates semiconductors in the range $ThS_{1.71-1.76}$.

conductivity at high temperature—usually very difficult to make—are readily performed on minute, irregularly shaped specimens as small as 0.2 cm^3. Although there were many semiconductors ready for measurement, it was felt that the small-area technique should be thoroughly investigated on one semiconductor (Ce–S) whose efficiency is roughly known. The technique is now to be extended to other materials to improve their thermoelectric performance.

The conduction mechanism in Ce–S and Th–S semiconductors differs from that associated with the semiconductors Ge, InSb, and PbTe, and with the ionic semiconductors such as AgCl in which the Ag^+ ion moves through the lattice. The control mechanism may be best ascribed to that of the polaron model. The basic attributes of this model are its consistency with the observed rise in the Seebeck potential with increasing temperature; a slowly decreasing electrical conductivity with increasing temperature; and an extremely small Hall coefficient.

MATERIAL PREPARATION

Ce_2S_3 is prepared from the interaction of CeO_2 and H_2S. The result of the interaction is then melted down to form the compounds $Ce_{2+x}S_{3+x}$ $(0 \leq x \leq 1)$ depending on how much sulfur is pumped off. Material preparation is now being developed along two main lines:

(1). The formation of solid solutions of Ce–S with sulfides of barium, strontium, and calcium.

(2). The synthesis of Ce–S and Th–S free of cracks for reasonably small samples. Some progress is being made in improving the strength of the Ce–S semiconductors by controlling the rate of freezing when the melt is solidifying. A faster rate of freezing provides obsidian-like lustrous material which can be cut by abrasion—which is not fracture-prone, and to which leads can be soldered without difficulty. The conductivity of such material runs high, approximately 500 mho cm^{-1}. A contributing factor to the ease of soldering is the high thermal conductivity of the material, which is associated with the high electrical conductivity. All other concentrations of the wide impurity range are made by sulfurization or pumping off of the sulphur at moderately high temperatures.

Two samples of Th–S have been prepared by freezing the melt while pumping off excess sulfur. These have been X-rayed; the results show a mixed phase. However, rough Seebeck potential measurements indicate *p*-type carrier transport at room temperature reverting to *n*-type at high temperatures. A need for better sample preparation is indicated and attempts to prepare single-phase materials are under way. As in Ce–S, the Th–S samples are very friable and give indications that the techniques used in the small-area-contact measurements will be applicable.

SMALL-AREA-CONTACT TECHNIQUES

Recently developed techniques (1) for the evaluation of the parameters γ (a dimensionless parameter equal to $(\alpha^2\sigma/\kappa)T$, where T is in °K) and α have been tested at high temperatures and the results compared with values obtained by more conventional measurement procedures. The results encourage use of the procedure for further testing of new materials Though the method requires a small-area, ohmic contact on the material, this requirement is not serious with the rare earth sulfides, because wires and crucibles of molybdenum are readily wetted by these compounds.

The jig used for small-area-contacts is shown in Fig. 1. Contacts are made through 0.010 in. molybdenum wire, in the tapered crucible *A*. Temperature is determined by the tungsten-rhenium-tungsten thermocouple *B*. The cap *C* is made of boron nitride; *D*, of course, is the semiconductor charge. Contacts 1 or 2 are used to measure voltage decay and permit resistance correction of the lead wire. Additional contacts 3 and 4 are used to check the readings observed through the center lead.

By this method, materials which crack readily at low or room temperature can be safely measured, for the material is kept above 700° C while

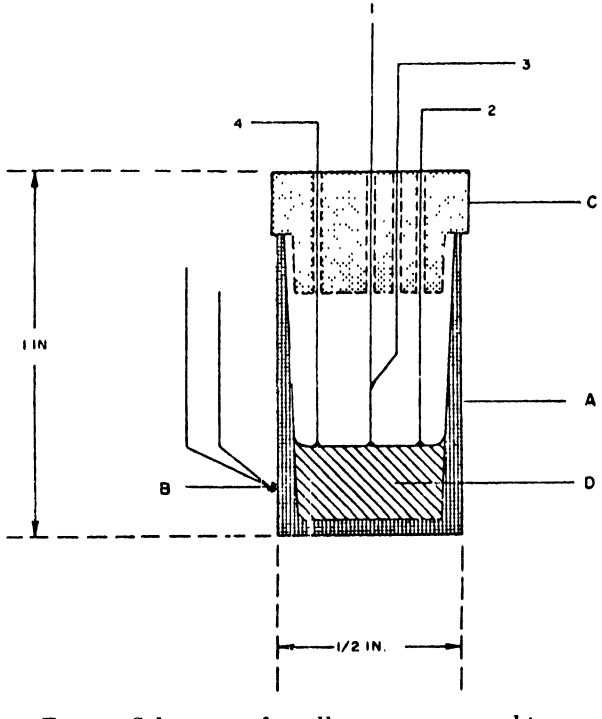


Fig. 1. Schematic of small-area gamma machine.

measurements are being taken. In this way, point contacts are inserted, the charge is melted at about 1900° C, and the point contacts are formed by inserting molybdenum wires into the melted material. Then the CeS semiconductor is frozen, but at no time is the frozen material permitted to descend below 800° K. Although this procedure was established as the only sure way to avoid sample loss, some samples show sufficient rupture strength to permit their cooling to room temperature. Because such samples were rare, most were preserved by being held at high temperature for some time; one sample was kept at 1100° K for four days. No noticeable change in the thermoelectric properties occurred. We believe that if the material shows sufficient promise, slow-cooling kiln practices could be employed to avoid cracking. The determination of the figure of merit $\gamma = T\alpha^2\sigma/\kappa$ at high temperature requires values for the thermal conductivity, which are usually extrapolated from room-temperature data. The most common technique for determining κ is that used in the comparison method described by Francl and Kingery.(2) Briefly, a block of the unknown material is sandwiched between two standard blocks of stainless steel or any other known reference material. When the thermal current has been established as being equal through both standards, the thermal current through the unknown gives the thermal conductivity. This technique is open to question at high temperatures, unless boundary conditions are arranged to limit stray thermal currents.

Measurements of thermal conductivity at small-area contacts have been continued, and the parameters α, σ, and κ derived from these techniques have been checked for consistency with the values derived by more conventional techniques. In the measurement of thermal and electrical conductivities of semiconductors, great care must be made to avoid cracks which will warp the potential and thermal distribution.

This approach is evaluated below for the Ce–S; the approach has already been verified for GaSb. In brief, voltages are applied through the molybdenum wire in ohmic contact with the semiconductor. After a short time of about a second (the time required for thermal equilibrium) the voltage is switched off rapidly, in about a microsecond. Since the small-area contact loses heat by thermal conduction, with no appreciable loss by radiation, the excess heating through the material dissipates and sets up a voltage which decays asymptotically according to

$$\delta V = \gamma V + \frac{\gamma}{2\alpha T} V^2$$

A typical pulse dissipation is shown in the scope picture in Fig. 2. Sweep time is of the order of a second. Table I lists the data involved in an experimental verification of small-area techniques using a Ce–S sample. In this table parameters measured by conventional techniques are marked

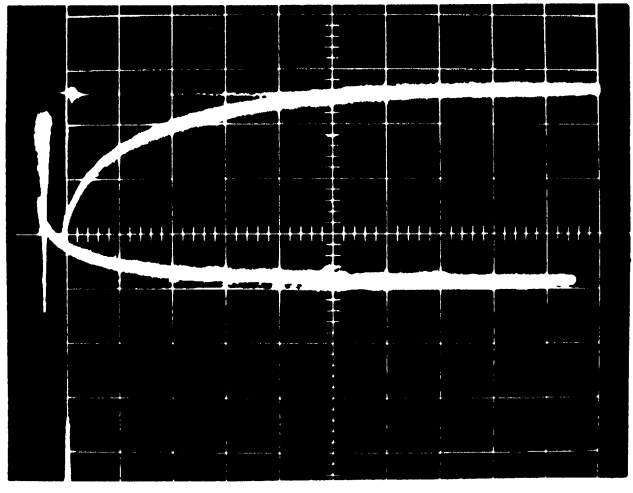


Fig. 2. Oscilloscope projection of pulsed δV as a function of time.

with a prime; those measured by the small-area-contact technique are unmarked. The γ and $\gamma/\alpha T$ data are measured from the reversal of the voltage V. Dividing γ by $\gamma/\alpha T$ gives the Seebeck potential α. The thermoelectric power is then measured as a function of temperature by more conventional techniques. The α' values devised by the conventional procedures agree generally within about 10 per cent with the α values derived from the small-area contacts. The agreement between α and α' supports strongly the validity of the small-area-contact values of γ and κ.

The κ values may be more precisely derived if the values for α and σ are determined independently from measurements on the materials used in the small-area γ machine. It must be remembered that the κ's so calculated are least accurate. However, the semiconductor efficiency γ is the most accurate term ($\sim$ 6 per cent) and is really the term which is of major interest in the field of thermoelectric semiconductors.

TABLE I: RESULTS OF MEASUREMENTS ON Ce–S SAMPLE A-26

T (°K)	$\gamma \times 10^2$	$\frac{\gamma}{\alpha T} \times 10^2$	α (μv/°C)	α' (μv/°C)	σ (mho/cm)	κ (w/cm-°C)	κ' (w/cm-°C)
1573	10.0	14.1	448	390	4.7	.015	.011
1523	9.2	14.2	425	380	5.12	.015	.012
1402	9.35	18.6	359	360	5.5	.011	.011
1273	7.85	13.9	442	335	6.0	.019	.011
1203	7.9	16.6	395	325	6.1	.014	.010
1103	6.38	14.1	404	320	6.37	.018	.011
973	7.2	15.2	485	275	6.3	.020	.007
300	0.07	5.92	40	40	8.7	.006	.006

The conductivity was measured in two ways. First, the potential around the fused-in wire was probed, but the results were invalid because of the occurrence of cracks in the sample. Second, a small filament was sliced from the material used in the crucible and its conductivity was measured by a movable four-probe potentiometric method. In this case, the conductivity was measured as 8.7 mho/cm^{-1} at room temperature. Since the resistance of the small-area probe could be measured at various temperatures, the conductivity could be determined by normalization.

Experimental error involved with the 300° K entry ($\kappa' = 0.006$) can be attributed to two causes: cracking already begun in the sample when it was lowered to room temperature; and, reading error in the lower γ's, which were at the lower limit of detection. The most significant difference between the α and α' values appears to be the sharper increase in α as compared to the change in α'.

There are indications in the temperature variations of γ, α, and κ of some leveling off at high temperatures. How sharply this occurs is not clear from the data thus far obtained. The values for κ above 973° K appear to be sufficiently invariant to be ascribed to the phonon transport.

Values for κ' from previous work at General Atomic and at Westinghouse are shown in Table II. The thermal conductivity measured by

TABLE II: MEASURED VALUES OF THERMAL CONDUCTIVITY

Average Temperature	κ'(w/cm-°C)
355	0.018*
650	0.014*
300	0.005†

*Data taken by stacked-disc method using stainless steel as the reference.
†Data from "Thermoelectricity Quarterly Progress Report No. 4," Westinghouse Research Report (November, 1959).

Westinghouse apparently does not agree with most of the data taken at our laboratories. The closeness of the values for 300° K shown in this table and in Table I is fortuitous for the reasons listed above. The value 0.014 w/cm-° C obtained at 650° K agrees well with the small-area values above 1000° K.

REFERENCES

1. M. Cutler, "Microphysics Measurements: Thermoelectric Parameters of GaSb from 25 to 140°C," General Atomic Report GAMD-1348 (April, 1960).
2. J. Francl, and W. D. Kingery, *J. Am. Ceram. Soc.*, 37, 80-84 (1954).

THEORY OF THE ELECTRON-TRANSPORT PROPERTIES OF THE 4f-ELECTRONS IN RARE EARTH COMPOUNDS

R. R. HEIKES

Westinghouse Research Laboratories, Pittsburgh, Pennsylvania

The band concepts have been adequate to interpret the electron-transport properties of most metals and semiconductors studied to date. However, there appear to be a group of substances that are more easily understood on a different basis. Examples of materials of this second type are to be found among the oxides of the metals of the first transition group. (1, 2, 3) In such substances it appears a better procedure to treat the electrons as localized particles and to treat their motion as a thermally activated diffusion process.

In order to appreciate the difference between the band and the localized concept, the energy-level diagram of Fig. 1 will be discussed. (4) Consider a crystal of a specified material to which we add an extra electron (for example, by an appropriate doping agent). If the charge carrier is free from the dopant, one of two situations will develop. First, let us keep all atoms fixed, but allow the added electron to occupy all the equivalent positions in the lattice. If one now removes the degeneracy by forming the appropriate linear combinations of all these configurations, one sees that a band of states is formed with a width E_B. If, on the other hand, one holds the added electron fixed and allows the atoms to move, the electron can then be trapped by its own polarization. (5) In this process the energy of the electron is lowered by an amount E_T. Now if $E_T > E_B/2$ the trapped state will be present in the crystal. The trapped state will, of course, be favored in the case of small overlap of the wave functions and small electronic polarizability. (5) In the case of many of the 3*d*-oxides both these conditions are met, and it is therefore reasonable to assume that the electrons are localized. (2, 3)

In the case of the transport phenomena in the rare earth compounds, it should also be expected that the energy bands would be relatively narrow, since conduction presumably takes place in the 4*f*-shell. Thus one might expect to find both band and localized behavior. Localized behavior would be favored, for example, in the oxides and sulfides, while band behavior should be expected in the selenides and tellurides.

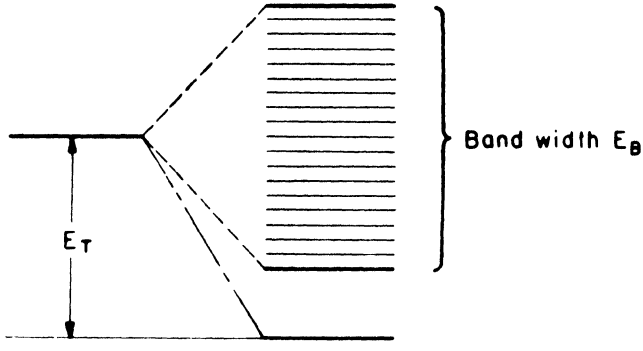


Fig. 1. Typical energy-level diagram.

Because the transport properties on the band model have been adequately treated in many places (6), the emphasis here will be on a discussion of the localized model. The results of the two models will be compared when appropriate.

ELECTRICAL CONDUCTIVITY

If one treats the charge-carrier motion as a thermally activated diffusion process, the electrical conductivity may be most simply derived from the Einstein diffusion relation:

$$\sigma = \frac{ne^2D}{kT} \tag{1}$$

where e is the electronic charge, k Boltzmann's constant, T the absolute temperature, n the charge-carrier density, and D the diffusion coefficient. Furthermore, for a cubic crystal one can write

$$D = \beta a^2 \tau^{-1} \tag{2}$$

where a is the diffusion distance (assumed here to be one lattice constant) and β is a structure-dependent factor (2β is the probability that an electron will leave a particular plane in a given jump). The remaining quantity τ^{-1}, the probability of a jump, forms the central problem. It has been proposed (2) that

$$\tau^{-1} = \tau_o^{-1} z e^{-\Delta G/RT} \tag{3}$$

where ΔG is the free energy of activation, and τ_o^{-1} is related to the lattice frequency; z is the number of empty nearest neighboring sites to the charge carrier. ΔG is related to the work necessary to remove the distortion surrounding the charge carrier and the site to which it will

jump, in such a way that neighboring sites are degenerate. Quantum mechanical transfer can then occur. Introducing the concentration of free carriers c and combining Eqs. (1), (2), and (3) one arrives at

$$\sigma = \frac{ce^2\beta z\tau_o^{-1}e^{-\Delta G/RT}}{akT} \tag{4}$$

At high temperatures it is expected that c will be equal to the concentration c_o of the doping agent (assuming each doping atom produces only a single carrier). At lower temperatures this will, of course, not be true and one must calculate the number of free carriers. In the limit of $c \ll c_o$ it is well known that

$$c \sim e^{-\Delta E/kT} \tag{5}$$

where ΔE is the binding energy of the dopant for the electron.

It is seen from Eq. (4) that the mobility essentially increases exponentially with temperature as long as $\Delta G \gg kT$. It should also be observed that one does not have problems with the degeneracy of the charge carriers on the localized model.

SEEBECK COEFFICIENT

On the localized model the conductivity calculation is straightforward; however, when one attacks the Seebeck coefficient and the thermal conductivity, a basic difficulty enters. In these phenomena one has to deal with a temperature gradient. In order to study the charge-carrier motion properly it is necessary to know the details of the motion. In other words, it is necessary to know precisely how the energy is supplied to the electron which is doing the jumping. In the absence of such specific knowledge it is necessary to resort to a model for the calculation. (It should be pointed out that a similar problem occurs for standard semiconductors, where one needs to know the energy dependence of the relaxation time.) The consequences of one simple model will now be examined.

Since the Peltier coefficient is simpler to treat theoretically, that will be done first; then the Seebeck coefficient, α, will be obtained from the Kelvin relation $\alpha = \pi/T$. The Peltier heat is simply defined as the heat absorbed or evolved at a junction of two materials on the passage of unit current. From the definition one may write, for a single material:

$$\pi = \frac{U^* - \mu}{e}, \quad \alpha = \frac{U^* - \mu}{eT} \tag{6}$$

where π is the Peltier coefficient, U^* is the total energy, except electrical, carried by a charge carrier in an isothermal region, and μ is the

chemical potential of the charge carrier. The quantity $U^* - \mu$ is simply the amount of heat needed to remove a particle from the solid. The calculation of π, therefore, reduces simply to a calculation of U^* and μ.

μ may be calculated as follows. First add a charge carrier to the system, with the restriction that the system be held rigid. For this case the charge in free energy is

$$G_1 = q\varphi + kT \ln \frac{c}{1-c} \tag{7}$$

where $q\varphi$ is the additional electrical energy, and the second term is the entropy of mixing. If the lattice is now allowed to relax around the site of the charge carrier, an amount of work ΔG_R will be done against an external agency. The free energy of the system then decreases by ΔG_R. Thus the total change in free energy per particle or the electrochemical potential $\tilde{\mu}$ may be written

$$\tilde{\mu} = q\varphi + kT \ln \frac{c}{1-c} - \Delta G_R \tag{8}$$

The chemical potential is then simply the last two terms of Eq. (8). To determine U^* the isothermal transfer of a particle from site one to site two must be considered (Fig. 2). In order to effect this transfer an amount of work W must be done at site one. Further, to maintain the region isothermal, heat Q must be added. Remembering that U^* is simply the total energy (except electrical) flux per particle under isothermal conditions, the first law of thermodynamics may be written

$$dU = W + Q + U^* dn \tag{9}$$

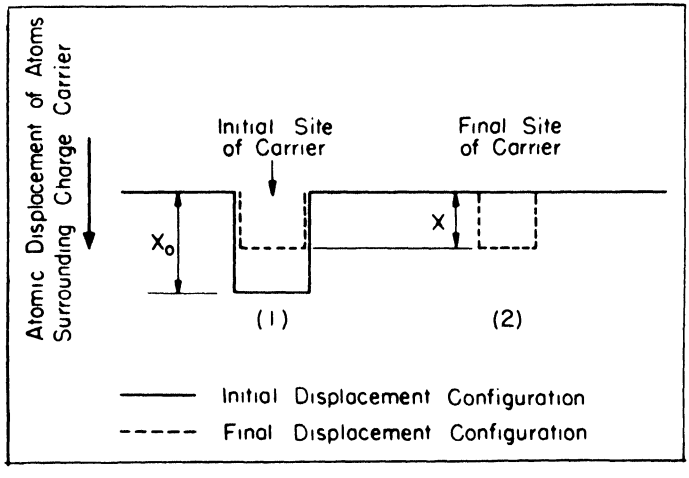


Fig. 2. Schematic transfer of particles.

Since this is an isothermal process the work W done on the system is equal to the increase in free energy. It follows also that $Q = -T\frac{dW}{dT}$. It is seen from Eq. (8) that the removal of a particle gives a change in the energy of $-\Delta H_R$. It remains to evaluate W. To do this one must resort to a specific model. It will be assumed that the free energy of activation is a function of the local force constants and atomic displacements. The local force constant at a site possessing a carrier will be denoted by k, while the force constant at an empty site will be denoted by k'. The equilibrium positions of the atoms surrounding an empty site will be taken as the zero of displacement. On the simple model presented here, a carrier will transfer whenever the atomic displacements surrounding the two sites are equal. The energy required for this process may be written

$$E = k\,(x_o - x)^2/2 + k'x^2/2 \tag{10}$$

Clearly, x must be such as to minimize E. This value is

$$x = \frac{x_o}{1 + (k'/k)} \tag{11}$$

Thus, we see that if $k = k'$, the free energy of activation is equally divided between the two sites.

Equation (9) can now be evaluated. W is easily seen to be

$$W = \Delta G_R\left[\frac{\gamma(\gamma - 1)}{(1 + \gamma)^2}\right] \tag{12}$$

where $\gamma = k'/k$ and $\Delta G_R = (1/2)kx_o^2$. Now, remembering that $Q = -T\frac{dW}{dt}$ and using Eq. (9), one can straightforwardly evaluate U^*. However, if one attempts to consider arbitrary temperature dependences of γ, the resulting expressions get unnecessarily complicated. Rather, the assumption will be made that γ is independent of temperature. Physically, such an assumption is not too unreasonable. (The consequence of removing this assumption will be mentioned later.) With this restriction, one finds that

$$U^* = -\Delta H_R\left[\frac{1 + 3\gamma}{(1 + \gamma)^2}\right] \tag{13}$$

Finally, from Eq. (6) one may write

$$\alpha = \frac{k}{q}\left\{\frac{-\Delta H_R}{kT}\left[\frac{1 + 3\gamma}{(1 + \gamma)^2}\right] + \frac{\Delta G_R}{kT} - \ln\frac{c}{1 - c}\right\} \tag{14}$$

It is seen that if $\gamma \approx 1$, the coefficient of $(\Delta H_R/kT) \approx 1$. Furthermore, for $\gamma < 1$ the coefficient of $\Delta H_R/kT$ remains of the order of unity. Thus, un-

less γ is significantly larger than unity, the Seebeck coefficient is rather insensitive to it.

It now also follows from Eqs. (10) and (11) that the free energy of activation occurring in Eq. (3) is simply

$$\Delta G = \Delta G_R \frac{\gamma}{1+\gamma} \tag{15}$$

To date, there have been relatively few systematic studies made on narrow-band materials. Of those that have been done (1, 3), it is found that, in order to get agreement with experimented data, it is necessary to set the coefficient of $\Delta H_R/kT$ in Eq. (13) equal to unity. Thus,

$$\alpha = -\frac{k}{q}\left[\frac{\Delta S}{k} + \ln\frac{c}{1-c}\right] \tag{16}$$

Let us consider now the alteration of Eq. (16) due to removal of the restriction that $(d\gamma/dT) = 0$. If one makes a power-series expansion of k and k' to terms linear in T, one has

$$\gamma = \frac{k'}{k} = \frac{k_o'(1+A'T)}{k_o(1+AT)} = \frac{k_o'}{k_o}(1+T\Delta A)$$

where it is expected that $T\Delta A \ll 1$. If one now revaluates Eq. (16), it is found that the first term is replaced by $\Delta S_R\,[1+0(T\Delta A)]$. In other words, the first order correction terms are of order $T\Delta A$. Thus, Eq. (16) should be a good approximation.

A rather close analogy may be drawn between Eq. (14) and the standard expression for the Seebeck coefficient for a nondegenerate extrinsic semiconductor, which may be written

$$\alpha = \frac{k}{q}\left\{A - \ln\frac{n}{2\left(\frac{2\pi m^* kT}{h^2}\right)^{3/2}}\right\} \tag{17}$$

The first term in this equation depends on the details of the motion, that is, the scattering mechanism. The first term in Eq. (14) also depends on details of the motion through the values of the force constants.

The analogy between the second terms requires further thought. It is desired to show that $\ln\frac{c}{1-c}$ is analogous to $\ln\frac{n}{2\left(\frac{2\pi m^* kT}{h^2}\right)^{3/2}}$

The equivalence of the numerators is clear. The denominator in the narrow band case, $(1-c)$, is simply the density of unoccupied sites. It

is easily seen that in the broad-band case the denominator can be given a similar interpretation. For it should be noted that the denominator is essentially the cube of the reciprocal wavelength of an electron of temperature T. Therefore, if one takes as the "size" of the electron, λ^3, the denominator is again the density of states, and the analogy in the broad-band and narrow-band case is rather complete.

Thus it is seen that the localized model is simply the limit of the broad-band semiconductor which is arrived at when the effective mass, m^*, is so large that γ^3 is less than a^3, the lattice constant, and therefore the electron may be considered as localized on a given site.

It should be recalled at this point that Eq. (13) has been derived for the temperature range where all charge carriers are free from impurity centers. Actually it is easily seen that Eq. (13) may be applied over the complete temperature range if one simply interprets c as the concentration of free (from impurity centers) carriers at that temperature.

It remains to examine the electronic contribution to the thermal conductivity. The following simple argument indicates that, on the model adopted here for localized carriers, the electronic thermal conductivity is zero. Consider Fig. 3; since the thermal conductivity is measured at

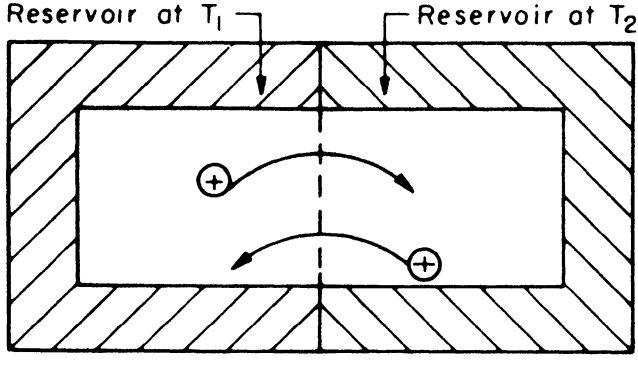


Fig. 3. Thermal conductivity model.

zero current, we need only consider the heat taken from the two reservoirs at T_1 and T_2, when the two particles jump across an imagniary plane as indicated. On the present model it is recognized that addition and removal of a particle require equal and opposite amounts of external work and heat from the reservoir. Therefore, the total amount of heat taken from either reservoir is zero, and thus the electronic thermal conductivity is zero.

As yet there are no experimental data available to check this result.

SUMMARY

At present there are relatively few data on the transport properties of the rare earth compounds. However, it is anticipated that the whole spectrum of behavior, that is, from broad band to localized properties will be found. An attempt has been made here to give a rather complete description of the localized case and its relation to the standard broad-band treatment.

REFERENCES

1. F. J. Morin, *Phys. Rev.*, 93, 1199 (1954).
2. R. R. Heikes and W. D. Johnston, *J. Chem. Phys.*, 26, 582 (1957).
3. S. Van Houten. Article to be published.
4. C. Zener and R. R. Heikes. Conference on Magnetism and Magnetic Materials, 1956.
5. R. W. Gurney and N. F. Mott, *Proc. Phys. Soc.* (London), 49, extra part 32 (1937).
6. W. Ehrenberg, *Electric Conduction in Semiconductor and Metals*. New York: Oxford University Press, 1958.

SAMARIUM SULFIDES FOR SEMICONDUCTOR APPLICATION

M. D. HOUSTON*

Magnetic and Ceramics Department, Westinghouse Materials Laboratories, Pittsburgh, Pennsylvania

The intensive search for new semiconductor materials, especially for higher temperature application, intuitively embraced the rare earth metals and their compounds. Refractory cerium sulfides reported by Eastman, Brewer *et al.* (1) displayed favorable electrical and stability characteristics. More recently, rare earth selenides and tellurides which possessed semiconductor properties were disclosed by Miller, Reid, and Himes. (2) Further data for these compounds (3a), gadolinium selenide (3b), and cerium sulfide (3c) are given in this publication and indicate a potential application in thermoelectric generation. In addition to these compounds, others in the samarium-sulfur system have displayed similar promising thermoelectric characteristics for high-temperature utilization.

PREPARATION

All sulfides were prepared by a vapor-solid interaction between the elements in an evacuated fused quartz chamber—a process very similar to that described by Iandelli. (3d) Precautionary measures were not taken to separate the reactants physically during the process, and no exothermic difficulties resulted. The sulfur vapor cloud which forms during the gradual temperature rise of 200°C per hour was observed to disappear near 600°C. The granular reaction product, analyzed by X-ray diffraction to be multiphase, was comminuted to pass through U.S. Series 120 mesh and then compacted into right cylinders by dry-pressing techniques, with pressures of 25 to 100 tons per square inch. These pellets were sealed in evacuated fused quartz chambers and fired at 1100 to 1250°C or were fired in a vacuum induction furnace which was

*The author wishes to express his appreciation to Drs. S. J. Angello and R. R. Heikes, Westinghouse Research Laboratories, for consultation; to R. C. Kuznicki, Westinghouse Materials Laboratories, for X-ray diffraction analyses; to the BuShips, U.S. Navy, for their sponsorship, in part, of the thermoelectric program; and to the Electrochemical Society for their kind permission to publish this article (presented at the Houston meeting of the Electrochemical Society in October 1960) in the proceedings.

capable of attaining 2000 °C. The thermoelectric data were obtained with the apparatus described by Duncan and Wilson. (4) The crystalline structures of the resultant compounds were determined by X-ray diffraction powder techniques.

DISCUSSION

The samarium-sulfur system consists of four distinct compounds and one solid-solution series. The apparent compounds are SmS, Sm_3S_4, Sm_2S_3, and SmS_2, of which the sesquisulfide is polymorphic and the disulfide may be polymeric (Sm_2S_4). The solid-solution series extends from Sm_3S_4 to Sm_2S_3, similar to the compositional range found in the cerium-sulfur system. The measured and reported (5) properties for polycrystalline specimens of the samarium compounds are given in Table I. All of the compounds are refractory and crystallize in some cubic structure. The electrical characteristics were observed to shift from insulating to semiconducting, as the sulfur concentration decreased.

TABLE I: PROPERTIES OF SAMARIUM SULFIDES

Property	Composition			
	SmS	Sm_3S_4	Sm_2S_3	SmS_2
Color	Black	Black	Yellow*	Brown
Bulk density, gm/cc	4.73	4.07	3.83*	4.43
Theoretical density (5), gm/cc	5.67	6.14	5.87	5.66
Melting point (5), °C	1500 °C	1800 °C	1780 °C	1730 °C
Electrical resistivity, ohm-cm	8.5×10^{-2}	5.9	8.2×10^{7}*	7.1×10^{5}
Crystal structure	Cubic-NaCl	Cubic-Th_3P_4	α-cubic-unk. γ-cubic-Th_3P_4	Cubic-unk.
Lattice constant, Å	5.967	8.556	8.448	7.87
Magnetic susceptibility (5), e.m.u. $\times 10^{-6}$	5070	2350	1120-α 1020-γ	1238
Ionic species	Sm^{+2}	Sm^{+2}, Sm^{+3}	Sm^{+3}	Sm^{+3}, unk.
Seebeck coefficient, μV/°C	−270	−150	...	...

*Multiphase specimen.

Compositions in the monosulfide region possess favorable properties for thermoelectric application. These parameters for the mono-preparation as a function of temperature are shown in Fig. 1. The rapid decay of the Seebeck coefficient is undesirable, and this feature leads to a maximum evaluation factor at a relative low temperature, 450 °C. With a preparation

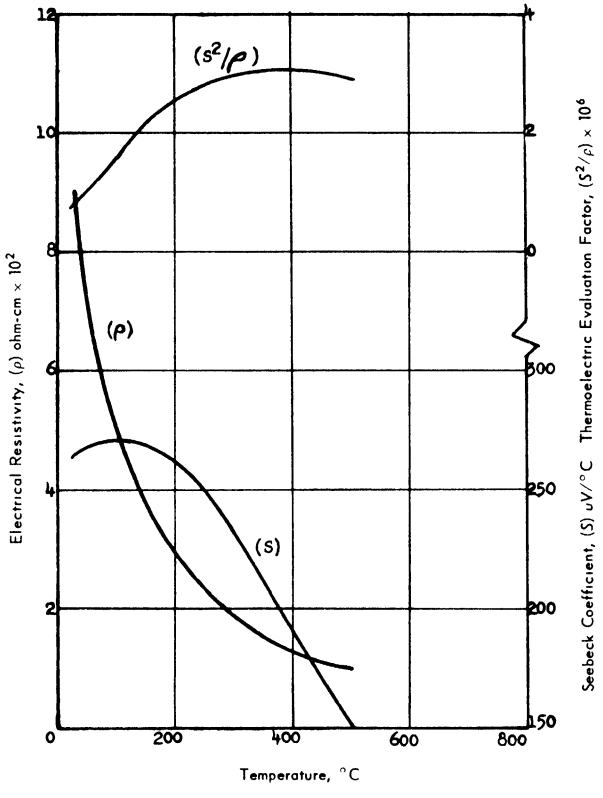


Fig. 1. Thermoelectric parameters *vs.* temperature for SmS.

corresponding to Sm_4S_3, the parameters are considerably stabilized up to higher temperatures (Fig. 2) and the maximum for the factor shifts upward to 600–650 °C. Room-temperature thermal conductivities for these two specimens are 0.0188 and 0.0358 w/°C-cm, respectively. For the latter composition, the thermoelectric efficiency (ε)* peaks at 1100 °K with a value of 10.3 per cent. This efficiency may appear low when compared to those reported for various intermetallic materials (15–20 per cent), but these more efficient materials fail at temperatures above 600 °C. Therefore, samarium subsulfides and other rare earth compounds appear quite favorable for high-temperature thermoelectric applications.

$$*\varepsilon = \frac{(1+ZT)^{1/2}-1}{(1+ZT)^{1/2}+1}. \quad Z = \frac{S^2}{\rho K},$$ where K = thermal conductivity, w/°C-cm; S = Seebeck coefficient, v/°C; ρ = electrical resistivity, ohm-cm.

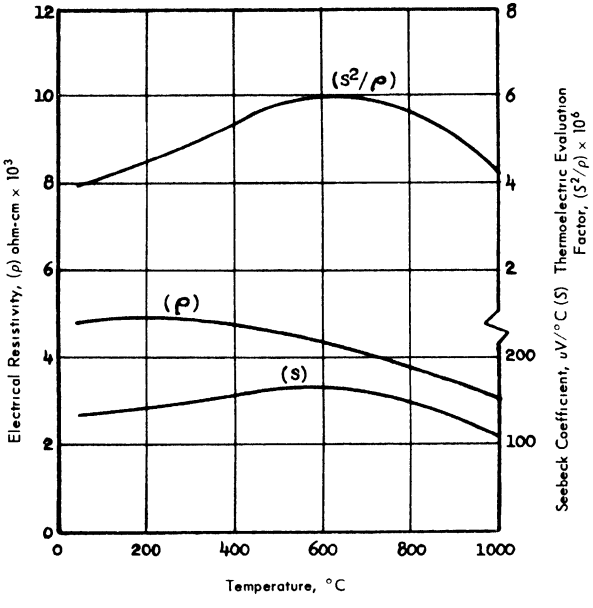


Fig. 2. Thermoelectric parameters *vs.* temperature for Sm_4S_3.

REFERENCES

1. E. D. Eastman *et al.*, *J. Am. Chem. Soc.*, 72, 2248 (1950).
2. J. F. Miller, F. J. Reid, and R. C. Himes, *J. Electrochem. Soc.*, 106, 1043 (1959).
3. Rare Earth Research Seminar: Paper by J. F. Miller and R. C. Himes. Paper by R. C. Vickery, and H. M. Muir. Paper by S. W. Kurnick *et al.* Paper by A. Iandelli.
4. C. S. Duncan and G. W. Wilson, *Elec. Engr.*, 79, 372 (1960).
5. M. Picon *et al.*, *Bull. Soc. Chim. France*, 2, 221 (1960).

PART FIVE

Mechanical and Metallurgical Properties of Metals, Alloys, and Intermetallics

SCANDIUM—ITS PREPARATION AND PROPERTIES

A. H. DAANE*

Ames Laboratory, AEC, and Chemistry Department,
Iowa State University, Ames, Iowa

Mendeleev predicted the occurrence of the element scandium in 1871 on the basis of his studies of the periodic relations among the elements of the periodic table. Shortly afterward, Lars Nilson (1) discovered scandium in some samples of the ore euxenite.

Scandium is a member of group IIIA of the periodic table, along with yttrium, lanthanum, the rare earth elements, and actinium, and occurs in the earth in smaller concentration (5 ppm) than most of the rare earths. However, this low concentration is only part of the reason why scandium has been relatively difficult to obtain for study. Due to a smaller ionic size than yttrium and the rare earths, it is not present in most rare earth ores. It has not, therefore, been produced in significant amounts in the recent work on the rare earths that made quantities of these elements available in high purity. Goldschmidt (2) has discussed the geochemical basis of the absence of scandium in yttrium and rare earth minerals, and has shown that the trivalent ionic radius of scandium would make it more likely to find this element in magnesium, iron, tin, zirconium, niobium, and tantalum minerals, as has been found to be the case. In spite of the general scarcity of scandium, one mineral, thortveitite, has been found that contains as much as 30 per cent Sc_2O_3, and samples of this material are much sought after in Norway; some thortveitite has also been found on the island of Madagascar. Much of the scandium that was available for study until the 1950's was obtained from the small amounts of this mineral that were found. Recently another significant source of scandium salts was discovered in the processing of uranium ores—in which scandium occurs in quite small amounts, but which may be removed and concentrated rather effectively. With an increasing interest in metals in general, the

*It is a pleasure to acknowledge the work on scandium done in our laboratory by D. H. Dennison, B. J. Beaudry, G. F. Wakefield, and C. E. Uebele. Reference has been made to the work of Dr. Doyle Geiselman at the Union Carbide Metals Laboratory; references to older literature have not been given, but it should be noted that work on scandium metal has been reported from French and Czechoslovak laboratories. Except for the crystallographic data, the physical properties reported here represent the first measurements found.

desire for modest quantities of scandium for study has prompted efforts to find additional sources of this element. As will be mentioned later, scandium appears to interact in an interesting manner with some other metals, but its scarcity would preclude its use as a general alloying agent in any but the most exceptional situations, unless the supply situation changes greatly.

If one considers the observed behavior of the group IIIA metals with other metals, the rather large sizes of the yttrium and rare earth atoms is apparent. For instance, as one passes across the rare earth group, the decreasing atomic radius resulting from the lanthanide contraction finds the heavy rare earths (Gd through Lu, and also Y) entering into limited solid solution with magnesium and titanium; the considerably smaller radius of scandium would suggest a greater interaction with these same metals, and studies of these alloys are now under way.

PREPARATION

The extraction of scandium from thortveitite to provide Sc_2O_3 for metal preparation may be accomplished by several processes. Spedding *et al.* (3) have described a process in which the 40 to 50 per cent SiO_2 in the thortveitite is removed as the volatile SiF_4 by heating the ground ore with ammonium bifluoride, and the resulting concentrate is purified by a combined thiocyanate-ether extraction and ion-exchange process. Solvent-extraction and ion-exchange methods have been used to obtain Sc_2O_3 from the processing of uranium ore.

As with yttrium and the rare earths, halides are the compounds of choice for the preparation of the metal, and the hygroscopic nature of the chloride, bromide, and iodide have made ScF_3 the most likely salt to be used in such metal-preparation studies.

PREPARATION OF ScF_3

Ammonium Bifluoride Process: In this reaction, the decomposition of ammonium bifluoride to yield ammonium fluoride and HF is utilized as a source of HF that may be easily metered out and controlled. Ammonium bifluoride and Sc_2O_3 are mixed in a 2.5 : 1 weight ratio to correspond to the reaction:

$$Sc_2O_3 + 6(NH_4)HF_2 \longrightarrow 2ScF_3 + 6NH_4F + 3H_2O$$

Although the reaction is written with the ammonium fluoride as a product, it is known that a significant amount of this salt decomposes at the reaction temperature, giving additional HF that participates in the reaction. The reaction mixture is placed in a platinum or Monel boat and is heated in a Monel furnace tube in a slow stream of dry air at 300 to 400° C for 8 to 12 hours. This gives a conversion of over 95 per cent, but the removal of the last amounts of oxygen requires a second ammonium bifluoride treat-

ment, using the same amount of this reagent with the product of the first reaction. The success of this treatment may be due to the initial solvent action of the molten ammonium bifluoride, which removes the ScF_3 layer from the unreacted Sc_2O_3 or ScOF, and permits direct contact with the fluorinating agent.

HF Process: A direct reaction between Sc_2O_3 and anhydrous HF may be used for the preparation of ScF_3:

$$Sc_2O_3 + 6HF \longrightarrow 2ScF_3 + 3H_2O$$

This reaction is carried out in platinum or Monel equipment at a temperature of 600 to 700° C, and requires 100 to 200 per cent excess HF through the furnace to achieve complete conversion to ScF_3.

Wet Process: ScF_3 has been prepared by precipitating the hydrated fluoride and drying the salt by one of the above treatments, or by a combined vacuum-heat drying. This latter variant generally leaves some ScOF in the product, and it generally is simpler to use one of the two preceding above methods directly.

REDUCTION OF ScF_3 *TO METAL*

To convert the ScF_3 to metal, an active metal reductant, such as calcium, barium, lithium, or sodium is employed. Calcium has been used in the preparations of scandium described in the literature, and is more easily handled than some of the other possibilities. Powdered ScF_3 and granular redistilled calcium are mixed in amounts to correspond to the following reaction:

$$2ScF_3 + 3Ca\ (+\ 10\ \text{per cent excess}) \longrightarrow 3CaF_2 + 2Sc$$

The charge is jolt-packed into a tantalum crucible having 0.010-in. or thicker walls (tungsten crucibles also serve well, but are not generally as available), and this is heated in a vacuum to about 500° C to remove adsorbed gases. At this temperature, one atmosphere of argon gas is admitted to the furnace, and the heating is continued to 1550–1600° C. During this heating period, the reaction is initiated, and proceeds with an even evolution of heat that does not get violent. At the upper temperature, the scandium metal and calcium fluoride slag cleanly separate into two layers, and on cooling the slag may be broken away to obtain the metal in a yield of greater than 95 per cent—and probably 99+ per cent. At this point, the scandium contains 0.5 per cent or more calcium and from 2 to 5 per cent tantalum, dissolved from the crucible walls. The calcium may be removed by holding the metal at 1550° C in a vacuum for several minutes; the tantalum is present in the scandium as elemental tantalum (as opposed to an intermetallic compound), and because of its very low vapor pressure may be separated from the scandium by vacuum distillation of the scandium as described below.

PURIFICATION OF SCANDIUM BY VACUUM DISTILLATION

The apparatus employed for vacuum distillation of scandium is shown in Fig. 1; tantalum radiation shields have recently been used in place of the BeO shields indicated, and the baffles may have concentric collimating holes instead of the staggered configuration shown. The assembly is evacuated and maintained at a vacuum of 10^{-5} mm Hg during the distillation, with small pressure excursions during the initial heating and outgassing. Distillation takes place at a reasonable rate when the scandium reaches a temperature of 1650 to 1700° C, and the condensing region remains at 800 to 1000° C; by keeping the condenser at this temperature, trace amounts of calcium and magnesium in the feed metal pass out

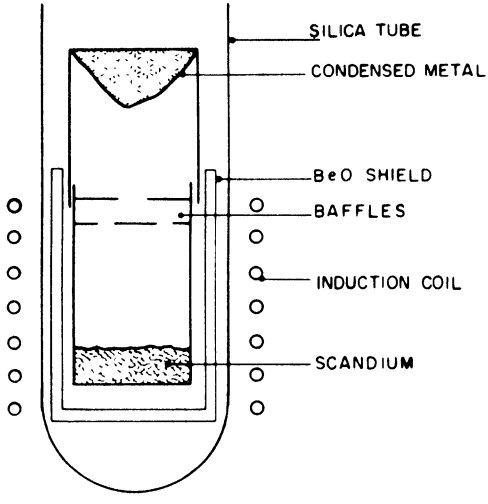


Fig. 1. Metal distillation system.

of the still without condensing with the scandium. In a 1-in.-diameter still of this type, a 25 g quantity of scandium may be condensed in several hours. When higher temperatures have been employed in an effort to increase the rate of distillation, the increased solubility of tantalum in the liquid scandium has caused crucible failures and loss of the liquid metal in the still.

The metal obtained by this distillation shows the following analyses:

Fe less than 0.05 per cent

Ca less than 0.02 per cent

Mg less than 0.03 per cent

Cr	less than 0.06 per cent
C	about 100 ppm
N	about 100 ppm

Oxygen analysis methods have not been perfected for scandium, but preliminary measurements indicate about 1000 ppm to be present. This is a higher figure than would be predicted on the basis of parallel studies with yttrium, but it is believed that this may be due in part to the existence of a volatile scandium oxide; the long time required for the distillation may be a contributing factor.

PROPERTIES OF SCANDIUM

MELTING POINT

The melting point of scandium has been measured on samples of distilled metal by the method of Pirani and Alterthum, obtaining a value of 1539° C, with a precision of ± 2° C; using this same method on metal samples of known melting point, an accuracy of ± 5° C was realized.

VAPOR PRESSURE

The vapor pressure of scandium is important in obtaining the pure metal by distillation as described above. Spedding *et al.* (4) report the measurements on the vapor pressure of scandium made with the Knudsen technique by means of a quartz fiber microbalance, and the data are plotted in Fig. 2. From these data, a heat of sublimation of 80.79 kcal/mole at 298° K, and an extrapolated normal boiling point of 3000° K, are obtained. The formula of the vapor pressure curve is

$$\log P_{mm} = \frac{-1.7177 \times 10^{-4}}{T°K} + 8.2979$$

These measurements indicate that the distillation of scandium is taking place at a pressure of about 0.5 mm, which is consistent with the low rate of distillation observed in this process, compared to the 2 mm recommended as the figure to consider for vacuum distillation of metals in Kroll's treatment. (5)

The entropy of vaporization of scandium from these data is 27.5 e.u. This is quite in line with values observed for metals having similar properties.

CRYSTAL STRUCTURES

The crystal structure of scandium has been examined by several workers. Older literature gave both a hexagonal and a face-centered cubic structure for scandium. Spedding *et al.* (4, 6, 7) have shown in

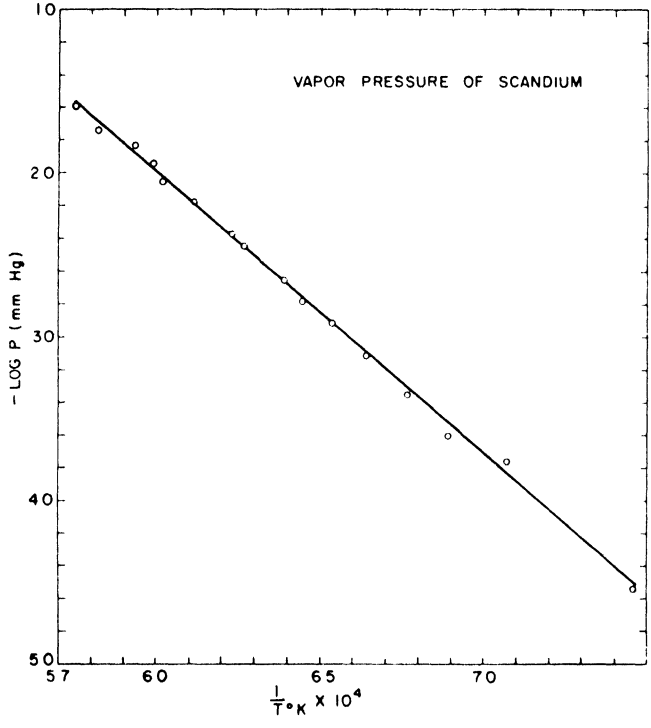


Fig. 2. Vapor pressure of scandium.

more recent work that the hexagonal form of scandium is the stable form from room temperature to near 1000° C, and that the face-centered cubic phase of scandium reported in the past is not characteristic of the pure metal, but is more probably due to a face-centered cubic impurity such as the nitride. The most recent measurements on scandium show the hexagonal form of the metal to have lattice constants of $a = 3.3080$, $c = 5.2653$, $c/a = 1.59$; an atomic volume of 15.028 cm^3; and a density of 2.922 g/cm^3. (7)

Beaudry has recently run thermal analyses on specimens of distilled scandium, and finds a transformation in the metal at 1339° C. This is not surprising in that a high-temperature transformation has been observed in yttrium and most of the rare earth metals, where the close-packed form of these metals transforms to the body-centered cubic structure on heating. Although it has not been possible to characterize this high-temperature form of scandium as being body-centered cubic, since it cannot be retained at room temperature by quenching, alloy system studies of scandium with other metals strongly indicate this to be the case.

ELECTRICAL RESISTIVITY

The electrical resistivity of scandium has been measured by Spedding *et al.* (4) and by Geiselman. (8) The values range between 54 and 66 microhm-cm, with Geiselman reporting the lower figure on a specimen of zone-melted metal. It is apparent that impurities exert an effect on this property. This range of values for the resistivity of scandium places it, along with yttrium and the rare earth metals, in the category of rather poor metallic conductors.

THERMAL EXPANSION COEFFICIENT

Spedding *et al.* (7) have measured the thermal expansion of scandium from room temperature to 1000° C by means of a high-temperature X-ray diffraction camera, and report a value of the average linear thermal expansion coefficient at 400° C of $11.4 \times 10^{-6}/°C$. The anisotropic nature of scandium is indicated in the expansion coefficients along the *a* and *c* axes of 9.3 and $15.2 \times 10^{-6}/°C$ respectively. These values are near those of yttrium and the heavy rare earth metals.

CORROSION RESISTANCE

Scandium is generally like the heavy rare earths in its corrosion properties. It does not tarnish rapidly in air and resists serious attack when heated in air until the temperature reaches several hundred degrees. The metal appears to form a stable nitride coating that tends to slow down further attack. In solutions, scandium is rapidly attacked by acids, but, like yttrium and the heavy rare earth metals, it is not seriously attacked by a 1 : 1 mixture of concentrated HNO_3 and 48 per cent HF.

MECHANICAL PROPERTIES

Geiselman (8) has studied some of the mechanical properties of scandium and finds it similar to yttrium and the heavy rare earth metals in that it is soft, but cracks on being worked more than a small amount. Hot swaging at 1000° C was found to be feasible. Tensile strengths of 23,000 to 37,000 psi were found on several specimens, with elongations of 3 to 5 per cent and reductions in area of 3 to 8 per cent; additions of titanium increased these values only slightly. A recrystallization temperature of about 500° C was reported.

ALLOY STUDIES

Scandium has been examined as an alloying agent with several metals, but in almost every case, the small amount of scandium metal available made it possible to prepare only one or perhaps two compositions; in no case has a complete alloy system of scandium with another metal been

reported. In these studies, scandium has been found to behave like a rare earth metal, forming compounds generally isostructural with similar rare earth compounds, and serving as a scavenger of nonmetallic impurities.

On an atomic-volume plot of the elements, scandium is seen to be in a position where it might be expected to form substantial solid solutions with several metals of current interest, including titanium, magnesium, and perhaps aluminum.

SCANDIUM-TITANIUM SYSTEM

Beaudry (9) has studied the Sc-Ti system and finds complete solid solubility across the beta region of this system (the beta form of scandium was discovered in this study). Some solid solubility occurs in the alpha form also. Geiselman (8) is studying the mechanical properties of Sc-Ti alloys and finds some increase in strength and ductility of scandium on adding titanium.

SCANDIUM-MAGNESIUM ALLOYS

Although detailed studies of Sc-Mg alloys have not been made, there appears to be some solid solubility in this system, and a similarity between it and some of the yttrium-and rare earth metal-magnesium systems. As has been noted in yttrium-and rare earth metal-magnesium studies, the rate of reaction between scandium and magnesium appears to rather slow.

SUMMARY

Scandium metal has been found to be very similar to yttrium and rare earth metals in most of its physical properties. It is sufficiently smaller as a metallic atom that it forms more extensive solid solutions with some other metals, and exhibits its individuality in its alloying behavior with other metals.

REFERENCES

1. Lars Nilson, *Compt. rend.*, 88, 645 (1879).
2. V. M. Goldschmidt, *Geochemistry*. Oxford, England: Clarendon Press, 1954.
3. F. H. Spedding *et al.*, *J. Electrochem. Soc.*, 105, 683 (1958).
4. F. H. Spedding *et al.* Paper accepted for publication in *Trans. AIME*
5. W. J. Kroll, *Trans. Am. Electrochem. Soc.*, 87, 571 (1945).
6. F. H. Spedding, A. H. Daane, and K. W. Herrmann, *Acta Cryst.*, 9, 559 (1956).
7. F. H. Spedding, J. J. Hanak, and A. H. Daane. Article to be published.
8. D. Geiselman. Quarterly progress reports, "The Metallurgy of Scandium," Union Carbide Metals Company, Air Force Contract AF 33(616)-6262 (1959-60).
9. B. J. Beaudry. Unpublished data.

MECHANICAL PROPERTIES OF RARE EARTH METALS*

B. LOVE AND C. KIRKPATRICK

Research Chemicals, Division of Nuclear Corporation of America, Burbank, California

Determination of the mechanical properties of the rare earth metals reflects growing availability and use of these materials. While the physical and chemical properties may be determined with some considerable precision on small quantities, the mechanical property evaluation requires much larger samples.

In mechanical-property determination, the properties of a given specimen may be said with certainty to apply to that specimen, and with reasonable certainty, to other specimens having the same composition, size, and shape, and which were prepared in the same manner.

Limitations in the quantity of material available in the earlier phases of this rare earth research necessitated the use of micro specimens for mechanical-property evaluation. As expected, properties obtained from near standard (0.250-in.-diameter reduced section) specimens are somewhat different from those obtained from the micro specimens. The differences are not large, however. While sample size was probably the major cause, the effect of other factors such as grain size and minor impurities must be considered.

MECHANICAL-PROPERTY-DETERMINATION SURVEY

Tables I and II show some results of mechanical-property determinations made at Research Chemicals in 1958. (1) Micro specimens were used to determine ultimate strength, tensile yield strength, and elongation at room and elevated temperatures. Room-temperature determinations were made of Izod impact properties.

The individual rare earth metals showed startling differences in ultimate tensile and tensile yield strengths. The lower atomic numbered elements had low strengths, while yttrium and the higher atomic numbered earths (except ytterbium) showed strengths which compared favorably

*This report is contribution number RC 155 from the laboratories of Research Chemicals, Division of Nuclear Corporation of America, Burbank, California. This work was supported in part by Wright Air Development Center under contract No. AF 33(616)-5905.

TABLE I: ROOM-TEMPERATURE MECHANICAL PROPERTIES OF CAST RARE EARTH METALS

Metal & No. of Samples	Ult. Tens. Strength (psi)	Tens. Yield Strength 0.2% Offset (psi)	Elongation (% in 0.375 in.)	Izod Impact (in.-lb)
Yttrium (5)	35,400	28,500	8.7	18.0
Lanthanum (5)	18,200	17,200	7.9	54.0
Cerium (4)	14,800	13,200	23.85	26.3
Praseodymium (4)	14,500	14,300	9.8	57.0
Neodymium (5)	23,900	22,900	10.6	99.4
Samarium (1)	18,000	16,200	2.5	6.5
Gadolinium (4)	26,400	25,100	7.8	15.4
Terbium (1)				38.4
Dysprosium (5)	35,100	32,600	5.6	19.8
Holmium (2)	37,500	32,100	4.9	85.8
Erbium (4)	38,700	38,000	4.0	14.0
Ytterbium (1)	10,400	9,500	5.7	63.7

with those obtained for the pure elements aluminum, magnesium, and titanium. The relatively low density of yttrium indicates a correspondingly high strength-to-weight ratio. In addition, the higher-strength metals showed quite good retention of tensile properties at temperatures up to 800 °F (427 °C). Impact tests showed the cast metals to be notch-sensitive, as expected.

ROOM-TEMPERATURE MECHANICAL PROPERTIES

On the basis of the above preliminary work, three metals, yttrium, dysprosium, and erbium were selected for further investigation. The

TABLE II: ELEVATED-TEMPERATURE TENSILE PROPERTIES OF CAST RARE EARTH METALS

	204 °C (400 °F)			427 °C (800 °F)		
	Ult. Tens. Strength (psi)	Tens. Yield Strength 0.2% Offset (psi)	Elongation (% in 0.375 in.)	Ult. Tens. Strength (psi)	Tens. Yield Strength 0.2% Offset (psi)	Elongation (% in 0.375 in.)
Yttrium	19,000	18,500	3			
Lanthanum	15,300	12,400	9.4	6,700	3,750	21
Cerium	5,700	4,700	21.4			
Praseodymium	20,100	14,700	15.8	6,740	5,850	30
Neodymium				6,000	5,700	13
Samarium	21,000	17,900	10.4	12,000	11,000	5.6
Gadolinium	17,950	15,600	6.8	14,100	13,050	11.3
Dysprosium	30,800	20,800	8.3			
Holmium	30,800	24,600	6.0			
Erbium	34,700	29,600	5.5	25,100	21,800	6.7
Ytterbium	10,200	7,800	10.8			

metals were prepared as nonconsumable, arc-melted blanks. All subsequent references to "cast" metals refer to specimens cut from these blanks. Some results of this work are shown in Table III. The use of near "standard" specimens—3 in. long, with a 0.250-in.-diameter reduced section, resulted in less scatter between samples of the same element. The elastic moduli in tension and compression were also determined from stress-strain measurements. Although larger specimens are generally recommended, the values thus determined are felt to be reasonably representative of the cast metal.

Tensile properties were found to be similar to those previously determined. Impact tests again showed notch-sensitivity, characteristic of cast metal.

WROUGHT RARE EARTH METALS

The tensile properties of wrought rare earth metals, both hot-and cold-swaged, are shown in Table IV. Dysprosium was the only metal which could be cold-worked to any extent, as cast, without intermediate annealing. Ductility, as measured by reduction of area, is improved when the cast structure is broken up by cold-working, although the uniform elongation is reduced to lower values than that for the cast structure.

Yttrium and erbium swage easily at 1800°F. For both metals, the ultimate yield strengths were improved somewhat by hot-swaging. Property increases probably are the result of breaking up of the original cast struc-

TABLE III: ROOM TEMPERATURE MECHANICAL PROPERTIES OF CAST RARE EARTH METALS

Metal & No. of Samples	Ult. Tensile Strength (psi)	Tens. Yield Strength 0.2% Offset (psi)	Elongation (% in 1 in.)	Red. of Area (%)	Youngs Mod. Tension (psi) $\times 10^{-6}$
Dysprosium (3)	31,400	18,300	5.0	13	8.3
Erbium (3)	33,200	17,600	5.0	14	9.3
Yttrium (4)	32,500	26,500	1.0	8	8.4

Metal & No. of Samples	Comp. Yield Strength 0.2% Offset (psi)	Youngs Mod. Compression psi $\times 10^{-6}$	Izod Impact (in.-lb)
Dysprosium (3)	18,700	6.7	27
Erbium (3)	20,300	12.0	13
Yttrium (4)			19

TABLE IV: ROOM-TEMPERATURE TENSILE PROPERTIES OF WROUGHT RARE EARTH METALS WORKED BY SWAGING

Metal & No. of Samples	Area Reduced by Working, & Swaging Temp.	Ult. Tens. Strength (psi)	Tens. Yield Strength 0.2% Offset (psi)	Elongation (% in 1 in.)	Red. of Area (%)	Tens. Modulus (psi × 10^{-6})
Dysprosium (1)	20% Cold	43,000	28,000	2.0	16.0	8.25
Dysprosium (1)	60% Cold	47,500	39,000	2.0	31.0	7.02
Dysprosium (2)	66% Cold	54,500	47,200	1.5	23.5	7.06
Erbium (3)	20% Hot	32,700	18,300	5.0	11.5	7.89
Erbium (2)	40% Hot	36,800	24,700	5.0	11.25	9.38
Erbium (2)	60% Hot	33,500	23,300	6.0	14.0	8.30
Erbium (1)	68% Cold	50,500	45,700	1.0	23.5	7.78
Yttrium (2)	20% Hot	27,800	19,700	2.0	16.0	8.62
Yttrium (2)	40% Hot	34,300	26,400	2.0	9.3	7.65
Yttrium (2)	60% Hot	39,000	28,500	7.0	20.5	8.17

ture and some "cold" working imparted during the swaging, since the working temperature probably did not remain above the recrystallization point at all times.

RECRYSTALLIZATION STUDIES

Specimens were taken for metallographic examination after each of the several steps in the deformation processes. Sections from cold-swaged rods of yttrium and erbium were given a number of different annealing cycles, and also prepared for metallographic examination.

WROUGHT STRUCTURES

Heating to 1800 °F without working does not result in any marked change in micro-structure, although impurities in the erbium seem to have a somewhat different distribution. The 60 per cent hot-worked yttrium showed evidence of recrystallization by the presence of relatively uniform equi-axed grains. The 20 per cent and 40 per cent metal showed no such evidence. This strongly suggests that the recrystallization temperature of yttrium is near 1800 °F (982 °C).

Erbium, hot-worked to 20, 40, and 60 per cent reductions at 1800 °F, showed no evidence of recrystallization.

RECRYSTALLIZED STRUCTURES

Specimens of yttrium which had been cold-worked 20 per cent (area reduction) after an initial hot swaging of 40 per cent (area reduction), were annealed for four hours at temperatures of 900, 1000, and 1100 °C. Recrystallization was essentially complete at 900 °C within four hours. Annealing at 1000 °C produced somewhat sharper grain definition. Marked grain growth was observed after annealing at 1100 °C.

Specimens of erbium which had been cold-swaged to a 60 per cent area reduction after initial hot-swaging to a 40 per cent area reduction were annealed for four hours at temperatures of 900, 1000, 1100, and 1200 °C. The structure after annealing at 900 °C was still that of the cold-worked metal. Recrystallization was almost complete after four hours at 1100 °C, the structure consisting principally of new equi-axed grains. After annealing at 1200 °C, appreciable grain growth was observed.

FATIGUE PROPERTIES

A smooth-bar fatigue specimen was used in this study. Stress range was from the maximum load to a minimum load—equal to 10 per cent of the maximum. Various stress levels were chosen to produce failures at various times from one thousand to over one million cycles. The testing speed was 1800 cycles per minute.

Fatigue data for dysprosium, erbium, and yttrium are presented in Fig. 1, 2, and 3.

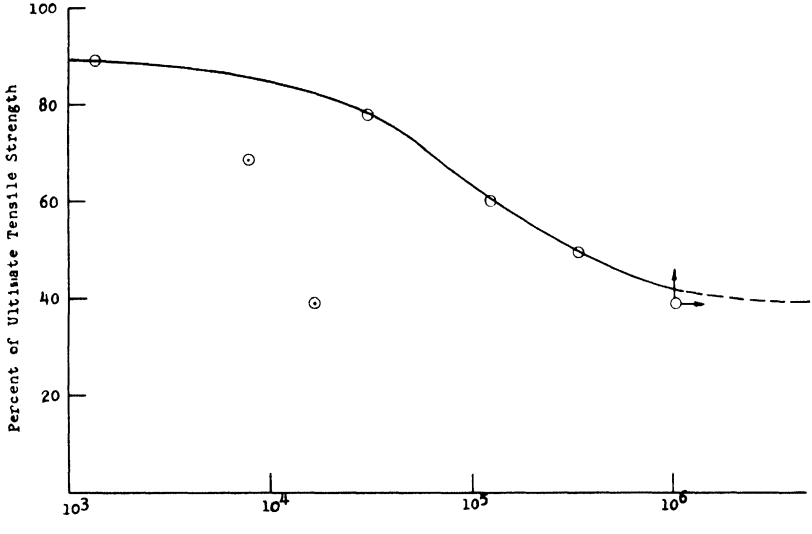


Fig. 1. Tensile fatigue properties of dysprosium.

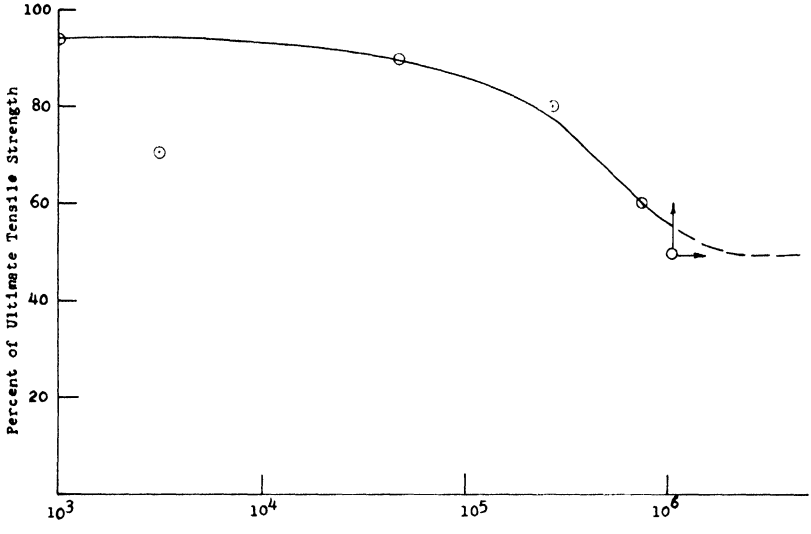


Fig. 2. Tensile fatigue properties of erbium.

The endurance limits for yttrium and erbium appear to be at a stress level equivalent to approximately 50 per cent of the ultimate tensile strength. The limit for dysprosium appears to be approximately 40 per cent of the ultimate tensile strength.

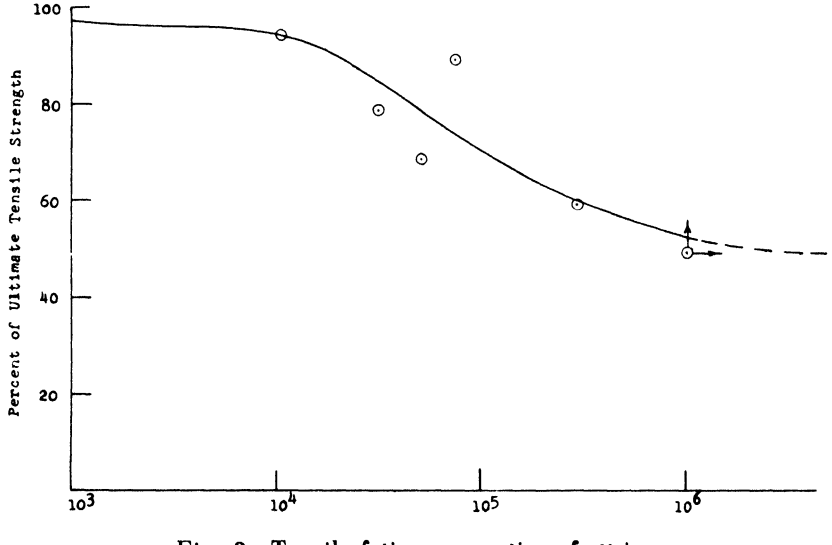


Fig. 3. Tensile fatigue properties of yttrium.

TENSILE PROPERTIES OF RARE EARTH-ZIRCONIUM ALLOYS

An investigation of binary alloys of rare earth metals with other elements suggested that, of those systems examined, zirconium would be most likely to effect improvement in mechanical properties. (2) The solubility of zirconium in erbium ranges from approximately 7 per cent at room temperature to 17 per cent at the eutectic temperature (1450 °C). Beyond this solubility limit, a second phase occurs which consists of a dilute solid solution of erbium in zirconium.

The mechanical properties of erbium could be enhanced by either solid-solution hardening (up to 7 per cent zirconium) or by solution annealing and aging (7 to 17 per cent zirconium). Two alloys were, therefore, selected for this work, one containing 7 per cent of zirconium and the second containing 11 per cent. The former alloy was examined as cast and also after four hours at 1000 °C (furnace-cooled). The latter alloy was examined (1) as cast, (2) after being solution-annealed two hours at 1100 °C. furnace-cooled, and aged eight hours at 600 °C, and (3) solution-annealed two hours at 1100 °C, oil-quenched, and aged 6 hours at 600 °C. The results of this series are shown in Table V, together with typical values for arc-cast unalloyed erbium for comparative purposes.

Metallographic examination of the cast 7 per cent alloy revealed a uniform well-delineated grain structure with no evidence of free zirconium. The tensile ultimate and tensile yield strengths of this alloy were found

TABLE V: TENSILE PROPERTIES OF ERBIUM-ZIRCONIUM ALLOYS

Alloy, Blank and Specimen Number		Heat Treatment	Ult. Tens. Strength (psi)	Tens. Yield Strength 0.2% Offset (psi)	Elongation (% in 1 in.)	Reduction of Area (%)
Erbium-7% Zirconium	(32-1)	As cast	52,000	37,500	1	1.5
	(32-3)	As cast	42,000	38,500	-	1.5
	(32-3)	Annealed at 1000 °C	47,500	30,000	3	5.5
Erbium-11% Zirconium	(33-1)	As cast	71,300	49,000	2	1.5
	(33-2)	Annealed at 1100°C Furnace-cooled Aged at 600°C	58,000	35,000	2	5.5
	(33-3)	Annealed at 1100 °C Oil-quenched Aged at 600 °C	60,500	34,500	3	7.0
Erbium (unalloyed)		As cast	33,000	17,000	5	14.0

to be markedly increased over values found for unalloyed cast erbium. This increase, however, is at the expense of ductility, as measured by reduction in area and uniform elongation. Annealing the alloy had little effect on the ultimate strength and improved the ductility, but reduced the yield strength.

Metallographic examination of the cast 11 per cent alloy showed a very small amount of zirconium-rich solid solution. Examination of the aged structure showed a more uniform distribution of zirconium-rich solid-solution particles, precipitated from the erbium-rich solid solution.

This alloy also exhibited a greater than twofold increase in tensile yield strength over unalloyed cast erbium. The tensile strengths were decreased, and the ductility, as measured by reduction of area, increased with subsequent heat treatment (solution annealing and aging).

All the two-phase alloys were stronger than the single-phase.

SUMMARY AND CONCLUSION

In general, the behavior of yttrium, dysprosium, and erbium is comparable to that of other, more common metals with a close-packed hexagonal crystal structure. The cast structures can be cold-worked, within limits, to improve mechanical properties. At a temperature of 1800 °F, all three are easily swaged to heavy reductions; the resulting structures are uniform and dense, and the properties are improved over those of the cast condition. The hardness and tensile strength of these cold-worked structures increase with increasing reductions, in a normal fashion.

Tensile properties were determined on both wrought and cast material. Values for the three metals were found to be quite comparable when the metals were under the same conditions. Ductility, as measured by reduction of area, was improved by working. The cast rare earth metals are notch-sensitive. The fatigue properties of cast yttrium, dysprosium, and erbium follow the normal patterns of increased life with decreased maximum applied load. Fatigue endurance limits in the order of 40–50 per cent of the corresponding ultimate tensile strength may be expected.

Recrystallization studies were made on cold deformed yttrium and erbium. The behavior follows a normal sequence of recovery, recrystallization, and grain growth. The temperature required for complete recrystallization of erbium, cold-worked 60 per cent, is approximately 1100 °C—a high value considering that the melting point of this rare earth metal is 1500 °C. This behavior suggests that the tensile properties of erbium may be retained at reasonably high operating temperature.

Studies of the tensile properties of erbium–zirconium alloys showed greatly increased tensile strengths over those of unalloyed erbium. The aging process is important for the development of maximum mechanical properties, and further studies of this process are being made.

REFERENCES

1. B. Love, *Selection and Evaluation of Rare or Unusual Metals: The Metallurgy of Yttrium and the Rare Earth Metals,* WADC Technical Report 57-666, Part II. Wright Air Development Center, Wright-Patterson Air Force Base, Ohio (1959).
2. B. Love, *The Metallurgy of Yttrium and the Rare Earth Metals: Phase Relationships,* WADD Technical Report 60-864, Part I. Wright Air Development Division, Wright-Patterson Air Force Base, Ohio (1960).

EFFECTS OF ALLOYING ADDITIONS OF Sc, Y, RARE EARTHS, Th, AND Pu ON THE γ-α TRANSFORMATION OF CERIUM

K. A. GSCHNEIDNER, JR., R. O. ELLIOTT, AND R. R. McDONALD*

University of California, Los Alamos Scientific Laboratory, Los Alamos, New Mexico

The γ-α transformation of pure cerium has been studied, and the present results are compared in this paper with the X-ray results of McHargue and Yakel. The effects of alloying additions of scandium, yttrium, most of the rare earths, thorium, and plutonium on the γ-α transformation of pure cerium have been determined. Experiments have been performed at room temperature under high pressure, and at low temperatures under atmospheric pressure. Plutonium and thorium were found to stabilize α-Ce with respect to γ-Ce, while the other alloying elements—at least under high pressure—did not. The results are discussed here in terms of the valence, size, number of unpaired *f*-electrons, and the magnetic moment of the solute element.

INTRODUCTION

Cerium, the first member of the 4*f*-transition group of elements, undergoes a 16.5 per-cent volume change both at high pressure ($\sim$ 8,000 atm at 298° K) (1) and at low temperatures ($\sim$ 100° K at 1 atm). (2) Zachariasen (3) and Pauling (4) suggested, independently, that this large volume change could be attributed to an electronic transition of a 4*f*-electron to the valence band. Trombe and Foëx (2), who were the first to discover this large volume change at low temperatures, also observed that another Ce allotrope was formed at slightly higher temperatures, between 100 and 273° K, under certain conditions. In accordance with the nomenclature used by Trombe and Foëx, we have used the Greek letters α, β, and γ to denote the allotropic forms of Ce normally existing at low, intermediate, and room temperatures, respectively. The room-temperature form, γ, is face-centered cubic (5), with $a = 5.1612$ A. (6) The β-form

*The information given at the Rare Earth Research Symposium has been submitted for publication in a journal. This work was performed under the auspices of the U. S. Atomic Energy Commission. The authors wish to thank F. E. Colvin, J. Louis, L. M. Lundgren, and M. Y. Prince for performing some of the experiments and calculations, and V. O. Struebing for preparing the alloys.

was originally reported by Hull (7) to be hexagonal with $c/a \sim 1.6$, but the recent data of McHargue and co-workers (8, 9) show that the lattice constants are $a = 3.68$ and $c = 11.92$ A, and that $c/a = 3.24$. Lawson and Tang (10) found that α-Ce is face-centered cubic, but with $a = 4.84$ A at 15,000 kg/cm^2 and room temperature. They were the first to propose that the high-pressure allotrope and the low-temperature alpha-phase were the same. A year later, Schuch and Sturdivant (11) published low-temperature X-ray diffraction results that proved the proposition to be correct.

Very little information has been published concerning the effects of alloying additions on the γ-α Ce transformation. Trombe (12) reported that 0.4% Si (not stated whether w/o or a/o) does not effect the γ-α transformation, while Ca prevents the formation of α-Ce, presumably as a result of the stabilization of β-Ce. Mahn (13) found that the addition of Mg lowers the γ-α transformation temperature, 1.0 w/o being sufficient to lower it to less than 77°K. Similarly, Clark and co-workers (14) found that as little as 0.44 w/o Fe lowered the γ-α transformation temperature to 77° K; Lawson and Tang (10) found that 0.2% Fe (not stated whether w/o or a/o) raises the γ-α transformation pressure to greater than 15,000 kg/cm^2. Gaume-Mahn (15) recently reported that tantalum appeared to raise the γ-α transformation temperature by about 5° K. Of these solutes (Ca, Fe, Mg, Si, and Ta) only Ta appears to stabilize the α-Ce allotrope; the others either have no effect on the γ-α transformation or tend to prevent the formation of α-Ce. Most of these solutes are known or thought to form very limited solid solutions with Ce—with the exception of Mg (16)—and it occurred to us that the effects of solutes that form extensive solid solutions should be investigated.

Recent information on the Ce-Th (17) and Ce-Pu (18) phase diagrams indicate that Ce alloys as the more dense or higher valent (α-Ce) form in Th-rich and Pu-rich solid solutions. Both Th and Pu appear to stabilize the α-Ce allotrope with respect to the γ-and β-Ce forms, and it seemed possible that they might cause the α-allotrope to be retained at room temperature and atmospheric pressure. It was also reasoned that if such stabilization occurred, and if it were due entirely to the smaller size of the Th and Pu atoms, then Sc and some of the smaller-size rare earths might also stabilize the α-allotrope. Lanthanum was examined because it is one of the few metals having a larger radius than either γ-or α-Ce, and is known to form extensive solid solutions (19, 20) with Ce. This investigation is concerned with the stabilization of α-Ce by alloying with these various solutes.

EXPERIMENTAL

The Ce used in this study was purchased from the Cerium Metals Corporation. Chemical analysis showed that it was 99.54 per cent pure.

Another Ce metal stock of higher purity (99.89 per cent) was obtained from the Bureau of Mines at Reno, Nevada. Sufficient quantities of the higher-purity metal were not available for the complete study, and thus it was used only to investigate the γ-α transformation behavior of the pure metal. The purities of the various solutes were of the order of 99 per cent.

A simple piston and cylinder device, having a pressure capability of 11,000 atm, and containing glycerol as the hydrostatic medium, was used. A Baldwin SR-4 load cell was used to measure the applied force delivered by a 50-ton Lombard press, and the pressure was calculated from the cross-sectional area of the piston, corrections being made for frictional forces. Volume changes were calculated from the linear displacement of the movable piston. This displacement was measured by means of two dial indicators which were attached to the movable piston. The observed volume changes were corrected for the expansion of the cylinder and shortening of the piston by using elastic theory calculations, and were also corrected by using Bridgman's values (1) for the compressibility of glycerol.

A dial-indicator dilatometer having a helium atmosphere was used in the low-temperature work. A glass Dewar (the inner Dewar) surrounding the quartz vacuum jacket was constructed in such a manner that liquid N_2 could be added, and the space above the liquid evacuated. The minimum temperature thus attained was of the order of 48 to 50 $^\circ$ K. The temperature of the specimen was measured by means of a copper-constantan thermocouple, which had its measuring junction resting on top of the specimen. A second Dewar surrounded the inner Dewar. The addition of liquid N_2 to only the outer Dewar permitted us to cool the sample at a rate of about 3 $^\circ$ K/min. When the sample had been cooled to about 75 $^\circ$ K, liquid N_2 was added to the inner Dewar, which was then evacuated to further cool the specimen. Rapid quenches down to 75 $^\circ$ K at rates of about 100 $^\circ$ K/min were attained by adding the liquid N_2 directly to the inner Dewar.

The samples were prepared by the induction-melting of weighed amounts of the two components. Nominal compositions are reported for all of the samples used in these experiments. The cast ingots were sealed within evacuated Pyrex capsules, homogenized at 725 $\pm$ 25 $^\circ$ K for a minimum of 200 hours (several were heat-treated for as long as 1000 hours) and air-cooled to room temperature. Cerium-plutonium alloys containing more than 10 a/o Pu were heat-treated at 875 $\pm$ 10 $^\circ$ K for at least 200 hours. After being heat-treated, the samples were machined to form right cylinders (0.434-in. diameter $\times$ 1.0 in. long) for the high-pressure runs. Later, these same samples were remachined to a diameter of 0.250 in. (1.0 in. long) for the dilatometric runs. Between runs the speci-

mens were reheat-treated at 725° K (at 875° K for the high-Pu, Pu-Ce alloys) for 4 to 24 hours to eliminate any β-Ce that may have formed during the runs. β-Ce forms at 263 ± 10° K upon cooling, and does not completely revert to the γ-Ce allotrope below 420 ± 5° K. (9)

RESULTS

PURE CERIUM

The γ-α transformation temperatures and pressures of Ce obtained from the Cerium Metals Corporation and from the Bureau of Mines are shown in Table I. The values for the transformation temperatures shown are significantly different from those reported by McHargue and Yakel

TABLE I: TRANSFORMATION TEMPERATURES AND PRESSURES OF TWO Ce STOCKS

Source	Trans. Temp. at 1 atm			Trans. Pressure at 296° K		
	γ ⟶ α (° K)	α ⟶ γ (° K)	$\left(\frac{\Delta l}{l_0}\right)^*$ (%)	γ ⟶ α (atm)	α ⟶ γ (atm)	$\left(\frac{\Delta V}{V_0}\right)$ (%)
Cerium Metals Corporation	106.4 ± 4.6	100.9 ± 4.0	3.67 ± 0.20	7,790	5,830	14.0
U.S. Bureau of Mines	116.5 ± 4.6	103.9 ± 3.8	3.40 ± 0.04	7,670 ± 80	5,680	13.6

*Value obtained by quenching.

(9), 96 ± 5 and 160 ± 10° K for the γ ⟶ α and α ⟶ ψ transformations, respectively. We believe that these discrepancies arise as a consequence of the inherent differences between our experimental method and that of McHargue and Yakel. At least 5 per cent of the α-Ce phase must be present to be detected by McHargue and Yakel's X-ray method, but as little as 0.3 per cent of the new phase can be identified by using the dilatometric method, which allowed us to detect the start of the γ ⟶ α or α ⟶ γ transformation. We estimate that McHargue and Yakel's Ce sample contained approximately 20% γ-Ce and 80% β-Ce at the γ ⟶ α transformation temperature (~100° K). Therefore 25 to 50 per cent of the γ-Ce present must have transformed before a sufficient amount of α-Ce was present to permit its detection by their X-ray method. Our dilatometric curves for the Bureau of Mines Ce show that the γ ⟶ α transformation temperature reported by McHargue and Yakel would be 15 to 30° K lower than our value when 25 to 50 per cent of the γ-Ce has transformed to α-Ce. In a typical dilatometric run our alloy consists of approximately 55% γ-Ce and 45% β-Ce at the γ ⟶ α transformation temperature. Since we could detect the formation of α-Ce as soon as 0.3% α-Ce had formed,

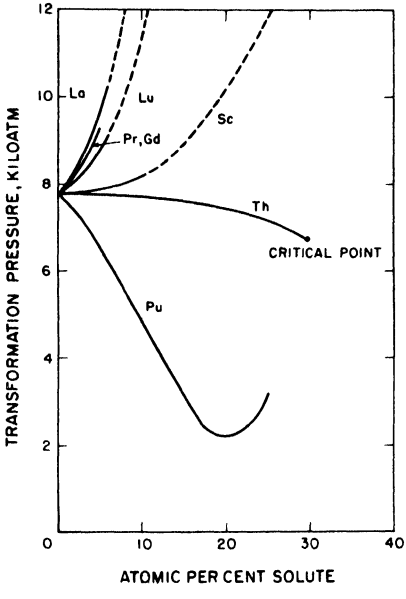
approximately only 0.5 per cent of the γ-Ce must have transformed to α-Ce before we were able to detect the beginning of the transformation. This deduction suggests that our transformation temperatures are about 0.3° K too low. We have not, however, corrected our values for the $\gamma \longrightarrow \alpha$ transformation temperatures by this amount, because it was not significant in view of the observed temperature variation. A similar argument suggests that McHargue and Yakel's $\alpha \longrightarrow \gamma$ transformation temperature should be decreased by about 65° K. If this correction is made, their result becomes 95 ± 10° K as compared with 103.9 ± 3.8° K for our result for the Bureau of Mines Ce. This large correction is necessary because the reverse transformation ($\alpha \longrightarrow \gamma$) appears to be quite sluggish in the temperature range from 104 to approximately 175° K; above 175° K the transformation proceeds to completion at a very rapid rate.

The results for the high-pressure transformation of the Bureau of Mines Ce agree reasonably well with the values reported in the literature. The mean value for the $\gamma \longrightarrow \alpha$ transformation pressure at 296° K is 7620 atm (1, 21, 22, 23, 24), while the mean value for the $\alpha \longrightarrow \gamma$ transformation pressure is 5490 atm (23, 24). Because the values for the $\gamma \longrightarrow \alpha$ transformation pressure in the literature lie between 7160 atm (21) and 8440 atm (23), the agreement between our value of 7670 atm and the mean literature value of 7620 atm is considered to be fortuitous.

EFFECT OF ALLOYING ON THE TRANSFORMATION PRESSURE

The effects of the solutes, Sc, La, Pr, Gd, Lu, Th, Pu, on the $\gamma \longrightarrow \alpha$ transformation under compression are shown in Fig. 1. The effects on the reverse transformation ($\alpha \longrightarrow \gamma$) are similar to those shown in Fig. 1. In general, the hysteresis between the transformation pressures obtained during compression and decompression becomes slightly less as the solute content is increased. For Th additions the hysteresis becomes zero at 18.6 a/o Th, and for alloys containing more than this amount of Th, the reverse transformation ($\alpha \longrightarrow \gamma$) occurs at higher pressures than does the $\gamma \longrightarrow \alpha$ transformation. A minimum in the curve for the Ce-rich alloys containing Pu occurs at about 20 a/o Pu.

The volume of transformation versus the solute concentration is shown in Fig. 2. It should be noted that the transformation curve for Ce-Pu alloys follows the theoretical curve expected for simple dilution, but that the Ce-Th volume-of-transformation curve drops off much faster than would be expected for simple dilution, becoming zero at 31.1 a/o Th. Thus a "critical point" appears to exist in the Ce-Th system. A 27 a/o Th alloy showed a small volume of transformation (2.2 per cent), whereas a 34 a/o Th alloy showed no evidence for a transformation. The data for Sc, La, Pr, Gd, and Lu also show a much larger decrease in the volume



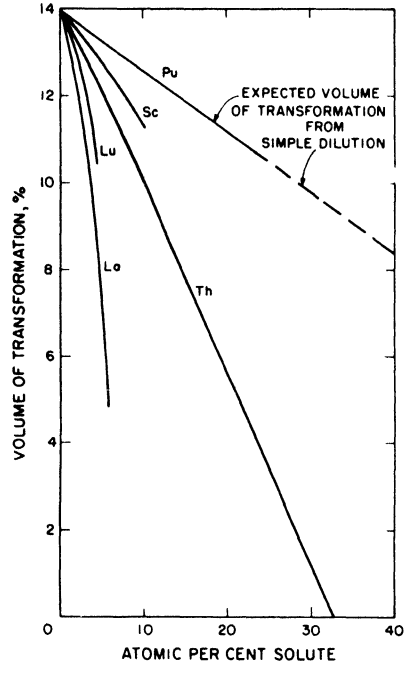


Fig. 1. Effects of alloying on the $\gamma \longrightarrow \alpha$ transformation pressure of cerium as a function of solute concentration.

Fig. 2. Effects of alloying on the volume of the $\gamma \longrightarrow \alpha$ cerium transformation under compression as a function of solute concentration.

of transformation than would be expected for simple dilution.* For La, Pr, Gd, and Lu, however, this large decrease may have resulted because the transformation could not be completed before the maximum pressure of safe operation was attained; that is, the transformation may not have gone to completion at the maximum pressure. It is not possible at this time for us to ascertain whether or not a "critical point" will be found in these Ce systems.

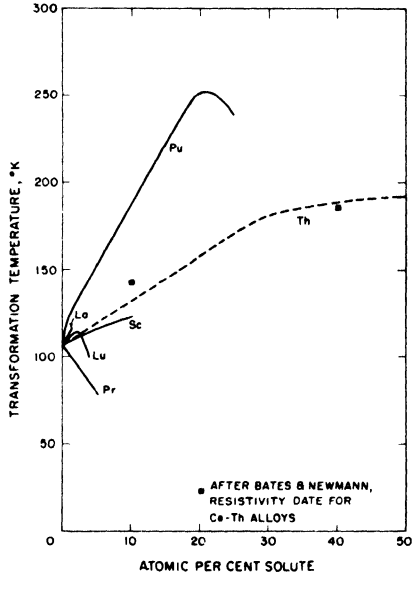
EFFECT OF ALLOYING ON THE TRANSFORMATION TEMPERATURE

The effects of the solutes Sc, La, Pr, Lu, Th, and Pu on the $\gamma \longrightarrow \alpha$ transformation temperature of Ce are shown in Fig. 3. In general the reverse transformation ($\alpha \longrightarrow \gamma$) behaves similarly to the $\gamma \longrightarrow \alpha$ transformation. The maxima in the curves for the Ce-Pu and Ce-Lu alloys occur at about 22 a/o Pu and 2 a/o Lu, respectively. The curve for the Ce-Th

*Data for Pr and Gd are not shown in Fig. 2.

alloys show a leveling off at higher Th contents, but it is uncertain whether or not the Ce-Th alloys would show a maximum at concentrations greater than 50 a/o Th. The transformation temperatures based on the electrical resistivity data of Bates and Newmann (25) for two Ce-Th alloys are also shown in Fig. 3. The data for Gd are not shown in Fig. 3, but the results for a Ce-5 a/o Gd alloy indicate that the $\gamma \longrightarrow \alpha$ transformation (if it occurs) would take place below 50° K.

The solute concentration versus the change in length of Ce specimens containing Sc, La, Lu, Th, and Pu is shown in Fig. 4. The theoretical curve obtained by assuming (1) simple dilution and (2) a length change of 5.5 per cent for pure Ce—based on Schuch and Sturdivant's X-ray data (11)—is also shown in Fig. 4. It should be noted that the data for Ce-Th and Ce-Pu alloys tend to approach, but do not reach, the simple dilution curve. The fact that these data do not meet the simple dilution curve may be explained by considering that alloys having compositions of less than 15-20 a/o Th or Pu did not transform completely to the α-phase at our minimum temperature of 50° K. This same consideration may also explain why the data for the Sc-, La-, and Lu-Ce alloys did not approach the theoretical curve. Furthermore, X-ray data for Ce-rich alloys show that both La and Lu tend to stabilize β-Ce with respect to γ-Ce, and



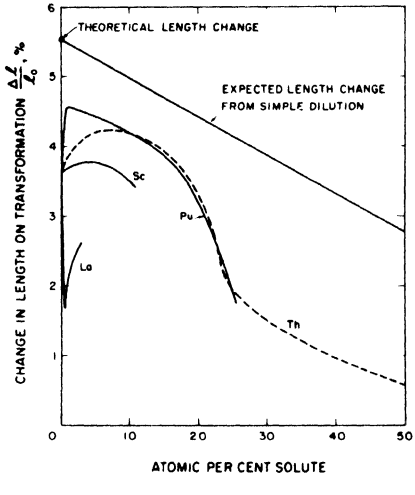


Fig. 3. Effects of alloying on the $\gamma \longrightarrow \alpha$ transformation temperature of cerium as a function of solute concentration.

Fig. 4. Effects of alloying on the length change of the $\gamma \longrightarrow \alpha$ cerium transformation at low temperatures as a function of solute concentration.

thus the observed length changes in the Ce–La and Ce–Lu alloys are much smaller than they would be theoretically.

DISCUSSION

Examination of the data in Fig. 1 and 3 shows that the expected inversion is exhibited by Th and Pu. The term *inversion* used in the above sense relates to the situation in which addition of a solute to a metal raises (or lowers) the temperature and lowers (or raises) the pressure of a transformation in the metal. Initial small additions of Sc, La, and Lu to Ce raise both the transformation temperature and pressure; however, larger additions of Lu lower the transformation temperature, and thus the Ce–Lu alloys also exhibit the expected inversion. It would appear that Pr and Gd alloys show this inversion effect, but the low-temperature data are insufficient to determine whether the curves (Fig. 3) are correct, or whether these two solutes behave like Lu.

It is interesting that the rate of rise of the transformation pressure per atomic per cent is dependent on the size of the trivalent solute atom. That is, the smaller the solute atom, the smaller the rate of rise. This effect is shown in Fig. 5.

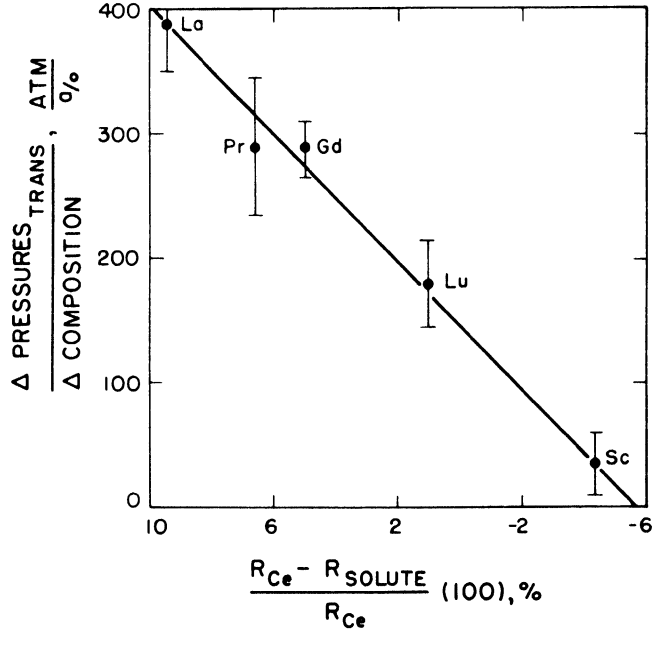


Fig. 5. The effect of size on the rate of rise of the $\gamma \longrightarrow \alpha$ transformation pressure per atomic per cent.

The ability of Pu, and to a certain extent that of Th, to stabilize α-Ce has been demonstrated. It has not, however, been possible to retain α-Ce at room temperature under atmospheric pressure, as we had hoped to be able to do at the outset of this study. α-Ce cannot be retained at room temperature in the Pu-Ce system because, at concentrations higher than 20 a/o Pu, the transformation temperature at atmospheric pressure is lowered, and the transformation pressure at 296° K is raised.

The "critical point" which was observed for the Ce-Th alloys at high pressure was not observed for these alloys at low temperature, at least up to 50 a/o Th. Extrapolation of these data, however, indicates that a "critical point" may exist at about 64 a/o Th (see Fig. 4). The low-temperature data for Pu also indicate that a "critical point" exists in this system at about 32 a/o Pu (see Fig. 4); however, no evidence for a "critical point" at high pressure exists for this alloy system.

REFERENCES

1. P. W. Bridgman, *The Physics of High Pressure*. London: G. Bell & Sons, Ltd., 1952.
2. F. Trombe and M. Foëx, *Compt. rend.*, 217, 501 (1943).
3. W. H. Zachariasen, quoted by A. W. Lawson and T. Tang, Phys. Rev., 76, 301 (1949).
4. L. Pauling, quoted by A. F. Schuch and J. H. Sturdivant, *J. Chem. Phys.*, 18, 145 (1950).
5. L. L. Quill, *Z. anorg. Chem.*, 208, 273 (1932); A. Rossi, *Nature*, 133, 174 (1934); and W. Klemm and H. Bommer, *Z. anorg. Chem.*, 231, 138 (1937).
6. F. H. Spedding, A. H. Daane, and K. W. Herrmann, *Acta Cryst.*, 9, 559 (1956).
7. A. W. Hull, *Phys. Rev.*, 18, 88 (1921).
8. C. J. McHargue, H. L. Yakel, Jr., and L. K. Jetter, *ibid.*, 10, 832 (1957); also see ORNL-2422, 207 (November, 1957).
9. C. J. McHargue and H. L. Yakel, Jr. Article accepted for publication in *Acta Met.* (1960).
10. A. W. Lawson and T. Tang, *Phys. Rev.*, 76, 301 (1949).
11. A. F. Schuch and J. H. Sturdivant, *J. Chem. Phys.*, 18, 145 (1950).
12. F. Trombe, *Rev. Met.*, 52, 2 (1956).
13. F. Mahn, *Ann. Phys.*, Series 12, 3, 393 (1948).
14. J. R. Clark, S. T. Pan, and A. R. Kaufmann, *Phys. Rev.*, 63, 139 (1943).
15. F. Gaume-Mahn. Sixteenth International Congress of Pure Applied Chemistry. (Inorg. Chem.) Paris (1957). London: Butterworth Scientific Publications, 1958.
16. K. A. Gschneidner, Jr., *The Rare Earth Alloys*. To be published.

17. R. T. Weiner, W. E. Freeth, and G. V. Raynor, *J. Inst. Metals*, 86, 185 (1957–58).
18. F. H. Ellinger, C. C. Land, and E. M. Cramer, in W. D. Wilkinson (ed.), *Extractive and Physical Metallurgy of Plutonium and Its Alloys*. New York: Interscience Publishers, Inc. In press.
19. R. Vogel and H. Kose, *Z. Metallk.*, 45, 663 (1954).
20. E. M. Savitskii and V. F. Terekhova, *Zhur. Neorg. Khim.*, 3, 756 (1958).
21. M. G. Gonikberg, D. P. Shakhovskhoi, and D. P. Butuzov, *Zhur. Fiz. Khim.*, 31, 350 (1957).
22. A. I. Likhter, Yu. N. Ryabinin, and L. V. Vereshchagin, *Zhur. Eksptl. i. Teoret. Fiz.*, 33, 610 (1957).
23. E. G. Ponyatovskii, *Doklady Akad. Nauk SSSR*, 120, 1021 (1958).
24. C. A. Swenson and R. Herman, *J. Chem. Phys.*, 29, 398 (1958).
25. L. F. Bates and M. M. Newmann, *Proc. Phys. Soc.* (London), 72, 345 (1958).

RARE EARTH METALS IN METALLURGY, CERAMICS, AND CERMETS

E. S. FUNSTON AND J. A. McGURTY

General Electric Company, ANP Division, Cincinnati, Ohio

The past decade has been a period of remarkable scientific and engineering advancements. One of the less publicized accomplishments of this period is the growth of the scandium, yttrium, and rare earth metal technology to industry. Scientists, engineers, and manufacturers can now obtain on a competitive basis, as off-the-shelf items, sixteen of the eighteen metallic elements and compounds of these elements which comprise the IIIA group of the periodic table. Stable isotopes of the other two elements of this group, promethium and actinium, do not exist.

Many people are under the mistaken impression that yttrium and the rare earth metals are truly rare elements. The contrary is the case. Ore reserves are known which are measured in millions of pounds. Hundreds of thousands of pounds of stockpile concentrates exist at manufacturer sites.

This present lush situation is for the most part a consequence of AEC and Air Force programs conceived to provide the General Electric–Aircraft Nuclear Propulsion Program with large quantities of ultrahigh-purity yttrium metal and compounds, and lesser quantities of the rare earth metals. The successful fulfillment of the requirements of this national effort was largely due to the pioneering work of Dr. Spedding and his associates at Iowa State University, not only on the all-important ion-exchange technique which makes possible the chemical separation of these elements in the highest purity form, but also for the research activities which provided processes for extracting these metallic elements in high-purity form from their compounds. Mention must also be made of the excellent work of the Michigan Chemical Company, Dow Chemical Company, the Lindsay Chemical Division, the Crane Chemical Company, and the Lunex Chemical Company, which established commercial facilities for producing yttrium, the rare earth metals and their compounds, in support of this program.

Having so ably satisfied a national need for yttrium and the rare earth metals, all those now concerned with this new field wonder what

new uses will now develop for these elements and their compounds, Production capabilities now far exceed present market demand, and producers must look to new products from the laboratories if this new industry is to grow strong. This paper reports on some of the uses for these materials which have been developed as a consequence of research at GE-ANPD.

GROUP IIIA ELEMENTS IN METALLURGY

The metallurgical industries will in time be heavy users of these new metals. Research has already established that certain of these metals when added to various commercially important alloys improve workability, strength, and oxidation resistance. They are helpful for achieving alloys of fine-grain structure and for raising recrystallization temperatures. These elements are also excellent scavengers, and are much more effective than either aluminum, silicon, or boron.

Two conditions must be corrected before tonnage customers develop for these metals. The first relates to price: One steel producer has found that rare earth additions improve both workability and mechanical properties of alloy steel. Unfortunately, with yttrium and the rare earth metals at their present price levels, he cannot produce this improved alloy and remain competitive. Second, considerable scientific and engineering research must be carried out in order to define the properties and usefulness of these elements. Since these elements appear to be most useful as additions to other metal systems, the nature of the binary systems of these elements must be defined. GE-ANPD has sponsored such work at Denver Research Institute and at Armour Research Foundation, with the result that the binary systems of yttrium with at least twenty-five elements are now fairly well defined. This research should be continued in order to evaluate these elements completely.

RARE EARTHS AND YTTRIUM IN FERROUS ALLOYS

Research carried out at Denver Research Institute and Battelle Memorial Institute in support of the GE-ANPD effort has shown that yttrium and the rare earth elements are only slightly soluble in iron-base alloys. The solubility data for Type-446 stainless steel (Fe–25 Cr) shown in Table I is typical. In spite of this low solubility, the effect of such additions, especially an yttrium addition, on oxidation resistance, workability, grain-refinement, and resistance to recrystallization is outstanding. For example, as Collins *et al.* (1) have previously shown, AISI Type-446 stainless steel, containing 25 w/o chromium with the balance primarily iron, is oxidation-resistant to about 2000° F. By the addition of a nominal 1 w/o yttrium to this system, a new alloy was obtained whose oxidation resistance is such that at 2300° F it has an

TABLE I: SOLUBILITY LIMIT OF RARE EARTH METALS AND YTTRIUM IN IRON-25 CHROMIUM ALLOY

Rare Earth	Solubility Limit, w/o
Lanthanum	< 25
Cerium	< 0.5
Praseodymium	< 0.5
Neodymium	< 0.5
Samarium	< 0.1
Gadolinium	< 0.5
Terbium	< 0.5
Dysprosium	< 0.2
Holmium	< 0.5
Erbium	< 0.5
Thulium	~ 0.19
Ytterbium	< 1
Lutetium	< 0.05
Yttrium	< 0.07

equivalent life expectancy equal to the parent metal without yttrium at 2000° F.

Lanthanum, gadolinium, dysprosium, and erbium were also found to improve oxidation resistance, but not as well as the yttrium additions. The specimens shown in Fig. 1 show the appearance of a Fe-30 Cr alloy and a Fe-30 Cr-1 Y alloy after being heated in air at 2300° F for 100 hours. The desirable effect of the yttrium addition is obvious.

Several tons of this alloy have been produced by vacuum melting techniques. Some caution should be exercised in the selection of raw materials in order to prevent excessive yttrium lossess. Materials low in carbon and oxygen impurities should be selected. The conversion of ingots into useful form differs little from that used to process Type-446 stainless steel.

The addition of 3 per cent Al to iron-chromium-base alloys produces metals which, when heated in air, are protected by an Al_2O_3 type coating rather than by the Cr_2O_3 type coating of the non-aluminum-bearing alloy. This aluminum oxide-type coating is more protective than the chromium oxide type. Yttrium additions (~ 1 per cent) to these iron-chromium-aluminum alloys also improve the protective qualities of this Al_2O_3 type coating.

In Fig. 2, the oxidation resistance of the yttrium containing Fe-Cr-Al alloy is compared with the Fe-Cr-Al alloy. The result is one of the most oxidation-resistant, workable base-metal alloys known. These metals, at temperatures as high as 2600° F, form an oxide coating that is smooth, hard, nonspalling, and thermal shock-resistant. A metallographic section of this alloy is shown in Fig. 3 after 450 hours service at 2300° F. The specimen, although only 0.007 in. thick, survived

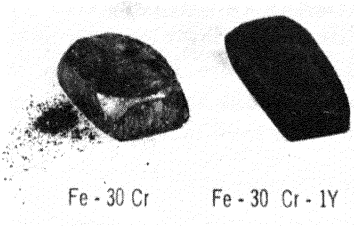


Fig. 1. Oxidation at 2300°F (100 hr).

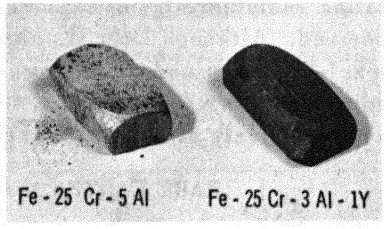


Fig. 2. Oxidation at 2300°F (100 hr).

numerous thermal cycles without spalling of the coating or loss of metal thickness. The alloy is single-phase, except for small oxide inclusions, and does not appear to be susceptible to intergranular oxidation.

In the iron-chromium-yttrium alloy, an aluminum content of at least 3 w/o is required to obtain the desired hard gray Al_2O_3 type film. At this composition, the alloy has good ductility and weldability, and remains relatively fine-grained at high temperatures. Alloys containing aluminum additions of from 4 to 5 w/o are somewhat more oxidation-resistant, but are more difficult to fabricate and to weld. Grain growth at high temperatures also proceeds fairly rapidly. Alloys containing about 7 w/o aluminum can only be hot-worked with difficulty.

Type-446 stainless steel ingots cost approximately seventeen cents a pound. Even were metallic yttrium or a ferro-yttrium alloy to become available at fifty dollars a pound, a 1 per cent yttrium addition would quadruple the price of this alloy. Yttrium additions of lower cost must be found.

The effects of yttrium additions to austenitic stainless steels has also been investigated. From the standpoint of oxidation resistance, only minor improvements were noted. Yttrium additions to nickel and nickel-base alloys were also found to have very little effect on the ox-



Fig. 3. Metallographic section of Fe-Cr-Al-Y alloy.

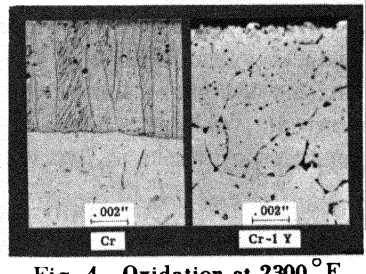


Fig. 4. Oxidation at 2300°F (100 hr).

idation resistance. Some improvement in metallurgical structures was observed. Although Lohr (2) claimed the life of heating elements of the nickel–chromium and nickel–iron–chromium alloys were improved by the addition of 0.5 w/o lanthanum, GE-ANPD studies did not find lanthanum to be decisively effective for improving oxidation resistance.

RARE EARTHS AND YTTRIUM IN CHROMIUM

Chromium-base alloys have for years been viewed by the metallurgist as potentially useful high-temperature materials. Although the element is moderately resistant to oxidation, it readily absorbs nitrogen from the air at temperatures above red heat, and loses all structural stability. Previous investigators have shown that additions of aluminum, silicon, boron, titanium, zirconium, and nickel—which in some instances improve the oxidation-nitrogen resistance of some metals—have no such desirable effect on chromium.

GE-ANPD research has shown that yttrium and some of the rare earth metals, and only these elements, are effective as additions to chromium for improving high temperature (to 2500° F) oxidation-nitration resistance. The photomicrographs shown in Fig. 4 reveal the micro-structure of unalloyed chromium and a chromium–1 w/o yttrium alloy which were heated in air at 2300° F for 100 hours. The unalloyed sample shows severe oxide attack to a depth of 10 mils and nitride-formation in the grain boundaries. The sample containing yttrium shows only superficial oxidation and no nitride precipitation.

If the ductile-brittle transition temperature of chromium–yttrium alloys can be reduced to below room temperature, tonnage applications for these alloys will develop. A number of chromium–1 per cent yttrium heats have been produced that could be hot forged and rolled into strip 0.30–0.40 mils in thickness. Small samples have also been hot rolled at 400° C to thicknesses of the order of 20 mils without cracking. This strip could be further reduced to 3 mils by cold pack-rolling after annealing at 800° C for 15 min. This very thin cold-worked material was found to be ductile at room temperature.

Investigations of chromium–rare earth element alloys were carried out to study the effects of rare earth element additions on hardness, oxidation resistance, and nitride formation. A tabulation of these data is shown in Table II. Some of the rare earth elements also improve the properties of chromium, but not as effectively as yttrium.

RARE EARTHS IN VANADIUM

Not too long ago vanadium was believed to be a hard, unworkable metal. However, as purer metal became available, it became apparent that pure vanadium like its congeners columbium and tantalum had ex-

TABLE II: RARE EARTH ADDITIONS TO CHROMIUM

Effect on hardness, oxidation, and nitrogen absorption of iodide-chromium at 2300°F, 100 hours

Rare Earth Added *w/o*	Rare Earth Analyzed *w/o*	As Cast Hardness R_A	Weight Gain mg/in.^{2} 100 hr	N_2 Absorption ppm
1 La	...	37	22	2400
2 La	...	35	55	1820
4 La	...	36	88	1850
0.5 Ce	...	42	30	220
2 Ce	...	36	30	170
0.5 Pr	0.03	39	15	650
1 Pr	...	39	15	...
2 Pr	1.71	42	8	30
4 Pr	...	41	38	...
0.5 Nd	0.11	38	15	1170
2 Nd	0.75	40	8	280
1 Sm	0.01	42	22	1170
2 Sm	0.02	41	20	1040
5 Sm	0.02	42	22	1112
0.5 Gd	0.50	38	15	430
2 Gd	1.85	41	8	230
0.5 Dy	0.11	41	66	1090
1 Dy	...	40	37	...
2 Dy	0.75	41	15	1170
4 Dy	...	40	8	...
6 Dy	1.95	42	22	1480
1 Ho	0.45	40	24	580
2 Ho	1.26	40	15	150
.5 Er	0.03	41	30	1250
2 Er	1.22	42	12	300
5 Er	3.38	41	8	60
1 Tm	0.12	40	140	850
2 Tm	0.16	42	90	1990
2 Tb	0.03	43	45	900
1 Lu	...	39	9	900
0.5 Y	...	39	15	110
1 Y	0.66	39	8	160
Unal. Cr	0	39	185	1.65 *w/o* N_2

cellent cold ductility. The problem is one of obtaining metal of adequate purity at reasonable cost. Only recently, a 20-mil sheet was selling for three dollars per square in.

During the course of a GE-ANPD sponsored study of the vanadium-yttrium phase diagram at Denver Research Institute, it was observed that the yttrium-vanadium system is characterized by no compounds and a

complete immiscibility in the solid state, and to temperatures several hundred degrees above the melting point of vanadium, except for some restricted terminal solubility. Examinations of the micro-structure of vanadium–yttrium compositions showed the vanadium phase to be cleaner than the starting material and of low yttrium content. The vanadium phase was also found to have the low hardness of very pure vanadium. DRI was able to reduce a 1/2-in.-thick arc-melted button to 0.7 mils in thickness by cold-rolling, without a single annealing treatment. Obviously, in retrospect, yttrium additions scavenge the impurities from liquid vanadium, and in excess do not contaminate the vanadium phase. Thus yttrium and and presumably some of the rare earths can be used to convert impure vanadium inexpensively to metal of good quality.

RARE EARTHS AND YTTRIUM IN CERAMICS

Ceramic producers are also potential customers of large quantities of yttrium and rare earth element compounds. Certainly the oxides of some of these elements are among the most stable and high-melting known materials.

Zirconia (ZrO_2), with a melting point of 2680° C (4850° F), is a very promising material for high-temperature applications. However, it has found very little use in the pure form because the compound undergoes a phase change at 1830° F which is accompanied by a significant volume change. Massive articles are subject to gross cracking on heating and cooling past this transformation temperature as a consequence of this property.

Various attempts have been made to modify the properties of zirconia with additions of other oxides to obtain a crystal structure which remains stable (no phase change) at all temperatures. Oxide additions found useful for this purpose are calcia, magnesia, thoria, titania, lanthana, neodymia, scandia, gadolinia, and yttria. The calcia addition has proved to be the most useful in this respect, and the tremendous quantity of zirconia ware produced by the ceramic industry is calcia-stabilized material. Unfortunately, at very high temperatures, especially in a reducing (H_2) or low-pressure environment, calcia is not as stable (volatile) as might be desired, and the maximum high-temperature capabilities of the ZrO_2 are not realized. A search of the stabilizing additions has thus continued.

The first investigation of yttria-stabilized zirconia bodies was that of Yavorsky and Geller (3) in 1945. Such materials have received very little attention since then because of the cost and scarcity of Y_2O_3. GE-ANPD investigators have found that, for melting such refractory materials as chromium and vanadium under low pressures at temperatures to 4000° F, the yttria (13 w/o) stabilized zirconia melting crucibles have the best high-temperature stability for such purposes. As a consequence

of this need, one vendor, Zirconium Corporation of America, now markets these bodies as standard commercial items.

The Norton Company has also been active in this field and is considering the marketing of fused ceria-stabilized zirconia ceramic ware for use in air to ultrahigh temperatures.

THE RARE EARTHS IN CERMETS

The primary interests in this field relate to combinations of rare earth compounds dispersed in metal matrices. GE-ANPD and other AEC installations make use of such materials for control-shielding applications.

The principal rare earths employed for this purpose, because of their high neutron absorption cross sections, are those of dysprosium, europium, gadolinium, and samarium.

An interesting way found to prepare such bodies was discovered at GE-ANPD. It was found that when additions of samarium or gadolinium were made to palladium, the resultant alloys could be worked into useful forms. The final shape could then be heated in air to a temperature at which the palladium alloy absorbed oxygen so as to bring about the internal oxidation of the rare earth metal, yielding a structure possessing the desirable high-temperature stability of palladium metal and refractory oxides. The nature of this rare earth-oxide formation is shown in Fig. 5.

SUMMARY

Research work on rare earths and yttrium at GE-ANPD has uncovered a number of interesting effects which have led to their useful applications in several fields. In metallurgy, small additions of rare earths and yttrium have enhanced the oxidation resistance of ferrous- and chromium-

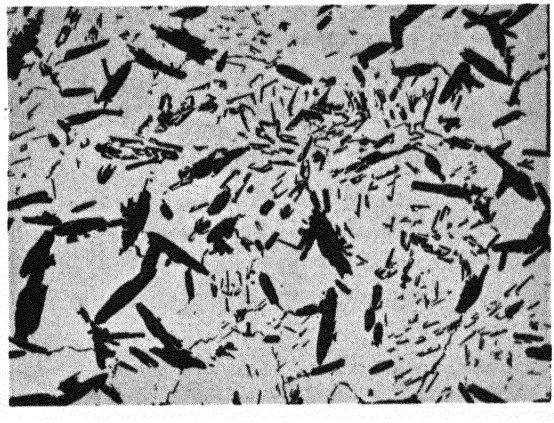


Fig. 5. Oxidized palladium rare earth alloy.

base alloys, as well as having improved their workability. Furthermore, the scavenging effect of yttrium has been utilized to produce a ductile vanadium metal. In ceramics the oxides of yttrium and rare earths are being used for high-temperature stabilization of zirconium. In cermets they find their widest use for nuclear-control applications.

Group IIIA element technology in the fields of metallurgy, ceramics, and cermets has only begun to be explored. As other investigators become interested in these metals and join with others presently working in this field, certainly much wider applications for these new metals will be found.

REFERENCES

1. J. F. Collins, J. A. McGurty, and V. P. Calkins, "Applications of Rare Earths to Ferrous and Non-Ferrous Alloys." Paper presented at American Society for Metals—Atomic Energy Commission Symposium on the Rare Earths and Related Metals, November, 1959.
2. J. M. Lohr, assignor to Driver Harris Company, U. S. Patents 2,687,954 and 2,687,956, *Alloy* (August, 1954).
3. R. F. Geller and P. J. Yavorsky, *J. Res. Natl. Bur. Stand.*, 35, 87 (1945).

RARE EARTH BORIDES AND NITRIDES*

HARRY A. EICK

Michigan State University, East Lansing, Michigan

This paper will deal primarily with the rare earth borides, which at the present time are of much greater interest than the corresponding nitrides. The nitrides will be discussed in a separate section at the end of the paper.

The rare earth borides were first investigated in 1932 by von Stackelberg and Neumann (1) and Allard (2) who prepared the hexaborides of lanthanum, cerium, praseodymium, neodymium, gadolinium, erbium, and ytterbium, along with other metals. These investigators established that the crystal structure was cubic of the cesium chloride type, in which the metal atom was held in the center of a cage of boron atoms (just as the cesium atom is in the CsCl crystal); six boron atoms in octahedral form were located at the corners of the cell in the same position as the chloride ion in cesium chloride. These hexaborides were then forgotten until Lafferty (3), in 1951, prepared LaB_6 and examined it to determine its thermionic properties.

Borides in which the boron-metal ratio differed from six had been found for many transition metals and for the actinides, and they were to be expected for the rare earths. Post, Moskowitz, and Glaser (4) reported in 1956 an MB_4 phase isostructural with UB_4 and an MB_x phase. Since their investigation, much activity has been centered on these and other borides. Probably the greatest activity has been expended in Russia by Samsonov and co-workers, who have prepared all of the rare earth hexaborides and most of the corresponding tetraborides and determined a few of their physical and chemical properties.

METHODS OF PREPARATION

The simplest method of preparation is by the reaction of the pure metal with boron. This method was used by Felten *et al.* (5) to prepare LaB_4. However, when this technique is used, great care must be taken to allow sufficient time for the product to become homogeneous. Galloway (6) has

*Based in part on work performed under the auspices of the U.S. Atomic Energy Commission.

observed that samples of samarium tetraboride can be prepared by direct reaction of the elements. However, even when excess metal is added to force the reaction path to SmB_4, trace amounts of SmB_6 are observed. Binder, LaPlaca, and Post (7) have reported that duodecaboride samples could not be prepared by this method.

A second method of reaction preferred by Samsonov (8) consists in reacting the sesquioxide with boron carbide (and carbon, if necessary), according to the equations:

$$M_2O_3 + 3\ B_4C \longrightarrow 2\ MB_6 + 3\ CO$$

$$M_2O_3 + 2\ B_4C + C \longrightarrow 2\ MB_4 + 3\ CO$$

These workers claim that the carbon is removed completely as carbon monoxide, and thus extremely pure specimens result. However, using a variation of this method, which consisted in mixing the sesquioxide with boron and carbon, and pressing a pellet, Post *et al.* (4) obtained an MB_x phase in which x was either 3 or 4. They did not present analytical data on their specimens, but the author has found this MB_x phase cannot be prepared in the absence of carbon. Hence, it is questionable if this should be considered a boride, and it more probably should be considered a rare earth boride-carbide.

A disturbing fact resulting from Samsonov's (8) work is that many of the lattice parameters reported by him differ considerably from those reported by other workers. This discrepancy is probably not a result of a carbon impurity (resulting from his method of preparation), but more likely indicates that the rare earth oxide specimens used by Samsonov were in reality mixtures of rare earth oxides. This supposition is supported by the analytical data on the sesquioxide samples used in the work of Tvorogov (Ref. a, Table I), for in his work the rare earth impurity varied from 3 to 10 per cent).

A third method of preparing borides is by the reaction of the metal oxide with boron, according to the equations:

$$2\ M_2O_3 + 22\ B \longrightarrow 4\ MB_4 + 3\ B_2O_2(g)$$

$$2\ M_2O_3 + 30\ B \longrightarrow 4\ MB_4 + 3\ B_2O_2\ (g)$$

Post *et al.* (4) first used this method to prepare the tetraborides by pressing a briquet and heating in a hydrogen atmosphere. Eick and Gilles (9) used the same method, but heated in vacuum to allow the $B_2O_2(g)$ to escape. This reaction proceeds equally well with either amorphous boron or crystalline boron. Again, however, it is difficult to obtain homogeneous samples. For example, YbB_4 may not be prepared by this method because of the high vapor pressure of ytterbium metal, and ErB_6 may not be prepared readily because of the instability of ErB_6 with respect to ErB_4 and boron at the temperatures necessary for the reaction. A second disadvan-

tage is that phases which are probably ternary metal-boron-oxide mixtures result from the preparations of some of the rare earths and are difficult to remove. According to Binder (7), however, MB_{12} compounds could be prepared only by this method. This may mean that a trace of oxygen is necessary to stabilize the phase. Although other methods of preparation have been reported, they do not seem to be of importance at the present time and will therefore be neglected.

TABLE I: LATTICE PARAMETERS OF RARE EARTH HEXABORIDES

Element	a(Å)
Y	4.128[a], 4.126[b], 4.08[c]
La	4.153[c,a]
Ce	4.141[a,c]
Pr	4.130[c], 4.132[a]
Nd	4.1260[d,a], 4.128[c]
Pm	
Sm	4.1333[d,a], 4.129[c]
Eu	4.178[e,a], 4.169[f]
Gd	4.1078[d,c], 4.121[a], 4.14[f]
Tb	4.1020[d], 4.092[a], 4.13[f]
Dy	4.0976[d], 4.07[c], 4.13[f]
Ho	4.096[d,a], 4.12[f]
Er	4.101[a], 4.110[c,f]
Tm	4.10[a]
Yb	4.1468[d], 4.140[a,c,f]
Lu	4.11[f]

(a) N. N. Tvorogov, *Zhur. Neorg. Khim.*, **4**, 1961 (1959); (b) G. A. Kudintseva, *et al.*, *Fiz. Metal i Metalloved*, **6**, 272 (1958); (c) Binder (11); (d) Eick and Gilles (9); (e) Felten (5); (f) values taken from Samsonov (8); (g) A. Zalkin and D. H. Templeton (14).

From the above descriptive information we can see that the most common borides are the cubic hexaboride and the tetragonal tetraboride. Various other borides have been reported, however. The diboride, reported by I. Binder (10), has been re-examined and is now no longer believed to exist (11). Some duodecaborides have been reported by Binder (7) for five rare earth metals and are isostructural with UB_{12} and ZrB_{12}. In addition Binder (7) has reported another crystalline boride possessing hexagonal symmetry in which the boron-metal ratio is either 4 or 5.

DISCUSSION OF THE STRUCTURES AND PROPERTIES

Table I lists the lattice parameters of the hexaborides as determined by various investigators. The table is by no means complete, but it is thought that the first listed lattice parameters are more accurate. Although the lattice parameters of lutetium, thulium, and erbium are probably in error by a small amount, it is readily noticeable that they do not decrease

in size proportionally to the other members. This very small decrease may indicate that the boride lattice can contract no further, and the smaller metal atoms are simply held, as it were, rather loosely in a boron cage. Other non-rare-earth hexaborides have larger lattice parameters. It is interesting to note the agreement among various investigators. Since it is extremely difficult to analyze accurately for boron, these data seem to indicate that the presence or deficiency of boron in the structure does not appreciably alter the lattice parameter.

As Post (7) has pointed out, the lattice parameters of the hexaborides of samarium, europium, and ytterbium are larger than would be expected if the elements were following the characteristic lanthanide contraction. The anomalous behavior of these three is characteristic of the metallic state, in which the atomic radii of these same elements is larger than would be expected. Therefore one may assume that the rare earth atom is present not as an ionic compound but in a more metallic nature. The hexaborides are conductors. S. Flodmark (12) has completed a theoretical study of bonding in MB_6 compounds and has concluded that several strongly bonding orbitals are in the conduction band, and hence, conductivity should be expected.

When a rare earth hexaboride is heated to a high temperature, two paths of decomposition may be followed. First, it may lose metal and become progressively richer in boron, as the following equation illustrates:

$$MB_6 \longrightarrow M\,(g) + 6\ B(s)$$

or secondly, it may disproportionate to give a lower boride and a free boron:

$$MB_6 \longrightarrow MB_4\,(s) + 2\ B\,(g)$$

Those rare earth metals which have a high vapor pressure would be expected to follow the first equation, while those which have a low vapor pressure should follow the second. Preliminary experiments tend to support this view, but there are exception. Neodymium, which possesses a rather low vapor pressure should follow Eq. (2). However, it apparently obeys Eq. (1). A possible reason for this unexpected behavior is interaction with the container.

When the hexaboride obeys Eq. (1), the boron-metal ratio progressively increases, until a point is reached at which the cubic structure collapses and the boron structure is left. After vaporization of about 40 per cent, by weight, of neodymium from a neodymium hexaboride sample, the specimen still retained its cubic structure, with only a slight variation in lattice parameter.

Table II lists the lattice parameter of the tetragonal rare earth tetraborides. Again, those values thought to be most reliable are listed first. Some lattice parameters reported by Neshpor and Samsonov (13) for the heavier rare earth tetraborides are very much in error, and, since the

error is such that the unit cells are larger, it is safe to assume that the samples were contaminated as stated previously. The lattice parameters decrease in a regular fashion characteristic of the +3 ions. From this regular decrease one may assume that the tetraborides are ionically bonded molecules. As would be expected, these molecules are not conductors.

The crystal structure of the MB_4 molecules, as determined by Zalkin and Templeton (14), consists of a three-dimensional network of boron atoms spread around the metal atoms. There are sixteen boron atoms in the unit cell, twelve of which are arranged in two octahedral forms of six each. The remaining four are in a plane, and these connect the octahedra together to make a continuous two-dimensional chain. The atoms of the octahedra above and below this plane are joined to similar boron atoms in neighboring cells, so that the network is continuous.

As would be expected, the high-temperature stability of the tetraborides may be directly related to the stability of the hexaboride. Those elements whose hexaborides decompose into the tetraboride may be heated to their melting points without appreciable decomposition. On the other hand, the tetraborides of those elements whose hexaborides disproportionate to give the elements will react according to the equation:

$$3\ MB_4 \longrightarrow 2\ MB_6 + M(g)$$

Very little information is available on other physical properties of this tetraboride phase.

TABLE II: LATTICE PARAMETERS OF TETRAGONAL RARE EARTH TETRABORIDES*

Metal	a(Å)	c(Å)
Y	7.09[c]	4.01
La	7.30[c]	4.17
Ce	7.205[g]	4.090
Pr	7.20[c]	4.11
Nd	7.219[d]	4.1020
Pm		
Sm	7.174[d]	4.0696
Eu		
Gd	7.144[d,a,c]	4.0479
Tb	7.118[d,a]	4.0286
Dy	7.101[d,c]	4.0174
Ho	7.086[d,a]	4.0079
Er	7.071[d,c]	3.9972
Tm		
Yb	7.01	4.00
Lu	6.98[f]	3.93

*References as for Table I.

Table III lists the lattice parameters of some of the rare earth duodecaborides. This cubic cell is isostructural with the phases ZrB_{12} and UB_{12}. The structure consists of a metal atom held in the center of a cage of 24 boron atoms. The cage, a regular polyhedron composed of squares and hexagons, shares its atoms with other similar cages to make a continuous three-dimentional network of boron atoms. Little is known about this difficultly prepared phase. As has been stated, it may be prepared only from boron and the sesquioxide. Other boride phases which are known—but not yet completely understood—are the following. The originally reported MB_2 phase, now believed to be a ternary metal-boride-

TABLE III: LATTICE PARAMETERS OF SOME DUODECABORIDES (7)

Metal	a(Å)
Dy	7.49
Ho	7.49
Er	7.48
Tm	7.48

oxide (11), has already been briefly discussed. Because of the difficulty encountered both in the preparation and analysis of these ternary boride phases, no additional data are available.

The tetragonal MB_x borides reported by Post *et al.* (4) can be easily prepared only when carbon is present. Hence, these are most likely boride-carbide phases, about which nothing except the lattice parameter is known (Table IV). The author prepared the ErB_4 phase by reacting ErB_4 with graphite in a high vacuum at elevated temperatures (> 2200° C). The phase was a hard, brittle substance which could not easily be removed from the reaction container.

TABLE IV: LATTICE PARAMETERS OF TETRAGONAL MB_x PHASE*

Metal	a(Å)	c(Å)
La	3.82	3.96
Pr	3.81	pseudo cubic(?)
Gd	3.79	3.63
Er	3.77_9	3.51_5

*All but Er from Ref. 7.

An additional hexagonal rare earth boride, MB_x in which $x = 4$ or 5, has been reported by Binder *et al.* (7) Lattice parameters for this phase are listed in Table V. The regular decrease in the lattice parameter indicates that the metal ion exists in its ionic + 3 oxidation state, as it

does in the tetragonal tetraborides. This MB_x phase is probably not a true boride, but is more likely a borate, MBO_3. (16)

From the above discussion it is apparent that much additional work must be performed before the rare earth-boron systems will be understood in even small detail.

TABLE V: LATTICE PARAMETERS OF HEXAGONAL MB_x PHASE (15)

Metal	a(Å)	c(Å)
La	3.90	4.33
Ce	3.87	4.39
Sm	3.86	4.47
Gd	3.83	4.45
Dy	3.78	4.41
Er	3.76	4.39
Tm	3.74	4.38
Yb	3.72	4.35

THE RARE EARTH NITRIDES

The rare earth nitrogen systems are of considerable interest to the author. The history of the nitrides can be summed in a paragraph. Iandelli and Botti (17) in 1938 prepared the nitrides of lanthanum, cerium, praseodymium, and neodymium, and Endter (18) in 1948 prepared gadolinium nitride. In 1956 Eick *et al.* (19) and Klemm and Winkelmann (20) prepared the remainder of the nitrides and reported the lattice parameters of these face-centered cubic phases (Table VI). It is apparent from the regular decrease in the lattice parameter that the lanthanide contraction is being followed, and hence that the metal-nitrogen bonds are somewhat ionic.

TABLE VI: LATTICE PARAMETERS OF RARE EARTH NITRIDES

Metal	a(Å)	Reference
La	5.29	(19)
Ce	5.01	(16)
Pr	5.15	(16)
Nd	5.14	(16)
Pm		
Sm	5.048	(18)
Eu	5.007	(18)
Gd	5.00	(19)
Dy	4.93	(19)
Ho	4.91	(19)
Er	4.84	(19)
Tm	4.81	(19)
Yb	4.785	(18)
Lu	4.77	(19)

In recent work the author has attempted to prepare pure nitrides by the reaction of the metal with hydrogen, followed by the removal of the hydrogen under vacuum to produce a very reactive powder. This powder is then reacted with either ammonia gas or nitrogen to produce the nitride. Samples produced in this manner do not contain the theoretical amount of nitrogen, but in the case of cerium nitride, for example, the composition is about N/Ce = 0.87 when only the nitride nitrogen is analyzed. However, the lattice parameters of such samples correspond to those reported in the literature.

When these cerium nitride samples have been annealed at 1600 to 1800° C in a high vacuum, the lattice parameter becomes considerably larger. At the present it is not known if this increase in size is the result of the formation of stoichiometric CeN, or if some oxygen, which dissolved when the samples were removed from the dry box, is being permanently located in the lattice.

CONCLUSION

An effort has been made to examine all of the now known rare earth boride phases briefly with respect to their methods of preparation, structures and high-temperature properties, with the hope that such an examination will show the areas in which current research effort is being expended. The rare earth nitrides have been briefly discussed with respect to their stoichiometry.

REFERENCES

1. M. von Stackelberg and F. Neumann, *Z. physik. Chem.*, 19B, 314 (1932).
2. G. Allard, *Bull. Soc. Chim. France*, 51, 1213 (1932).
3. J. M. Lafferty, *J. App. Phys.*, 22, 299 (1951).
4. B. Post, D. Moskowitz, and F. W. Glaser, *J. Am. Chem. Soc.*, 78, 1800 (1956).
5. E. J. Felten, I. Binder, and B. Post, *ibid.*, 80, 3479 (1958).
6. G. L. Galloway and H. A. Eick. Unpublished work.
7. I. Binder, S. LaPlaca, and B. Post. Conference on Boron sponsored by the U. S. Army Signal Research and Development Laboratory, Asbury Park, N. J., Sept. 18–19, 1959.
8. G. V. Samsonov, *Uspekhi Khemii*, 28, 189 (1959).
9. H. A. Eick and P. W. Gilles, *J. Am. Chem. Soc.*, 81, 5030 (1959).
10. I. Binder, *Powder Met. Bull.*, 7, 74 (1956).
11. I. Binder, *J. Am. Ceram. Soc.*, 43, 287 (1960).
12. S. Flodmark, *Arkiv Fysik*, 14, 513 (1959).
13. V. S. Neshpor and G. V. Samsonov, *Dopovidi Akad. Nauk Ukr. RSR*, 478 (1957), *Zhur. Fiz. Khim.* 32, 1328 (1958).
14. A. Zalkin and D. H. Templeton, *Acta Cryst.*, 6, 269 (1953).

15. S. LaPlaca. Private communication.
16. E. J. Felten. Private communication.
17. A. Iandelli and E. Botti, C. A., 32, 5274[5] (1938).
18. F. Endter, *Z. anorg. Chem.*, 257, 127 (1948).
19. H. A. Eick, N. C. Baenziger, and L. Eyring, *J. Am. Chem. Soc.*, 78, 5987 (1956).
20. W. Klemm and G. Winkelmann, *Z. anorg. Chem.*, 288, 87 (1956).

A STRUCTURAL SURVEY OF THE HEAVY RARE EARTH SILICIDES

CHARLES E. LUNDIN*

Denver Research Institute, University of Denver
Denver, Colorado

The existence of silicides of yttrium and the heavy rare earth metals with the stoichiometric ratio, M_3Si_5, has been established, whereas disilicides of these metals have not been confirmed. M_3Si_5 compounds of yttrium and the heavy rare earths are structurally isomorphous. Two structural forms have been determined for the M_3Si_5 compounds: hexagonal and orthorhombic. The anomalous formation behavior of these two closely associated structures and the factors which control their occurrence have also been the object of study.

INTRODUCTION

The use of transition metal–silicides as a class of materials for structural and other specialized applications in a high-temperature environment has received considerable attention. The melting points of these silicides are considered to be in the refractory range. Thus, for the requirements that have been imposed by missile and reactor technology for higher-temperature materials, the silicides have favorable characteristics. In particular, the rare earth–silicon systems such as gadolinium, dysprosium, and europium–silicon have been considered for reactor control-rod materials because of their high-neutron capture in conjunction with their high-temperature properties. However, much basic information regarding silicides must yet be developed in order to comprehend their potential usefulness more fully. The present study is an effort in this direction.

In the course of an investigation of the binary phase diagram of the yttrium–silicon system at the University of Denver, Denver Research

*The author is indebted to the following sponsors: The yttrium–silicon phase diagram study was sponsored by the General Electric Company, Aircraft Nuclear Propulsion Department under Subcontract AT-33. The studies of the heavy rare earth silicides were internally sponsored by the University of Denver, Denver Research Institute. The author also wishes to thank Mr. Robert McCune for conducting the X-ray diffraction analysis.

Institute, under sponsorship of the General Electric Company, Aircraft Nuclear Propulsion Department, anomalous compound formation was observed in the system. Further studies were thereby stimulated to examine the compound formation more thoroughly and to extend the study to the heavy rare earth metal silicides. These latter studies have been internally sponsored by the University of Denver. The studies have been conducted by metallographic and X-ray diffraction techniques.

The compound in the yttrium–silicon system and in each of the heavy rare earth metal–silicon systems—which is the object of this study—is of the stoichiometric ratio, M_3Si_5. The existence of M_3Si_5 compounds of yttrium and the heavy rare earth metals has been confirmed, both by metallographic and X-ray diffraction techniques. No evidence for the formation of MSi_2-type silicides with these metals could be found. Furthermore, the study of this compound divulged the presence of two crystal forms, a hexagonal form and an orthorhombic form. The conditions necessary for the existence of one form in preference to the other has been the object of considerable investigation, and is still being pursued.

To date, more emphasis has been placed on investigations of the Y_3Si_5 compound. Similar behavior in the heavy rare earth metal systems has been found, but additional studies must be conducted to prove complete isomorphism in these systems.

BACKGROUND

Previous investigations of both the phase equilibria and the crystal structures of intermediate phases of rare earth metal–silicon systems have been very limited. The only data which are available on the phase equilibria of these systems are those for the cerium–silicon system by Vogel (1), and then the phase diagram is only a partial diagram. No other phase diagrams are known to exist. Also, the structural data on intermediate phases of these systems are very meager. The efforts at structure determination have been primarily of disilicides.

The existence of $CeSi_2$ was reported by Zachariasen (2), Brauer and Haag (3), and Krikorian (4) and was determined to have a body-centered tetragonal structure of the $ThSi_2$ type. In addition, Brauer and Haag reported the same structures for lanthanum, praseodymium, and neodymium disilicides. However, the X-ray patterns of samarium and yttrium disilicides displayed extra lines which indicated that the tetragonal symmetry had diminished as the atomic number of the rare earth increased. The assumption was made that all of the rare earth metal disilicides exist and are related to the same structure-type, $ThSi_2$, on the basis of the structural determination of the light rare earth silicides. In a later study by Perri, Binder, and Post (5, 6), two allotropic forms of rare earth disilicides were reported, a high-temperature, body-centered tetragonal form, and a

low-temperature, orthorhombic form. These were referred to as β- and α-MSi_2, respectively. The transformation temperature from β- to α-MSi_2 was reported to increase with decreasing atomic radii or with increasing atomic number. Thus, the stable room-temperature form of MSi_2 changes from tetragonal to orthorhombic, as the transformation temperature increases from below room temperature to above room temperature with an increase in atomic number.

It is interesting to note that these authors observed a deficiency of silicon in the "α-$GdSi_2$." The stoichiometric composition was found to be close to $GdSi_{1.4}$. In the case of YSi_2, the transformation from α to β was reported to be $450 \pm 50^\circ$ C. The structures and lattice parameters given are as follows: (1) α-YSi_2 is orthorhombic, $a = 4.04$A, $b = 3.95$A, c = 13.33A; and (2) β-YSi_2 is body-centered tetragonal of the $ThSi_2$ type, $a = 4.04$A, c = 13.42A.

Since the rare earth silicide form which is reported to be β-MSi_2 (5, 6) is isostructural with that of thorium disilicide—namely, body-centered tetragonal—a search of the literature concerning the structural characteristics of thorium disilicide reveals an anomalous but related relationship with the rare earth silicides. The form α-$ThSi_2$ was established by Brauer and Mitius (7) as body-centered tetragonal. Later, Jacobson, Freeman, Tharp, and Searcy (8) obtained a hexagonal silicide, but observed that the silicon content was somewhat lower than that of the α-$ThSi_2$. They designated it β-$ThSi_2$. Recently, in a study by Brown and Norreys (9), this same phase was described as Th_3Si_5. Also, a new phase designated β-$ThSi_2$, was established with a similar hexagonal structure, but with the axial ratio changing from greater-than-one to less-than-one, respectively. These authors suggest that the atomic arrangement of Th_3Si_5 can be derived from β-$ThSi_2$ by omission of one-sixth of the silicon atoms. Thus the Th_3Si_5 is presumably a defect lattice. As a result of this omission, the axial ratio is purported to change.

The considerable variance and anomalous behavior in the findings from one author to the other is evidence that the structural characteristics of this type of silicide needs clarification.

EXPERIMENTAL PROCEDURES

All of the alloys were prepared by melting carefully weighed charges in a nonconsumable electrode arc furnace under a purified argon atmosphere. Nominal compositions were maintained to very close tolerances by noting weight differences after melting—which generally indicated very little change. The typical purities of the yttrium, the other rare earth metals, and the silicon are presented in Table I.

Metallographic techniques were as follows: The alloys, after mounting in bakelite, were ground on successively finer silicon-carbide discs

TABLE I: TYPICAL PURITY OF METAL COMPONENTS

	(%)
Yttrium	99.2
Gadolinium	99.5
Dysprosium	99.0
Erbium	99.0
Lutetium	99.0
Silicon	99.99

of grit sizes 1, 0, 00, and 000. Final polishing was accomplished with two stages of lapping on Microcloth with 5-micron and 1-micron diamond paste abrasive. The silicides were etched with a solution consisting of 75 ml of Keller's etch and 25 ml of HNO_3.

The annealing of the silicides was done in quartz capsules, which were either evacuated or partially evacuated with argon gas as the remaining atmosphere. The encapsulated specimens were annealed in either Globar or Nichrome-wire tube furnaces with appropriate temperature control.

X-ray diffraction analyses were conducted with powder samples on a Norelco diffractometer and basic unit. Standard preparation of powder samples for X-ray analyses was employed.

RESULTS AND DISCUSSION

As a result of the original phase-equilibria study of the yttrium–silicon system, the phase diagram in Fig. 1 was established. Four intermediate phases were found—Y_5Si_3, Y_5Si_4, YSi, and Y_3Si_5 (10). Structural data for the phases are as follows: (1) Y_5Si_3 is hexagonal of the Mn_5Si_3 ($D8_8$) type, $a = 8.418 \pm 0.005$A, $c = 6.337 \pm 0.005$A; 2) Y_5Si_4—structure not determined; (3) YSi is orthorhombic, $a = 4.257 \pm 0.005$A, $b = 10.527 \pm 0.008$A, and $c = 3.839 \pm 0.005$A; (4) Y_3Si_5 is hexagonal, $a = 3.836 \pm 0.001$A, $c = 4.139 \pm 0.001$A. Since Brauer and Haag, and Perri, Binder, and Post have reported the existence of YSi_2, alloys were carefully prepared at this stoichiometric ratio and above and examined metallographically. The micro-structures of these alloys were always two phase, consisting of primary dendrites of Y_3Si_5 phase and the Y_3Si_5-Si eutectic. X-ray diffraction analysis of alloys prepared in the composition range between the Y_3Si_5 phase and silicon did not give the hexagonal Y_3Si_5 pattern. Another distinct set of lines was present. Analysis of the pattern revealed as orthorhombic structure—$a = 4.05 \pm 0.01$A, $b = 3.95 \pm 0.01$A, and $c = 13.36 \pm 0.01$A. Thus, the author postulates that this structure was established by Perri, Binder, and Post; however, they report the phase as α-YSi_2. In this investigation, silicon lines were always detected in alloys with compositions above that of Y_3Si_5, confirm-

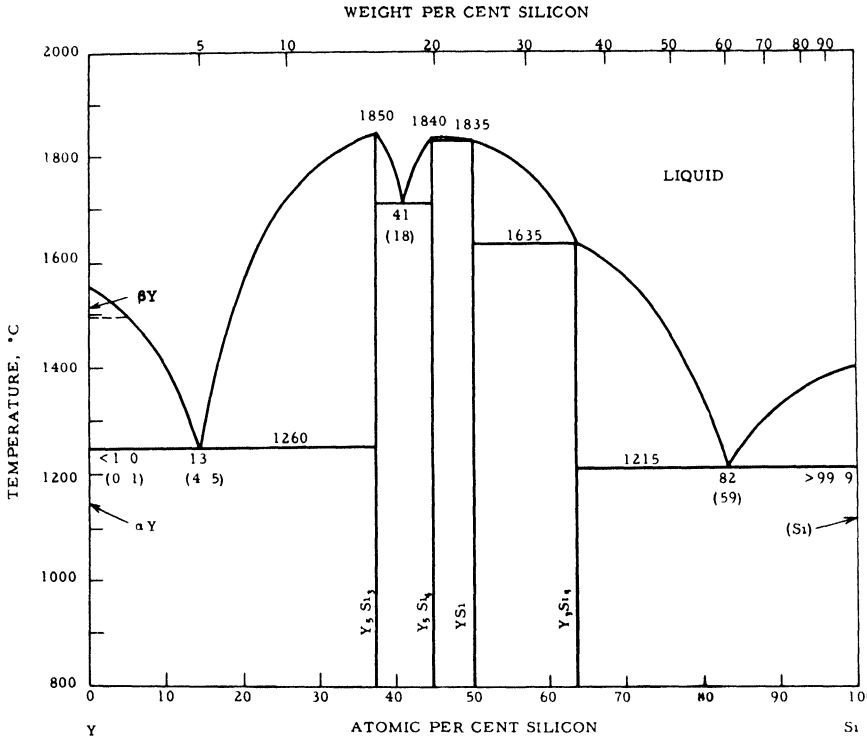


Fig. 1. The yttrium-silicon phase diagram.

ing the metallographic interpretation that a two-phase region exists between the Y_3Si_5 phase and the silicon phase. Thus, the author believes that Perri, Binder, and Post were, in actuality, analyzing a two-phase structure, wherein the orthorhombic phase was an allotropic modification of Y_3Si_5, rather than YSi_2.

An annealing study was next undertaken to determine the temperature level of the allotropic transformation. Specimens of both the Y_3Si_5 and YSi_2 compositions were subjected to heat treatments at 1150, 950, and 450° C, and then water-quenched. Also samples of both compositions were immersed in a liquid nitrogen bath. Metallographic and X-ray diffraction techniques were used to study these treated samples. No changes were seen in either alloy composition in either of their metallographic or crystal structures, compared to those of the as-cast state. Thus, the attempt to locate a phase transformation in the Y_3Si_5 compound by these treatments was unsuccessful. The stable form of Y_3Si_5 seems to be primarily dependent on composition. If a high-temperature form of the orthorhombic phase exists, as suggested by Perri, Banks, and Post, it

could not be detected by the anneal-and-quench technique. However, the presence of this phase is not discounted, since the heat treatments and rapid quenches might not have been able to suppress the transformation sufficiently well to retain the body-centered tetragonal phase at room temperature. Moreover, if the body-centered tetragonal phase does exist at higher temperatures, another question which arises is the temperature relationship of coexistence of the body-centered tetragonal, orthorhombic, and hexagonal phases at the same stoichiometric ratio, Y_3Si_5. The possibility of defect-type lattices, wherein small differences in silicon content could affect the stable crystal form, suggests itself as a mechanism of existence of the orthorhombic and hexagonal forms—and possibly the body-centered tetragonal form. High-temperature X-ray diffraction studies must be undertaken to resolve these questions.

Another factor that was studied which could affect the crystal structure type is the interstitial element content of the phase. The stabilization in M_5Si_3 compounds of one form in preference to another, depending on the interstitial content, has been well established. These phases have been termed *Nowotny phases* (11), after the author who detected the phenomenon. The stoichiometry of these phases are in reverse of the rare earth silicides under study, but the structural relationships are very closely related. A typical example is Nb_5Si_3 with a β-high-temperature form which is body-centered tetragonal of the W_5Si_3 type, and an α-low-temperature form which is body-centered tetragonal of the Ta_5Si_3 type. When carbon is added, a hexagonal form is stabilized (Nowotny phase). It is presumed the other interstitials act similarly. The impurity carbon and oxygen contents of the components used to prepare the yttrium-silicon alloys were checked and found to be less than 1000 ppm, combined. If the hexagonal form of Y_3Si_5 is an interstitial-stabilized form, this interstitial content might be sufficient to effect the change. However, the alloys used by Perri, Binder, and Post were prepared by silicon reduction of the metal oxides (or carbon and silicon reductions in some cases), but no hexagonal structures were developed. Thus, it would seem that interstitially stabilized silicide structures do not occur with the rare earths. To determine what the effect may be with the Y_3Si_5 phase, carbon was added to alloy buttons, with compositions at the ratios, Y_3Si_5 and YSi_2. No change in their metallographic structures or their crystal structures were noted.

Since the anomalous existence of the two crystal forms associated with the Y_3Si_5 phase have not been fully resolved, it was thought that the extension of the study to include the heavy rare earth metals might shed some light on this phenomenon. The supposition that isomorphism exists between the heavy rare earth silicides and yttrium silicides is

sound, because the properties of yttrium—even though it is not a member of the lanthanide series—are very similar to those of the heavy rare earths.

Representative heavy rare earth metals, gadolinium, dysprosium, erbium, and lutetium, were alloyed with silicon to the M_3Si_5 ratio. The as-cast alloys were metallographically examined, and samples were analyzed by X-ray diffraction techniques. The micro-structures in all cases were single-phase, proving the existence of the M_3Si_5 type. X-ray diffraction analysis of the alloys also confirmed the existence of the same hexagonal structure which was found with Y_3Si_5. The lattice parameters of these structures are presented in Table II. The corresponding yttrium silicide is included for comparison.

TABLE II: LATTICE PARAMETERS OF HEXAGONAL M_3Si_5 COMPOUNDS

	a	*c*	*c/a*
Gd_3Si_5	3.877 ± 0.001A	4.172 ± 0.001A	1.076
Y_3Si_5	3.836	4.139	1.079
Dy_3Si_5	3.831	4.121	1.076
Er_3Si_5	3.788	4.090	1.080
Lu_3Si_5	3.745	4.042	1.079

A gradual decrease in both the *a* and *c* parameters is observed with increase in atomic number of the rare earth, while the *c/a* ratio remains practically constant. Since the rare earth metals undergo a contraction of atomic radius with increase in atomic number, it follows that the size of the unit cell of the silicide will decrease. The size of the yttrium-silicide unit cell falls between gadolinium and dysprosium silicides, which is the same location of yttrium metal within the relative size range of the elemental rare earth metals.

In the same manner, gadolinium, dysprosium, erbium, and lutetium were alloyed with silicon to an MSi_2 composition. These as-cast alloys were metallographically examined, and samples were analyzed by X-ray diffraction techniques. The micro-structures of these alloys were two-phase, with M_3Si_5 plus a small amount of silicon. X-ray diffraction analysis of the MSi_2 two-phase alloys provided a somewhat different situation. In all cases, excess silicon lines were detected, thus confirming the metallographic data. However, the structures determined from the line patterns were orthorhombic for gadolinium and dysprosium, and isomorphic with that of yttrium, while the patterns for erbium and lutetium were hexagonal, and isomorphic with the alloys prepared to the M_3Si_5 ratio. The lattice parameters and structures of these compositions are presented in Table III.

TABLE III: STRUCTURES AND LATTICE PARAMETERS OF THE M_3Si_5 PHASE IN ALLOYS PREPARED AT THE MSi_2 COMPOSITION

	a	*b*	*c*	*Structure*
Gd_3Si_5	4.09 ± 0.01A	4.01 ± 0.01A	13.44 ± 0.01A	Orthorhombic
Y_3Si_5	4.05	3.95	13.36	Orthorhombic
Dy_3Si_5	4.03	3.94	13.33	Orthorhombic
Er_3Si_5	3.799 ± 0.001	...	4.090 ± 0.001	Hexagonal
Lu_3Si_5	3.745	...	4.042	Hexagonal

Again, a gradual decrease in the *a*, *b*, and *c* parameters of the orthorhombic structure, with increase in atomic number, is observed in gadolinium and dysprosium. The orthorhombic yttrium silicide falls between gadolinium and dysprosium in cell size, as it did in the hexagonal structure.

High-temperature X-ray diffraction studies must be undertaken to prove which of these two phases is the high-temperature form. The study of the compositions prepared at the MSi_2 ratio would indicate that the transformation temperature from one phase to the other is changing with increase in atomic number, and the change-over occurs at room temperature between dysprosium and erbium.

REFERENCES

1. R. Vogel, *Z. anorg. Chem.*, 84, 323-327 (1913).
2. W. Zachariasen, *Acta Cryst.*, 2, 94-99 (1949).
3. G. Brauer and H. Haag, *Z. anorg. Chem.*, 267, 198-212 (1952).
4. O. Krikorian, USAEC Publ. UCRL-2888, 1955, 16–17.
5. J. Perri, I. Binder, and B. Post, *Journal of Phys. Chem.*, 63, 616 (1959).
6. J. Perri, E. Banks, and B. Post. *Dissertation Abstracts*, 17, 3, 436 (1958).
7. G. Brauer and A. Mitius, *Z. anorg. Chem.*, 249, 325 (1942).
8. E. Jacobson *et al.*, *J. Amer. Chem. Soc.*, 78, 4850 (1956).
9. A. Brown and J. Norreys, *Nature*, 1959, 673.
10. C. Lundin and D. Klodt, "Fundamental Alloy Development Studies," APEX 449. Denver Research Institute for the General Electric Company, ANPD Subcontract AT-33, May 20, 1958.
11. E. Parthe, B. Lux and H. Nowotny, *Monatsh Chem.*, 86, 859 (1955).